

University of Alberta

**Freeze-Thaw Dewatering of Oil Sands Tailings As Part of a Natural Remediation
Strategy**

by

Bryan Jon Robert Bale

A thesis submitted to the Faculty of Graduate Studies and Research
in partial fulfillment of the requirements for the degree of

Master of Science

in

Geotechnical Engineering

Civil and Environmental Engineering

Edmonton, Alberta

Spring 2007



Library and
Archives Canada

Bibliothèque et
Archives Canada

Published Heritage
Branch

Direction du
Patrimoine de l'édition

395 Wellington Street
Ottawa ON K1A 0N4
Canada

395, rue Wellington
Ottawa ON K1A 0N4
Canada

Your file *Votre référence*
ISBN: 978-0-494-29935-7
Our file *Notre référence*
ISBN: 978-0-494-29935-7

NOTICE:

The author has granted a non-exclusive license allowing Library and Archives Canada to reproduce, publish, archive, preserve, conserve, communicate to the public by telecommunication or on the Internet, loan, distribute and sell theses worldwide, for commercial or non-commercial purposes, in microform, paper, electronic and/or any other formats.

The author retains copyright ownership and moral rights in this thesis. Neither the thesis nor substantial extracts from it may be printed or otherwise reproduced without the author's permission.

AVIS:

L'auteur a accordé une licence non exclusive permettant à la Bibliothèque et Archives Canada de reproduire, publier, archiver, sauvegarder, conserver, transmettre au public par télécommunication ou par l'Internet, prêter, distribuer et vendre des thèses partout dans le monde, à des fins commerciales ou autres, sur support microforme, papier, électronique et/ou autres formats.

L'auteur conserve la propriété du droit d'auteur et des droits moraux qui protègent cette thèse. Ni la thèse ni des extraits substantiels de celle-ci ne doivent être imprimés ou autrement reproduits sans son autorisation.

In compliance with the Canadian Privacy Act some supporting forms may have been removed from this thesis.

Conformément à la loi canadienne sur la protection de la vie privée, quelques formulaires secondaires ont été enlevés de cette thèse.

While these forms may be included in the document page count, their removal does not represent any loss of content from the thesis.

Bien que ces formulaires aient inclus dans la pagination, il n'y aura aucun contenu manquant.


Canada

University of Alberta

Library Release Form

Name of Author: Bryan Bale

Title of Thesis: Freeze-Thaw Dewatering of Oil Sands Tailings as Part of a Natural Remediation Strategy

Degree: Master of Science

Year This Degree Granted: 2007

Permission is hereby granted to the University of Alberta Library to reproduce single copies of this thesis and to lend or sell such copies for private, scholarly or scientific research purposes only.

The author reserves all other publication and other rights in association with the copyright in the thesis, and except as herein before provided, neither the thesis nor any substantial portion thereof may be printed or otherwise reproduced in any material form whatsoever without the author's prior written permission.

University of Alberta

Faculty of Graduate Studies and Research

The undersigned certify that they have read, and recommend to the Faculty of Graduate Studies and Research for acceptance, a thesis entitled Freeze-Thaw Dewatering of Oil Sands Tailings as Part of a Natural Remediation Strategy, submitted by Bryan Bale in partial fulfillment of the requirements for the degree of Master of Science in Geotechnical Engineering.

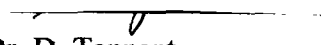
September 8, 2006



Dr. D.C. Segó



Dr. K.W. Biggar



Dr. D. Tannant



Dr. C. Mendoza

Abstract

The natural process of freeze-thaw dewatering has shown promise as a method to reclaim high moisture content mine tailings generated in Alberta's oil sand mining industry.

Dewatering of these deposits during freezing occurs due to the structural changes within the frozen soil, and from the removal of water from the underlying thawed soil during the creation of ice lenses. By determining the segregation potential of the tailings, the extent of water removal from the deposit can be predicted. Conventional freezing test methods were found to be ineffective for measuring the freezing characteristics of the compressible tailings. A method involving time-lapse photography was developed to determine the segregation potential of soft soils. Soil thermal conditions at Fort McMurray were modeled and thaw strain and frost heave were predicted for two tailings deposits.

Acknowledgements

I wish to thank Dr. Dave Segó for suggesting this research topic and providing guidance during my time at the University of Alberta. I also appreciate the input from Dr. Kevin Biggar and Dr. Lukas Arenson.

Work in the laboratory would not have been possible without the help of Christine Hereygers. Your patience and helpfulness is greatly appreciated. Also, thanks to Gerry Cyre for your help with the field-sampling program, and to Dung Anh Nguyen for your assistance with the TDR measurements.

Thank you Syncrude Limited for your financial support, access to research materials, and help from the staff at the Edmonton Research Centre. I am also grateful for the funding from NSERC and Luscar Limited.

Table of Contents

Chapter 1 - Introduction.....	1
1.1 Background.....	1
1.1.1 Oil Sands Overview	1
1.1.2 Past and Present Fine Tailings Management	3
1.1.3 Requirements for Land Reclamation	7
1.1.4 Previous Freeze-Thaw Dewatering Studies	8
1.1.5 Current Natural Remediation Strategy.....	9
1.2 Objectives	10
1.3 Methodology.....	10
1.4 Organization of Thesis.....	11
1.5 References.....	12
Chapter 2 - Freeze-Thaw Mechanisms	13
2.1 Freezing	13
2.1.1 Analytical Solutions for Freezing Thermodynamics	13
2.1.2 Overview of Freezing Mechanisms	14
2.1.3 Open and Closed System Freezing	18
2.1.4 Segregation Potential	19
2.2 Thawing	22
2.2.1 Model for Thawing of Soil	22
2.2.2 Freeze-Thaw Impact on Hydraulic Conductivity	24
2.2.3 Freeze-Thaw Impact on Consolidation Characteristics	26
2.3 Freeze-Thaw Settlements and Consolidation	26
2.3.1 Consolidation During Freeze	26
2.3.2 Thaw and Post-Thaw Consolidation.....	28
2.4 Additional Consolidation Mechanisms.....	28
2.4.1 Desiccation.....	29
2.4.2 Seepage Consolidation and Drainage	29
2.5 Conclusions.....	29
2.6 References.....	30
Chapter 3 - Material Sampling.....	32

3.1	Sampling Technique	33
3.2	Site Characterization.....	36
3.3	Observations of Frozen Soil Structure.....	40
3.4	Conclusions.....	44
3.5	References.....	46
Chapter 4 - Previous Related Work and Material Characterization		47
4.1	Freeze-Thaw Dewatering of Oil Sand Fine Tailings	47
4.2	Segregation Potential	49
4.3	Summary of Material Characteristics	50
4.3.1	Grain Size Distribution	50
4.3.2	Geotechnical Characteristics.....	51
4.3.3	Freezing Point Depression	52
4.4	References.....	53
Chapter 5 - Laboratory Freeze-Thaw Testing.....		54
5.1	Test Theory	54
5.2	Freezing Test Apparatus 1: Heave and Flow Measurements	57
5.2.1	Equipment.....	58
5.2.2	Test Operation.....	59
5.2.2.1	Sample Preparation	59
5.2.2.2	Testing Procedure	59
5.2.3	Test Results.....	60
5.2.4	Conclusions from First Test Series.....	63
5.3	Freezing Test Apparatus 2: Suction, Flow, and Heave Measurements	65
5.3.1	Equipment.....	65
5.3.2	Test Operation.....	66
5.3.3	Test Results.....	67
5.3.4	Conclusions from Second Test Series.....	68
5.4	Freezing Test Apparatus 3: Time Lapse Photography.....	72
5.4.1	Equipment.....	73
5.4.2	Test Operation.....	73
5.4.3	Test Results.....	73

5.4.4	Conclusions from Third Test Series	75
5.5	Conclusions.....	75
5.6	References.....	77
Chapter 6 -	Interpretation of Freeze-Thaw Testing	78
6.1	Overview of Laboratory Freezing Tests	78
6.2	Pore Pressure During Freezing	79
6.3	Qualitative Observations of Heave and Flow	84
6.4	Temperature Distribution During Freezing	88
6.5	Segregation Potential	91
6.5.1	Methods for Determining the Segregation Potential	91
6.5.1.1	Surface Heave or Inflow	91
6.5.1.2	Final Lens Thickness	92
6.5.1.2.1	Validity of Final Ice Lens Thickness for Determining Segregation Potential	96
6.5.1.3	Ice Penetration Rate	97
6.5.1.4	Final Moisture Content	97
6.5.2	Segregation Potential Results	97
6.6	Solids Content Distribution After Freezing.....	105
6.7	Photographs from Freezing Tests	109
6.8	Thaw Strain.....	112
6.9	Conclusions.....	120
6.10	References.....	123
Chapter 7 -	Modeling for Field Predictions	124
7.1	Temperature Distribution.....	125
7.1.1	Bottom Boundary Condition.....	125
7.1.2	Upper Boundary Condition.....	125
7.1.3	Basic Geotechnical Parameters.....	126
7.1.4	Thermal Analysis Parameters	128
7.1.4.1	Unfrozen Water Content	128
7.1.4.2	Heat Capacity	128
7.1.4.3	Thermal Conductivity	129

7.1.5	Numerical Analysis Method	132
7.1.6	Numerical Analysis Results.....	133
7.1.6.1	Initial Temperature Distribution	133
7.1.6.2	Frost Penetration	135
7.1.6.3	Temperature Gradient.....	136
7.2	Segregation Potential	136
7.3	Frost Heave Determination.....	137
7.3.1	Thaw Strain and Consolidation.....	138
7.4	Conclusions.....	138
7.5	References.....	139
Chapter 8 -	Summary, Conclusions, and Recommendations.....	140
8.1	Summary of Thesis	140
8.2	Conclusions.....	142
8.3	Recommendations.....	143
Appendix A -	Summary of Test Results	145
A.1	Test Series 1	146
A.1.1	S1T1 – Devon Silt.....	146
A.1.2	S1T2 – Suncor Pond 2/3 MFT	148
A.1.3	S1T3 – Suncor Pond 2/3 MFT	150
A.1.4	S1T4 – Suncor Pond 2/3 MFT	153
A.2	Test Series 2.....	156
A.2.1	S2T2 – Suncor Pond 2/3 MFT	156
A.2.2	S2T3 – Suncor Pond 2/3 MFT	159
A.2.3	S2T4 – Suncor Pond 2/3 MFT	161
A.3	Test Series 3.....	163
A.3.1	S3T1 – Syncrude SWSS Sump Fines - Bulk	163
A.3.2	S3T2 – Syncrude SWSS Sump Fines - Bulk	170
A.4	Test Series 4.....	177
A.4.1	S4T1 - Syncrude SWSS Sump Fines – Frozen Core	177
A.4.2	S4T2 - Syncrude SWSS Sump Fines – Frozen Core	181
A.4.3	S4T3 - Syncrude SWSS Sump Fines – Frozen Core	183

A.5	Test Series 5.....	185
A.5.1	S5T1 and S5T2 – Devon Silt	185
A.6	Test Series 6.....	188
A.6.1	Syncrude SWSS Sump Fines – Frozen Core	188
Appendix B -	Testing Procedure and Details	189
B.1	Sample Preparation	189
B.1.1	Bulk MFT Samples	189
B.1.2	Frozen Sump Core	189
B.1.3	Devon Silt	189
B.2	Material Characterization	190
B.3	Equipment Accuracy.....	190
B.4	Testing Procedures.....	191
B.4.1	Setup 1	191
B.4.2	Setup 2	192
B.4.3	Setup 3	192
B.5	Final Solids Content Determination	193
B.5.1	Frozen Sample	193
B.5.2	Refreezing from Thawed Sample	193
B.5.3	Freezing Remainder of Frozen Sample.....	193
B.5.4	Thawed Sample.....	193
Appendix C -	Frozen Core Photographs.....	194
C.1	Sampling Location S2.....	195
C.2	Sampling Location S3.....	196

List of Tables

Table 2-1 - Factors Affecting Segregation Potential (Konrad 1990).....	22
Table 3-1 - Summary of Sampling Locations (Universal Transverse Mercator)	35
Table 4-1 - Segregation Potential of Devon Silt (Xia 2006)	50
Table 4-2 – Properties of Materials Reported in Literature	51
Table 4-3 – Initial Properties of Materials Tested in Laboratory Program.....	51
Table 6-1 - Summary of Laboratory Tests.....	79
Table 6-2 - Comparison of SP Values for Test Series 5 Using Various Calculation Methods.....	97
Table 6-3 - Segregation Potential for All Tests	98
Table 6-4 - Summary of Average Thaw Strain and Corresponding Solids Content	118
Table 7-1 - Parameters for Thermal Analysis for Sump Material	127
Table 7-2 - Parameters for Thermal Analysis for MFT	127
Table 7-3 - Segregation Potential Used for Frost Heave Analysis	136
Table A-1 - Overview of Tests	145
Table B-1 - Material Characteristics and Associated ASTM Standards.....	190
Table B-2 - Equipment Accuracy for Test Setup 1.....	191
Table B-3 - Equipment Accuracy for Test Setup 2 and 3.....	191

List of Figures

Figure 1-1 - Oil Sands Deposits in Alberta, Canada (Morgenstern et al. 1988).....	1
Figure 1-2 - Stratigraphy of Athabasca Deposit (Morgenstern et al. 1988)	2
Figure 1-3 - Segregation Chart Showing Syncrude Tailings Stream Properties (Modified after Morgenstern and Scott 1995).....	5
Figure 1-4 - Fine Tailings Management Alternatives (After Morgenstern and Scott 1995)	7
Figure 2-1 - Frost Heave in an Idealized One Dimensional Soil Column (Modified after Andersland and Ladanyi 2004).....	15
Figure 2-2 - Formation of Ice Lenses with Reduction in Temperature Gradient (Modified after Konrad and Morgenstern 1980).....	17
Figure 2-3 - Open and Closed System Freezing: A) closed system, B) open system, C) pea gravel changes upper part into closed system (Modified after Andersland and Ladanyi 2004)	18
Figure 2-4 - Characteristics of the Frozen Fringe: a) Simplified, b) Actual Shape (Modified after Andersland and Ladanyi 2004)	20
Figure 2-5 - Hydraulic Conductivity Increase Due to Freeze-Thaw (Modifed after Proskin 1998)	25
Figure 2-6 - Hydraulic Conductivity Ratio as a Funciton of Temperature Gradient for 1, 3, and 5 Freeze-Thaw Cycles (Modified after Benson and Othman 1993)	25
Figure 2-7 - Consolidation Curve for Frozen-Thawed and Never Frozen MFT (Modified after Proskin 1998).....	26
Figure 3-1 - Abnormally Warm Winter Results in Shallow Frost Penetration (Environment Canada 2006).....	33
Figure 3-2 Location of Sump Relative to Storage Reservoir (Syncrude Ltd 2006)	34
Figure 3-3 - Approximate Locations of Sampling Sites (Syncrude Ltd 2006).....	34
Figure 3-4 - Schematic of Sampling Device.....	36
Figure 3-5 - Solids Content S1.....	37
Figure 3-6 - Solids Content S2.....	37
Figure 3-7 - Solids Content S3.....	38
Figure 3-8 - Solids Content - All Holes	38

Figure 3-9 - Shear Strength - S1	39
Figure 3-10 - Shear Strength - S2	39
Figure 3-11 - Shear Strength - S3	40
Figure 3-12 - Shear Strength – All Holes	40
Figure 3-13 - Site 1b - Depth 0-10.5cm.....	41
Figure 3-14 - Site 1b - Depth 10.5-16 cm.....	42
Figure 3-15 - Site 2 - Depth 14-21.5 cm.....	42
Figure 3-16 - Site 1b - Depth 47.5-53 cm.....	43
Figure 3-17 - Laboratory Frozen Sample - Test S2T2.....	44
Figure 4-1 - Bench-Scale Thaw Strain Results for Oil Sand MFT (Modified after Dawson et al. 1999)	48
Figure 4-2 - Freeze-Thaw Dewatering of Suncor MFT (Modified after Proskin et al. 1996)	49
Figure 4-3 - Grain Size Distribution for All Materials Studied	50
Figure 4-4 - Freezing Point Depression of Suncor Pond 2/3 MFT	52
Figure 5-1 - Initial Test Apparatus (Arenson et al. 2005).....	58
Figure 5-2 - Temperature in Soil During Freezing	61
Figure 5-3 – External Water Supply During Freezing.....	62
Figure 5-4 - Heave During Freezing	62
Figure 5-5 - Ice Penetration During Freezing.....	63
Figure 5-6 - Schematic of Modified Testing Apparatus (Modified after Arenson et al. 2005)	65
Figure 5-7 - Schematic of Pressure Sensor for Measurement of Suction	66
Figure 5-8 – Measured Pore Pressure During Freezing.....	67
Figure 5-9 - Automated and Manual External Water Supply Readings	68
Figure 5-10 - Suction at the Middle Sensor During Freezing.....	69
Figure 5-11 - Suction Profile for Champlain Sea Clay and MFT	70
Figure 5-12 - Vertical Ice Needles in Frozen MFT	71
Figure 5-13 - Segregation Potential During Transient Freezing for MFT.....	74
Figure 5-14 - Segregation Potential During Transient and Steady Thermal Conditions (After Konrad 1987a).....	75

Figure 6-1 - Pore Pressure in Top Sensors.....	80
Figure 6-2 - Pore Pressure in Middle Sensor - Full Test Duration	81
Figure 6-3 - Pore Pressure in Middle Sensor - Transient Freezing.....	82
Figure 6-4 - Pore Pressure in Bottom Sensor - Full Test Duration.....	83
Figure 6-5 - Pore Pressure in Bottom Sensor – Transient Freezing	83
Figure 6-6 - Inflow for All Tests.....	84
Figure 6-7 - Heave for All Tests - Full Scale.....	85
Figure 6-8 - Heave for All Tests – Reduced Vertical Scale	85
Figure 6-9 - Heave at 2 Days as a Function of Liquidity Index	86
Figure 6-10 - Freeze-Thaw Cycle Affect Upon Inflow – MFT Sump – S3T1 and S3T2.	87
Figure 6-11 - Freeze-Thaw Cycle Affect Upon Heave - MFT Sump – S3T1 and S3T2..	87
Figure 6-12 - Heave for Test Series 5 – Devon Silt.....	88
Figure 6-13 - Location of Freezing Point of Pore Fluid and Observed Ice Lens Location During Freezing – Test S2T4.....	89
Figure 6-14 - Temperature Distribution During Test – S1T2.....	90
Figure 6-15 - Temperature Gradient During Freezing - Test #2	91
Figure 6-16 - Final Ice Lens Thickness - S4T1	93
Figure 6-17 - Final Lens Thickness for Devon Silt	94
Figure 6-18 - Final Ice Lens Thickness - All Tests	95
Figure 6-19 - Segregation Potential of Devon Silt.....	100
Figure 6-20 - Segregation Potential of MFT.....	101
Figure 6-21 - Segregation Potential of MFT Bulk Sump	102
Figure 6-22 - Ice Lens Penetration - S3T1.....	103
Figure 6-23 - Ice Lens Penetration - S3T2.....	103
Figure 6-24 - Segregation Potential of MFT Sump Frozen Core	104
Figure 6-25 - Average Segregation Potential of All Soils Tested	105
Figure 6-26 - Solids Content After Freezing for MFT	106
Figure 6-27 - Solids Content After Freezing for MFT Sump - Bulk Sample.....	108
Figure 6-28 - Solids Content After Freezing for Frozen Core from MFT Sump	108
Figure 6-29 – Solids Content After Freezing and Re-application of Consolidation Pressure for Series 5 Tests	109

Figure 6-30 - Ice Structure in Devon Silt (10g/L NaCl).....	111
Figure 6-31 - Ice Structure in MFT.....	111
Figure 6-32 - Advancing Freezing Front in MFT Bulk Sump - S5T1.....	112
Figure 6-33 - Thaw Strain for All Tests.....	114
Figure 6-34 – Thaw Strain vs. Density for Soils Tested and McKenzie Valley Soils (After Andersland and Ladanyi 2004).....	115
Figure 6-35 - Thaw Strain vs. Water Content for Soils Tested and McKenzie Valley Soils (After Andersland and Ladanyi 2004).....	115
Figure 6-36 - Thaw Strain for Test Series 3	116
Figure 6-37 - Thaw Strain For MFT Sump Frozen Core.....	117
Figure 6-38 - Thaw Strain for MFT Sump Frozen Core - Series 4.....	118
Figure 6-39 - Freeze-Thaw Dewatering of 1992/93 Suncor Field Core (Modified after Proskin et al. 1996).....	119
Figure 6-40 - Bench Scale Freeze-Thaw Dewatering – (Modified after Dawson et al. 1999).....	120
Figure 7-1 - Flow Chart for Frost-Heave Prediction (After Konrad 1999).....	124
Figure 7-2 - Average Daily Temperature and Snow Depth at Ft. McMurray from 1983-2003.....	126
Figure 7-3 - Unfrozen Water Content for Sump Material	128
Figure 7-4 - Volumetric Heat Capacity Function for MFT and Sump	129
Figure 7-5 – Thermal Conductivity of MFT.....	131
Figure 7-6 - Thermal Conductivity for Sump Material	132
Figure 7-7 - Mesh for Finite Element Analysis	133
Figure 7-8 - Initial Temperature Distribution of Sump and MFT Deposits at Start of Freezing Period.....	134
Figure 7-9 - Annual Soil Temperature Variation in Sump and MFT	135
Figure 7-10 - Frost Penetration for Sump and MFT	135
Figure 7-11 - Temperature Gradient at Freezing Front for Sump and MFT	136
Figure 7-12 - Frost Heave During Freezing Period.....	137
Figure A-1 – Temperature in Sample During Test – S1T1	146

Figure A-2 - Water Supply and Heave - S1T1	146
Figure A-3 - Base of Ice Lens Penetration - S1T1.....	147
Figure A-4 - Final Ice Lens Growth - S1T1	147
Figure A-5 - Surface Heave and Final Ice Lens Growth - S1T1	148
Figure A-6 - Temperature in Sample During Test - S1T2.....	148
Figure A-7 - Water Supply and Heave - S1T2	149
Figure A-8 - Base of Fringe Penetration - S1T2.....	149
Figure A-9 - Temperature in Sample During Test - Cycle 1 - S1T3	150
Figure A-10 - Water Supply and Heave - Cycle 1 - S1T3.....	150
Figure A-11 - Temperature in Sample During Test - Cycle 2 - S1T3	151
Figure A-12 - Water Supply and Heave - Cycle 2 - S1T3.....	151
Figure A-13 - Ice and Fringe Penetration - S1T3	152
Figure A-14 - Solids Content Profile – After 2 Cycles - S1T3.....	152
Figure A-15 - Temperature in Sample During Test - Cycle 1 - S1T4	153
Figure A-16 - Water Supply and Heave - Cycle 1 - S1T4.....	153
Figure A-17 - Final Ice Lens Growth – Cycle 1 - S1T4	154
Figure A-18 - Temperature in Sample During Test - Cycle 2 - S1T4	154
Figure A-19 - Water Supply and Heave - Cycle 2 - S1T4.....	155
Figure A-20 - Base of Ice Lens Penetration - S1T4.....	155
Figure A-21 - Solids Content Profile - After 2 Cycles - S1T4	156
A-22 - Temperature in Sample During Test – S2T2.....	156
Figure A-23 - Pore Pressure During Freezing - 54.6 kPa Back-Pressure – S2T2	157
Figure A-24 - Water Supply and Heave – S2T2.....	157
Figure A-25 - Final Ice Lens Growth – S2T2.....	158
Figure A-26 - Surface Heave and Final Ice Lens Growth – S2T2.....	158
Figure A-27 - Solids Content Profile – S2T2	159
Figure A-28 - Temperature in Sample During Test – S2T3	159
Figure A-29 - Pore Pressure During Freezing – S2T3.....	160
Figure A-30 - Water Supply – S2T3.....	160
Figure A-31 - Temperature in Sample During Test – S2T4	161
Figure A-32 - Pore Pressure During Freezing – 106 kPa Back Pressure – S2T4.....	161

Figure A-33 - Water Supply – S2T4.....	162
Figure A-34 - Base of Ice Lens Penetration – S2T4.....	162
Figure A-35 - Temperature in Sample During Test - Cycle 1 – S3T1	163
Figure A-36 - Pore Pressure During Freezing - 78 kPa Back-Pressure – Cycle 1 – S3T1	163
Figure A-37 - Water Supply - Cycle 1 – S3T1	164
Figure A-38 - Final Ice Lens Growth – S3T1.....	164
Figure A-39 - Temperature in Sample During Test - Cycle 2 – S3T1	165
Figure A-40 - Pore Pressure During Freezing - Cycle 2 – S3T1	165
Figure A-41 - Water Supply and Heave - Cycle 2 – S3T1	166
Figure A-42 - Final Ice Lens Growth – Cycle 2 – S3T1	166
Figure A-43 - Temperature in Sample During Test - Cycle 3 – S3T1	167
Figure A-44 - Pore Pressure During Freezing - Cycle 3 – S3T1	167
Figure A-45 - Water Supply and Heave - Cycle 3 – S3T1	168
Figure A-46 - Final Ice Lens Growth - Cycle 3 – S3T1	168
Figure A-47 - Surface Heave and Final Ice Lens Growth – Cycle 3 – S3T1	169
Figure A-48 - Base of Ice Lens Penetration – S3T1.....	169
Figure A-49 - Temperature in Sample During Test - Cycle 1 – S3T2	170
Figure A-50 - Pore Pressure During Freezing - Cycle 1 – S3T2.....	170
Figure A-51 - Water Supply and Heave - Cycle 1 – S3T2	171
Figure A-52 - Final Ice Lens Growth - Cycle 1 – S3T2.....	171
Figure A-53 - Surface Heave and Final Ice Lens Growth – Cycle 1 – S3T2	172
Figure A-54 - Temperature in Sample During Test – Cycle 2 – S3T2.....	172
Figure A-55 - Pore Pressure During Freezing – Cycle 2 – S3T2	173
Figure A-56 - Water Supply and Heave – Cycle 2 – S3T2	173
Figure A-57 - Surface Heave and Final Ice Lens Growth – Cycle 2 – S3T2	174
Figure A-58 - Temperature in Sample During Test - Cycle 3 – S3T2	174
Figure A-59 - Pore Pressure During Freezing - Cycle 3 – S3T2.....	175
Figure A-60 - Water Supply and Heave - Cycle 3 – S3T2	175
Figure A-61 - Base of Final Lens and Heave - Cycle 3 – S3T2.....	176
Figure A-62 - Base of Ice Lens Penetration – S3T2.....	176

Figure A-63 - Solids Content Profile After 3 Cycles – S3T2	177
Figure A-64 - Temperature in Sample During Test – S4T1	177
Figure A-65 - Pore Pressure During Freezing – S4T1.....	178
Figure A-66 - Water Supply and Heave – S4T1.....	178
Figure A-67 - Final Ice Lens Growth – First Ice Lens – S4T1	179
Figure A-68 - Final Ice Lens Growth - Retreated Ice Lens – S4T1	179
Figure A-69 - Surface Heave and Final Ice Lens Growth – S4T1.....	180
Figure A-70 - Solids Content Profile After Thaw – S4T1.....	180
Figure A-71 - Temperature in Sample During Test – S4T2	181
Figure A-72 - Pore Pressure During Freezing – S4T2.....	181
Figure A-73 - Water Supply and Heave – S4T2.....	182
Figure A-74 - Final Ice Lens Growth – S4T2.....	182
Figure A-75 - Solids Content Profile After Thaw – S4T2.....	183
Figure A-76 - Temperature in Sample During Test – S4T3	183
Figure A-77 - Water Supply and Heave – S4T3.....	184
Figure A-78 - Solids Content Profile After Thaw – S4T3.....	184
Figure A-79 - Temperature in Sample During Test - S5T1 and S5T2	185
Figure A-80 - Water Supply and Heave - S5T1 and S5T2.....	185
Figure A-81 - Measured Heave and Heave Due to Inflow - S5T1 and S5T2.....	186
Figure A-82 - Heave Throughout S5T1 and S5T2 Freeze and Final Thaw.....	186
Figure A-83 - Final Ice Lens Growth - S5T1	187
Figure A-84 - Final Ice Lens Growth - S5T2	187
Figure A-85 - Final Solids Content After Thaw and Re-application of Consolidation Pressure – S5T1 and S5T2.....	188
Figure A-86 - Thaw Strain for Test Series 6.....	188

List of Symbols

Symbol	Definition
c_f	Volumetric heat capacity of frozen soil
c_u	Volumetric heat capacity of unfrozen soil
e	Void ratio
H	System enthalpy
h	Heave at the surface of the soil
H_i	Height of ice increase at lens
H_w	Height of water increase at lens
k_b	Bitumen thermal conductivity
k_f	Soil thermal conductivity
k_i	Ice thermal conductivity
k_w	Water thermal conductivity
L	Latent heat of fusion
n	Porosity of soil
P	Pressure
P_i	Ice pressure
P_w	Pore water pressure
SC	Solids content
SP_0	Segregation potential with no overburden pressure
SP_l	Segregation potential at the ice lens
T	Temperature
T_i	In situ freezing temperature
T_s or T_f	Segregational freezing temperature
V	Molar volume
v	Velocity of water flowing through fringe
V_c	Volume of water expelled due to consolidation
v_m	Velocity of water generated within the fringe
V_i	Specific volume of ice

Symbol	Definition
v_l	Velocity of water arriving at ice lens
v_u	Velocity of water arriving from external supply
v_{uc}	Velocity of water generated due to consolidation
v_{ucl}	Velocity of water generated due to consolidation at the ice lens
V_w	Specific volume of water
W_s or M_s	Weight of solid particles
W_t or M	Total soil weight
W_w	Weight of water
z or X	Vertical depth scale in soil
α	Fraction of water released due to consolidation that freezes at the ice lens
ε	Factor for the amount of unfrozen water remaining in the fringe
γ	Soil unit weight
γ'	Soil effective unit weight
γ_d	Dry soil unit weight
γ_w	Unit weight of water
κ_f	Diffusivity of frozen soil
κ_u	Diffusivity of unfrozen soil

List of Abbreviations

Abbreviation	Full Name
AEC	Alberta Environmental Centre
ASTM	American Society for Testing and Materials
CRREL	Cold Regions Research and Engineering Laboratory
CT	Composite Tailings
FPD	Freezing Point Depression
FTFC	Fine Tailings Fundamentals Consortium
LI	Liquidity Index
MFT	Mature Fine Tailings
MLSB	Mildred Lake Settling Basin
OSLO	Other Six Lease Owners
PI	Plasticity Index
SP	Segregation Potential
SWSS	South West Sand Storage
TDR	Time Domain Reflectometry
USCS	Unified Soil Classification System

Chapter 1 - Introduction

The research conducted as part of this study focused on the potential for the use of natural freeze and thaw cycles as a mechanism to dewater and strengthen mine tailings generated in the recovery of bitumen from Alberta's oil sands deposits. This chapter presents an overview of the oil sands operations, the past and present tailings management strategies, and a proposed natural remediation strategy. The objectives and methodology of the research are explained, and the organization of the thesis is outlined.

1.1 Background

1.1.1 Oil Sands Overview

With a combined estimated reserve of between 1.7 and 2.5 trillion barrels of bitumen, the Athabasca, Cold Lake, and Peace River deposits form a massive petroleum resource in Alberta, Canada (Figure 1-1). Much of the current mining focuses on the Athabasca deposit in the area of Fort McMurray, Alberta. The Athabasca deposit is the largest petroleum resource in the world. Of the estimated reserves, 300 billion barrels are recoverable with existing technologies. The crude oil recovered from the oil sands accounts for 34% of Canada's domestic production with production expected to grow by more than 50% by 2010 (Synkrude Ltd. 2003).

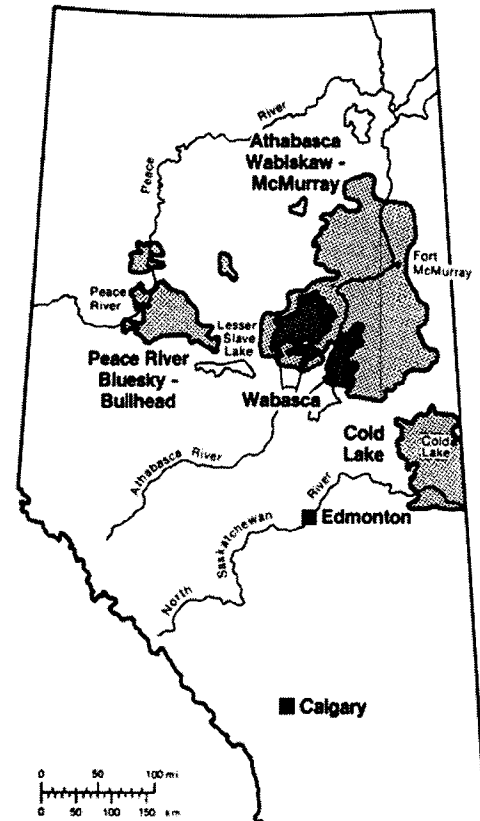


Figure 1-1 - Oil Sands Deposits in Alberta, Canada (Morgenstern et al. 1988)

The oil sands in the Athabasca deposit are composed of the Lower Cretaceous McMurray Formation, which rests on the Upper Devonian strata consisting of mainly limestone and calcareous shales. The soils of the McMurray Formation were deposited in a variety of fluvial – deltaic environments. The Middle and Upper McMurray Formation, which hold the high-grade bitumen ore, were deposited in a tidal environment during the Cretaceous period. The sediments originated from successive deposition in fluvial estuarine and marine environments. Atop the McMurray Formation lie variable depths of overburden consisting of peat and surficial deposits such as clay, silt, sand, glacial till, clay shale, and low-grade oil sand (Morgenstern et al. 1988).

See Figure 1-2 for an illustration of the stratigraphy of the Athabasca deposit. At present, mining is economical with overburden depths up to 50 metres (Syncrude Ltd. 2003).

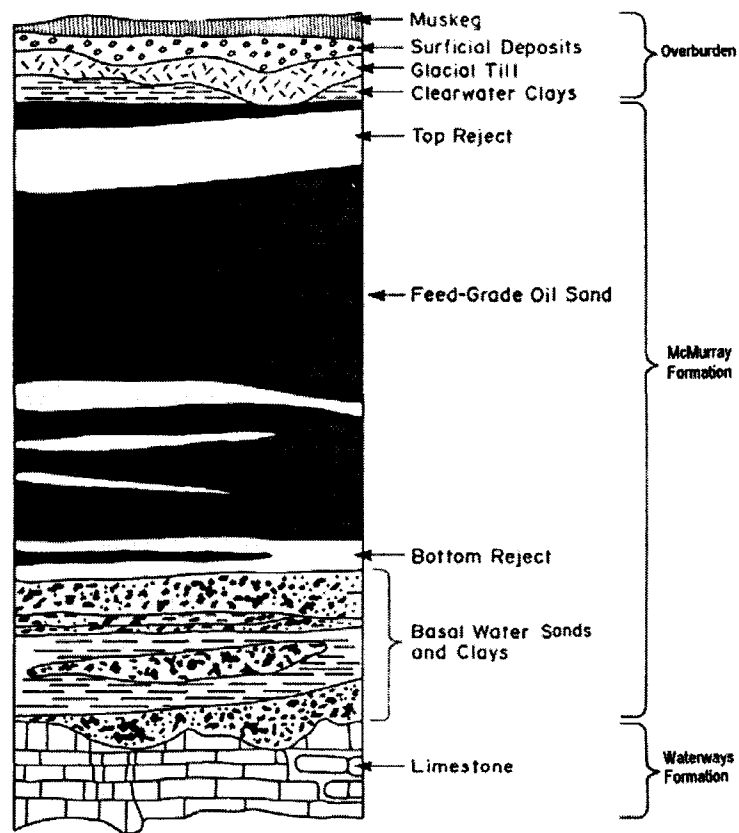


Figure 1-2 - Stratigraphy of Athabasca Deposit (Morgenstern et al. 1988)

The oil sands consist predominantly of a quartz sand matrix surrounded by a thin film of water and fines, with the remaining pore space filled with bitumen and some associated gases. The ratios of these ingredients are approximately 5% water, 11% bitumen, 12% fines, and 72% sand. It is the thin water layer surrounding the sand that allows the extraction of the bitumen from the sand through the addition of hot water, steam, and sodium hydroxide (chemical dispersant). Using this process, the fines are dispersed resulting in three streams: a predominantly sand-water stream, a high water content fines stream, and a bitumen froth. Air flotation is used to recover some of the bitumen from the fines stream before it is mixed with the sand stream, and pumped out as waste (tailings). As it is the fines in the tailings that pose reclamation difficulties, it is of interest to note that most of the fines in the insitu deposits are found in separate seams and lenses (Caughill et al. 1993).

The following paragraph, from the Fine Tailings Fundamentals Consortium (FTFC), explains the fine tailings problem:

It took about a year from the commencement of commercial extraction of bitumen from oil sand in 1967 to fully recognize that the tailings pond was filling rapidly with a slowly dewatering suspension of fine mineral particles, now called “fine tailings”. It was necessary to provide storage for this unanticipated fluid volume, which accumulated at a rate of more than 20% of the volume of oil sand excavated from the mine. Provision for containment of this fluid layer represents a direct incremental operating cost and continues to be the source of major logistical planning headaches. Additionally, it is necessary to accommodate these large volumes of fluid fine tailings in the development of an environmentally acceptable reclamation plan (FTFC 1995).

1.1.2 Past and Present Fine Tailings Management

During initial mining operations, tailings were disposed of by overboarding into containment ponds. The mixture of sand, fines, and bitumen, would segregate upon entering the pond, forming sand beaches nearest the deposition outlet, and a slurry of fines and residual bitumen that accumulated in the centre of the pond. This slurry is

termed “Thin Fine Tailings” and has a solids content of approximately 6% (Proskin et al. 1996).

There are several drawbacks involved with using this disposal technique. Firstly, the pond requires a large area of land to be covered with a wet landscape. This pond hinders mining operations in that it may lie atop mineable ore, as is the case at Syncrude Limited (Caughill et al. 1993). In addition, the water atop the pond is toxic. Napthenic acids and selenium occur in the tailings water and are toxic to life. Increased turbidity and unrecovered hydrocarbons can also be toxic to fish (Morgenstern and Scott 1995). However, it is the formation of a fine tailings deposit through using this disposal technique that will be of interest in this study.

When the fine tailings stream is mixed with the sand stream and overboarded into a containment pond, some of the fines are entrapped with the sand forming the beaches. Much of the fines, approximately 40-50%, enter the settling basin as thin fine tailings and accumulate in the centre of the pond. Here the fines settle relatively quickly to form a deposit with solids content in excess of 30%. At this point, the material is called Mature Fine Tailings (MFT). The average particle size of MFT is 5-10 microns, the solids content is 33%, and the void ratio is greater than 5. There is a large amount of this material produced. For every cubic metre of oil extracted, roughly 2 cubic metres of fluid fine tails are generated (Morgenstern and Scott 1995).

Fine tailings are a difficult material to dispose of and reclaim in the oil sands mining operations. When allowed to settle under quiescent conditions in the containment pond, the fines form MFT. This material is problematic in that it is resistant to consolidation and remains in a soft, fluid state for decades. The hydraulic conductivity of mature fine tails is in the range of 1×10^{-6} to 1×10^{-9} m/s. It also exhibits thixotropic character that influences long term densification (Banas 1991). It is the charged clay particles and bitumen clogged voids that cause this hindered consolidation. There are other methods that can be used to deal with fine tailings that either involves restricting its formation, or treating it after MFT has been formed (Morgenstern and Scott 1995).

A recent method currently being used by Syncrude Ltd. to prevent the formation of MFT is to create non-segregating tailings, known as composite tailings (CT). Mixing fine tails with sand and adding gypsum creates CT. It takes only a small change in solids content to make Syncrude tailings non-segregating. See Figure 1-3 for the segregation chart associated with Syncrude tailings as well as the materials tested as part of this research. Composite tailings have the benefit of containing the fine tailings in a sand matrix, allowing greater strength to be obtained from the tailings without the formation of MFT. Difficulties with using CT include hindered settling of the CT deposit and problems in controlling the CT mixture. If the ingredients in CT are not controlled tightly, the mixture can segregate.

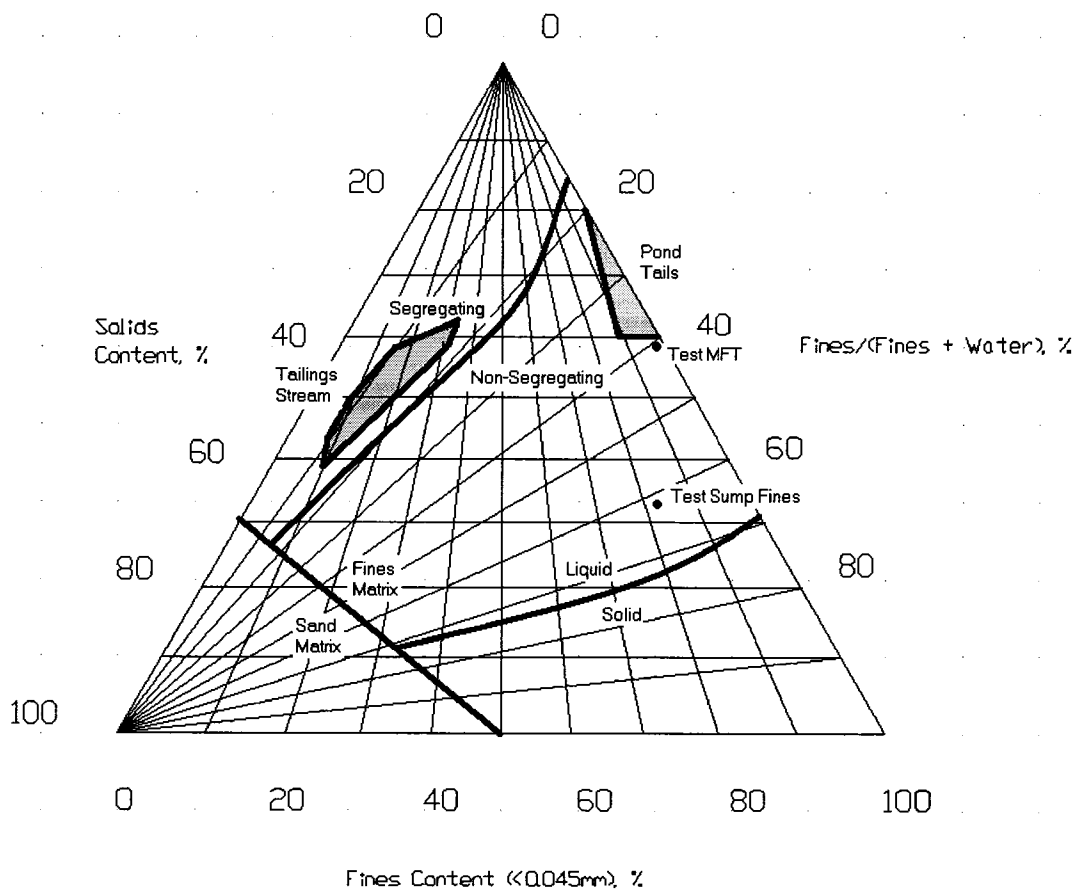


Figure 1-3 - Segregation Chart Showing Syncrude Tailings Stream Properties (Modified after Morgenstern and Scott 1995)

There are several other options available for the handling of fine tailings. Figure 1-4 presents options that could be employed (Morgenstern and Scott 1995). Many of these options have either been studied or are currently in use. Alternatives include:

Selective Mining:

Since most of the fines in the oil sands deposit occur in distinct layers or lenses, often as clay shales, avoiding these materials by selective mining will result in less fine tailings being generated (Morgenstern and Scott 1995).

Controlling Fines Dispersion During Mining:

The use of a chemical dispersant to aid with the extraction process causes additional problems due to hindered settling in the tailings stream. Modifications to the extraction process could change the degree of fines dispersion and the density of the tailings (Morgenstern and Scott 1995).

Non-Segregating Chemical Treatment:

Non-segregating tailings such as CT contain the fine tailings within the sand matrix, and do not allow MFT to form.

Water Capped Tailings Ponds:

Providing a water cap on the tailings ponds was the initial method of handling tailings, and a large volume of fine tailings remain in these ponds.

Tailings Entrained in Overburden:

Mixing the fine tailings with sand or overburden could be used to thicken the tailings stream and allow for different methods of storage or reclamation (Morgenstern et al. 1988).

Accelerated Dewatering by Mechanical, Chemical, or Other:

It may be possible to use other processes to directly treat the fine tailings. This is an area of active research at the University of Alberta.

Aggressive Drainage, Natural Drying, Freeze-Thaw:

Providing drainage for the fine tailings and using natural processes including natural drying (desiccation), and freeze-thaw may be used to treat fine tailings. This area is the focus of this study.

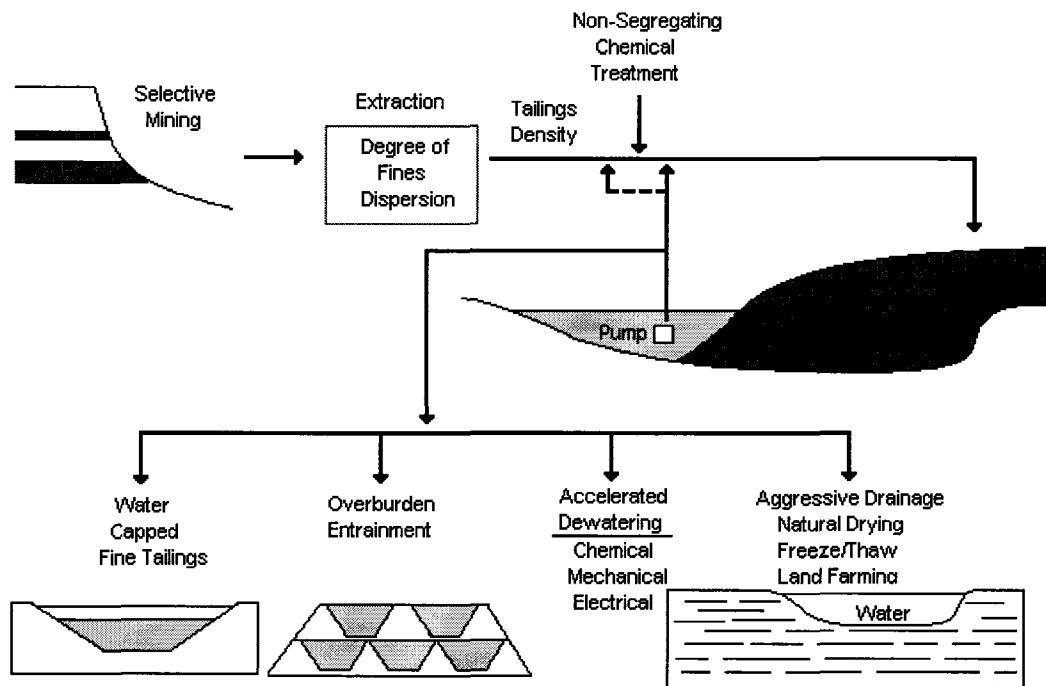


Figure 1-4 - Fine Tailings Management Alternatives (Modified after Morgenstern and Scott 1995)

1.1.3 Requirements for Land Reclamation

As part of the mining lease, the land must be reclaimed after mining has finished. Requirements for the reclamation include that the land must be geotechnically stable and non-erosive. It must have a productive capability at or above the levels of pre-disturbance, and be maintenance free. In addition, the resulting environment must develop into an ecosystem that is self-sustaining and diverse, with natural communities of plants and animals. Since wetlands were initially present at the site, they may be part of the reclamation strategy. It is apparent, however, that some of the fine tailings deposits will need to be strengthened and dewatered in order to support reclamation efforts. A surface strength of 5 kPa has been deemed sufficient to support reclamation efforts, including a 1 metre thick capping layer of soil (Morgenstern and Scott 1995).

1.1.4 Previous Freeze-Thaw Dewatering Studies

Freeze-thaw dewatering has been studied at the University of Alberta since 1990. Earlier work by Proskin, Dawson, and Segó has investigated the potential for using freeze-thaw dewatering to strengthen and dewater MFT ((Dawson and Segó 1993; Dawson et al. 1999; Proskin 1998; Segó et al. 1993)). Much of this work focused on using thin layer freeze-thaw dewatering. Thin layer freeze-thaw dewatering involves pumping thin layers of MFT (0.1 to 0.5 m thick), into a freezing cell during the winter. Each layer is allowed to freeze rapidly without access to water. Fort McMurray is well suited to freeze-thaw dewatering since the average annual temperature is 0°C. More material can be frozen at Fort McMurray than can thaw during the warm months. Freezing causes the structure of the MFT to compress, resulting in large thaw strains. The effects of using chemically amended MFT for improved freeze-thaw dewatering have also been studied (Dawson et al. 1999).

Johnson et al. (1993) conducted research at the Alberta Environmental Centre (AEC). This included small and large-scale laboratory freeze-thaw tests as well as field scale experiments. This work examined the effects of freeze-thaw dewatering, improved drainage during thaw, and multilayer freezing.

The previous work indicates that freeze-thaw has the potential to be a successful mechanism in treating the fine oil sand tailings. Work by Segó and Dawson suggests that a volume reduction of 70% is possible after five years of thin layer placement. Field tests carried out at Suncor Ltd. found that after one year, the MFT had undergone an increase in solids content of approximately 95%. This is higher than the 33% increase in solids content that the laboratory tests had indicated. Post thaw processes of consolidation, desiccation, and drainage likely contributed to the increased dewatering not found in the laboratory. Shear strength at the surface was measured to be 2.5 kPa. This represents a large increase over the initial 20 Pa of never frozen MFT (Proskin et al. 1996).

1.1.5 Current Natural Remediation Strategy

A current plan for the use of freeze-thaw dewatering differs from the thin layer dewatering that has been previously studied. The intent of the current study is to use a combination of natural remediation techniques that can act year round to create a strengthened capping layer atop the soft tailings. The strategy will involve pumping a mixture of ingredients on top of the fine tailings. This mixture could be composed of a variety of materials including MFT, CT, sand, overburden, plants, or other additives. The top capping mixture is to serve the following functions:

Be Frost Susceptible

During the freezing months, the highly frost susceptible capping layer will act as a dewatering pump. Frost susceptible soils form ice lenses, which draw water from depths due to suctions created at the ice lens. The frost action compresses the frozen soil and creates fractures within the frozen mass. The result is dewatering of the capping layer and fine tailings beneath, and improved drainage through the overlying material. Further explanation of the freeze-thaw process can be found in Chapter 2.

Deliver Plants

Previous research has shown that the fine tailings are capable of supporting plants. Laboratory tests showed that the dewatering effects of plant transpiration are appreciable (Silva 1999). Placing plants on the soft fine tailings is a challenge, however, due to the poor trafficability of the tailings. The capping layer is to serve as a delivery mechanism for the vegetation.

Support Vegetation

The capping layer must be able to support plant life. This may include altering the pH, adding fertilizer, or other soil types.

Allow Soil Development

The capping layer would ideally be able to evolve into a self-sustaining soil, capable of maintaining other plant species.

The four related studies serve to dewater the soil by freeze-thaw and evapo-transpiration. This research will focus on the use of freeze-thaw dewatering as part of the natural remediation scheme.

1.2 Objectives

The main objective of this research is to evaluate in the laboratory the frost susceptibility of MFT, and another waste soil obtained from a freshly exposed sump at Syncrude Ltd (south-west sand storage sump, SWSS). The sump material will be sampled frozen, and will be studied to examine the ice structure that develops during the first season of freezing insitu. Never-frozen MFT and the frozen samples will then be subjected to freezing tests to establish the compatibility of using laboratory tests to predict field conditions, and to study the potential for freeze-thaw dewatering over several seasons. This research will indicate whether never-frozen samples can be tested in the laboratory to represent field conditions. Following the laboratory study, a frost heave prediction model that couples the climatic conditions, frost penetration, and underlying material characteristics will be developed to predict water transfer to the surface.

The knowledge garnered from this research is intended to serve as part of the natural remediation strategy outlined in the previous section. It may also stand alone as a reclamation technique that can be used to strengthen fresh, dry deposits of MFT.

1.3 Methodology

This research program began with a literature review of the oil sands industry fine tailings reclamation problem. Previous efforts to strengthen fine tailings using natural processes such as freeze-thaw effects, desiccation, and consolidation were examined. Laboratory experiments to quantify the potential for the use of freeze-thaw dewatering on tailings was undertaken, and comparisons to insitu field samples were made. This

information was used to create numerical predictions for the effectiveness of a field scale freeze-thaw dewatering program in Fort McMurray.

1.4 Organization of Thesis

Chapter 1 of this thesis has presented an overview of the oil sands industry as it relates to the generation of fine tailings. The past and present tailings management methods have been presented as well as previous studies of freeze-thaw dewatering. A current natural remediation strategy has been discussed. The objectives, methodology, and outline of the thesis are also given.

Chapter 2 presents background theoretical knowledge of the freeze-thaw mechanisms including desiccation and seepage consolidation. Chapter 3 outlines the sampling program employed, and presents the geotechnical characteristics of the sampled material for comparison. Chapter 4 summarizes the past research in the area of freeze-thaw dewatering and the physical and chemical properties of the mine tailings used in this research. Chapters 5 and 6 give the summary of laboratory testing and interpretation of the results, respectively. Chapter 7 presents a frost heave prediction model for Fort McMurray. Conclusions of the thesis are stated in Chapter 8.

1.5 References

- Banas, L. (1991). "Thixotropic behaviour of oil sands tailings sludge." PhD thesis, University of Alberta, Edmonton, Alberta.
- Caughill, D. L., Morgenstern, N. R., and Scott, J. D. (1993). "Geotechnics of nonsegregating oil sand tailings." *Canadian Geotechnical Journal*, 30(5), 801-811.
- Dawson, R. F., and Segó, D. C. (1993). "Design concepts for thin layered freeze-thaw dewatering systems." *Canadian Geotechnical Conference*, 283-288.
- Dawson, R. F., Segó, D. C., and Pollock, G. W. (1999). "Freeze-thaw dewatering of oil sands fine tails." *Canadian Geotechnical Journal*, 36(4), 587-598.
- FTFC (Fine Tailings Fundamentals Consortium). (1995). "Advances in oil sands tailings research", Edmonton, Alberta.
- Johnson, R. L., Bork, P., Allen, E. A. D., James, W. H., and Koverny, L. (1993). "Oil sands sludge dewatering by freeze-thaw and evapotranspiration." *Rep. No. RRTAC 93-8*, Alberta Conservation and Reclamation Council, Edmonton, Alberta.
- Morgenstern, N. R., Fair, A. E., and McRoberts, E. C. (1988). "Geotechnical engineering beyond soil mechanics - a case study." *Canadian Geotechnical Journal*, 25(4), 637-661.
- Morgenstern, N. R., and Scott, J. D. (1995). "Geotechnics of fine tailings management." *Proceedings of the Specialty Conference on Geotechnical Practice in Waste Disposal. Part 2 (of 2), Feb 24-26 1995*, ASCE, New York, NY, USA, New Orleans, LA, USA, 1663-1683.
- Proskin, S. A. (1998). "A geotechnical investigation of freeze-thaw dewatering of oil sands fine tailings." PhD thesis, University of Alberta, Edmonton, Alberta.
- Proskin, S. A., Segó, D. C., and Burns, R. (1996). "Field tests evaluating freeze-thaw dewatering of fine tailings." *Proceedings of the 1996 3rd International Conference on Tailings and Mine Waste, Jan 16-19 1996*, Fort Collins, CO, USA, 189.
- Segó, D. C., Proskin, S. A., and Burns, R. (1993). "Enhancement of solids content of oil sand fine tails by chemical treatment and freeze-thaw." *Canadian Geotechnical Conference*, 293-296.
- Silva, M. J. (1999). "Plant dewatering and strengthening of mine waste tailings." PhD thesis, University of Alberta, Edmonton, Alberta.
- Syncrude Ltd. (2003). *Syncrude Fact Book*. Syncrude Canada Ltd., Fort McMurray, Alberta.

Chapter 2 - Freeze-Thaw Mechanisms

This chapter is to serve as an overview of the mechanisms responsible for freeze-thaw dewatering. Since some of the topics outlined in this chapter are complex and beyond the scope of this thesis, the reference list following this chapter can be consulted for further detail.

The processes involved with a freeze-thaw dewatering scheme include both the freeze and thaw cycles, as well as post-thaw settlement and consolidation, desiccation, and seepage consolidation. The relevant concepts relating to a freeze-thaw dewatering study are presented in this chapter. Topics that are covered briefly and are not integral to this research are provided as background for understanding freeze-thaw testing reported in the literature.

2.1 Freezing

Soil subjected to freezing will undergo changes during the freeze cycle. These arise from the negative pressure generated due to the thermodynamics associated with the freezing process. A general overview of these changes and a means to predict the magnitude of the impact of freezing is presented in order to provide an understanding of the laboratory testing undertaken.

2.1.1 Analytical Solutions for Freezing Thermodynamics

The relationship between temperature, pressure, and volume for a closed system with a constant composition at equilibrium is defined by the Clapeyron equation (Equation 2-1):

Equation 2-1 (Anderson and Morgenstern 1973)

$$dP = \frac{\Delta H}{T(\Delta V)} dT$$

where P is the absolute pressure (N/m^2), H is the change in system enthalpy (J/kg), V is the change in molar volume (m^3/kg), and T is the temperature (K). For a system containing ice and water, the Clapeyron equation becomes (Equation 2-2):

Equation 2-2 (Konrad 1994)

$$(\Delta V_i)dP_i + (\Delta V_w)dP_w = L \ln \frac{T}{T_0}$$

where V_w and V_i are the change in specific volumes (m^3/kg) of water and ice respectively; dP_w and dP_i are the changes in pore water and ice pressures (N/m^2) respectively; L is the specific latent heat of fusion of water ($334 \text{ kJ}/\text{kg}$); T is the equilibrium temperature (K); and T_0 is the freezing temperature (K) of pure water under atmospheric pressure. This equation gives the variation in pressure and temperature for a system at constant composition.

This equation has been demonstrated to be accurate near the ground surface experimentally. For a 1°C temperature drop, 1250 kPa suction is generated. These suctions are likely responsible for the growth of ice lenses and the cause of frost heave (Proskin et al. 1996).

2.1.2 Overview of Freezing Mechanisms

A temperature drop beneath the frozen/thawed soil interface causes a decrease in pressure in the thawed soil as is indicated by Equation 2-1 and Equation 2-2. This is the driving mechanism that brings water towards the freezing front and contributes to the development of frost heave. However, there are other mechanisms also involved in the freezing process.

When water changes phase to become ice, it undergoes a 9% volumetric expansion. This expansion can compress the fabric of the soil surrounding the ice (Andersland and Ladanyi 2004).

During initial freezing, the temperature gradient is large, with large differences existing between the cold air temperature and the warm ground temperature. As freezing is initiated into the ground, the freezing front advances quickly. Suctions are created beneath the advancing freezing front. Water thus has the tendency to migrate to the freezing front due to the suction, but due to the rapidity of the advancing freezing front

compared to the ability of the soil to transmit water as controlled by the hydraulic conductivity, it is not able to reach the freezing front. As a result, during initial freezing, there is an outflow of water due to the 9% expansion of pore water freezing (Konrad and Morgenstern 1980).

Once the rate of the advance of the freezing front slows, water from within the thawed soil or from an external source is able to reach the frozen soil, and the formation of ice lenses begins. Figure 2-1 can be used as a guide in understanding this process.

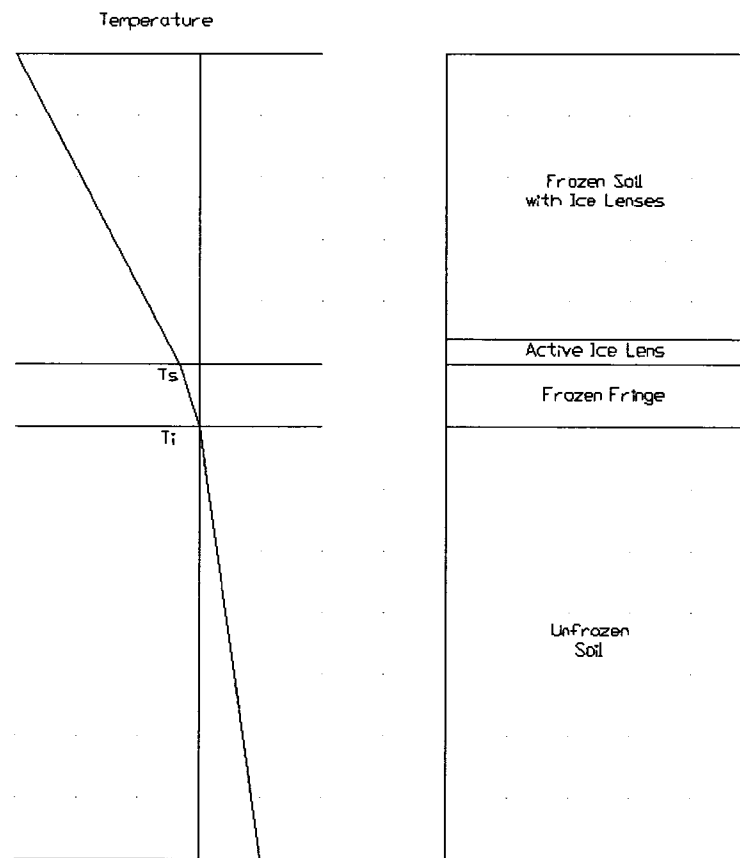


Figure 2-1 - Frost Heave in an Idealized One Dimensional Soil Column (Modified after Andersland and Ladanyi 2004)

As a soil is cooled, the water within freezes at different rates depending on its location within the soil structure. The first water to freeze is within the pore spaces in the soil. This freezing begins at the insitu freezing temperature (T_i). A thin film of unfrozen water remains surrounding the soil particles. At a lower temperature, called the segregation-

freezing temperature (T_f), an ice lens forms. The ice lens serves to cutoff any flow from the thawed soil below, to the frozen soil above. The zone between these two temperatures consists of ice and water films, and serves to progressively restrict the flow of water near the ice lens. This zone is termed the frozen fringe (Konrad and Morgenstern 1980).

Figure 2-1 can be divided into a zone of frozen soil, thawed soil, and the frozen fringe. As water is drawn towards the ice lens from the thawed soil, it must travel through the frozen fringe. Continued cooling of the fringe causes more water to freeze, in turn reducing the hydraulic conductivity of the fringe. The water slows, and at some point when the advancing freezing front has established the segregational-freezing temperature below the last ice lens, and the water is flowing slowly enough, a new ice lens forms. The water within the fringe freezes in place and the entire process repeats until the temperature gradient becomes steady (Konrad and Morgenstern 1980).

For pure water, the size that an ice lens will grow depends on the amount of time it spends as the lowest ice lens and on the overburden pressure. Initial ice lenses are closely spaced and are thin, while ice lenses that form under lower temperature gradients deeper in the soil are thicker and spaced further apart. See Figure 2-2 for a schematic of this process (Konrad and Morgenstern 1980).

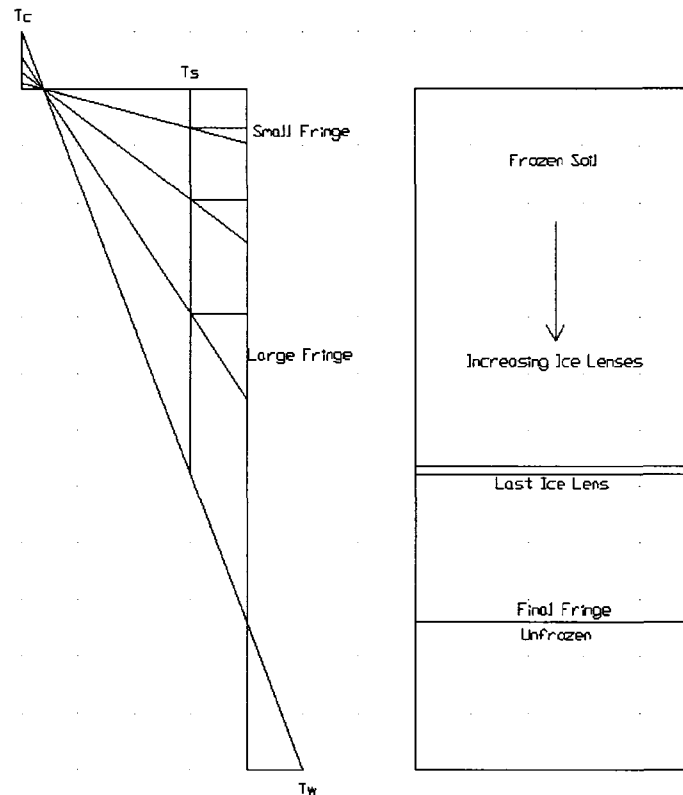


Figure 2-2 - Formation of Ice Lenses with Reduction in Temperature Gradient (Modified after Konrad and Morgenstern 1980)

The formation of ice lenses causes the soil surface to heave. The heave rate is given in Equation 2-3:

Equation 2-3 (Andersland and Ladanyi 2004)

$$\frac{dh}{dt} = 1.09v + 0.09n \frac{dz}{dt}$$

where v is the velocity of the arriving water, n is the porosity, and z is the depth of the frost front. Ice lenses will form in a frost sensitive soil (dirty sand, silt, or silty clay), if the freezing rate is slow enough and there is access to water (Andersland and Ladanyi 2004).

The orientation of the ice lenses depends on the direction of the temperature gradient. Ice lenses can form both perpendicular and parallel to the direction of heat flow. Ice lenses

will typically form perpendicular to the temperature gradient, as was shown in Figure 2-1. If the upward flow of water is impeded due to the formation of perpendicular ice lenses, water can be drawn in laterally through the fringe. This forms a reticulate ice structure surrounding lumps, or peds, of soil (Andersland and Ladanyi 2004).

Ice that forms surrounding a ped of soil consolidates the soil. Water is drawn from the soil ped to form the ice lens, resulting in a consolidated soil ped. The creation of peds results in a soil that is stiffer, stronger, and denser than the never frozen soil. The freezing process also draws water from depths to create the ice lenses, resulting in dewatering and strengthening of the soil beneath the frozen zone (Proskin et al. 1996).

2.1.3 Open and Closed System Freezing

Freezing can be considered as either having an unlimited water supply (open) or no supplied water (closed). Figure 2-3 presents three cases as examples of open and closed freezing systems.

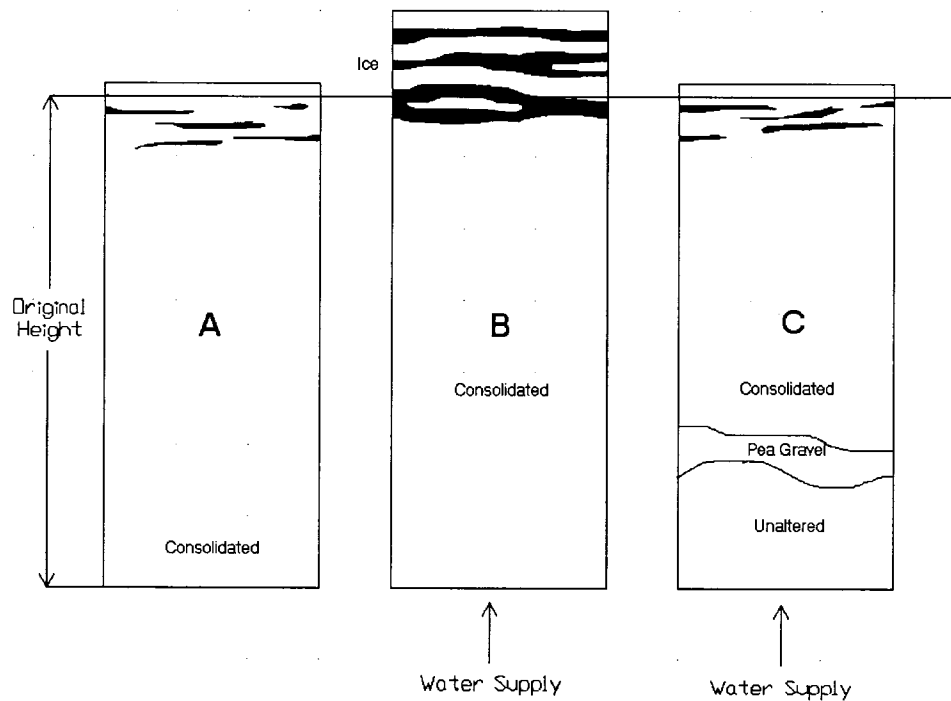


Figure 2-3 - Open and Closed System Freezing: A) closed system, B) open system, C) pea gravel changes upper part into closed system (Modified after Andersland and Ladanyi 2004)

In a closed system, only the water in the soil can be supplied for freezing. An impermeable boundary or a layer that cannot support suction or capillary rise can create a closed system. An open system exists when water is available to the frozen soil. Close proximity to the water table, within the range of capillary rise, creates an open system (Andersland and Ladanyi 2004).

2.1.4 Segregation Potential

A concept that can be used to quantify the frost susceptibility of a soil, and that will be used as part of this research, is the segregation potential (SP). Evaluating the segregation potential at near steady-state thermal conditions under negligible overburden pressure may be considered as a soil index property that uniquely characterizes the frost-heave susceptibility (Andersland and Ladanyi 2004).

The concept of segregation potential is based on several assumptions. It is assumed that flow towards an ice lens occurs through the frozen fringe and Darcy's law is valid. The ice lens is assumed to be impermeable, so flow from above the ice lens in the frozen soil is not possible. The theory is also based on the Clausius-Clapeyron equation being valid. Some simplifying assumptions for the temperature, permeability, and suction profiles are also made, and are shown in Figure 2-4 (Andersland and Ladanyi 2004).

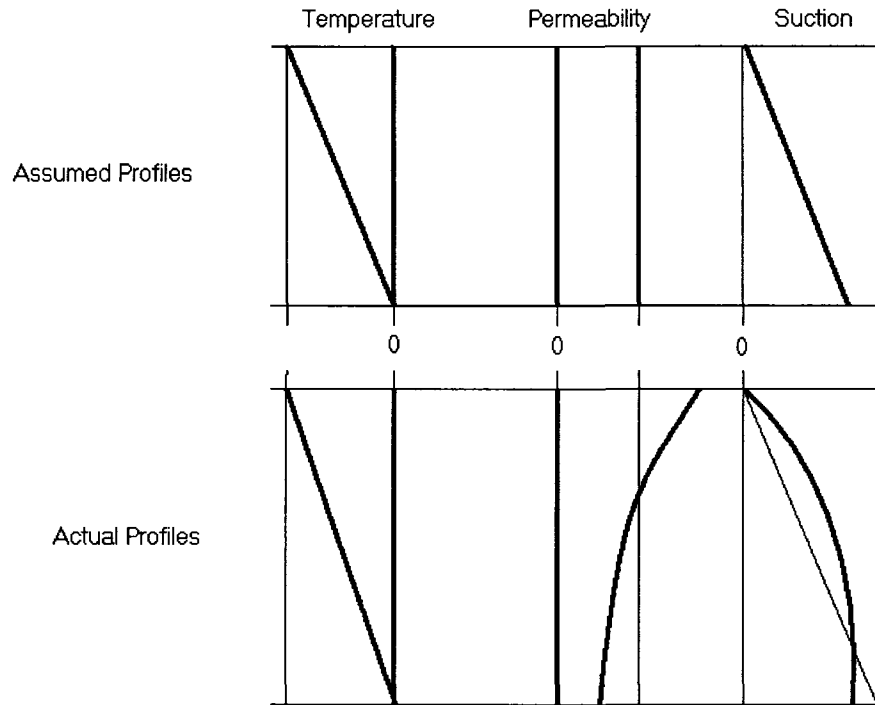


Figure 2-4 - Characteristics of the Frozen Fringe: a) Simplified, b) Actual Shape (Modified after Andersland and Ladanyi 2004)

Noting that there is a linear relationship between the temperature gradient and the water intake velocity under steady thermal conditions and negligible overburden pressure (Konrad and Morgenstern 1981), SP is defined as:

Equation 2-4 (Konrad and Morgenstern 1981)

$$v_0 = SP(gradT)$$

where v_0 is the water intake rate, and $gradT$ is the temperature gradient in the frozen fringe.

Segregation potential is dependant on several factors other than the temperature gradient of the fringe and the water intake rate. It is also impacted by the total suction potential at the freezing front, the segregation and freezing temperature, and the hydraulic conductivity of the fringe (Andersland and Ladanyi 2004). Using SP does not require the consideration of these factors since SP is normalized (Konrad 1990).

The applied pressure, or the overburden pressure affects SP by reducing the suction. There is a theoretical pressure where frost heave is no longer possible, called the “shut off pressure”, but this is usually very high and beyond the range of engineering problems (Konrad and Morgenstern 1982a).

The temperature gradient in the frozen fringe also has an affect upon the segregation potential in the laboratory. In the field, however, the frost penetration rates are usually much smaller, and hence so are the temperature gradients. To achieve cooling rates similar to field cooling rates in the laboratory, it is possible to use step freezing and assess SP near thermal steady state (Konrad 1990).

The SP for a soil can be defined as a surface that is unique for a given soil. Determining SP at various heat extraction rates and overburden pressure allows a unique surface to be plotted (Konrad and Morgenstern 1982b).

The segregation potential can be calculated by measuring the surface heave rate and the temperature gradient in the fringe. Alternatively, the net water intake can be measured instead of the total heave. If there is no consolidation within the soil due to the suction generated during freezing, the two methods will yield the same results. For weak structured or soft soils, these techniques will significantly underestimate the frost susceptibility of a soil. More information on the determination of SP can be found in Chapter 5 (Konrad and Seto 1994).

By conducting a small number of frost heave tests, a relationship can be defined between the segregation potential and overburden pressure for a soil. This can then be used to find the velocity of the water flowing through the fringe. Combined with a thermal model, the expected frost heave for field conditions can be found (Konrad and Morgenstern 1984).

Table 2-1 lists the factors that impact the segregation potential of a soil.

Table 2-1 - Factors Affecting Segregation Potential (Konrad 1990)

Factor	Explanation
Soil type	Includes gradation, mineralogy of the fine fraction, specific surface area, and surface charge density. These factors affect how well water can be transferred through the soil.
Porosity	Reflects the degree of packing of the soil. Impacts the rate that water can be supplied.
Pore fluid	Quantity and type of exchangeable ions. Affects the soil grain's affinity to hold water.
Cooling rate in fringe	Ice lens formation depends on the rate of heat removal. Low rates are representative of natural conditions.
Pressure	Suction at the ice front controls water transfer. This suction is in turn impacted by externally applied pressure, and friction at the cell wall.
Freeze-thaw cycles	Repeated freeze-thaw cycles cause a reduction of the void ratio of the soil and a subsequent decrease in segregation potential.

2.2 Thawing

In addition to the effect of freezing that is of interest in this study, the impact of thaw is also of significance. Significant research has been done on the topic of thaw and thaw strain as it relates to freeze-thaw dewatering of oil sands tailings (Dawson et al. 1999; Johnson et al. 1993; McKenna and Dawson 1999; Proskin 1998; Sego and Dawson 1992). This section will briefly outline some theory that can be used in the analysis of thawing soil.

2.2.1 Model for Thawing of Soil

In analyzing the behaviour of a thawing soil, it is important to know the movement of the thaw or frost front. One method that has been shown to be accurate for saturated soils is the Stefan equation. This equation assumes a linear temperature distribution in the thawed soil while temperature in the frozen soil is ignored (Equation 2-5).

Equation 2-5 (Andersland and Ladanyi 2004)

$$L \frac{dX}{dt} = k_f \frac{v_s}{X} \Rightarrow X = \left(\frac{2k_f}{L} \int v_s dt \right)^{1/2}$$

where X is the depth, t is time, L is the latent heat of the soil, k_f is the frozen soil thermal conductivity, and v_s is the difference between the ground surface temperature and the freezing temperature of the soil moisture. Imposing the Neumann model in which a step

increase in temperature is applied to the surface of the soil, it is found that the movement of the interface between the frozen and thawed zones is given by Equation 2-6 (Nixon and McRoberts 1973). Nixon and McRoberts found that the relationship between the thaw depth and time can be expressed as is shown in Equation 2-7 (Nixon and McRoberts 1973).

Equation 2-6 (Andersland and Ladanyi 2004)

$$X = \alpha\sqrt{t}$$

Equation 2-7 (Proskin 1998)

$$\frac{L\sqrt{\pi}}{2\sqrt{\kappa_u c_u T_s}} \alpha = \frac{e^{-\alpha^2/4\kappa_u}}{\operatorname{erf}\left(\frac{\alpha}{2\sqrt{\kappa_u}}\right)} - \frac{T_g k_f}{T_s k_u} \sqrt{\left(\frac{\kappa_u}{\kappa_f}\right)} \frac{e^{-\alpha/4\kappa_f}}{1 - \operatorname{erf}\left(\frac{\alpha}{2\sqrt{\kappa_f}}\right)}$$

where α is the root of the transcendental equation; L is the volumetric latent heat of soil (J/m^3); k_f and k_u are the thermal conductivity of the frozen and unfrozen soils (W/m K); c_f and c_u are the volumetric heat capacity of the frozen and unfrozen soils (J/m^3); κ_f and κ_u are the diffusivities of the frozen and unfrozen soils (m^2/s) with $\kappa = k/c$; T_s and T_g are the surface and initial ground temperatures, respectively (Proskin et al. 1996). Assuming that $T_g \sim 0^\circ$, this reduces to:

Equation 2-8 (Andersland and Ladanyi 2004)

$$\alpha = 2\sqrt{\alpha_u} \left(\frac{Ste}{2}\right)^{\frac{1}{2}} \left(1 - \frac{Ste}{8}\right)$$

Equation 2-9 (Andersland and Ladanyi 2004)

$$Ste = c_u T_s (L)^{-1}$$

where T_s the constant surface temperature. Assuming a linear temperature distribution in the soil:

Equation 2-10 (Andersland and Ladanyi 2004)

$$X = \left(\frac{2k_u T_s}{L}\right)^{\frac{1}{2}} \sqrt{t}$$

This solution is often used for the prediction of thaw depth (Andersland and Ladanyi 2004).

Other solutions for the temperature distribution within a soil exist and vary in their rigor and simplifying assumptions. The Stefan solution has been used commonly in past research.

2.2.2 Freeze-Thaw Impact on Hydraulic Conductivity

In addition to the changes to the soil caused during freezing, changes are also noted during thaw. One of the main changes in the thawed soil is an increase in hydraulic conductivity of the frozen portion of the soil. As the freezing front advances into the soil, the cooling soil contracts and cracks. These cracks fill with water and form a reticulate ice structure. Water is continually drawn to these ice lenses during freezing, resulting in the consolidation of the peds they surround. Upon thaw, the ice melts away, leaving an open drainage network and greatly increasing the hydraulic conductivity of the frozen soil. The hydraulic conductivity is typically increased by a factor of 2-10, but can be higher for soils such as MFT, which can increase by about 100 times (Proskin 1998; Sego and Biggar 2006). The changes in permeability occur primarily during the first three cycles, with the greatest impact from the first cycle (Andersland and Ladanyi 2004). Work by Chamberlain reported no change in the permeability after 9 cycles (Benson and Othman 1993).

Figure 2-5 illustrates how the hydraulic conductivity increases after one freeze-thaw cycle. The data is from consolidation tests performed on Syncrude MFT (Proskin 1998). Note that the greatest increase is at low void ratios.

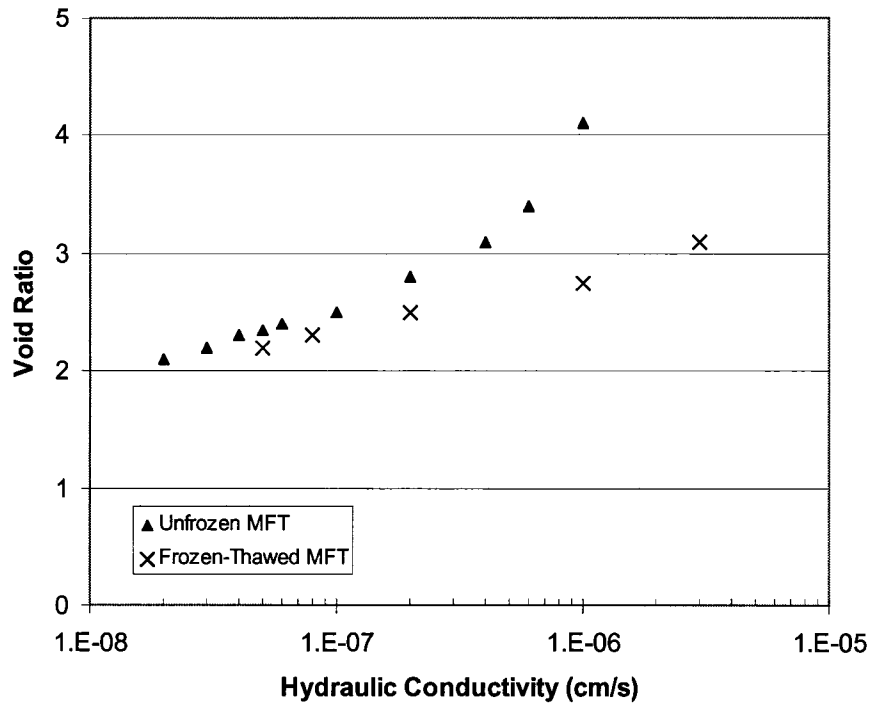


Figure 2-5 - Hydraulic Conductivity Increase Due to Freeze-Thaw (Modified after Proskin 1998)

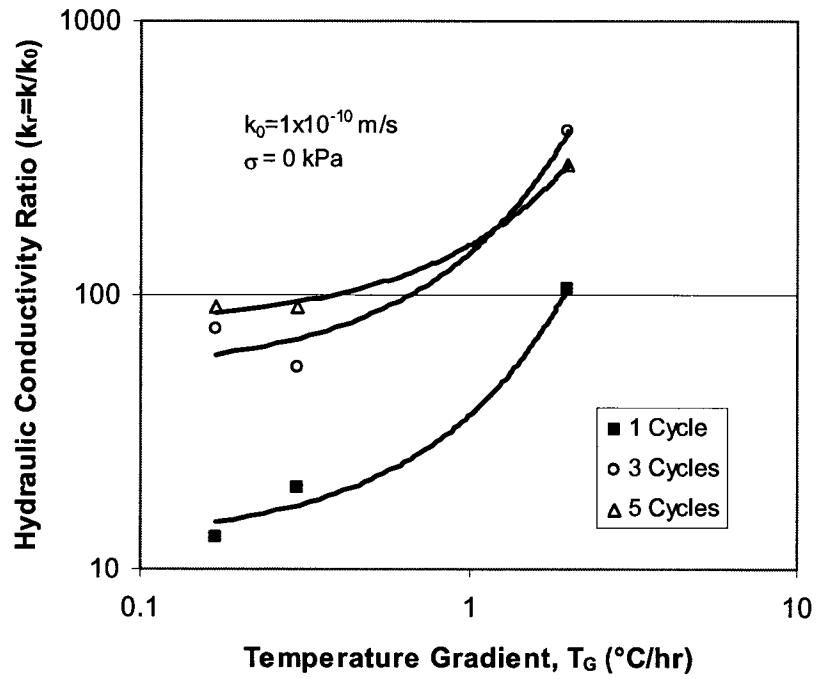


Figure 2-6 - Hydraulic Conductivity Ratio as a Function of Temperature Gradient for 1, 3, and 5 Freeze-Thaw Cycles (Modified after Benson and Othman 1993)

2.2.3 Freeze-Thaw Impact on Consolidation Characteristics

The changes to the hydraulic conductivity due to freeze-thaw also impact the consolidation characteristics of the soil. Figure 2-7 shows the change in the consolidation curve for MFT (Proskin 1998). Notice that the greatest influence is at low effective stress levels.

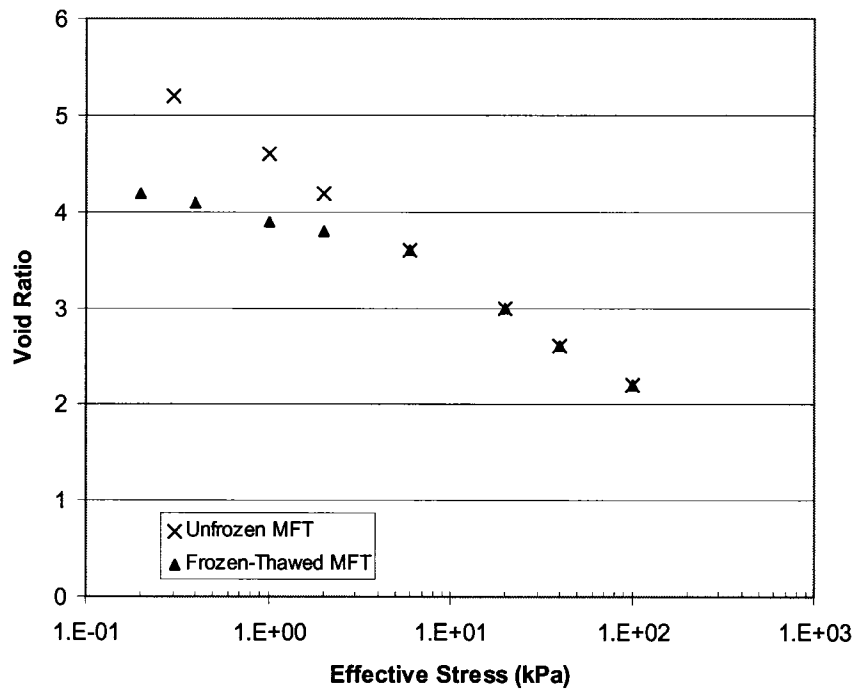


Figure 2-7 - Consolidation Curve for Frozen-Thawed and Never Frozen MFT (Modified after Proskin 1998)

2.3 Freeze-Thaw Settlements and Consolidation

Decreasing the volume of tailings through dewatering increases the strength of the deposit and is the final goal of a freeze-thaw dewatering program. Volume reductions are gained through several processes during the freeze and thaw cycle.

2.3.1 Consolidation During Freeze

During freeze, the suctions generated beneath the active ice lens cause an increase in the effective stress. For a typical soil, this effective stress increase is minor compared to the preconsolidation pressure of the soil. Most soils near the ground surface that are in the zone of frost penetration are either mechanically placed and overconsolidated, or are

naturally overconsolidated due to desiccation, freeze-thaw, etc. As the soil freezes and ice lenses develop, the ground surface heaves. The suction generated beneath the lowest ice lens does consolidate the soil further, but this reduction in volume of the unfrozen soil beneath the ice lens is negligible. For a soft soil, such as MFT, the suctions beneath the ice lens can cause a large amount of consolidation. As a result, surface heave will be less for a soft soil than it would be for a stiff soil, since the increasing ice lens thickness is accompanied by reductions to the thawed soil volume. The differences in the amount of heave noted, and the amount of consolidation occurring for soft and stiff soils is due to the initial state of stress relative to the preconsolidation pressure, and the compressibility of the soil (Konrad and Seto 1994).

Much of the previous freezing tests performed at the University of Alberta have used Devon Silt (Xia et al. 2005). In the analysis from these tests, consolidation during freeze was neglected. This was justified for two reasons. Since the soil was consolidated to 100 kPa before freezing, the preconsolidation pressure was likely not exceeded by suction, or if it was, the zone of high suction would have only impacted a small volume of soil nearest to the final ice lens. Secondly, the compressibility coefficient of Devon Silt is 0.257 (Proskin 1998). Compared to MFT, which has a compressibility coefficient of approximately 2.89 above a void ratio of one and 0.429 below (Proskin 1998), the MFT is more than ten times more compressible at high void ratio than the Devon Silt. Added to this is the fact that the MFT used in this testing was not consolidated in advance of testing, so any increase in effective stress due to suction acted on the soil in its virgin state. Thus, consolidation during freezing cannot be neglected when performing freezing tests on MFT. It has been noted that consolidation of layers adjacent to an ice lens can cancel the heave normally associated with ice segregation, particularly where the water supply is limited and soil permeability is low (Andersland and Ladanyi 2004). Tests involving x-ray photography of the frozen soil have been used to show this consolidation effect in the unfrozen soil (Yoneyama et al. 1983).

2.3.2 Thaw and Post-Thaw Consolidation

During and after thaw, the soil will continue to consolidate. Due to the advancing thaw front, a moving boundary problem is created. The movement rate of the thaw front controls the rate of liberation of excess pore water; hence thaw rate is important in predictions of thaw consolidation. Terzaghi's one-dimensional theory of consolidation can be used, but if the ice content is greater than the normal soil pore volume, it may be largely inaccurate (Andersland and Ladanyi 2004).

The consolidation of soft tailings, such as MFT, does not obey Terzaghi's one-dimensional consolidation theory due to the large strains involved and the changing compressibility and hydraulic conductivity properties. The void ratio versus log effective stress is nonlinear at low stress and is dependant upon freezing history (Proskin 1998).

Attempts to model the consolidation characteristics of MFT have been made by Somogyi and Pollock based on the finite strain consolidation theory (Pollock 1988; Somogyi 1980). From this work it was deemed that an additional mechanism is contributing to the consolidation, possibly thixotropy and creep (Proskin 1998). Details of these methods can be found in the above-mentioned sources.

2.4 Additional Consolidation Mechanisms

In addition to the dewatering effects due to consolidation during freeze, settlement upon thaw, and post thaw consolidation, there are several other mechanisms that can contribute to the overall dewatering that has been noted during field tests (Proskin 1998). These include desiccation and seepage consolidation. Field tests performed at Suncor Limited found that after one year the MFT had undergone an increase in solids content of approximately 95%. This is higher than the expected increase from laboratory testing (33%). The post thaw processes of consolidation, desiccation, and drainage are thought to have contributed to the increased dewatering (Proskin et al. 1996).

2.4.1 Desiccation

An important mechanism that can increase the strength of soft mine tailings in a dry landscape is desiccation, or surface drying. Due to desiccation, the surface of the soil layer settles, and cracks initiate and propagate downward forming cracked soil columns with a desiccated surface crust. The desiccation effect greatly improves the trafficability of a thin layer of soil atop the soft mass. This surface may have adequate strength to support workers and equipment, and is often part of the reclamation criteria for a soft, cohesive, waste-disposal site. Methods for predicting the impact of desiccation include empirical or semi-empirical models, or a finite element computer program. More can be found on this topic in the paper by Naser Abu-Hejleh and Znidarcic (1995).

2.4.2 Seepage Consolidation and Drainage

Downward flow of water towards a drainage boundary results in increased consolidation rates compared with laboratory consolidation predictions. The provision for aggressive drainage of the tailings ponds will increase the consolidation rates of the tailings. Seepage consolidation and drainage are additional mechanisms that increase the solids content of the soft tails, and have been noted in field tests (Proskin 1998).

2.5 Conclusions

This chapter has provided the background knowledge required to understand the results of the laboratory and field-testing performed as part of this thesis. It has also briefly covered some topics that are not specifically used in this thesis, but are useful for understanding the literature. The following chapters use the theories presented here to examine the suitability of using a freeze-thaw dewatering program to aid with the strengthening of soft mine tailings.

2.6 References

- Andersland, O. B., and Ladanyi, B. (2004). *Frozen Ground Engineering*. John Wiley & Sons, Inc., Hoboken, New Jersey.
- Anderson, D.M., and Morgenstern, N.R. (1973). "Physics, chemistry, and mechanics of frozen ground: a review." *Permafrost: The North American Contribution to the Second International Conference on Permafrost*, Yakutsk, National Academy Science, Washington, D.C., 257-288
- Benson, C. H., and Othman, M. A. (1993). "Hydraulic conductivity of compacted clay frozen and thawed in situ." *Journal of Geotechnical Engineering*, 119(2), 276-294.
- Dawson, R. F., Sego, D. C., and Pollock, G. W. (1999). "Freeze-thaw dewatering of oil sands fine tails." *Canadian Geotechnical Journal*, 36(4), 587-598.
- Johnson, R. L., Bork, P., Allen, E. A. D., James, W. H., and Koverny, L. (1993). "Oil sands sludge dewatering by freeze-thaw and evapotranspiration." *Rep. No. RRTAC 93-8*, Alberta Conservation and Reclamation Council, Edmonton, Alberta.
- Konrad, J. M. (1990). "Segregation potential - pressure - salinity relationships near thermal steady state for a clayey silt." *Canadian Geotechnical Journal*, 27(2), 203-215.
- Konrad, J.M. (1994). "Sixteenth Canadian Geotechnical Colloquium: Frost heave in soils: concepts and engineering." *Canadian Geotechnical Journal*, 31, 223-245.
- Konrad, J. M., and Morgenstern, N. R. (1984). "Frost heave prediction of chilled pipeline buried in unfrozen soils." *Canadian Geotechnical Journal*, 21(1), 100-115.
- Konrad, J. M., and Morgenstern, N. R. (1982a). "Effects of applied pressure on freezing soils." *Canadian Geotechnical Journal*, 19(4), 494-505.
- Konrad, J. M., and Morgenstern, N. R. (1982b). "Prediction of frost heave in the laboratory during transient freezing." *Canadian Geotechnical Journal*, 19(3), 250-259.
- Konrad, J. M., and Seto, J. T. C. (1994). "Frost heave characteristics of undisturbed sensitive Champlain sea clay." *Canadian Geotechnical Journal*, 31(2), 285-298.
- Konrad, J. M., and Morgenstern, N. R. (1981). "Segregation potential of a freezing soil." *Canadian Geotechnical Journal*, 18(4), 482-491.
- Konrad, J. M., and Morgenstern, N. R. (1980). "Mechanistic theory of ice lens formation in fine-grained soils." *Canadian Geotechnical Journal*, 17(4), 473-486.
- McKenna, G., and Dawson, R. (1999). "1995/1996 MFT freeze-thaw prototype at Syncrude's Base Mine Lake." Syncrude Ltd, Edmonton, Alberta.

- Naser Abu-Hejleh, A., and Znidarcic, D. (1995). "Desiccation theory for soft cohesive soils." *Journal of Geotechnical Engineering*, 121(6), 493-502.
- Nixon, J. F., and McRoberts, E. C. (1973). "A study of some factors affecting the thawing of frozen soils." *Canadian Geotechnical Journal*, 10 439-452.
- Pollock, G. W. (1988). "Large strain consolidation of oil sand tailings sludge." PhD thesis, University of Alberta, Edmonton, Alberta.
- Proskin, S. A. (1998). "A geotechnical investigation of freeze-thaw dewatering of oil sands fine tailings." PhD thesis, University of Alberta, Edmonton, Alberta.
- Proskin, S. A., Segó, D. C., and Burns, R. (1996). "Field tests evaluating freeze-thaw dewatering of fine tailings." *Proceedings of the 1996 3rd International Conference on Tailings and Mine Waste, Jan 16-19 1996*, Fort Collins, CO, USA, 189.
- Segó, D. C., and Dawson, R. F. (1992). "Freeze thaw dewatering of OSLO cold water process fine tails." Imperial Oil Resources Canada Ltd.
- Segó, D. C., and Biggar, K. W. (2006). "Permafrost engineering course lecture." University of Alberta, Edmonton, Alberta.
- Somogyi, F. (1980). "Large-strain consolidation of fine-grained slurries." *Annual Conference - Canadian Society for Civil Engineering*, University of Manitoba, Winnipeg, Manitoba, 12.
- Xia, D., Arenson, L. U., Biggar, K. W., and Segó, D. C. (2005). "Freezing process in Devon Silt – Using time-lapse photography." *Submitted to Canadian Geotechnical Journal*, .
- Yoneyama, K., Ishizaki, T., and Nishio, N. (1983). "Water redistribution measurement in partially frozen soil by x-ray technique." *Proceedings - Permafrost, 4th International Conference*. Natl Acad Press, Washington, DC, USA, Fairbanks, AK, USA, 1445-1450.

Chapter 3 - Material Sampling

On February 9th and 10th 2006, a sampling program was performed at an external sump at Syncrude Limited in Fort McMurray. The sump was used during construction of the Southwest Sand Storage Dump (SWSS) dyke, and was known to contain the fine particles and MFT that were rejected during the construction. The sump had been maintained with a water cap of several metres until the dyke surrounding the sump was breached in the summer of 2005. The fine material in the sump was then allowed to dry out and freeze for the first time since its deposition. This provided an opportunity to sample a freshly frozen deposit, rich in MFT. The intent of the sampling program was to gather bulk material for testing in the laboratory and to examine and compare the frozen material to the soil frozen in the laboratory.

When the sampling was performed, the tailings were frozen to an approximate depth of 55 to 70 centimetres, with 2 to 4 metres of unfrozen tailings beneath. The frost penetration was much shallower than expected, due to the fact that the winter had been one of the warmest on record. According to Environment Canada, the winter of 2005/2006 was the warmest winter Canada has experienced since nationwide records began in 1948, 3.9°C above normal, based on preliminary data (Environment Canada 2006). From Figure 3-1, it can be seen that Fort McMurray experienced a warmer winter by approximately 7 degrees.

In previous field-scale freezing tests performed at Syncrude's Mildred Lake tailings pond, it was found that the MFT froze to a depth of 165 cm in one winter, if the snow was removed periodically. If the snow cover was left in place, freezing was restricted to 30 cm (Johnson et al. 1993).

TEMPERATURE DEPARTURES FROM NORMAL
Winter (Dec, Jan, Feb) 2005/2006
ANOMALIES DE LA TEMPÉRATURE PAR RAPPORT A LA NORMALE
Hiver (dec, jan, fev) 2005/2006

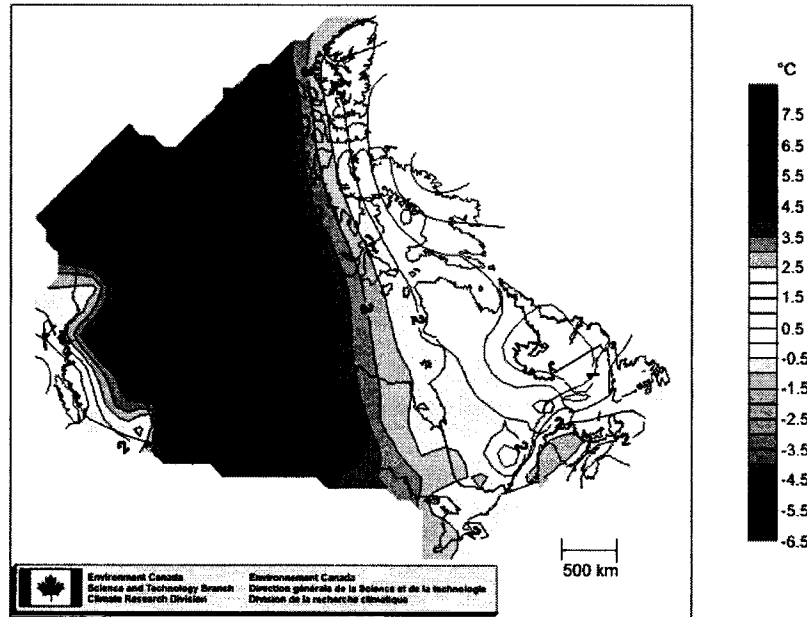


Figure 3-1 - Abnormally Warm Winter Results in Shallow Frost Penetration (Environment Canada 2006)

3.1 Sampling Technique

Three locations within the sump were used for sampling, each separated by approximately 90 metres. See Figure 3-2 for the location of the sump relative to the storage reservoir, Figure 3-3 for the approximate locations of the sampling sites within the sump, and Table 3-1 for the coordinates of the sampling sites.



Figure 3-2 Location of Sump Relative to Storage Reservoir (Syncrude Ltd 2006)

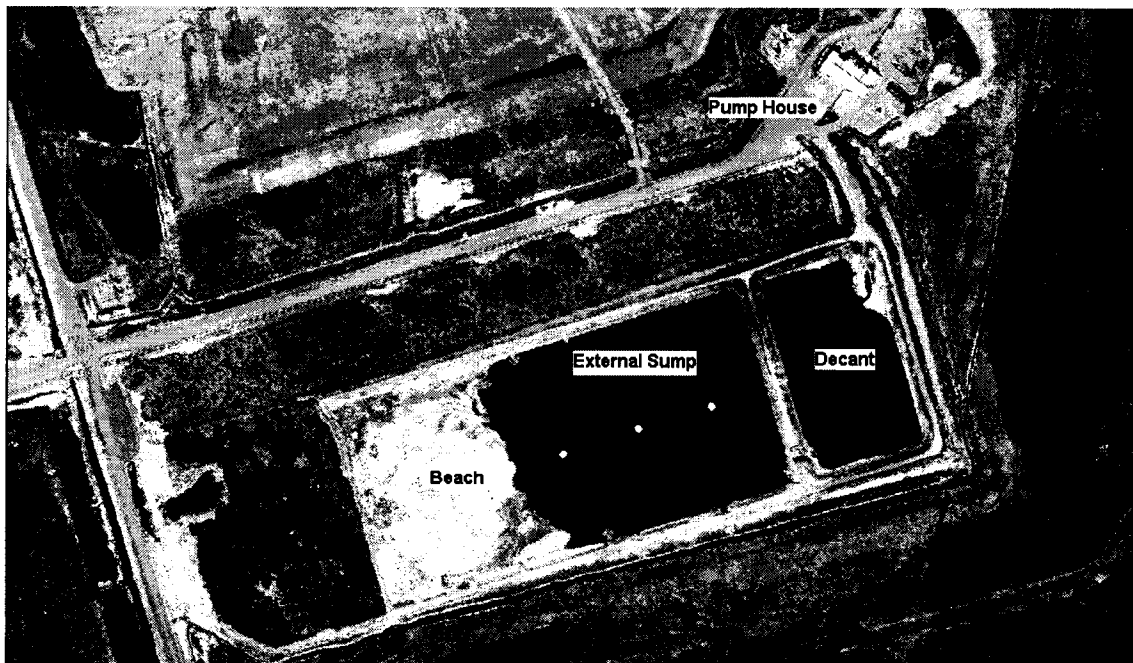


Figure 3-3 - Approximate Locations of Sampling Sites (Syncrude Ltd 2006)

Table 3-1 - Summary of Sampling Locations (Universal Transverse Mercator)

Location	Easting	Northing	Depth of Sump (m)
S1	0456427	6317835	4.1
S1b	0456427	6317835	4.1
S2	0456340	6317807	3.6
S3	0456241	6317788	4.1

Coring of the frozen material was performed using a 10 cm internal diameter CRREL barrel (Cold Regions Research and Engineering Laboratory), driven by a gas powered hand auger. The core was extruded from the barrel, typically in 10 to 20 cm lengths, and was immediately wrapped in plastic bags and placed in a cooler packed with snow. The cores exhibited no signs of damage due to melting or transportation upon being examined in the laboratory. They were then placed in a freezer for storage prior to future study.

After coring through the frozen crust, a field shear vane was used to measure the shear strength profile from the bottom of the frozen MFT to the base of the sump. Testing was performed at 30 cm intervals.

Following the shear vane tests, a one-metre long piston sampler was used to sample the unfrozen material. The samples were extruded into plastic bags.

After the three sites were sampled, an additional hole was cored at site S1, and 20 litre bulk samples were taken from depths of 1.0 metres, and 2.0 metres. The samples were gathered using a 5 cm diameter PVC pipe, with a cap on the bottom, and an entry hole cut into the wall of the pipe. The pipe was pushed into the soil so the entry hole was at the required depth, and held in place until enough material had flowed into the pipe. The pipe was then withdrawn and dumped into buckets. This was repeated until enough material was obtained. A schematic of this device is presented in Figure 3-4.

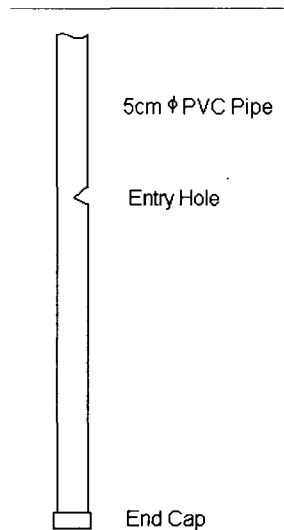


Figure 3-4 - Schematic of Sampling Device

3.2 Site Characterization

Figure 3-5 to Figure 3-8 illustrate the solids content profile with depth for the three sampled sites. It is important to note that the definition for solids content used here is the traditional geotechnical definition, shown below.

Equation 3-1 (Scott 2003)

$$SC = \frac{M_s}{M}$$

where M_s is the mass of the bitumen, fines, and sand, and M is the total mass of the tailings.

The solids content was determined from samples obtained in the thawed state using the piston sampler, as well as from the frozen core samples. The solids content at all three sites is quite similar, and differs by no more than 5%. Only S1 was sampled to the bottom of the sump, due to troubles with the piston sampler at sites S2 and S3. At site S1 there is an increase in solids content with depth, but a decrease towards the bottom of the sump. This could be due to variation in the material placed in the sump over time or water inflow at the base of the sump. Sites 2 and 3 have a slightly higher solids content, possibly because they are nearer to the deposition beach. All samples show a varied solids content in the frozen material, with low solids content in areas with extensive ice lens development.

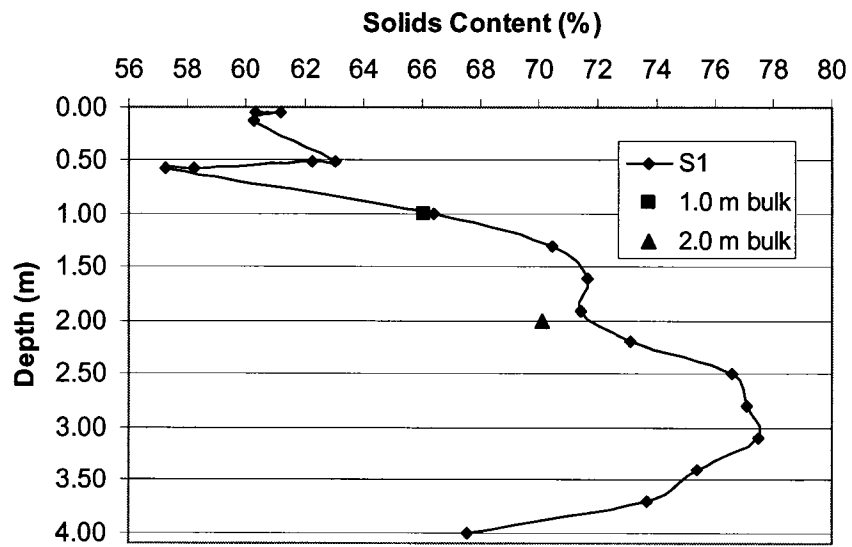


Figure 3-5 - Solids Content S1

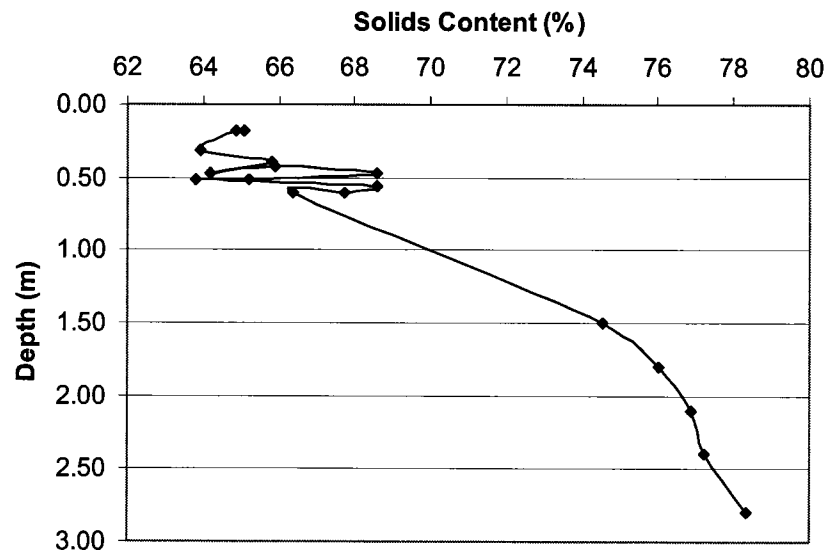


Figure 3-6 - Solids Content S2

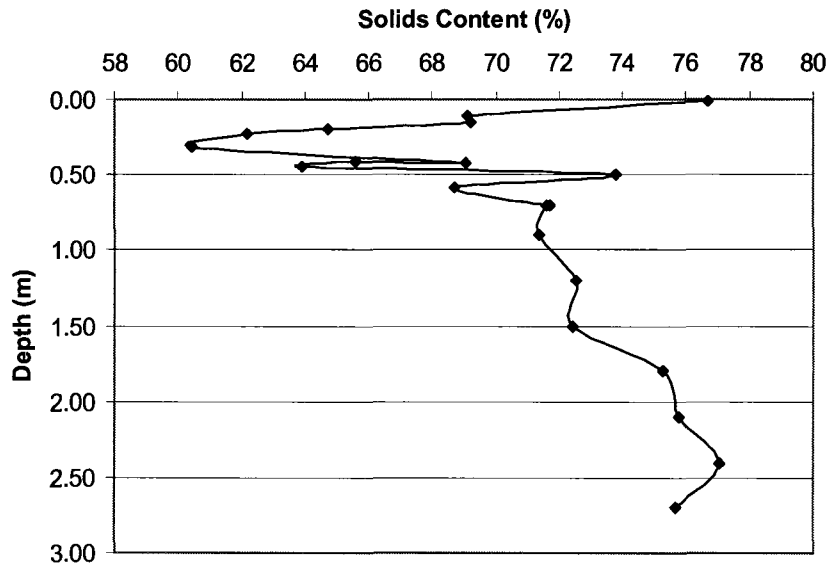


Figure 3-7 - Solids Content S3

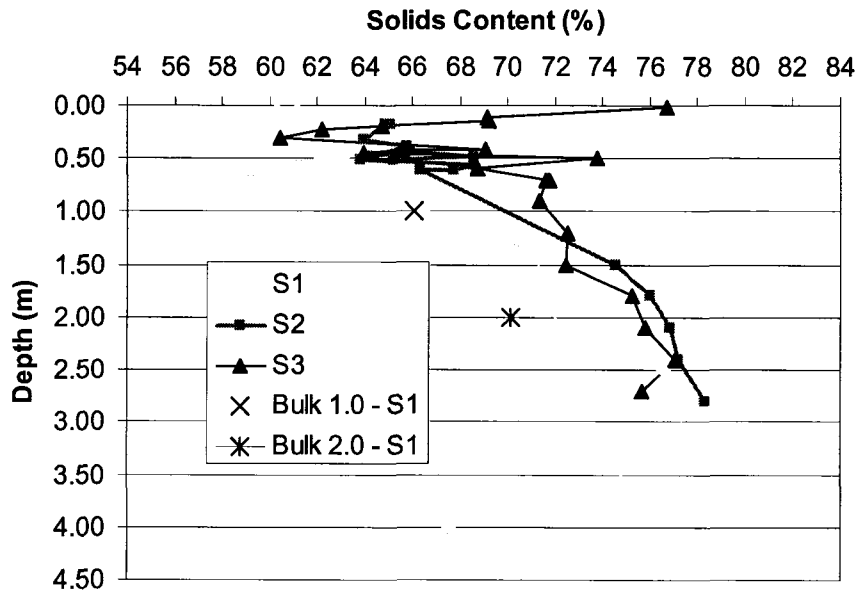


Figure 3-8 - Solids Content - All Holes

The shear strength of the deposit at each sampling site is reported in Figure 3-9 to Figure 3-12. Site S1 was not tested to the base of the sump. All sites show an increase in shear strength with depth, as well as a slight increase just below the frozen soil interface. Site S3 is unique in that it shows a rather large strength increase near the surface of the deposit, and a greater difference between the peak and residual strengths compared to the other sample sites. This may be due to the change in gradation due to the closer proximity

to the deposition beach at this site. It is possible that the soil here has a sensitive structure.

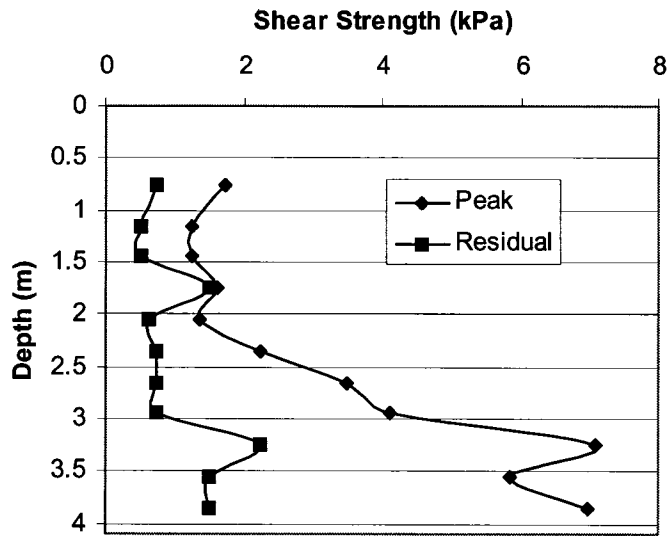


Figure 3-9 - Shear Strength - S1

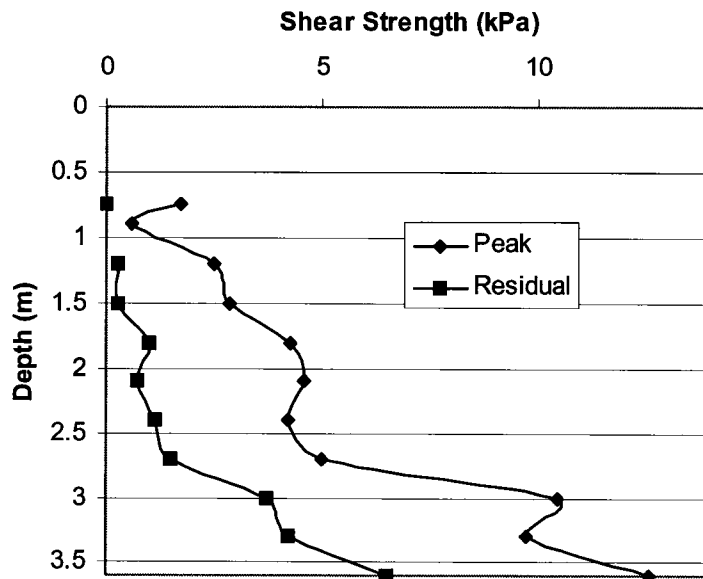


Figure 3-10 - Shear Strength - S2

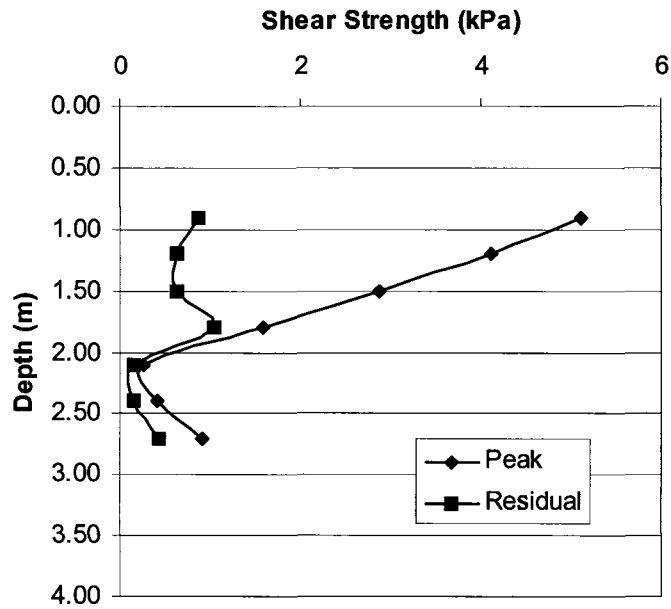


Figure 3-11 - Shear Strength - S3

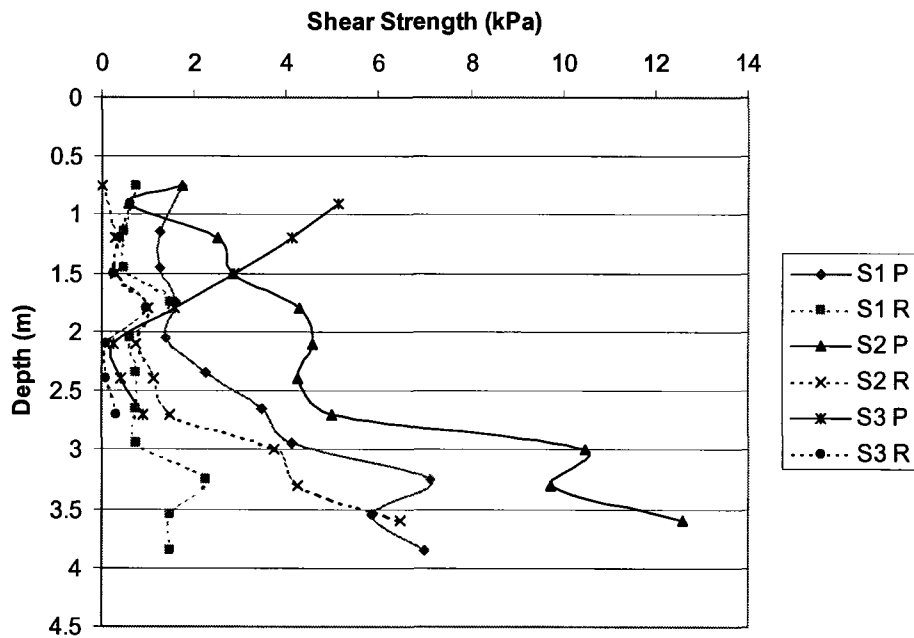


Figure 3-12 - Shear Strength - All Holes

3.3 Observations of Frozen Soil Structure

Several sections of the frozen core that were too small for freeze-thaw testing were cut vertically with a diamond saw and shaved smooth with a knife blade to study the ice

structure variation with depth into the profile, and to compare the field frozen soil with laboratory frozen soil. Photographs of these sections are given in Figure 3-13 to Figure 3-16.

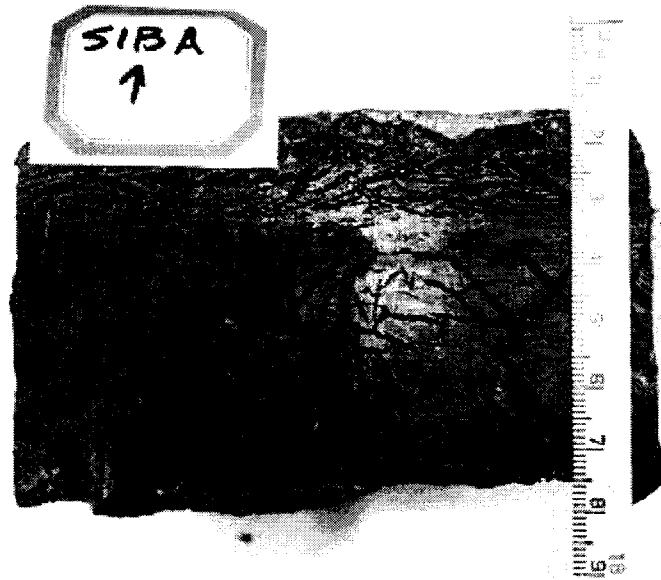


Figure 3-13 - Site 1b - Depth 0-10.5cm

The ice structure near the surface consists of three centimeters of horizontal lenses. This structure was not expected, and may be due to effects other than freezing such as unsteady heat flow. For example, a period of warm weather could cause the surface to thaw while the soil at depth remains frozen. This would reverse the direction of heat flow, cause water migration down into the soil, and allow horizontal lenses to form.

At a slightly greater depth the ice surrounds large peds of tailings. In laboratory tests there was no ped structure of this type observed near the surface of a sample subjected to one-dimensional freezing.

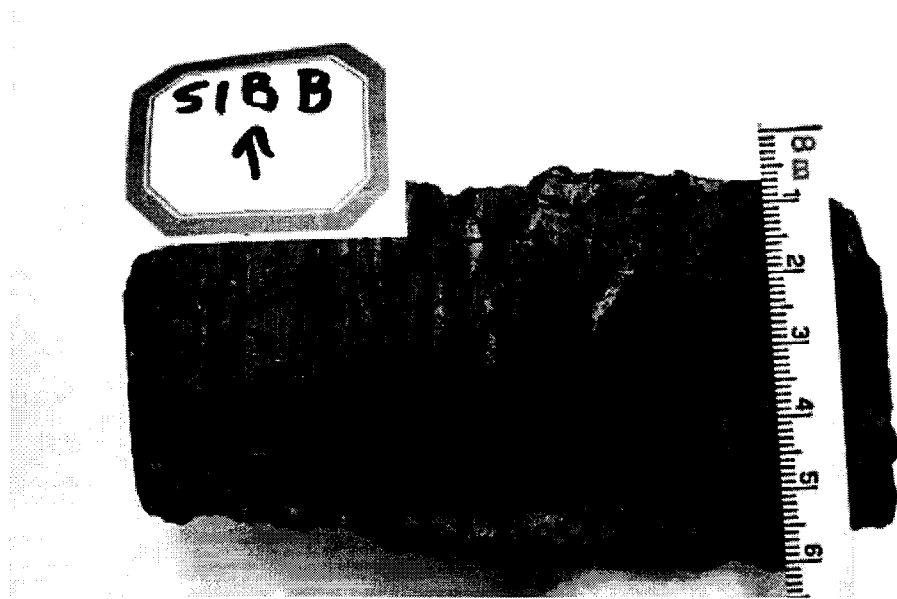


Figure 3-14 - Site 1b - Depth 10.5-16 cm

At a depth of 10.5-21.5 cm, the ice structure consisted of both vertical and horizontal lenses, with a needle like form. This was also noted in the laboratory frozen tests.

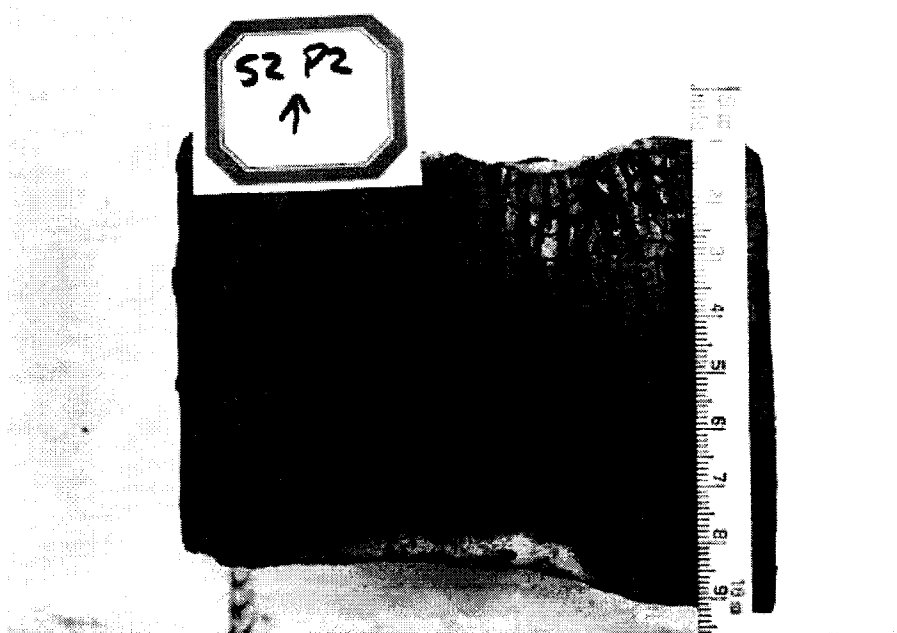


Figure 3-15 - Site 2 - Depth 14-21.5 cm

The ice structure nearest the bottom of the frozen soil was primarily horizontally aligned. This is similar to the ice structure observed near the final ice lens in the laboratory frozen samples.



Figure 3-16 - Site 1b - Depth 47.5-53 cm

For comparison, a photo showing a frozen sample of MFT obtained during a laboratory-freezing test is provided in Figure 3-17. The sample is of the same diameter as the core samples from the sump site.

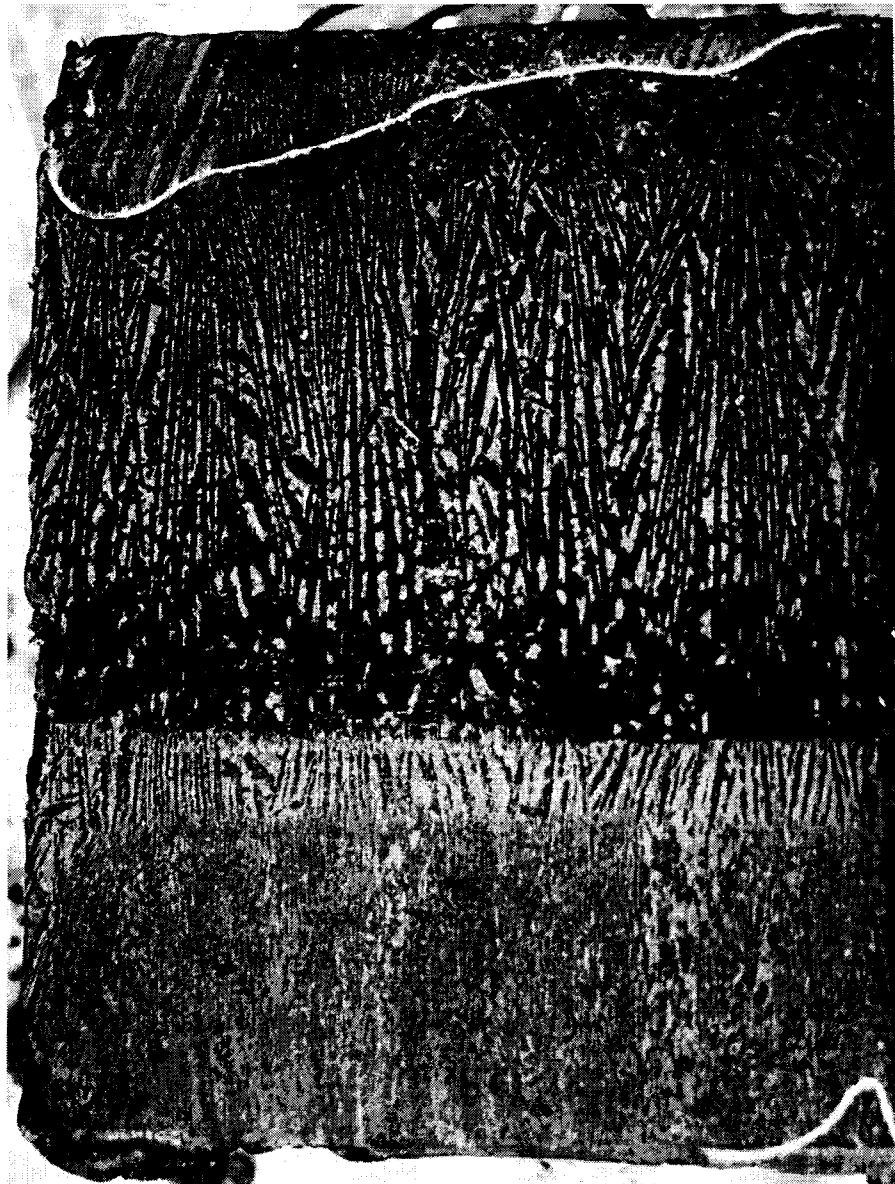


Figure 3-17 - Laboratory Frozen Sample - Test S2T2

Appendix C may be consulted for a more complete profile of photographs.

3.4 Conclusions

The field sampling program allowed the effect of freezing to be studied in a freshly frozen mine waste deposit. Comparison between the laboratory behaviour of the sump material, MFT, and Devon Silt, will be made in the following chapters. This chapter allows qualitative examination of the ice structure observed from the field samples

compared to the laboratory frozen samples. Future testing of the sump in which shear strength and moisture content are measured again would make it possible to determine the increase in density and strength of the deposit after freeze and thaw, and allow the laboratory results to be compared to the field results.

3.5 References

Environment Canada. (2006). "Climate trends and variations bulletin, temperature & precipitation in historical perspective, winter 2005/2006."

http://www.msc.ec.gc.ca/ccrm/bulletin/national_e.cfm (03/23, 2006).

Johnson, R. L., Bork, P., Allen, E. A. D., James, W. H., and Koverny, L. (1993). "Oil sands sludge dewatering by freeze-thaw and evapotranspiration." *Rep. No. RRTAC 93-8*, Alberta Conservation and Reclamation Council, Edmonton, Alberta.

Scott, D. J. (2003). "Multiphase mass-volume relationships for tailings." University of Alberta Geotechnical Centre.

Syncrude Ltd. (2006). "Aerial photographs of Syncrude Limited." .

Chapter 4 - Previous Related Work and Material Characterization

A summary of work performed previously on materials mentioned in this study is presented, including thaw strain and segregation potential. The characteristics of these materials are also provided.

4.1 Freeze-Thaw Dewatering of Oil Sand Fine Tailings

Several studies have been performed in the past on the topic of thaw strain due to freeze-thaw cycles for oil sand tailings. Most of these studies report thaw strains in the form of initial and final solids content. Since the solids content is difficult to determine in a freezing test involving cyclic freezing, the thaw strain is usually measured as a change in the height of the sample. For comparison to thaw strain values reported in previous work as initial and final solids content, thaw strain based upon settlement can be converted to final solids content. This is done by assuming or measuring the specific gravity of the soil, assuming complete saturation, and calculating the various components of the soil by mass using fundamental geotechnical engineering soil properties equations (Budhu 2000).

The effects of freeze-thaw cycles on the dewatering of soft tailings have been investigated on several occasions. In 1971, the United States Bureau of Mines completed a laboratory study of freeze-thaw dewatering of phosphate rock slime. This study found that the freezing rate is important for thaw strain. Rapidly frozen samples showed little thaw strain compared to more slowly frozen samples (Dawson et al. 1999). With this in mind, freezing tests should be performed with identical freezing rates to remove the effect of freezing rate from the comparison.

Research has been performed at the Alberta Environment Centre on oil sand fine tails, using MFT from the Mildred Lake Settling Basin at Syncrude Ltd. By combining MFT at 25% solids content with sand to increase the solids content to 29-35%, the final thaw strain was 52-54% after several cycles. This corresponds to an increase in solids content

of approximately 49%. The study also examined MFT at lower initial solids content and found an exponential decrease in the thaw strain with increasing initial solids content (Johnson et al. 1993).

Work by Dawson (Dawson and Seg0 1993), with Syncrude and Suncor MFT is presented in Figure 4-1. This figure represents the results of laboratory bench-scale tests, similar to the work performed as part of this research. Note that the thawed solids content approaches the zero thaw strain

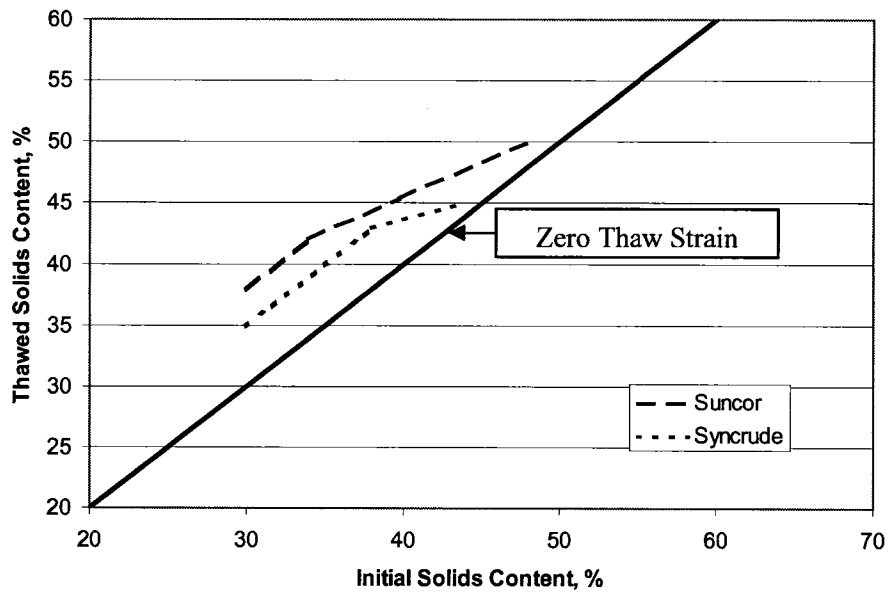


Figure 4-1 - Bench-Scale Thaw Strain Results for Oil Sand MFT (Modified after Dawson et al. 1999)
 Proskin (Proskin 1998), studied field frozen chemically amended MFT from Suncor, as well as untreated Suncor MFT and OSLO MFT. Thaw strain from this work for the untreated Suncor MFT is provided in Figure 4-2.

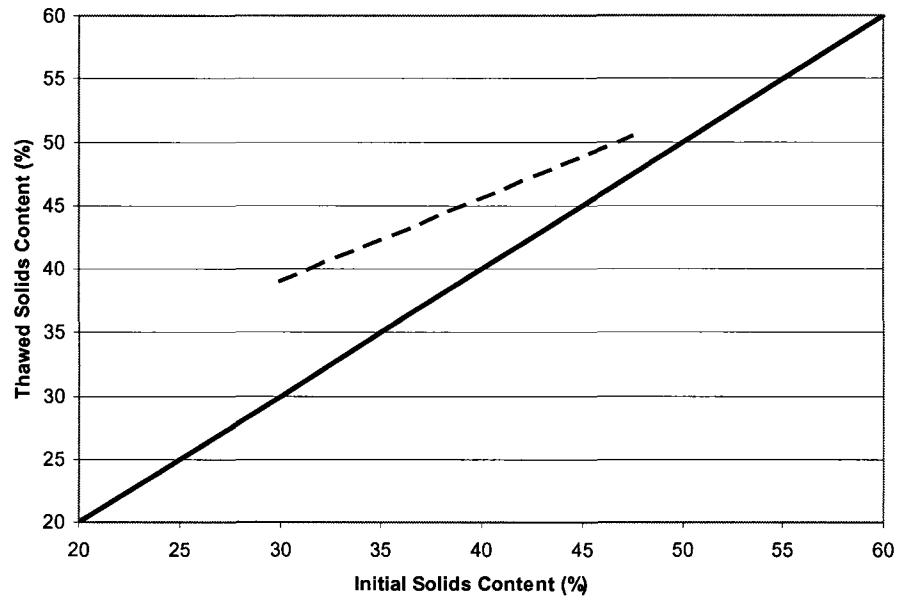


Figure 4-2 - Freeze-Thaw Dewatering of Suncor MFT (Modified after Proskin et al. 1996)

Figure 4-2 shows results that are similar to those shown in Figure 4-1. These figures are provided for comparison with the thaw strains determined as part of this research, presented in Chapter 6.

4.2 Segregation Potential

The segregation potential was determined for MFT, Syncrude sump fines, and Devon Silt, and is provided in Chapter 6. For comparison, the segregation potential of Devon Silt is listed in Table 4-1 (Xia 2006). These results are from recent testing at the University of Alberta, and were performed on samples that had been consolidated to 100kPa or to the specified overburden pressure, and frozen with varying overburden pressure.

Table 4-1 - Segregation Potential of Devon Silt (Xia 2006)

Test	Overburden Pressure (kPa)	Segregation Potential ($\text{cm}^2 \cdot \text{s}^{-1} \cdot \text{°C}^{-1}$)
1	0	4.6E-07
2	0	4.4E-07
3	0	4.8 E-07
4	100	4.4 E-07
5	200	2.7 E-07
6	400	2.4 E-07

4.3 Summary of Material Characteristics

Characteristics of the materials tested as part of this research are presented in this section.

4.3.1 Grain Size Distribution

The grain size distribution of all the materials studied, or used for comparison in this research are presented in Figure 4-3. Grain size distribution of the SWSS sump material at 1 and 2 m depths (Hereygers 2006), Syncrude MFT (Sego and Biggar 1996), Suncor MFT (Proskin 1998), OSLO MFT (Dawson et al. 1999), and Devon Silt (Xia 2006) are plotted.

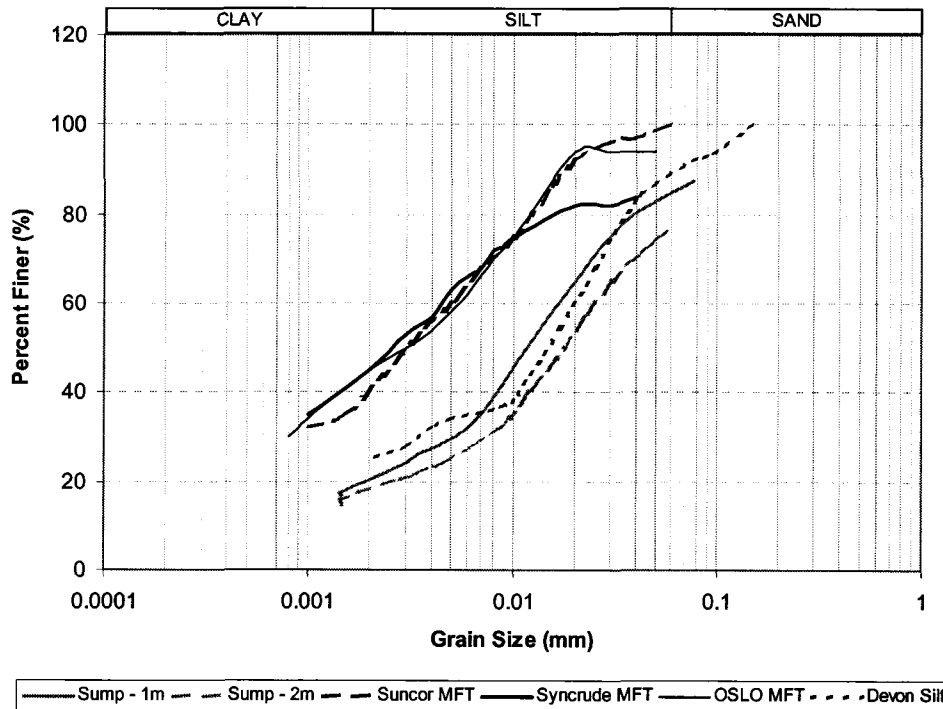


Figure 4-3 - Grain Size Distribution for All Materials Studied

4.3.2 Geotechnical Characteristics

The Atterberg limits and Unified Soil Classification System (USCS) classification for the soils used for comparison are listed in Table 4-2. The properties of the materials tested in this study are provided in Table 4-3.

Table 4-2 – Properties of Materials Reported in Literature

Material	Liquid Limit (%)	Plastic Limit (%)	USCS Classification	Specific Gravity
Devon Silt	32 ₁	20 ₁	ML	2.65 ₄
Syncrude/Suncor MFT	40-75 ₃	10-20 ₃	CL/CH/ML/MH ₃	2.40-2.44 ₅
OSLO MFT	50-55 ₂	20-25 ₂	CH	N/A

1. (Xia et al. 2005)
2. (Dawson et al. 1999)
3. (FTFC 1995)
4. (Xia 2006)
5. (Proskin 1998)

Table 4-3 – Initial Properties of Materials Tested in Laboratory Program

Material	Initial Moisture Content (%)	Initial Solids Content (%)	Liquid Limit (%)	Plastic Limit (%)	USCS Classification	Specific Gravity
Suncor Pond 2&3 MFT	144	41.0	N/A	N/A	N/A	N/A
Syncrude SWSS Sump Fines (1.0m depth)	51.4	66.1	30.1 ₁	17.2 ₁	ML	2.45 ₁
Syncrude SWSS Sump Fines (2.0m depth)	42.7	70.1	N/A	N/A	N/A	N/A

1. (Hereygers 2006)

The bitumen content for Syncrude MFT was determined during a trial freeze-thaw test (McKenna and Dawson 1999). It was found that the bitumen content was most commonly 2.0-2.5%.

4.3.3 Freezing Point Depression

The freezing point depression curve for Suncor Pond 2/3 MFT is given in Figure 4-4. The freezing point depression is only noted for the decant water, and was found to be -0.15°C . This was determined by ASTM standard D5918-96 (2001). During freezing the soil will become super cooled. As it freezes it will warm to the freezing point depression temperature. This is shown in the following figure.

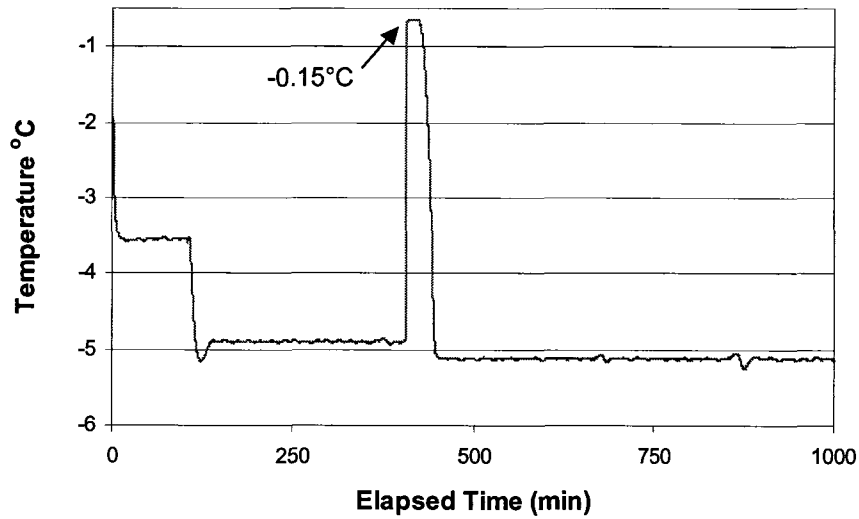


Figure 4-4 - Freezing Point Depression of Suncor Pond 2/3 MFT

4.4 References

Andersland, O. B., and Ladanyi, B. (2004). *Frozen Ground Engineering*. John Wiley & Sons, Inc., Hoboken, New Jersey.

Budhu, M. (2000). "Physical characteristics of soils and soil investigations." *Soil mechanics & foundations*, W. Anderson, ed., John Wiley & Sons, New York, New York, 14-17.

Dawson, R. F., and Segoo, D. C. (1993). "Design concepts for thin layered freeze-thaw dewatering systems." *Proceedings of the 46th Annual Canadian Geotechnical Conference*, Saskatoon, Saskatchewan, Sep 27-29 1993, 283-288.

Dawson, R. F., Segoo, D. C., and Pollock, G. W. (1999). "Freeze-thaw dewatering of oil sands fine tails." *Canadian Geotechnical Journal*, 36(4), 587-598.

FTFC (Fine Tailings Fundamentals Consortium). (1995). *Advances in oil sands tailings research*. Alberta Department of Energy, Oil Sands and Research Division, Edmonton, Alberta.

Johnson, R. L., Bork, P., Allen, E. A. D., James, W. H., and Koverny, L. (1993). "Oil sands sludge dewatering by freeze-thaw and evapotranspiration." *Rep. No. RRTAC 93-8*, Alberta Conservation and Reclamation Council, Edmonton, Alberta.

McKenna, G., and Dawson, R. (1999). "1995/1996 MFT freeze-thaw prototype at Syncrude's Base Mine Lake." Report. Syncrude Ltd, Edmonton, Alberta.

Proskin, S. A. (1998). "A geotechnical investigation of freeze-thaw dewatering of oil sands fine tailings." PhD thesis, University of Alberta, Edmonton, Alberta.

Proskin, S. A., Segoo, D. C., and Burns, R. (1996). "Field tests evaluating freeze-thaw dewatering of fine tailings." *Proceedings of the 1996 3rd International Conference on Tailings and Mine Waste, Jan 16-19 1996*, Fort Collins, CO, USA, 189.

Segoo, D. C., and Biggar, K. W. (1996). "The behaviour of a layer of frozen MFT placed on top of a layer of unfrozen MFT." Report. University of Alberta, Edmonton, Alberta.

Xia, D. (2006). "Frost heave studies using digital photographic technique." PhD thesis, Department of Civil and Environmental Engineering, University of Alberta, Edmonton, Alberta.

Xia, D., Arenson, L. U., Biggar, K. W., and Segoo, D. C. (2005). "Freezing process in Devon Silt – Using time-lapse photography." *Submitted to Canadian Geotechnical Journal*.

Chapter 5 - Laboratory Freeze-Thaw Testing

The type of freezing cell used, and the parameters measured when performing a freezing test are important. Most natural soils can be tested with a different method than is required for highly compressible soils such as MFT. This chapter presents the suitability of using three types of freezing test apparatus available at the University of Alberta to determine the freezing characteristics of soft mine tailings.

As a soil freezes, the suction generated beneath the ice lens induces an increase in effective stress on the soil near the ice lens. Depending on the magnitude of the suction and the compressibility of the soil, this effective stress change and associated void ratio change may be negligible. Reconstituted soils with high overconsolidation ratios, or stiff natural soils approach the ideal case of an incompressible soil (Konrad and Seto 1994). Therefore, the consolidation effects during freeze can be neglected for these soils. Much of the frost heave testing reported in the literature was performed using soils that were relatively stiff compared to soft mine tailings. Accordingly, only one paper was found in which frost heave testing was performed where consolidation during freeze was not assumed to be negligible. This paper reported the results of freezing tests performed on sensitive Champlain Sea clay (Konrad and Seto 1994). See Section 2.3.1 for a more detailed explanation of the consolidation during freezing process.

Soft mine tailings present unique challenges when they are used in freezing tests. Three methods were used to characterize the segregation potential for MFT from Suncor Limited's Pond 2 and 3, and the MFT rich sump material from Syncrude, described in Chapter 3. These test methods are described in the following sections.

5.1 Test Theory

This section discusses the mechanisms involved during the freezing of a soil, whether it is compressible or not. One purpose in performing freezing tests is to find the segregation potential (SP), an important index property that can be used to predict frost heave behaviour in the field (Konrad and Morgenstern 1984).

The amount of freezing-induced consolidation in the soil depends on its stress history and compressibility. Natural fine-grained soils may approach the ideal incompressible soil assumption when they are near the surface in the zone of frost influence. Surface desiccation and freeze-thaw may cause these soils to be highly overconsolidated and result in negligible consolidation due to the small recompression index.

Compressible soils, such as MFT, require the consideration of the effect of consolidation during freezing when calculating SP in the laboratory. If the consolidation effects are neglected, and only surface heave measurements are used to find SP, as is typical for stiff soils, then the laboratory tests may significantly underestimate the frost susceptibility of the soil (Konrad and Seto 1994). No surface heave was noticed during the initial testing program with MFT, which would indicate that MFT has no frost susceptibility. This is known to be untrue, as MFT exhibits substantial ice lens growth during freezing.

During freezing, there are three distinct water sources that supply water to the freezing front. The total water flow rate arriving at the ice lens (v_l), is the sum of the flow rates from three sources: from the external supply (v_u), from within the soil due to consolidation (v_{uc}), and from water generated within the frozen fringe (v_{fn}). See Equation 5-1.

Equation 5-1 (Konrad and Seto 1994)

$$v_l = v_u + v_{uc} + v_{fn}$$

During transient freezing, water is expelled from the fringe due to volume expansion during the phase change. The flux from the fringe (v_{fn}), can be approximated by Equation 5-2.

Equation 5-2 (Konrad and Seto 1994)

$$v_{fn} = n \cdot \varepsilon \cdot \frac{dX}{dt}$$

where n is the porosity, ε is a factor taking into account the amount of unfrozen water remaining in the frozen fringe, and dX/dt is the rate of frost penetration. At the segregational-freezing front (steady-state thermal conditions), the flux from the fringe no longer contributes water to the freezing front (Konrad and Seto 1994).

Segregation potential at the ice lens (SP_i) is defined as the ratio of the velocity of the water reaching the ice lens (v_i), to the temperature gradient in the frozen fringe ($gradT_f$):

Equation 5-3 (Konrad and Seto 1994)

$$SP_i = \frac{v_i}{gradT_f}$$

The velocity of the water reaching the ice lens in a soil that has negligible consolidation effects is related to the heave rate (dh/dt) and the 9% expansion during the phase change from water to ice. This is given in Equation 5-4.

Equation 5-4 (Konrad and Seto 1994)

$$v_i = \frac{dh/dt}{1.09}$$

If consolidation effects are not negligible, then the velocity of water reaching the ice lens also depends on the rate of water expelled from the soil during consolidation (v_{uc}), as is shown in Equation 5-5. The rate of water expelled during consolidation (v_{uc}) is given in Equation 5-6, where V_c is the total volume of water expelled during consolidation, and t is the time interval.

Equation 5-5 (Konrad and Seto 1994)

$$v_i = v_{uc} + \frac{dh/dt}{1.09}$$

Equation 5-6 (Konrad and Seto 1994)

$$v_{uc} = \frac{V_c}{\Delta t}$$

The water released per unit area during consolidation is calculated using Terzaghi's 1-dimensional theory of consolidation, shown in Equation 5-7.

Equation 5-7 (Konrad and Seto 1994)

$$V_c = \sum_{i=1}^n \frac{\Delta e_i}{1 + e_0}$$

where e_i is the void ratio in a layer of soil, and e_0 is the initial void ratio in that layer.

Equation 5-7 is applied to the discretized soil sample of n layers, where the measured suctions in each layer, (i), are applied to a consolidation curve for the material to find the change in void ratio for the measured suction.

Not all the water that is released during consolidation will reach the ice lens, as some will fill shrinkage cracks beneath the ice lens. The water migration rate to the ice lens is modified to account for this with Equation 5-8.

Equation 5-8 (Konrad and Seto 1994)

$$v_{ucl} = \alpha \cdot v_{uc}$$

In Equation 5-8, α is the fraction of water released during consolidation that actually freezes at the active ice lens. The water that freezes in shrinkage cracks will not contribute to heave. The α parameter can be calculated in two ways (Konrad and Seto 1994):

- The water flux reaching the ice lens is equal to the ratio of soil area to shrinkage crack area near the ice lens.
- The water flux reaching the ice lens is equal to the ratio of heave strain in the frozen soil to consolidation strain of the entire soil sample.

Since freezing tests on compressible soils are much more complicated than for incompressible soils, and the knowledge of the water fluxes due to external supply and consolidation are required, compressible soils require testing with the measurement of suction and temperature throughout the profile, as well as heave and water supply. Suction is a difficult parameter to measure, as most pore pressure transducers will not work under suction or are not small enough. One approach is to use an applied backpressure and measure the pressure reductions in the sample (suctions). Freezing with applied backpressure has been shown both theoretically and experimentally by Konrad and Seto to be practically equivalent to those obtained from conventional freezing tests (Konrad and Seto 1994).

5.2 Freezing Test Apparatus 1: Heave and Flow Measurements

The initial attempts to determine the SP for MFT were based on the procedure used by Xia for testing Devon Silt. This apparatus provides sufficient detail to determine SP provided that consolidation during freezing is negligible.

5.2.1 Equipment

The frost heave apparatus used for the initial testing phase is shown in Figure 5-1. The sample height was typically 12-14 cm.

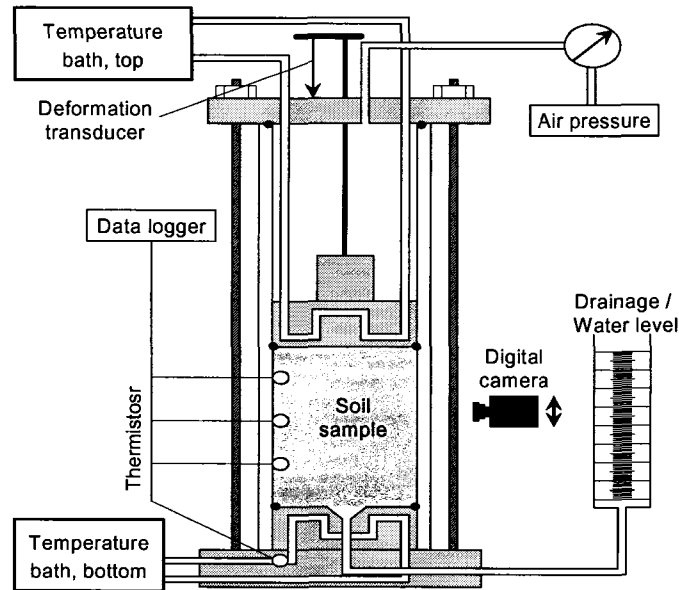


Figure 5-1 - Initial Test Apparatus (Arenson et al. 2005)

The cell wall is made of clear acrylic, which allowed high-resolution digital photos to be taken through the cell walls. Silicone vacuum grease is applied to the inner cell walls to minimize friction during heave. The upper and lower cooling plates are made of aluminum with channels within for the circulation of glycol from temperature regulated cooling baths. Stainless steel pore plates and filter paper are placed between the soil sample and water supply on the lower cooling plate. The temperature gradient within the soil is measured by four thermistors, placed through the cell walls, as well as one attached to the exterior of the base plate. Water flow from the sample is measured manually with a burette attached to the bottom of the sample. The soil is frozen under open conditions with free access to water from the bottom. The top cooling plate is free to heave with the soil and a deformation transducer is used to measure the heave. Digital photographs are taken through a macro lens to track the ice lens development. Fluorescein mixed with the soil indicates the phase change of the water in the soil. Viewed under ultraviolet light, the fluorescein is green when it is dissolved in water, and brown when it precipitates due to freezing. The thermistors, pressure sensor, and

displacement gauge are recorded automatically using a Data Dolphin or a Benchlink data logger. The camera is operated remotely and automatically through a personal computer. Appendix B contains the accuracy of the instrumentation, as well as sample preparation and testing procedures.

5.2.2 Test Operation

This section briefly describes the sample preparation and testing procedure. Consult Appendix B for more detail.

5.2.2.1 Sample Preparation

Sample preparation involved adding 5 g/L of fluorescein ($C_{20}H_{12}O_5$) to the sample, and stirring thoroughly. The fluorescein does not affect the freezing point of the water (Arenson et al. 2005). The agitation and suction did not cause any notable consolidation of the soil as no water was found to have separated from the soil.

After mixing the fluorescein into the sample, the solids content was determined, and the soil was then placed into the freezing cell. The soil was agitated with a shaker table while suction was applied to the top of the soil to remove any entrained air. It has been found that this method produces a sample that is fully saturated (Xia et al. 2005).

5.2.2.2 Testing Procedure

After the sample was placed in the freezing cell, and the top of the cell was assembled, the thermistors were placed through the ports into the sample. Any excess pore pressure generated by the disturbance of installing these sensors must be allowed sufficient time to dissipate. Dissipation was very rapid for the samples used in this testing but several hours were allowed before freezing commenced to be certain. Coolant and water supply lines were connected, and the displacement gauge was installed. The freezing cell was wrapped with insulation. If photographs were to be taken, a glass window with a still air gap between the window and the cell was installed. Failure to use an insulated viewing window caused a difference in the depth of the ice advance and the extent of the ice lensing when compared to the soil wrapped with insulation, due to increased heat transfer

at the cell wall. Prior to beginning the test, initial readings of water level and sample height were noted.

Before beginning the freezing test, the soil was allowed to cool to the ambient room temperature of 1-2°C. The warm end coolant supply was turned on several hours prior to freezing to establish the correct warm end temperature in the soil. If the sample was not cooled prior to freezing, there was excess heat that needed to be removed from the soil, and the test was not representative of actual freezing conditions. When the cold end coolant supply was turned on, photographs and water supply readings were taken at short time intervals. Fifteen minutes was appropriate. Once steady state thermal conditions were reached, the readings were taken every hour, or longer.

5.2.3 Test Results

This section presents a brief overview of the type of data obtained with this test method. Complete results from these tests can be found in Appendix A. Figure 5-2 presents the temperature within the soil during freezing. This plot can then be used to find the temperature gradient in the sample for determining the segregation potential. The daily spikes are due to warming of the cold room during the refrigeration unit defrost cycle.

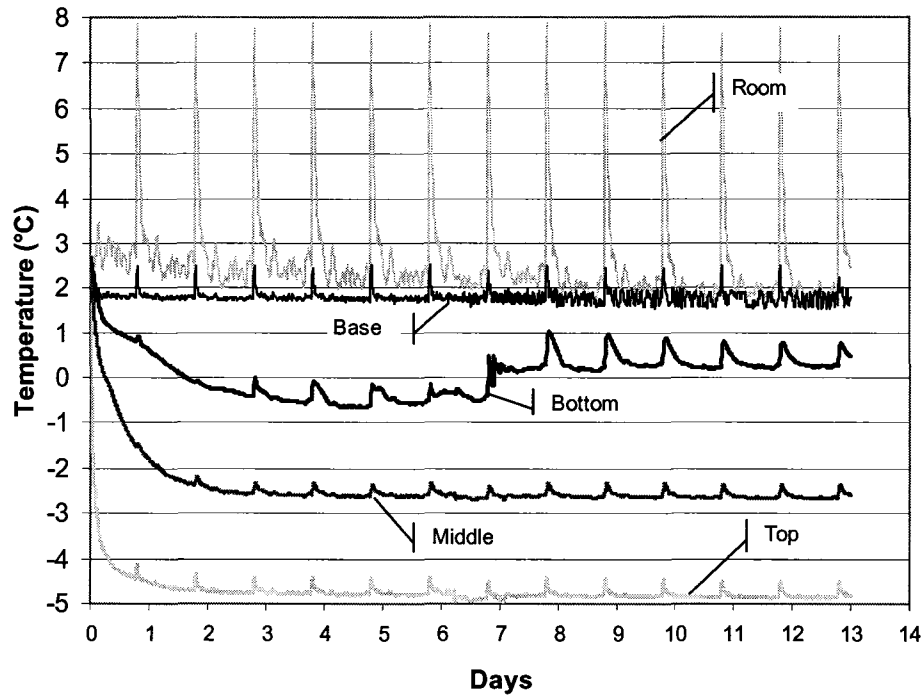


Figure 5-2 - Temperature in Soil During Freezing

Figure 5-3 shows the external water supply measurement during freezing for a typical test. Initially, water flows from the sample due to the expansion of water during the phase change to ice. At rapid freezing rates there is no ice lens formation so the water supply plot simply shows water expulsion due to the phase change expansion. As the temperature gradient becomes smaller, the plot shows the inflow towards the ice lenses. At steady state, and for a soil that is incompressible, the inflow will be equal to the volume of water forming the final ice lens. This final inflow rate can be used to find the velocity of the water reaching the final ice lens. Combined with the temperature gradient obtained from Figure 5-2 the segregation potential can be calculated.

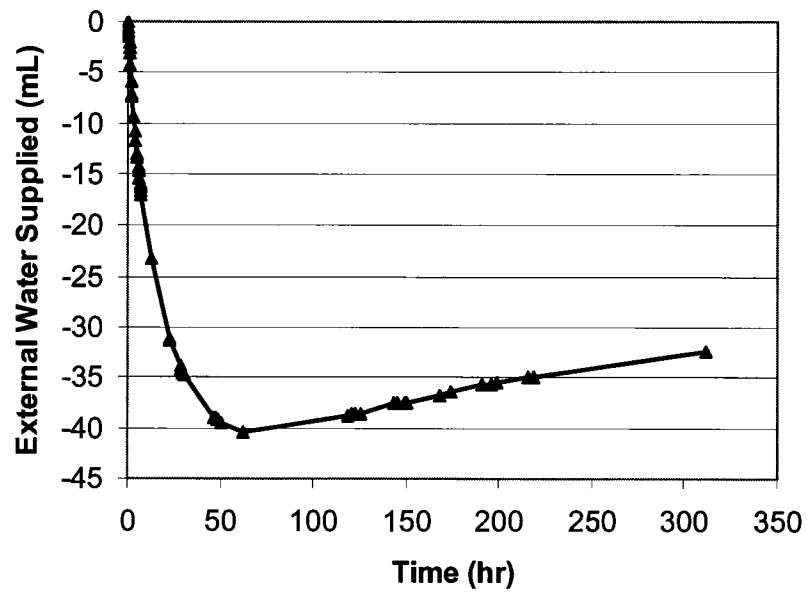


Figure 5-3 – External Water Supply During Freezing

Figure 5-4 presents a typical plot of surface heave during freezing. For an incompressible soil, the heave rate should be equal to horizontal ice lens formation rate. It is possible to determine SP by using either the flow or heave measurements for an incompressible soil. Note that there was practically no heave measured during this freezing test using a sample of MFT.

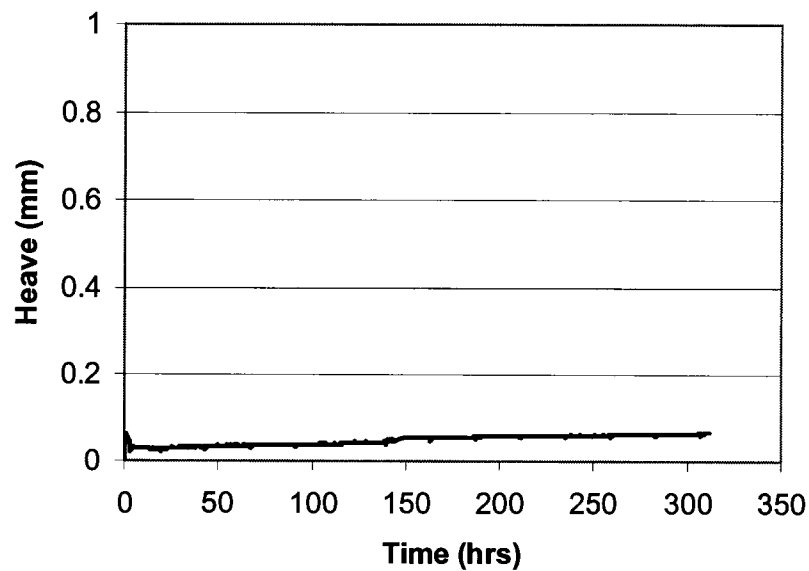


Figure 5-4 - Heave During Freezing

Figure 5-5 illustrates the location of the bottom of the ice lenses in the sample during freezing. This figure corresponds with the location of the -0.65°C isotherm, inferred from Figure 5-2. Based on this figure, the segregational freezing temperature is -0.65°C for this sample.

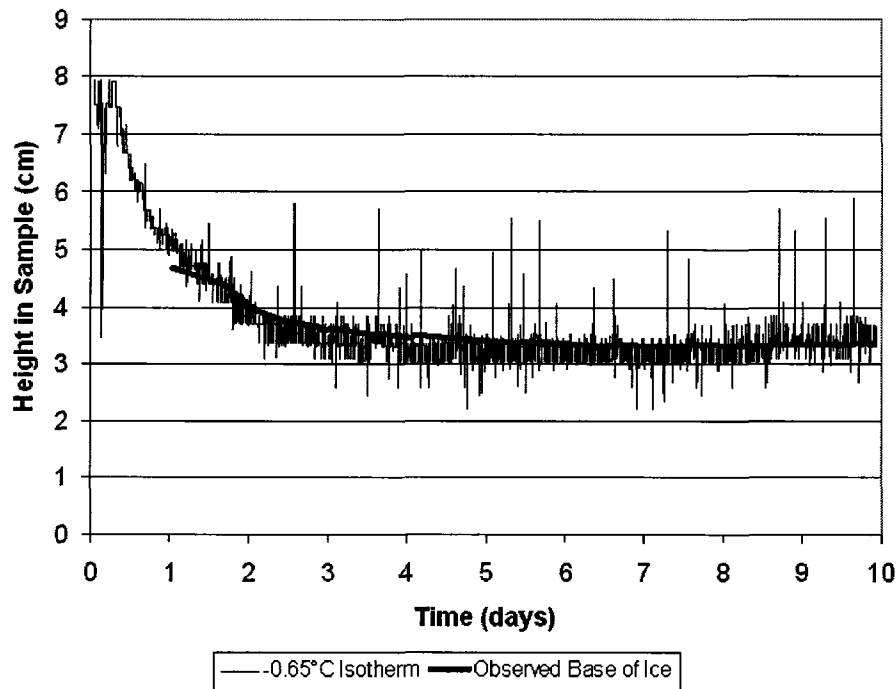


Figure 5-5 - Ice Penetration During Freezing

5.2.4 Conclusions from First Test Series

Figure 5-2, showing the temperature distribution in the sample, was sufficiently accurate to determine the temperature gradient in the soil. It was noted that a linear temperature distribution over the sample length was obtained after approximately two days. This correlates well with the photographs taken of the ice lens development. Near day two, the final ice lens forms. The temperature gradient could have been more accurately determined if the following deficiencies were addressed:

- It is difficult to ascertain the exact height of the thermistor in the sample, due to the flexibility of the wire housing used. A rigid mounting would allow the location of the thermistors to be more accurately determined but would restrict heave.

- The exact temperatures imposed on the soil by the coolant baths are unknown. Additional thermistors placed directly on the cold and warm end plates in contact with the soil would more accurately indicate the step freezing temperatures.

Figure 5-3, showing the external water supply during freezing, illustrates a condition that was not expected. Typical soils will have a net outflow for only an initial short period of time. This outflow occurs only while ice lenses are absent during the initial stage of freezing. During ice lens formation, there is usually a net inflow into the sample, with the rate becoming linear with time when the final ice lens forms. The discrepancy between MFT and typical soils is due to the lack of heave shown for the MFT (See Figure 5-4). A typical soil will heave while the ice lenses develop because the thawed soil beneath the ice lens is rigid enough to support the total stress increase caused by the ice expansion, and overcome the static friction between the soil and the cell wall. The MFT below the ice lens was too soft to overcome the friction. Expansion due to pore water freezing and ice lens development resulted in consolidation of the underlying thawed soil by the compressive force generated. This is shown in the external water supply graph. There was an inflow of water in the test shown in Figure 5-3, of approximately 8 mL, which accounts for merely 1mm of the observed 4mm thick ice lens.

Another process that likely occurred with the MFT was consolidation during freezing. With this process, water for ice lens growth is supplied from within the thawed MFT due to the suction generated at the base of the ice lens. This induces a reduction in pore pressure and a change in effective stress, leading to consolidation of MFT in the unfrozen zone. Again, this would be reflected in a reduction in the rate of inflow on the water supply graph.

The water supply graph allows the determination of the segregation potential when typical incompressible soils are tested. The rate of water arriving at the ice lens can be easily determined from the external supply graph. This was not possible for the MFT. Another technique to determine SP is to simply use the rate of heave to find the rate of

water arriving at the ice lens. The rate of heave is due to the 9% volumetric expansion of the water arriving at the lens. This was also not applicable for testing the MFT.

5.3 Freezing Test Apparatus 2: Suction, Flow, and Heave Measurements

After the first attempts with freezing MFT, the shortcomings of freezing test apparatus 1 were noted. Realizing that suction-induced consolidation was occurring during freezing, a test apparatus and method based on work by Konrad and Seto with Champlain Sea Clay was used (Konrad and Seto 1994).

5.3.1 Equipment

A few modifications were made to the testing apparatus used in the initial testing to include the consolidation effects during freezing, to improve the accuracy of the temperature measurements, and to automate the water flow readings. See Figure 5-6 for a schematic of the modified apparatus.

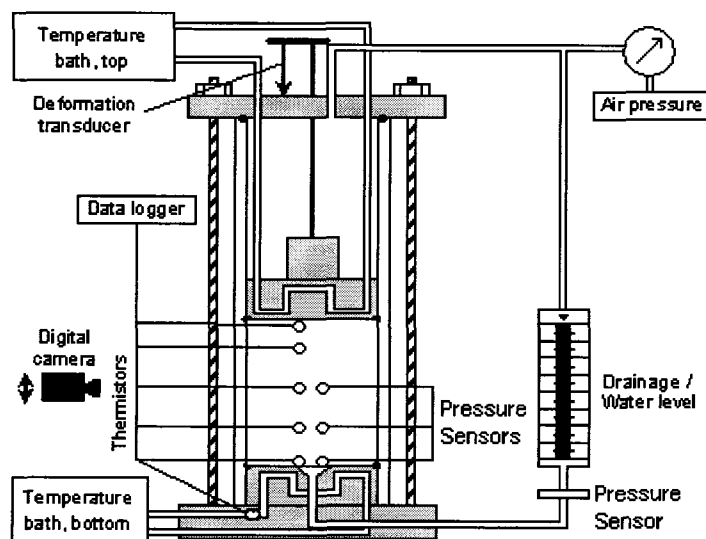


Figure 5-6 - Schematic of Modified Testing Apparatus (Modified after Arenson et al. 2005)

To quantify the consolidation effects during freeze, the apparatus was modified to resemble the apparatus used by Konrad and Seto in testing a sensitive Champlain Sea clay (Konrad and Seto 1994). The modifications included creating a manometer and

applying an arbitrary backpressure to the top of the cell, as well as to the bottom of the cell through the manometer fluid, resulting in no effective stress change in the soil. The pressure was required to be greater than the maximum suction and 100 kPa was used. Four ports equipped with Swagelok fittings were then placed in the cell wall adjacent to the existing thermistor ports. Rigid plastic tubing was fitted into these ports and attached to a pressure sensor. A schematic of the pressure sensor is shown in Figure 5-7. The tubes were filled with mineral oil and placed directly into the soil. This enabled the suction to be measured as a reduction in pressure relative to the applied backpressure.

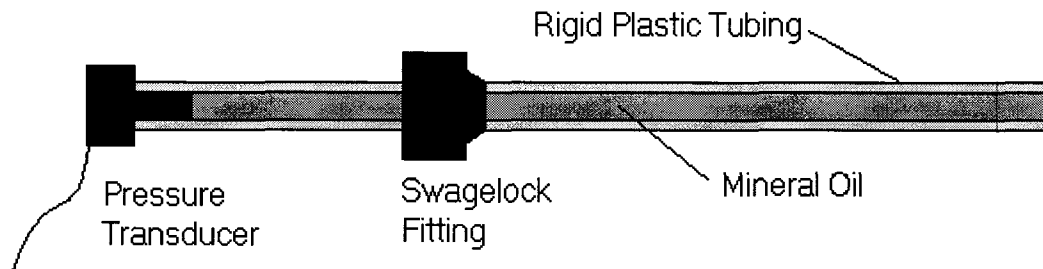


Figure 5-7 - Schematic of Pressure Sensor for Measurement of Suction

To improve the temperature data for interpreting the temperature gradient, a thermistor was mounted at the base of the top load plate. This allowed the exact cold end temperature to be determined, and allowed the thermistor to move with the load plate during heave and thaw settlement.

Water flow measurements were automated by using a differential pressure sensor mounted at the base of the manometer. This allowed a more thorough understanding of the external water supply response.

5.3.2 Test Operation

The testing was operated much in the same manner as is described in Section 5.2.2. The pressure sensors were installed at the same time as the thermistors. Before initiating freezing, the backpressure was slowly applied to the sample. A steady manometer reading indicated that there were no leaks or blockages in the pressure system. All other testing procedures are the same as for Setup 1.

5.3.3 Test Results

This freezing test apparatus allowed the measurement of suction within the soil. Figure 5-8 presents the pore pressure measured in a sample of MFT during freezing, including the 100 kPa backpressure. The apparatus was successful in measuring suctions of approximately 70 kPa in the thawed soil. An increase in the pressure in the sensor surrounded by frozen MFT near the top of the sample was due to the pressure generated by the expansion of water during the phase change in the freezing MFT, and the lack of surface heave. This stress increase was higher than 100 kPa, but the exact magnitude is unknown since the pressure sensor range was exceeded.

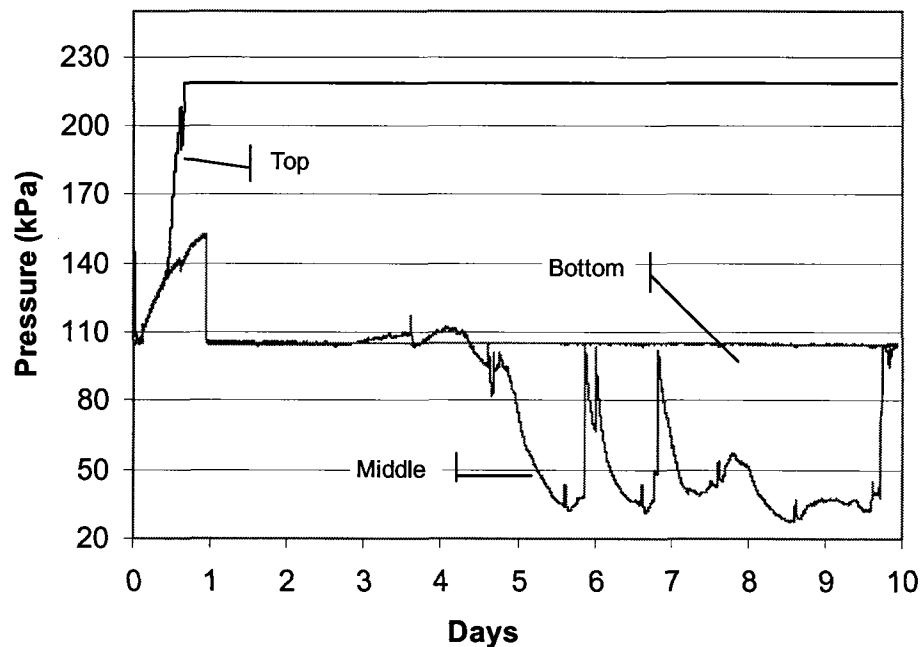


Figure 5-8 – Measured Pore Pressure During Freezing

Figure 5-9 presents the external water supply plots for the automated and manual readings. The manual readings were taken less frequently, but are known to be more accurate (See Appendix B for details). The automated readings allow the shape of the manual readings curve to be more accurately determined. The figure shows that both the manual and automated flow plots are of similar shape, but were often of slightly different magnitudes. The manual readings were known to be more accurate.

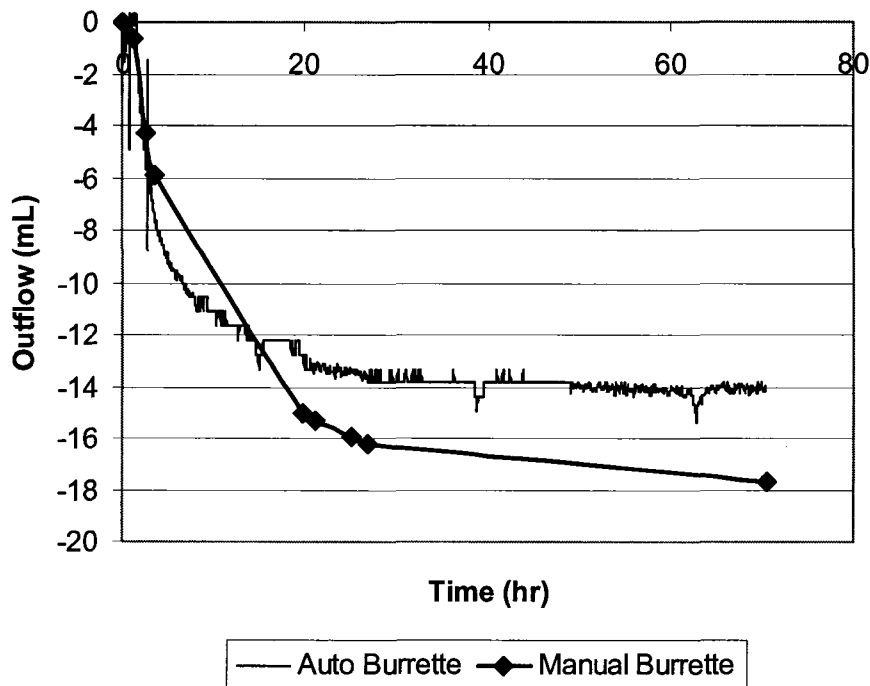


Figure 5-9 - Automated and Manual External Water Supply Readings

5.3.4 Conclusions from Second Test Series

Measuring the suction generated during the freezing of a soil is not an easy task. The measurement of suction is sensitive to the saturation of the soil, air bubbles in the pressure sensor, and blockage of the pressure sensor. Several attempts at designing the pressure sensors were required before accurate measurements of suction were obtained. The diameter of the tube leading from the soil to the pressure sensor was 5 mm. Any suctions measured are an average over the diameter of the sensor.

Suction is inferred from a reduction in the applied back pressure measured by pressure sensors in the soil. To apply the theory for calculating segregation potential, which includes the water generated by consolidation during freezing, it is necessary to determine the suction profile throughout the unfrozen soil. For this to be possible, suction must be measured in front of the advancing ice front to infer the suction profile ahead of the freezing front. Figure 5-10 presents the suction measured at the middle sensor while the ice front advanced past.

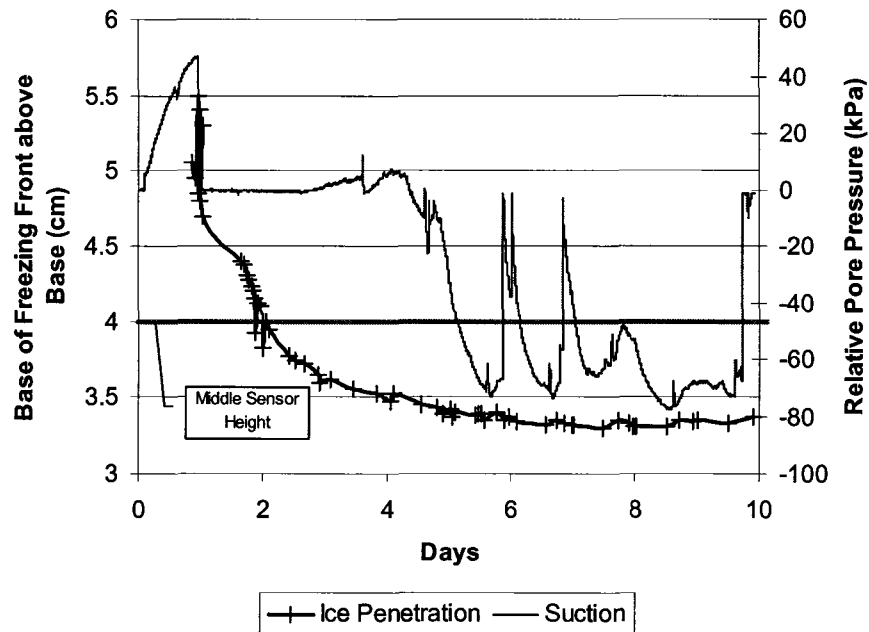


Figure 5-10 - Suction at the Middle Sensor During Freezing

Several interesting observations arise when examining this data.

No suction was noted in the sensor until more than two days after the ice front advanced past the sensor. It was expected that the suction would have been measured in advance of the ice front passing the sensor.

Suction of approximately 70 kPa was measured intermittently at the pressure sensor. There are periodic interruptions where no suction is measured. This is likely due to the slight warming that occurs in the cold room once each day while the refrigeration unit defrosts. A slight warming of the sample has been noted and causes the bottom ice lens to thaw and retreat very slightly. This would account for the loss of suction.

Suctions are measured after the ice has advanced past the pressure sensor by approximately 7 mm. If the pressure sensor were encased in ice, no suction would be noted. It is likely that the advancing ice front arrived at the pressure sensor and pushed the sensor downward as the ice lens continued to develop. If this were the

case, the pressure sensor would be embedded in the frozen fringe, and would therefore be measuring the maximum suction.

No suctions were measured at the lower pressure sensor at the bottom of the sample. The lack of any measured suction at any measurable distance from the advancing ice lens indicates that the suction generated at the ice lens does not extend very far into the thawed soil. It is possible that the suction profile extends only slightly deeper than the diameter of the pressure sensor. See Figure 5-11 for a schematic of the expected suction profiles in Champlain Sea Clay used by Konrad and Seto (Konrad and Seto 1994), and MFT.

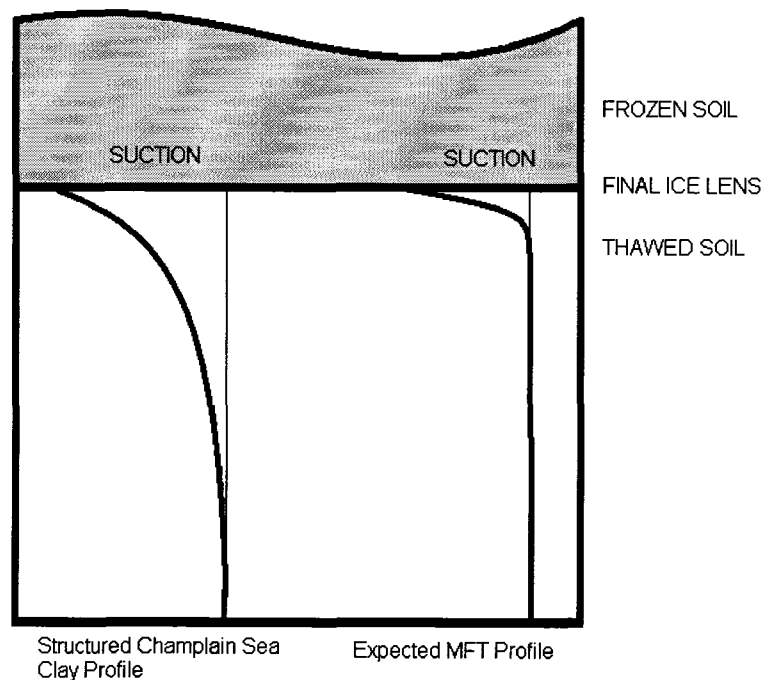


Figure 5-11 - Suction Profile for Champlain Sea Clay and MFT

The theory for considering consolidation during freezing described in Section 5.1 is based upon applying the measured suction gradient to the thawed soil profile. Since it was not possible to determine any suctions in advance of the ice lens, this type of analysis will not work with MFT. The extent of the suction profile depends on the magnitude of the suction generated at the ice lens, and on the hydraulic conductivity of the thawed soil.

This test apparatus likely revealed the reason for the lack of any surface heave. The high pressure recorded in the sensor trapped in the ice near the top of the sample indicates that there is significant stress increase in the sample. It would be expected that this stress would be released by heave. The fact that the pressure is noted continuously throughout freezing indicates that the stress has been locked in. An examination of the ice structure in the frozen MFT provides insight into this phenomenon. Figure 5-12 is a photo of the ice needle structure that was observed in the upper portion of a sample of MFT during a freezing test.

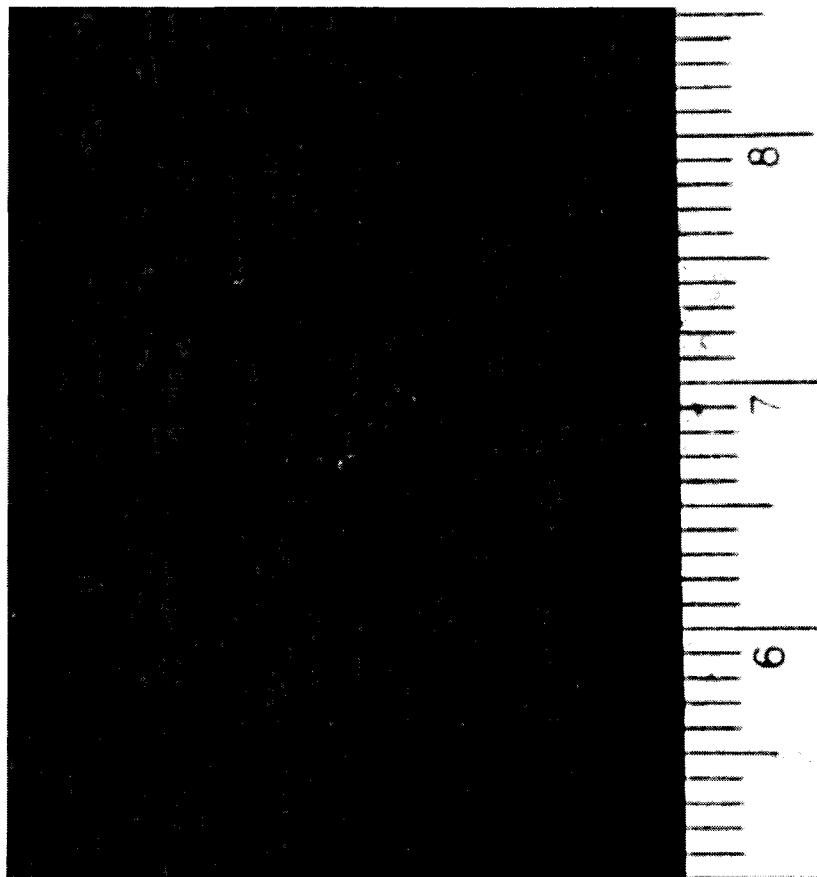


Figure 5-12 - Vertical Ice Needles in Frozen MFT

Note that the ice lens structure in Figure 5-12 is aligned primarily in the vertical direction. These needles form from water drawn out of the soil peds during periods of restricted water flow from below. Section 2.1.2 describes the mechanism responsible for vertically aligned ice lenses. As the vertical ice lenses form, the direction of expansion is

primarily in the horizontal direction. In turn, the stress caused by this expansion is also aligned horizontally. The stress acts against the cell wall and restrains the sample from heaving.

This test apparatus was able to provide details into the magnitude and extent of the suction being generated during freezing. For MFT, the extent of the suction ahead of the ice lens is too small to apply the theory for consolidation during freezing. This apparatus would likely work well for soils that exhibit a larger suction profile throughout the thawed soil.

5.4 Freezing Test Apparatus 3: Time Lapse Photography

The first two test methods were quite rigorous, but were unsuitable for soft, compressible mine tailings. These methods aimed to provide the temperature gradient and water flow rate to the ice lens to calculate the segregation potential during the entire freezing period. The difficulty is in finding the true water flow rate. The third method provides a technique to determine the flow rate at steady thermal conditions, but is not suitable for finding the flow rate during transient freezing. However, the segregation potential at steady thermal conditions is the main interest of this research and for application to many engineering problems.

The use of high-resolution digital photographs taken through a macro lens allows the measurement of the growth rate of the final ice lens. The photographs are taken with a scale in view, which is placed on the inside of the cell wall in contact with the soil. At steady thermal conditions, when the final ice lens has formed, all water arriving at the freezing front adds to the final ice lens. The final ice lens serves as a cutoff, with the assumption that no flow of water occurs through it. By photographing the final ice lens, the ice lens growth rate can be easily determined. The following equation is used to find the rate of water transfer through the fringe knowing the ice growth rate.

Equation 5-9

$$\frac{dH_w}{dt} = \frac{dH_i}{dt} / 1.09$$

where H_w and H_i are the height increase of water and ice, respectively, at the final ice lens between successive photographs.

5.4.1 Equipment

This method can be applied to any test where photographs are taken of the final ice lens, and temperature in the soil is recorded. The use of a fluorescein tracer aids in determining the advance of the ice front. The tests performed using Apparatus 1 and 2 were later examined using the theory for Apparatus 3, and the segregation potential at steady state was determined.

5.4.2 Test Operation

The tests were conducted in the same manner as described in Section 5.3.2. Photographs were taken of the final ice lens, with or without the use of ultraviolet lighting to view the fluorescein tracer. At steady thermal conditions, extra insulation was placed over the viewing window of the cell between photographs to ensure that the ice lens being photographed was not influenced by the room temperature.

Photographs were taken with a scale in view. When viewing the final ice lens, the following information is determined from the photographs:

- Vertical pixel coordinate at some arbitrary location on the scale to ensure that the scale is not moving relative to the cell wall.
- Number of pixels between adjacent millimeter divisions on the scale to determine the number of pixels per millimeter.
- Vertical pixel coordinate of the top and bottom of the final ice lens, taken at the same location on the ice lens for each photograph. This determines if the ice lens is stationary, as well as the thickness of the final lens.

5.4.3 Test Results

The segregation potential was determined for all tests performed in which the photographs were of sufficient quality to locate the final ice lens. By viewing the photographs, and plotting the elevation of the bottom of the ice lens based on the scale

included in the cell, the determination of the rate of ice growth was possible. During transient freezing this technique does not indicate the rate of water arriving at the ice lens. Ice lenses do form during transient freezing, but they form in succession. The assumption that the location of the lowest ice lens corresponds to the water transfer rate is valid only for the final ice lens, when thermal conditions are not responsible for the ice penetration into the sample. Figure 5-13 shows a plot of the segregation potential for transient and steady thermal conditions. Steady conditions are reached at approximately two days of freezing. The curve indicates a decrease in segregation potential during transient freezing. This is in error, as the assumption that the ice lens growth is proportional to the water transfer rate does not apply during transient freezing. For this method to be valid, there must be a developed final ice lens that acts as a cutoff. Figure 5-14 presents a plot of segregation potential calculated with a method suitable for both transient and steady freezing conditions for comparison. Figure 5-13 is only valid at steady thermal conditions.

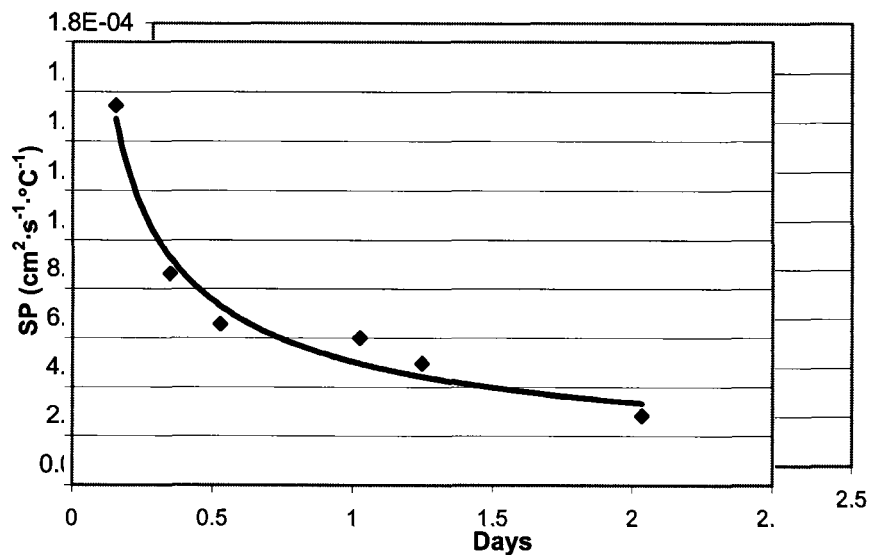


Figure 5-13 - Segregation Potential During Transient Freezing for MFT

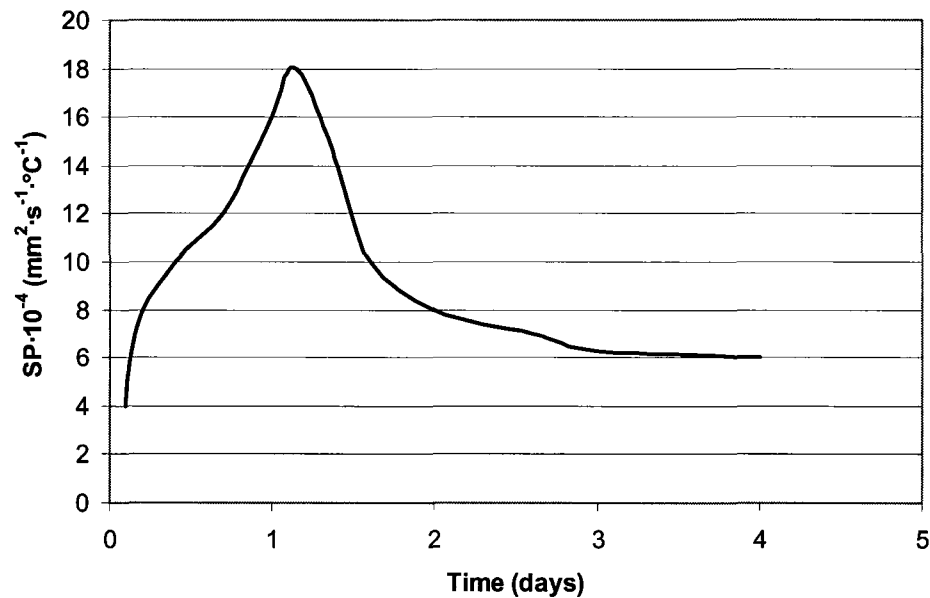


Figure 5-14 - Segregation Potential During Transient and Steady Thermal Conditions (Modified after Konrad 1987a)

5.4.4 Conclusions from Third Test Series

This test method was suitable for finding the segregation potential at steady thermal conditions (small temperature gradient), but not for transient freezing (large temperature gradient). In nature, small temperature gradients are typical (Konrad 1987b). Therefore, this method should be suitable for obtaining the segregation potential for predicting the freezing behaviour of natural soils.

Accuracy is likely limited when using this test method. Since photographs were taken at only one location in the freezing sample, they may have not been representative of the ice structure forming over the entire sample. Photographs at multiple viewing ports would be an improvement. More discussion on the suitability of this method is presented in Chapter 6.

5.5 Conclusions

Three freezing test devices were tested to determine the segregation potential of soft mine tailings including MFT. Apparatus 1 measured the total surface heave and temperature within the soil to find SP. This method works for soils that behave as incompressible, but

not for high void ratio mine tailings. Apparatus 2 includes the effects of consolidation during freezing, and is suitable for soils that consolidate during freeze and develop a suction profile that impacts a measurable portion of the thawed soil. This apparatus did not work for MFT due to the very small suction profile that was measured. Apparatus 3 determines SP based solely upon photographs of the final ice lens growth at steady thermal conditions. It was the only method that was found to be suitable for testing MFT.

5.6 References

Arenson, L. U., Xia, D., Segó, D. C., and Biggar, K. (2005). "Brine and unfrozen water migration during the freezing of Devon silt." *Proceedings of the 2005 Conference on Assessment and Remediation of Contaminated Sites in Arctic and Cold Climates (ARCSACC), May 8-10, Edmonton, AB, CAN*, 35-44.

Konrad, J. M. (1987a). "Procedure for determining the segregation potential of freezing soils." *Geotechnical Testing Journal*, 10(2), 51-58.

Konrad, J. M. (1987b). "The influence of heat extraction rate in freezing soils". *Cold Regions Science and Technology*, 14, 129-137.

Konrad, J. M., and Morgenstern, N. R. (1984). "Frost heave prediction of chilled pipeline buried in unfrozen soils." *Canadian Geotechnical Journal*, 21(1), 100-115.

Konrad, J. M., and Seto, J. T. C. (1994). "Frost heave characteristics of undisturbed sensitive Champlain sea clay." *Canadian Geotechnical Journal*, 31(2), 285-298.

Xia, D., Arenson, L. U., Biggar, K. W., and Segó, D. C. (2005). "Freezing process in Devon Silt – Using time-lapse photography." *Submitted to Canadian Geotechnical Journal*.

Chapter 6 - Interpretation of Freeze-Thaw Testing

This chapter serves to explain the test data and interpret the results. Full details of each test are available in Appendix A.

6.1 Overview of Laboratory Freezing Tests

Tests are labeled according to the series and test number. For example, the first test of the first series is S1T1. When a new soil or testing technique was used, a new series was started. Devon Silt was tested first to verify that the test equipment was operating properly and to serve as a reference for the MFT tested next in Series 1. The effect of multiple freeze-thaw cycles was studied during this test series. After these tests it was noted that heave was not occurring and it was realized that the underlying thawed soil was consolidating. Three tests were performed with a longer freezing duration and suction measurements for Series 2. With the lack of a notable suction profile in the MFT, the sump fines were tested next in Series 3 and were put through 3 freeze-thaw cycles to further examine this effect. A comparison of the freezing behaviour for naturally and laboratory frozen samples was made next in Series 4. Series 5 attempted to determine the segregation potential of Devon Silt by the time-lapse photography method for comparison with other methods. Series 6 was designed to measure the thaw strain of the sump fines.

Table 6-1 - Summary of Laboratory Tests

Test	Material	Test Procedure	Suction Measured
S1T1b	Devon Silt, 10 g/L NaCl	1 Freeze-Thaw Cycle	No
S1T2	MFT	1 Freeze-Thaw Cycle	No
S1T3	MFT	2 Freeze-Thaw Cycles	No
S1T4	MFT	2 Freeze-Thaw Cycles	No
S2T2	MFT	1 Freeze-Thaw Cycle, 12 Days Freezing	Yes
S2T3	MFT	1 Freeze-Thaw Cycle	Yes
S2T4	MFT	1 Freeze-Thaw Cycle, 10 Days Freezing	Yes
S3T1	MFT Sump	3 Freeze-Thaw Cycles	Yes
S3T2	MFT Sump	3 Freeze-Thaw Cycles	Yes
S4T1	MFT Sump – Frozen Core	Thawed and 1 Freeze-Thaw Cycle	Yes
S4T2	MFT Sump – Frozen Core	Thawed and 1 Freeze-Thaw Cycle	Yes
S4T3	MFT Sump – Frozen Core	Thawed and 1 Freeze-Thaw Cycle	No
S5T1	Devon Silt	1 Freeze-Thaw Cycle	No
S5T2	Devon Silt	1 Freeze-Thaw Cycle	No
S6T1	MFT Sump – Frozen Core	Thawed	No
S6T2	MFT Sump – Frozen Core	Thawed	No
S6T3	MFT Sump – Frozen Core	Thawed	No
S6T4	MFT Sump – Frozen Core	Thawed	No
S6T5	MFT Sump – Frozen Core	Thawed	No
S6T6	MFT Sump – Frozen Core	Thawed	No
S6T7	MFT Sump – Frozen Core	Thawed	No
S6T8	MFT Sump – Frozen Core	Thawed	No

6.2 Pore Pressure During Freezing

Freezing tests from S2T2 through S4T2 were performed using pressure sensors to measure the pore pressure within the soil during freezing. The maximum suctions

measured were in the range of 20-40 kPa, however test S2T4 generated 70 kPa suction after 5 days freezing. Details of this test are given in Sections 5.3.3 and 5.3.4.

Figure 6-1 presents the pore pressure above the applied back pressure (datum) measured at the top sensor for all tests (8 cm above base). The legend indicates the soil type. Some sensors were damaged during testing. As a result, some locations have less data. The intent of these figures is to illustrate the pore pressure reaction for all the soils. For a clearer look at a specific test, see Appendix A.

Note that there is typically an increase in pressure followed by a gradual reduction. The pressure increase is likely due to the expansion of water to ice. The reduction that occurs in some cases may be related to stress relief in the form of heave or consolidation. The high stresses measured at the top sensor, which is embedded in frozen soil, are likely squeezing the soil against the cell walls and limiting surface heave.

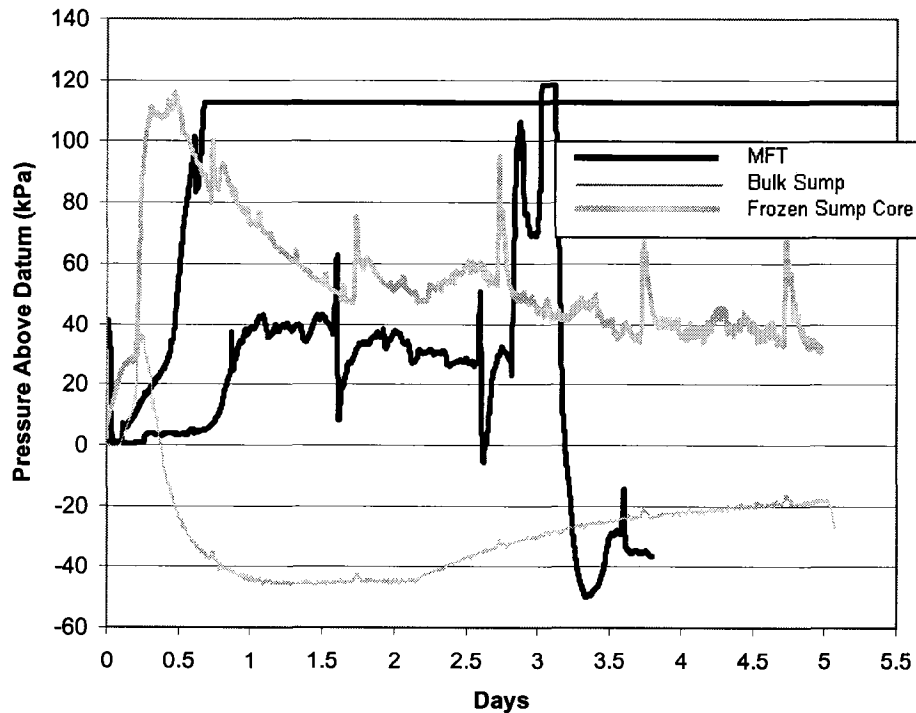


Figure 6-1 - Pore Pressure in Top Sensors

Figure 6-2 illustrates the pore pressure measured at the middle sensor (4 cm above base).

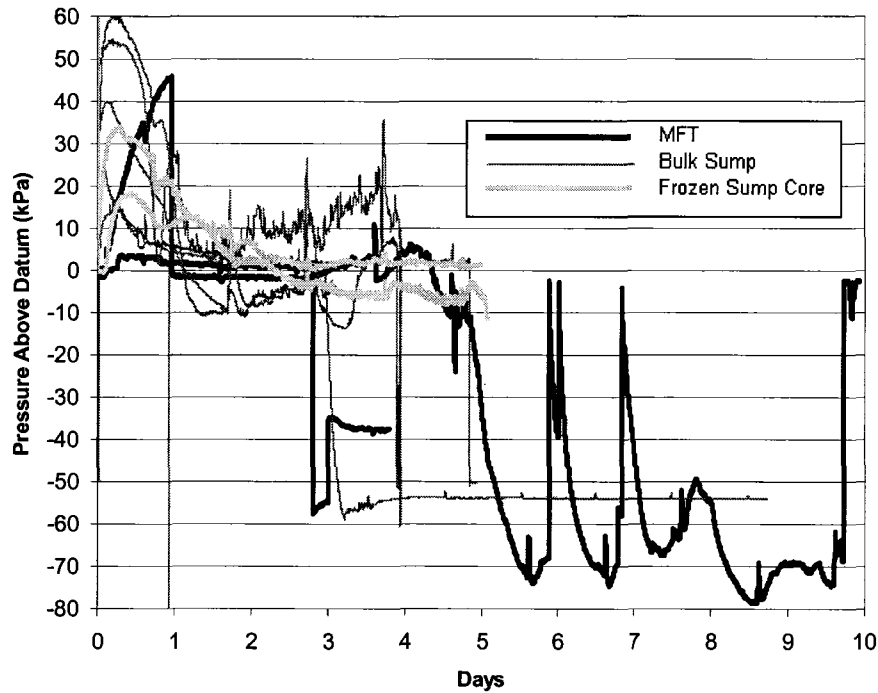


Figure 6-2 - Pore Pressure in Middle Sensor - Full Test Duration

Most tests show a spike in pressure during transient freezing that remains for the duration of some of the tests. Several tests indicate that suction is occurring after the transient freezing period. Figure 6-3 shows the same data as Figure 6-2, but only for the transient freezing period.

The line for test S2T4 in Figure 6-2 that illustrates suction over the period of 5 to 10 days is of interest (also shown in Figure 5-9). By tracking the location of the freezing front for this test, it is noted that the final ice lens likely pushed the sensor downwards as it formed and grew. The sensor was therefore measuring suction within the frozen fringe. The peak suction was approximately 70 kPa, which is the average pressure over the diameter of the pressure sensor, and is the best estimate for the maximum suction developed directly beneath the final ice lens. There are also spikes in the line at 1 day intervals that are probably due to the cold room cooling unit entering a defrost cycle. This increase in the air temperature may cause a shift in the temperature distribution in the sample, a recession of the final ice lens, and a loss of suction.

Figure 6-3, showing the transient freezing period for the middle sensor, indicates that suction was noted at approximately 28 hours for two of the 2 bulk sump tests. Examining the photographs taken during the freezing test, it is found that the ice lens was 4 mm above the sensor at 28 hours. This indicates that the depth of suction penetration may extend only 4 mm below the growing ice lens. However, this is not conclusive since only 2 tests measured suction at the middle sensor. The remaining tests do not indicate suction but do show the same pattern of elevated pore pressure during transient freezing.

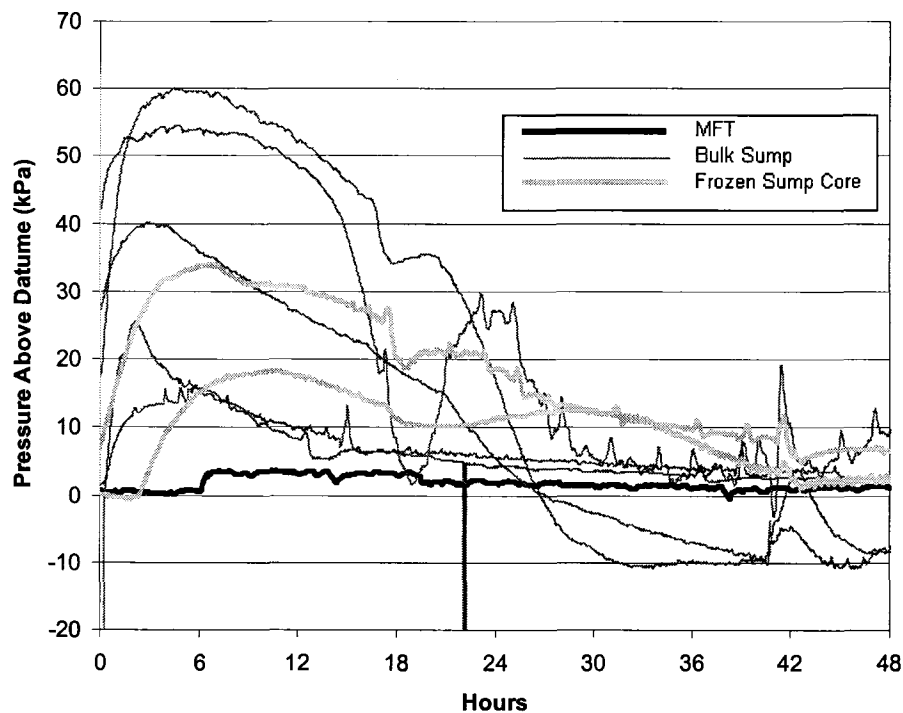


Figure 6-3 - Pore Pressure in Middle Sensor - Transient Freezing

Figure 6-4 and Figure 6-5 present the pore pressure measured at the bottom sensor (0.65 cm above base). Only one test indicated a notable suction. For this same test, no suction was noted at the middle sensor. After the transient freezing stage, the pressure reduces to the datum pressure. It is also noted that the steady pressure obtained after the transient freezing period is often not equal to the initial datum pressure. This may be due to temperature sensitivity of the pressure sensor or a sample response. For example, warming of the air in the cold room during the freezing unit defrost cycle by

approximately 4°C results in a pressure change of 3 kPa. This is likely occurring in the sample as temperature drops during freezing.

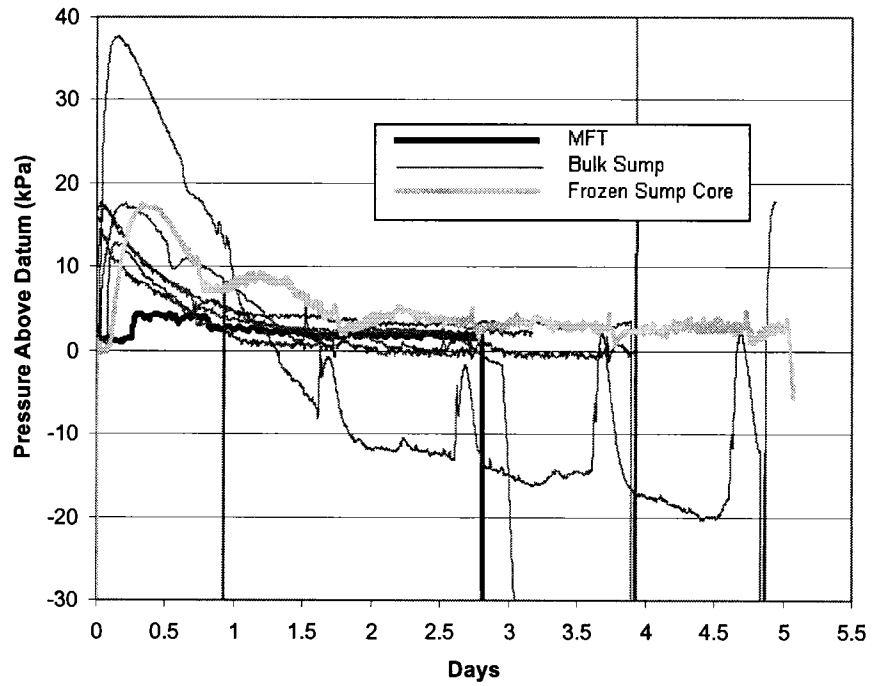


Figure 6-4 - Pore Pressure in Bottom Sensor - Full Test Duration

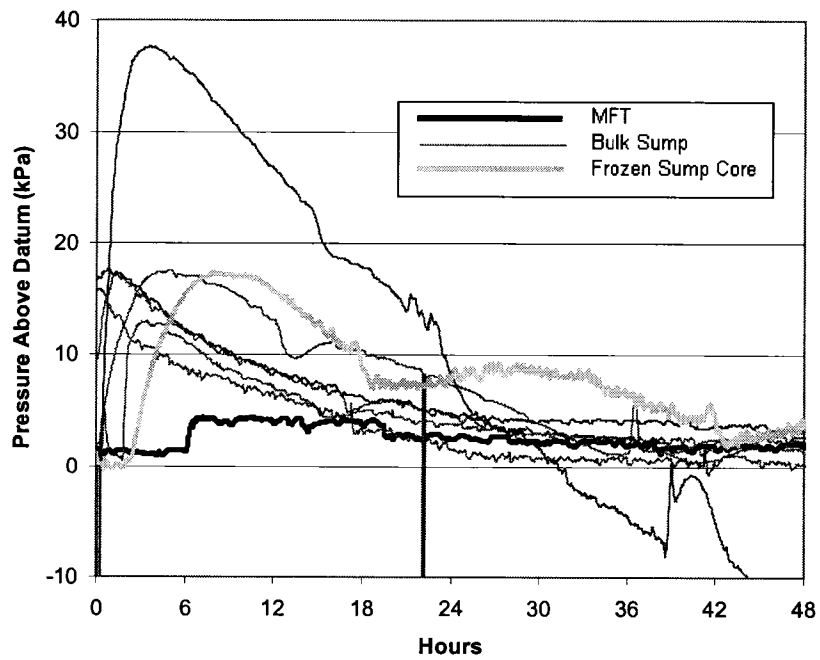


Figure 6-5 - Pore Pressure in Bottom Sensor – Transient Freezing

6.3 Qualitative Observations of Heave and Flow

The common technique to determine the segregation potential in a freezing test is to measure the surface heave or the water inflow rate. This section examines the results of the heave and inflow measurements, and identifies the limitations with applying this technique to high moisture content mine tailings.

Figure 6-6 plots the inflow for all tests. Only the Devon Silt tests that were consolidated to 100 kPa show a net inflow. The third Devon Silt test was not properly consolidated. The extent of its consolidation is unknown. All other tests were not consolidated.

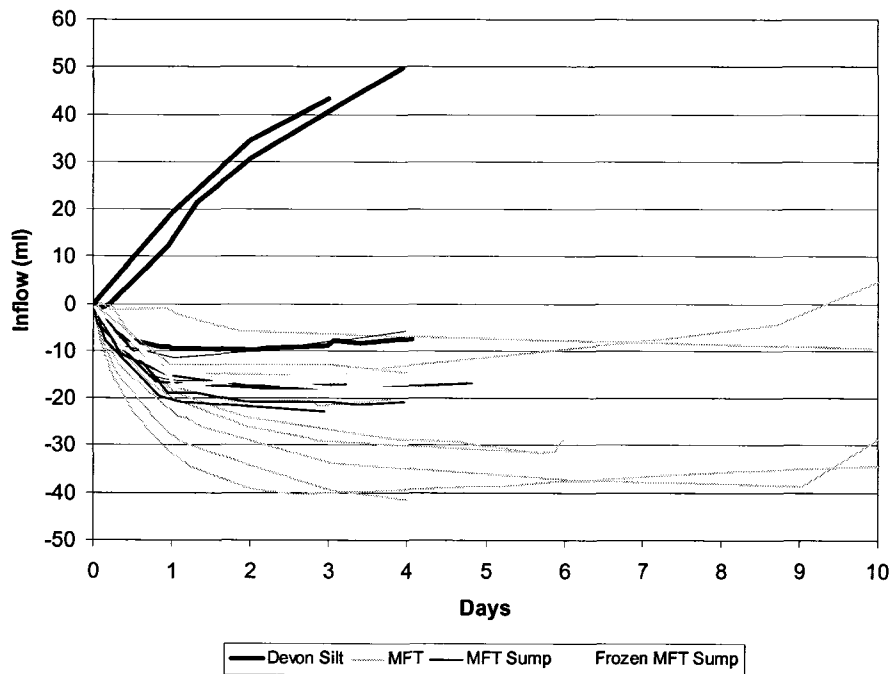


Figure 6-6 - Inflow for All Tests

Figure 6-7 and Figure 6-8 present the surface heave for all the tests. The heave is dramatically greater for the Devon Silt that was consolidated. Heave was negligible for MFT. It appears that the amount of heave may be related to the Liquidity Index of the soil, although more tests at varying LI would be required to prove this hypothesis (See Figure 6-9).

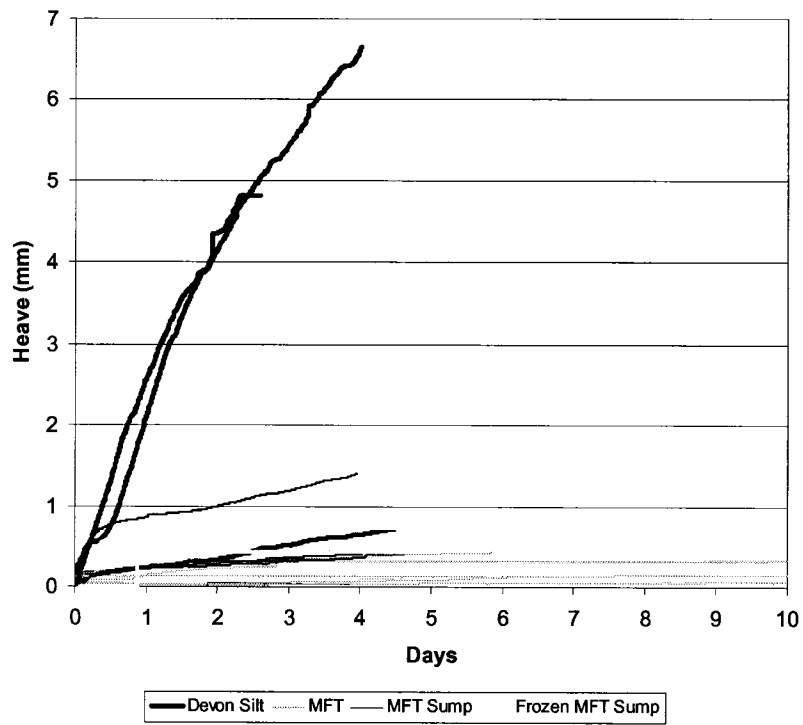


Figure 6-7 - Heave for All Tests - Full Scale

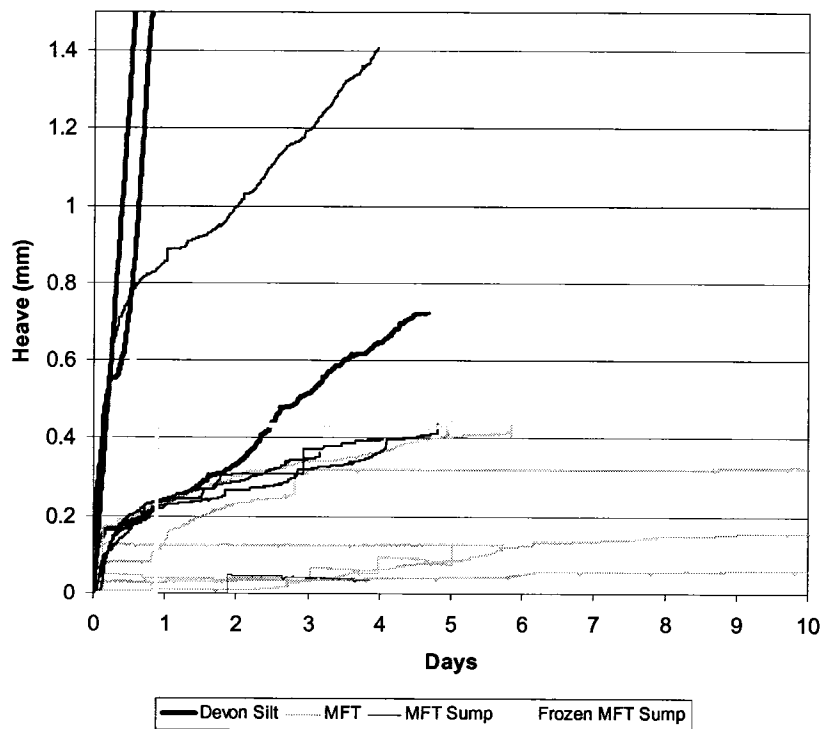


Figure 6-8 - Heave for All Tests - Reduced Vertical Scale

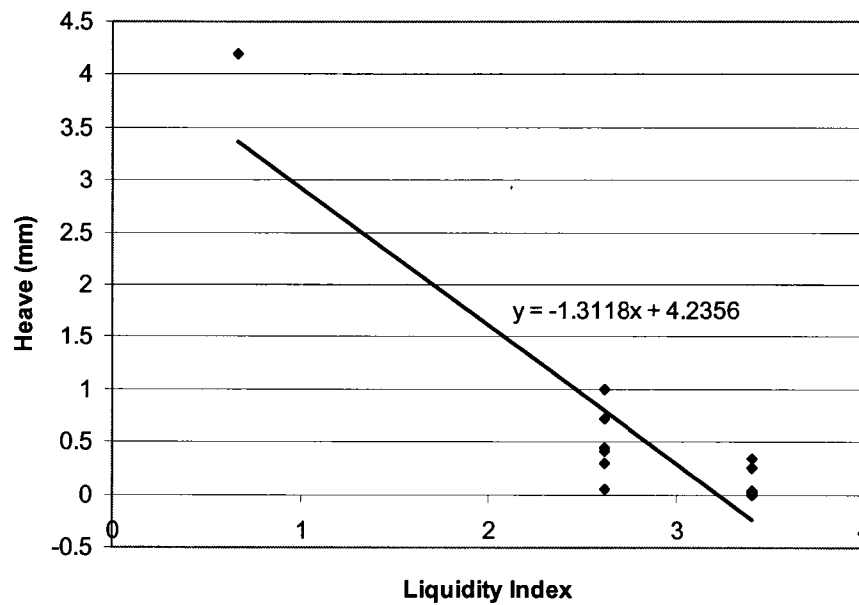


Figure 6-9 - Heave at 2 Days as a Function of Liquidity Index

Figure 6-10 and Figure 6-11 demonstrate the effect of repeated freeze-thaw cycles on the MFT sump material shows that with repeated cycles, the soil transitions from having only outflow during freezing, to having some inflow. Figure 6-11 illustrates that with repeated freeze-thaw cycles, heave increases. Both figures indicate that consolidation of the underlying soil is occurring, and with repeated cycles, the soil is gaining strength while decreasing in void ratio. Consolidation reduces the amount of water available within the soil that can be supplied to the developing ice lens. As the soil is consolidated, some water begins to be drawn from the external supply to meet the demand during freezing. Also, if the soil does not heave, the inflow will be approximately matched by the outflow. The 9% expansion from water to ice will cause a slight net outflow during freezing. As consolidation occurs and the thawed soil strengthens, some heave is possible, and the inflow becomes apparent.

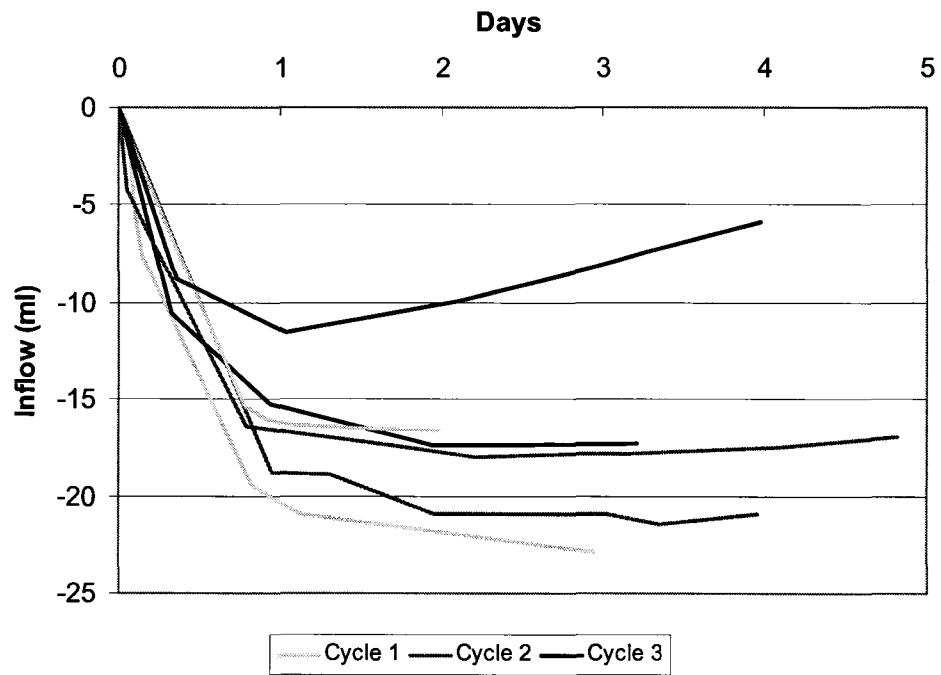


Figure 6-10 - Freeze-Thaw Cycle Affect Upon Inflow – MFT Sump – S3T1 and S3T2

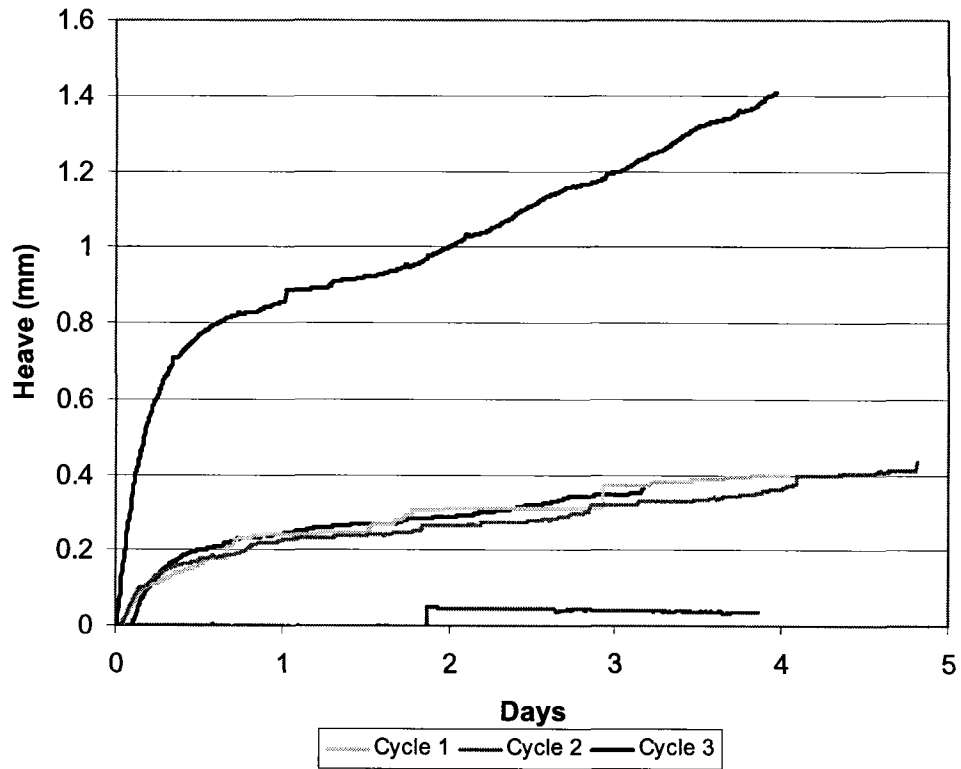


Figure 6-11 - Freeze-Thaw Cycle Affect Upon Heave - MFT Sump – S3T1 and S3T2

For a soil that is incompressible, the heave and inflow measurements are closely matched, as is shown in Figure 6-12. In this figure, the heave is plotted along with the heave determined from the water inflow. The water inflow, increased by 9% due to the phase change expansion of water to ice, yields approximately the same result as the measured heave.

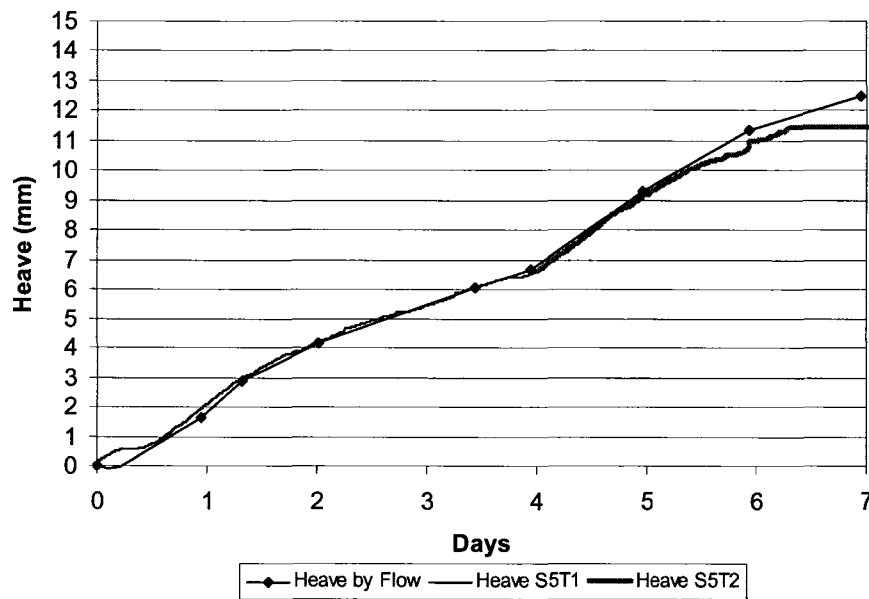


Figure 6-12 - Heave for Test Series 5 – Devon Silt

6.4 Temperature Distribution During Freezing

The temperatures measured within the soil can be used to track the location of the frozen fringe. Figure 6-13 provides an example of this for test S2T4. In the figure, the location of the -0.15°C isotherm, as well as the location of the base of the observed ice lenses, are plotted. The -0.15°C isotherm is the freezing point depression for the pore water from the Suncor MFT, and is the temperature at which ice begins to form in the pore spaces in the MFT. This was found in the laboratory and the details are available in Section 4.3.3 (Hereygers 2006). The temperature where ice can form in needles and lenses, called the segregational freezing temperature, is colder than the frost front temperature (Konrad and Morgenstern 1980). Examining the location of the -0.15°C isotherm and the observed base of the ice lens in Figure 6-13, and using the temperature gradient at these depths for this test, it appears that the segregational freezing temperature is approximately -0.6°C for MFT, and the fringe is approximately 1 cm thick (after 3 days freezing). The

segregational freezing temperature determined from this figure is also plotted in Figure 5.9.

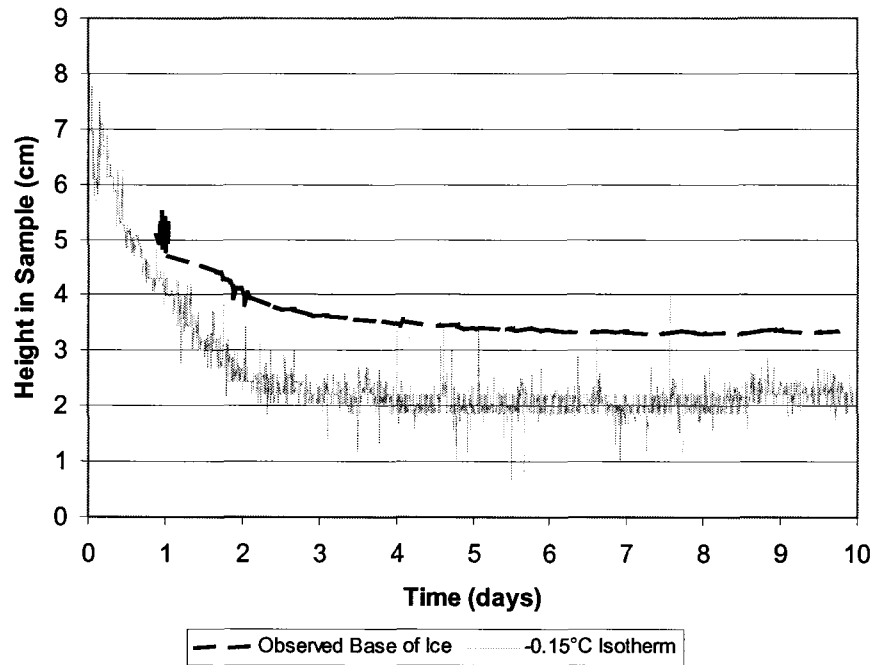


Figure 6-13 - Location of Freezing Point of Pore Fluid and Observed Ice Lens Location During Freezing – Test S2T4

The important parameter obtained from the temperature measurements during freezing is the temperature gradient within the frozen fringe. The fringe encompasses the area between the initial freezing temperature where ice begins to form (-0.15°C for MFT), to the active ice lens (-0.64°C for MFT). In these tests, the fringe was approximately 1 cm thick during steady thermal conditions.

Although the locations of the fringe and ice lenses can be predicted from the temperature measurements, this was found to be unnecessary. When it is assumed that the temperature gradient at the ice lens is equal to the gradient in the fringe, the location of the freezing front is not required (Konrad 1987). Also, if photographs are used, there is no need to locate the freezing front by using the temperature within the soil, since the photographs provide the location of the segregational freezing temperature with greater certainty.

The freezing tests were performed with 4 to 5 thermistors in the soil sample. Plotting the temperature at the location of these thermistors at various times allows the determination of the temperature gradient throughout the sample and especially within the frozen fringe. Figure 6-14 demonstrates one such plot. By knowing the freezing point depression, the location of the freezing front and the temperature gradient at the fringe can be determined from this figure. From Figure 6-14, it can be noted that steady thermal conditions are achieved at approximately 47 hours. This is in accordance with the observations from the photographs, which show the onset of the development of the final ice lens at this time.

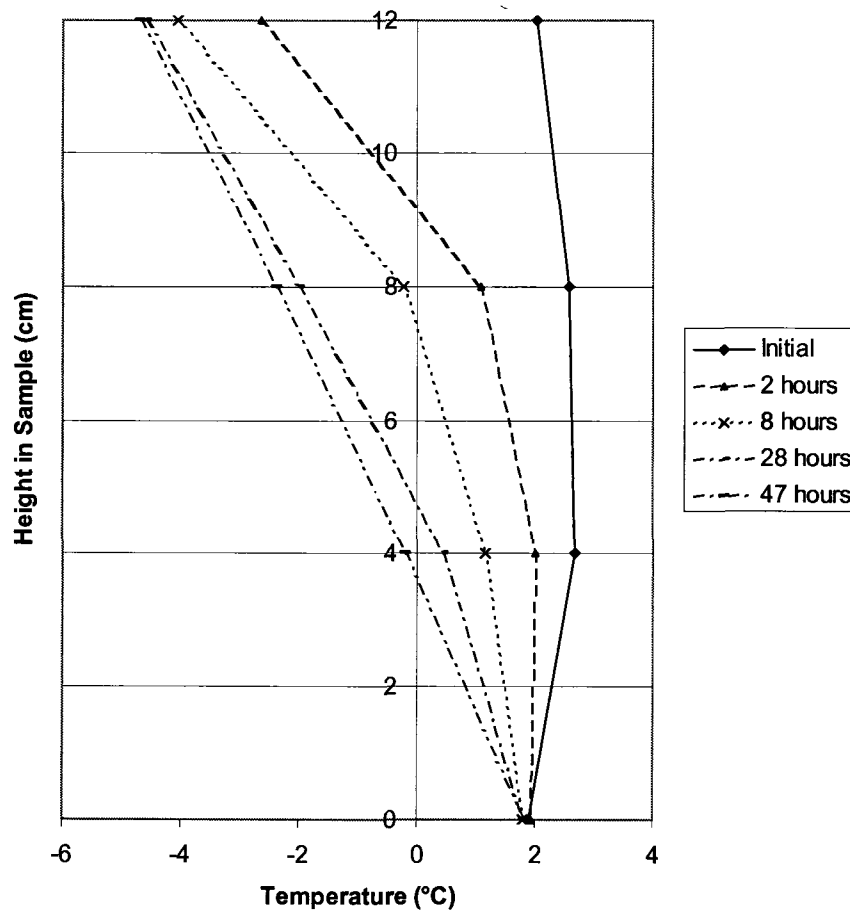


Figure 6-14 - Temperature Distribution During Test – SIT2

Figure 6-15 presents the same data as Figure 6-14, but in a format that is more useful for analysis. Here the temperature gradient is calculated for each third of the sample height. At steady state, all are approximately equal.

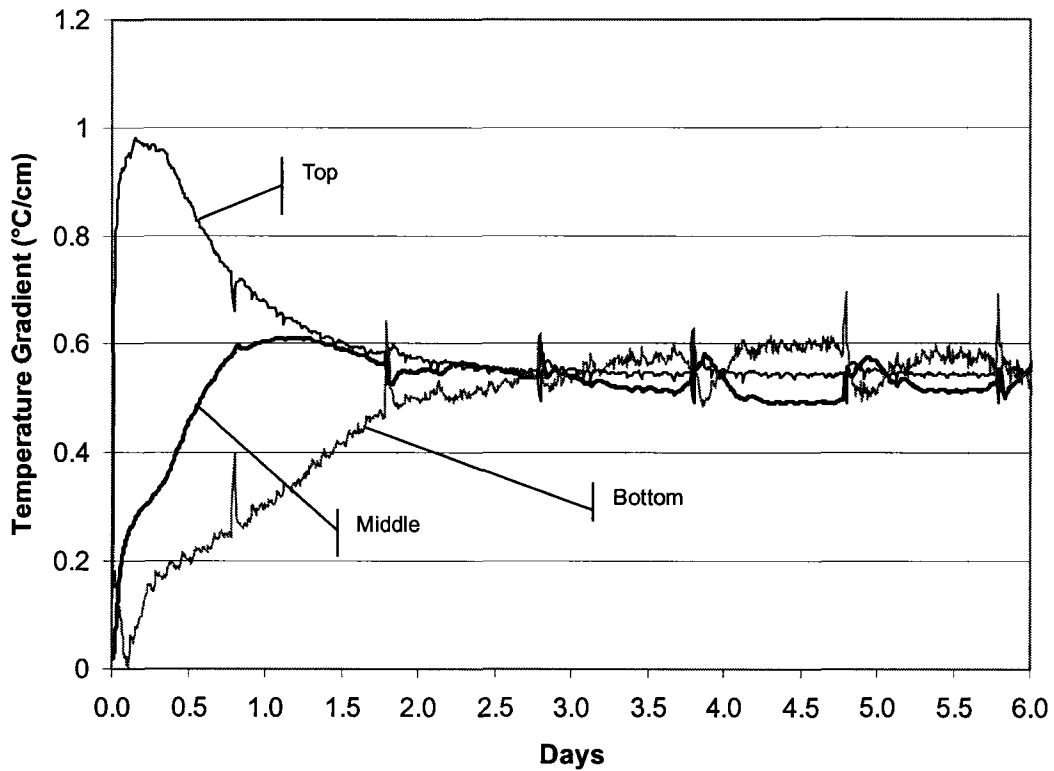


Figure 6-15 - Temperature Gradient During Freezing - Test #2

6.5 Segregation Potential

Methods for determining the segregation potential as well as the results of these methods are presented in this section.

6.5.1 Methods for Determining the Segregation Potential

Several of the methods that can be used to find the Segregation potential, mentioned in Chapter 5, will be more thoroughly discussed in terms of their suitability for high moisture content mine tailings.

6.5.1.1 Surface Heave or Inflow

For a typical incompressible soil, where consolidation of the underlying thawed soil does not occur, the flow of water through the fringe towards the active ice lens is supplied entirely by the external water supply under open drainage conditions. The rate of water arriving from the external supply is therefore equal to the rate flowing through the fringe

and can be used directly to calculate the segregation potential (Equation 5.3). Since there is no consolidation occurring, all water that arrives at the final lens will freeze and cause surface heave. The rate of surface heave is 9% greater than the rate of water arriving at the final ice lens due to the expansion of water during its phase change as it adds to the ice lens. Therefore, the rate of surface heave can be used as input into the equation for determining segregation potential after dividing it by 1.09. These two methods are similar, and yield comparable results.

This method was suitable only for the Devon Silt tests that were consolidated to 100 kPa prior to freezing, and then tested with zero overburden pressure. All other tests exhibited notable consolidation of the unfrozen soil during freezing, resulting in the measurement of only a portion of the heave visually observed via photographs.

6.5.1.2 Final Lens Thickness

Using time-lapse photographs of the final ice lens, the location of the top and bottom of the lens and its thickness are obtained. There are four distinct cases that arise when examining these photographs:

1. The location of the bottom of the ice lens remains fixed while the top of the lens moves upwards.
2. The top of the ice lens remains fixed while the bottom of the lens moves downwards.
3. The top of the ice lens is moving upwards while the bottom is moving downwards.
4. Both the top and the bottom of the ice lens are moving upwards or downwards.

Case 1 is the typical situation for an incompressible soil that exhibits surface heave equal to the rate of water migration to the fringe.

Case 2 reflects when the soil is compressible. Consolidation is occurring and this water is being supplied to the final ice lens while the surface of the sample is not heaving.

In case 3 behaviour the soil is likely exhibiting both heave and consolidation below the final lens.

In Case 4 behaviour it's likely that ice lens growth is occurring at another ice lens simultaneously. This could occur if the final ice lens has not completely blocked the water supply to the frozen soil above the nominal final ice lens.

Figure 6-16 presents the information obtained from the photographs for test S4T1. The locations of the top and bottom of the final ice lens are plotted according to their pixel coordinate. The final lens thickness is calculated from these and is also plotted along with a linear trendline used to determine the average final ice lens growth rate. The entire ice lens is moving downwards. It is thought that the top of the ice lens can be assumed to be stationary and the lens thickness increased to account for growth at another ice lens. This is a hypothesis that cannot be proven yet.

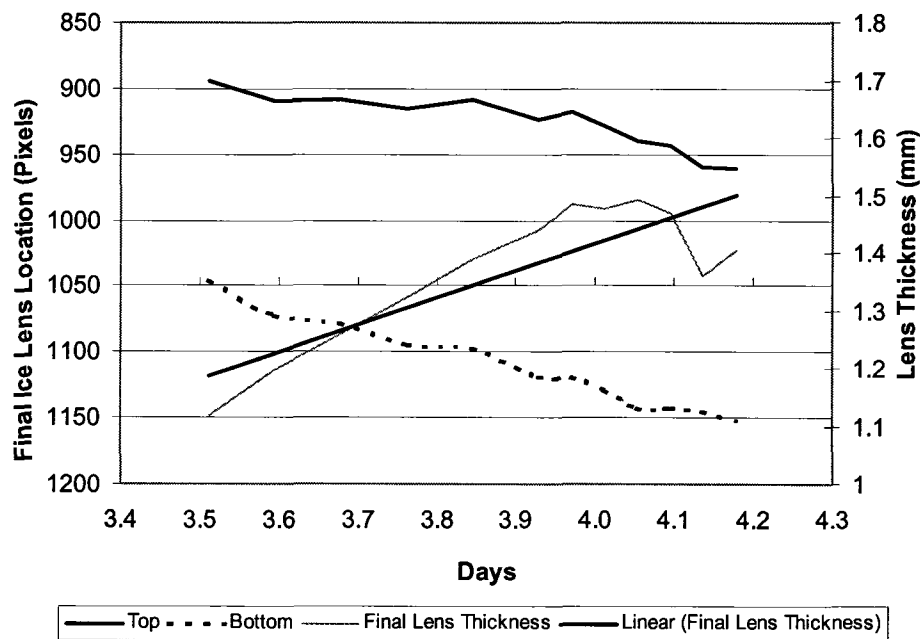


Figure 6-16 - Final Ice Lens Thickness - S4T1

Figure 6-17 presents the final ice lens growth rate for three tests using Devon Silt. The final ice lens growth rate is different for the S1T1b and S5 tests. Tests S5T1 and S5T2

were consolidated to 100 kPa. A problem with the consolidation process for test S1T1b resulted in insufficient consolidation for the test. It is not known to what value this sample was consolidated except that it is likely less than for tests S5T1 and S5T2. The S5 tests also had a lower temperature gradient (See Table A-1 in Appendix A). These factors are likely the cause of the difference in the ice lens growth rate between the two test series.

Also presented in Figure 6-17 are the results from recent work with Devon Silt (Xia et al. 2005). These tests were prepared in the same manner as the Devon Silt tested in this work, and used varying temperature gradients. Note that the results are similar to the tests performed as part of this work, and that there is considerable variation between the ice lens growth rates.

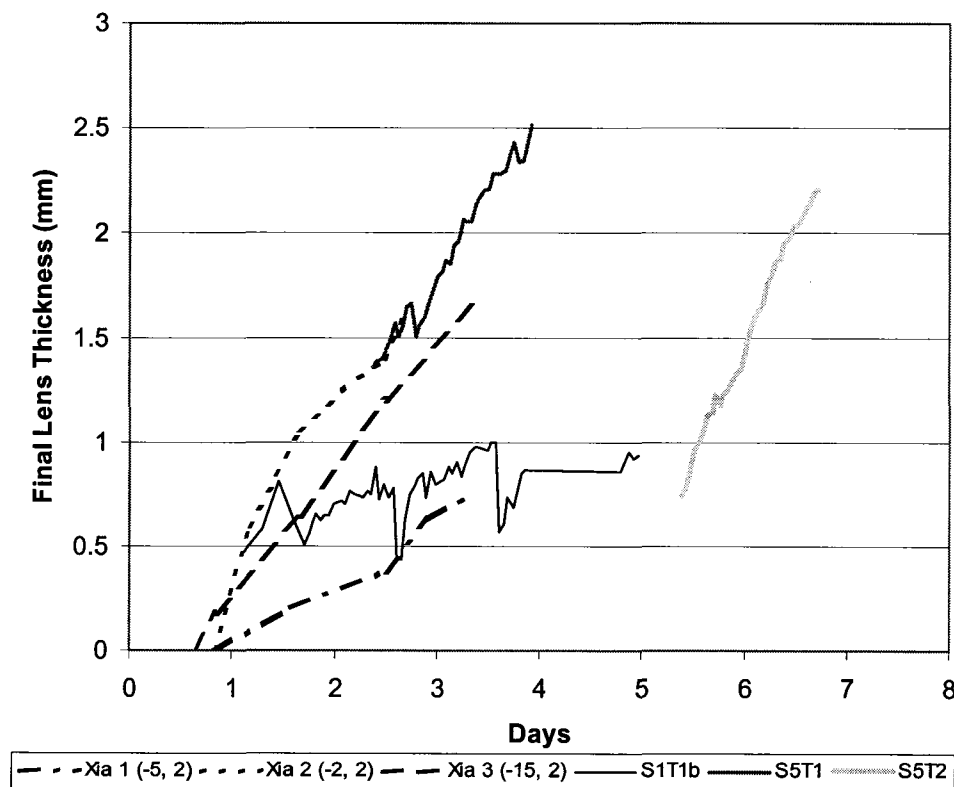


Figure 6-17 - Final Lens Thickness for Devon Silt

Presenting all the final ice lens growth rates for tests where the photographs were of sufficient quality allows a better understanding of the water transfer rate through the

frozen fringe for each soil type (see Figure 6-18). The temperature gradient also affects the ice lens growth rate.

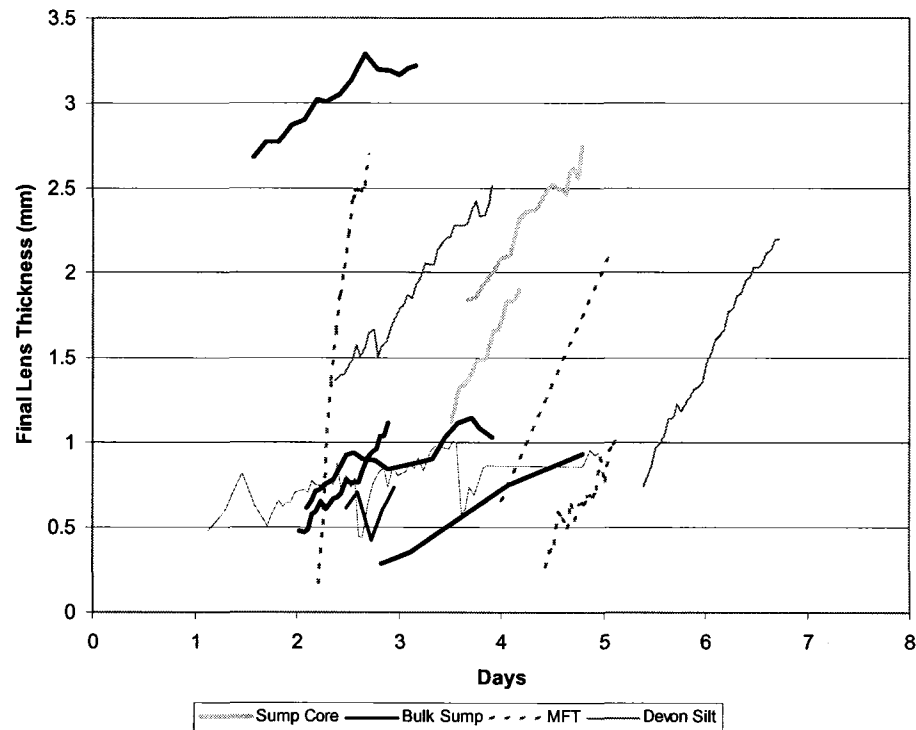


Figure 6-18 - Final Ice Lens Thickness - All Tests

Figure 6-18 is a useful indication of the frost susceptibility of the group of soils tested when the temperature gradient is constant. Freezing temperatures and temperature gradients varied slightly between test series. The following observations can be made from these results:

- The final ice lens growth rate for the MFT bulk sump samples is similar for all tests.
- The ice lens growth rate for MFT is rather variable. Although the material properties did not change, it is known that the temperature gradient was altered between some of these tests.
- The ice lens growth rate for the MFT sump frozen core is higher than for the bulk sump material. One difference is that the previous natural freezing of the soil, and

the macrostructure created in the soil during this freezing, increased the hydraulic conductivity and density of the soil allowing a higher ice lens growth rate.

Observation of the final ice lens can provide an important understanding of the soil behaviour and of the validity in choosing a method of analysis to determine the segregation potential from a freezing test.

6.5.1.2.1 Validity of Final Ice Lens Thickness for Determining Segregation Potential

Several factors contribute to error in the use of time-lapse photography of the final ice lens to assist in determining the segregation potential.

- Photographs were taken through a macro lens, which limits the field of view to approximately 2.2 by 1.5 cm. This represents only a small portion of the final ice lens in the freezing sample and requires the assumption that the growth rate observed in the field of vision is representative of the entire ice lens.
- The ice lens growth at the cell wall may be influenced by the external room temperature. Efforts to limit this were taken by providing a dead air space between a glass viewport and the cell wall, by maintaining the air temperature in the room near 0°C, and wrapping the test cell with insulation.
- The scale placed between the cell wall and the soil was made of steel, and may impact the growth of the final ice lens nearby by conducting heat better than the surrounding soil and ice.

For tests S5T1 and S5T2 with Devon Silt, in which the segregation potential could be determined by using the measured surface heave and inflow measurements, the time-lapse photography method was also performed to compare the results and establish the validity of using this method. Table 6-2 lists the results from these tests.

Table 6-2 - Comparison of SP Values for Test Series 5 Using Various Calculation Methods

Test	Method	SP ($\text{cm}^2 \cdot \text{s}^{-1} \cdot \text{°C}^{-1}$) $\times 10^{-6}$
S5T1	Final Ice Lens Photographs	2.1
	Surface Heave	3.3
	Water Inflow	3.6
S5T2	Final Ice Lens Photographs	3.1
	Surface Heave	4.6
	Water Inflow	4.5

The values for segregation potential using the time-lapse photography method and the conventional heave or inflow methods are similar, with the time-lapse photography method giving slightly lower SP values. Variations in segregation potential of less than one order of magnitude are considered acceptable (Sego 2006).

6.5.1.3 Ice Penetration Rate

This method was suitable only when the final ice lens had formed, and when the top of the ice lens was stationary as it grew. It is better to use the final ice lens thickness, which provides a better indication of the water transfer rate to the final ice lens.

6.5.1.4 Final Moisture Content

This method was applied for several tests that had an accurate final moisture content distribution determined by segmenting the soil in its frozen state. The accuracy of this method is limited, due to assumptions required for the calculation. In determining the segregation potential with this method, the solids content and thickness of the final ice lens is measured. The time from the first appearance of the ice lens, or the onset of steady thermal condition, to the end of freezing is used as the ice lens formation period. It is assumed that the flow to the ice lens is steady during this period. Using this information, the rate of water flow arriving at the final ice lens is determined.

6.5.2 Segregation Potential Results

Table 6-3 lists the segregation potential for all tests. Following the table are plots presenting this data.

Table 6-3 - Segregation Potential for All Tests

Test	Cycle	Material	SP ($\text{cm}^2\text{s}^{-1}\text{.}^\circ\text{C}^{-1}$)	Period (days)		Method	Confidence
				Start	End		
Xia1	1	Devon Silt	4.6E-07			Heave/Flow	
Xia2	1	Devon Silt	4.4E-06			Heave/Flow	
Xia3	1	Devon Silt	4.8E-07			Heave/Flow	
Xia4	1	Devon Silt	4.4E-07			Heave/Flow	
Xia5	1	Devon Silt	2.7E-07			Heave/Flow	
Xia6	1	Devon Silt	2.4E-07			Heave/Flow	
S1T1b	1	Devon Silt	4.2E-07	1	5	Final Lens Thickness	High
S5T1	1	Devon Silt	2.1E-06	2.4	3.9	Final Lens Thickness	High
S5T1	1	Devon Silt	3.3E-06	2	4	Heave	High
S5T1	1	Devon Silt	3.6E-06	2	4	Inflow Graph	High
S5T2	1	Devon Silt	3.1E-06	5.4	6.7	Final Lens Thickness	High
S5T2	1	Devon Silt	4.6E-06	5	7	Heave	High
S5T2	1	Devon Silt	4.5E-06	5	7	Inflow Graph	High
S1T2	1	MFT	6.0E-05	0	1	Slope of frost penetration	Low
S1T2	1	MFT	5.0E-05	0	1.25	Slope of frost penetration	Low
S1T3	1	MFT	2.8E-05	0	2	Slope of frost penetration	Low
S1T4	1	MFT	1.4E-05	2.2	2.7	Final Lens Thickness	High
S1T4	2	MFT	4.4E-05	2	5	Slope of frost penetration	Low
S1T4	2	MFT	1.1E-06	4	5	Final Lens Thickness	Low
S2T2	1	MFT	2.8E-06	2	12	Final Moisture Content	Medium
S2T2	1	MFT	1.4E-06	3	12	Inflow Graph	Low

Test	Cycle	Material	SP ($\text{cm}^2\text{s}^{-1}\text{.}^\circ\text{C}^{-1}$)	Period (days)		Method	Confidence
				Start	End		
S2T2	1	MFT	2.4E-06	4	5	Final Lens Thickness	Medium
S2T4	1	MFT	5.2E-06	2	4	Slope of frost penetration	Low
S2T4	1	MFT	8.0E-04	0	2	Slope of frost penetration	Low
S2T4	1	MFT	2.2E-04	0	4	Slope of frost penetration	Low
S2T4	1	MFT	3.7E-05	0	6	Slope of frost penetration	Low
S3T1	1	MFT Sump	2.8E-06	1	3	Slope of frost penetration	Medium
S3T1	1	MFT Sump	2.5E-07	1	3	Final Lens Thickness	Medium
S3T1	2	MFT Sump	4.1E-07	2	4	Final Lens Thickness	High
S3T1	3	MFT Sump	6.2E-07	2	3	Final Lens Thickness	High
S3T1	3	MFT Sump	8.5E-07	2	3	Slope of frost penetration	Low
S3T2	1	MFT Sump	1.3E-06	2	3	Final Lens Thickness	Medium
S3T2	1	MFT Sump	1.9E-06	2	3	Assumption for above case	High
S3T2	2	MFT Sump	5.9E-07	3	5	Final Lens Thickness	High
S3T2	3	MFT Sump	5.7E-07	2	4	Water Inflow	High
S4T1	1	MFT Sump Core	2.6E-06	4.6	5	Final Lens Thickness	High
S4T2	1	MFT Sump Core	1.3E-06	3.7	4.8	Final Lens Thickness	High

Figure 6-19 presents the segregation potential values for Devon Silt. The plot has been divided into three areas. In area A, the results of previous work by Xia are plotted. His tests were performed one year before this current work, and used the same equipment (Xia 2006). The samples in his tests were prepared with non-saline water, consolidated to

100 kPa (or to the overburden pressure, if greater), and frozen under various overburden pressures.

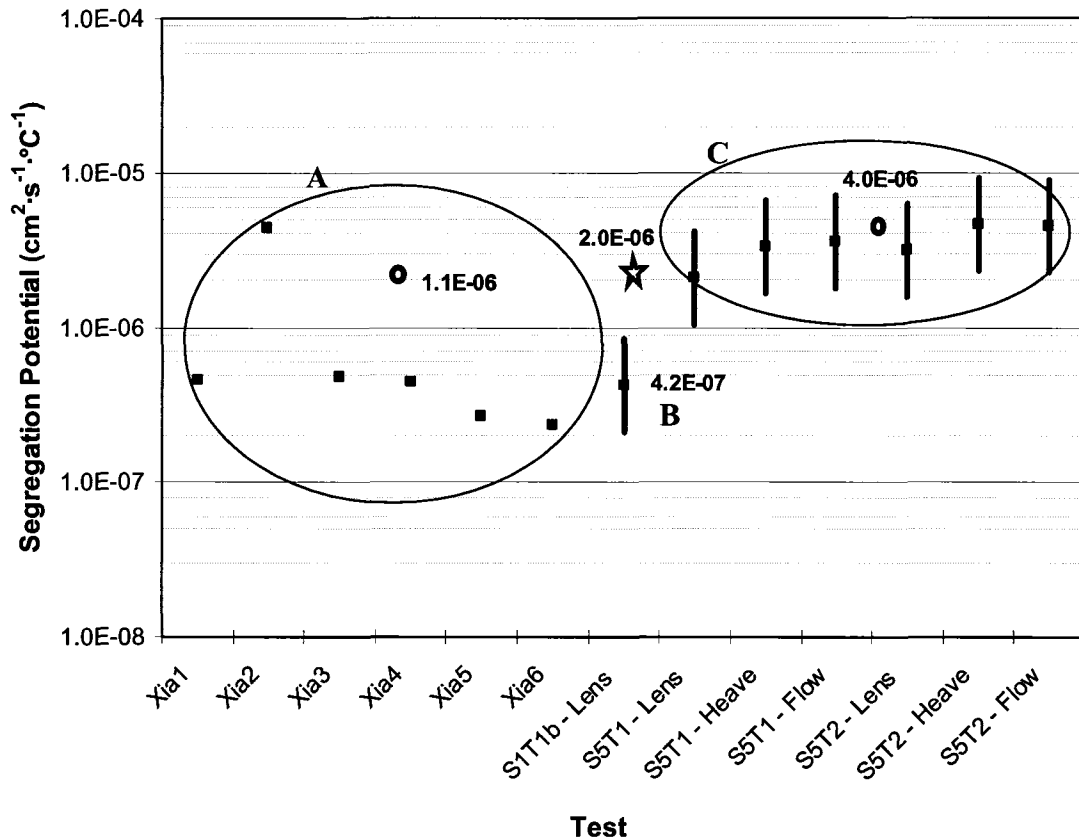


Figure 6-19 - Segregation Potential of Devon Silt

Test S1T1b, shown in area B, was performed on a sample that did not receive proper consolidation due to an error in the consolidation stage (Point 4.2E-07). Area C contains the Series 5 tests, performed on samples that were consolidated to 100 kPa.

The variation bars shown in the figure represent the confidence in the measurement, due to factors such as photograph quality, test operation, or validity of the analysis method. The size of the bar indicates high, medium, or low confidence. The length of the bars is arbitrary, and is only meant to serve as a visual clue to the accuracy of the measurement. Only the best readings were used in determining the average segregation potential, shown in Figure 6-19 with a star.

Of interest in Figure 6-19 is the fact that the segregation potential calculated by the final ice lens growth rate is approximately equal to the value found by heave or flow. Also, all tests are within one order of magnitude. There are some discrepancies between identical tests, such as Xia 1-3. In general, all results are quite similar.

Figure 6-20 illustrates the segregation potential for the Suncor Pond 2/3 MFT tested. Five tests, some analyzed using different methods, are plotted with the average labeled (shown with a 0). Each test is grouped together by a circular shape. There is considerable variation between these tests, likely due to the range of methods used before the time lapse-photography method was discovered and special attention was paid to photographing the final lens to ensure its accuracy. The average for the S1T2 tests only considered the third measurement, as the other two were not at steady state.

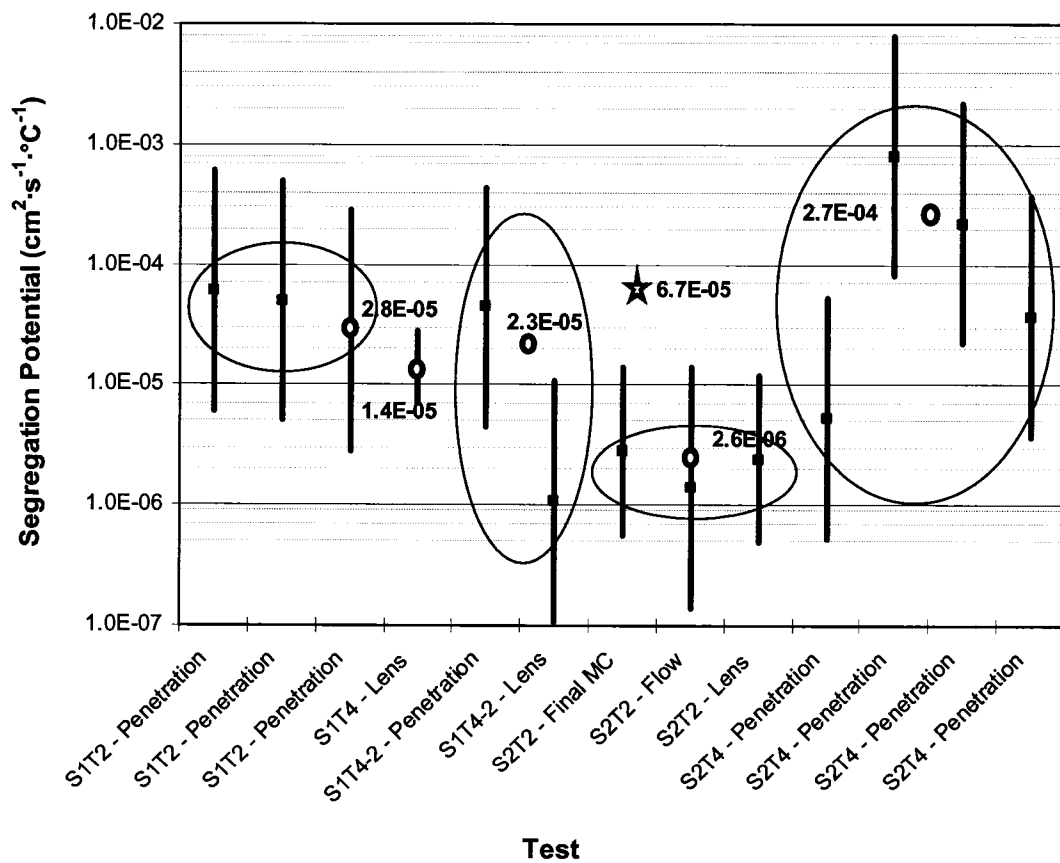


Figure 6-20 - Segregation Potential of MFT

Figure 6-21 contains the calculation of the segregation potential for the bulk samples from the Syncrude SWSS sump. These results have less variability than the MFT results in Figure 6-20. Due to the realization that the final ice lens method would provide the best results, the author focused on ensuring that quality photographs were obtained.

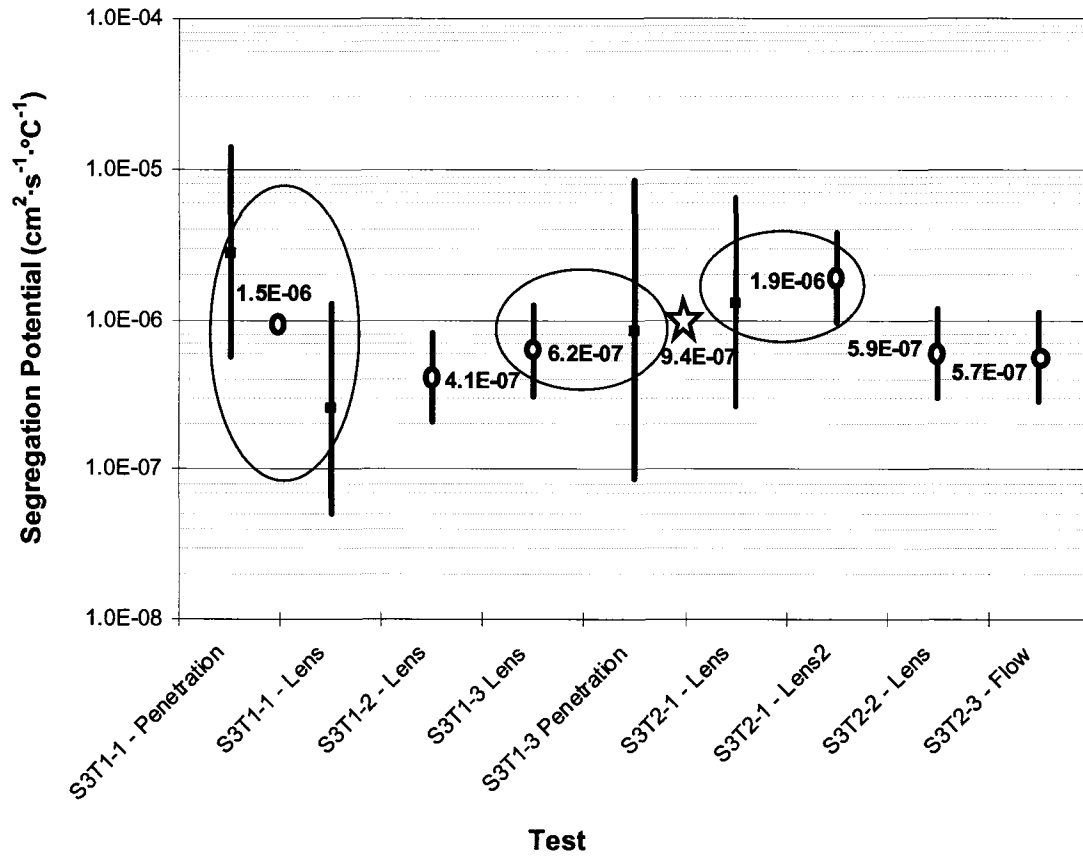


Figure 6-21 - Segregation Potential of MFT Bulk Sump

For the bulk sump material, the effect of multiple freeze-thaw cycles was studied. There was no observable increase or decrease for the SP with subsequent cycles. Konrad (1989), found that multiple freeze-thaw cycles can have two effects on the segregation potential. When the freezing front advances into fresh, never before frozen soil, the segregation potential increases. This is due to the higher void ratio in the virgin material. For a freezing front that remains in previously frozen soil, the segregation potential decreases with successive freeze-thaw cycles. Figure 6-22 and Figure 6-23 illustrate the ice lens advance for the S3T1 and S3T2 tests for multiple freeze-thaw cycles.

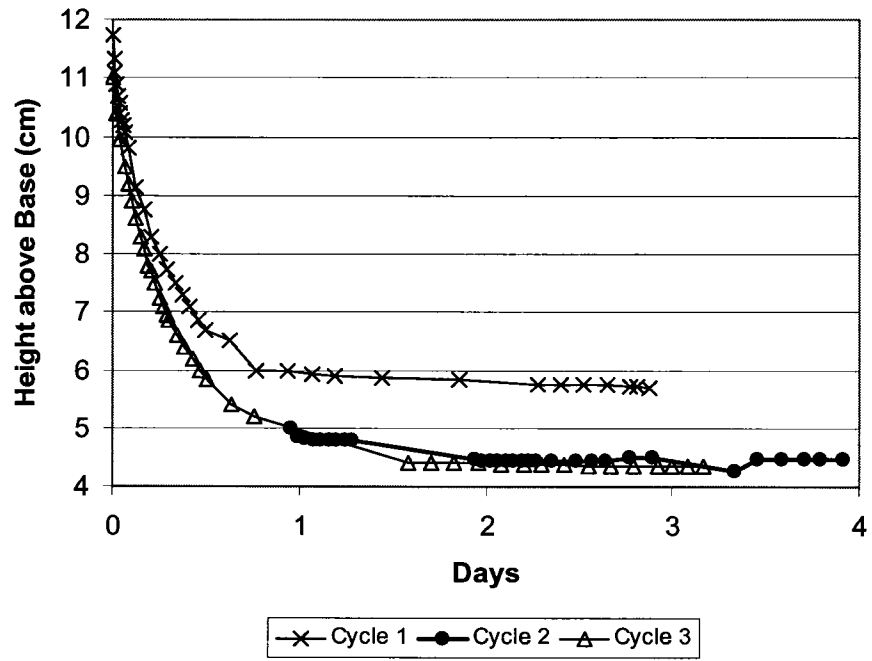


Figure 6-22 - Ice Lens Penetration - S3T1

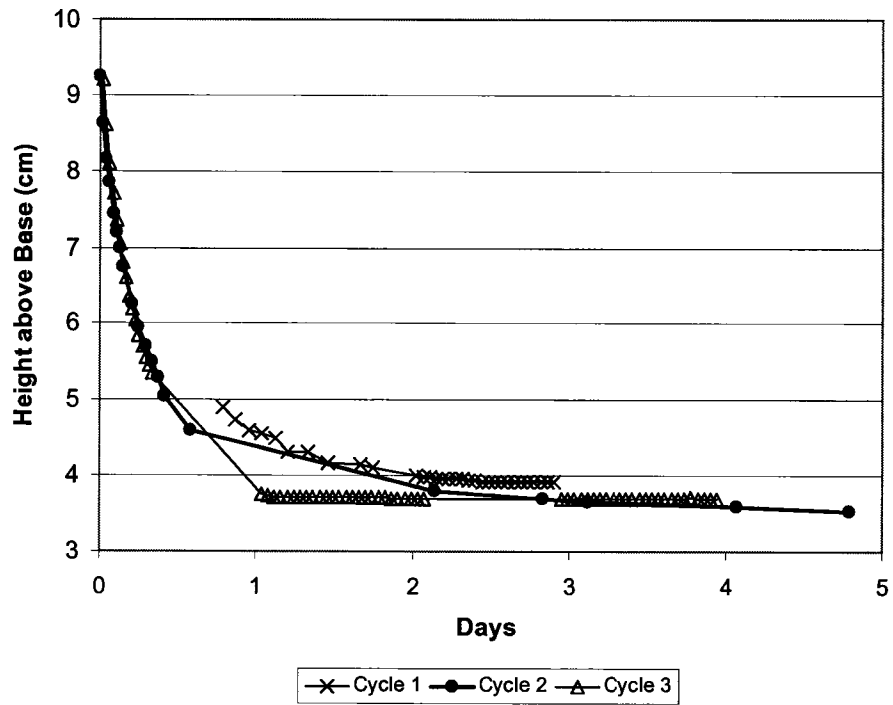


Figure 6-23 - Ice Lens Penetration - S3T2

Based on the plots shown in Figure 6-22 and Figure 6-23, it would be expected that the segregation potential should have increased since the freezing front advanced into fresh material for both tests. However, Konrad's work was based on overconsolidated, non-compressible soils. It is known that the bulk sump material used in S3T1 and S3T2 did consolidate during freezing, thus decreasing the void ratio of the unfrozen soil beneath the final ice lens. This is similar to the void ratio reduction due to the freeze-thaw, hence the segregation potential decreased.

Figure 6-24 shows the segregation potential for the frozen core samples from the Syncrude SWSS sump. Following this, the average segregation potential for all test materials is plotted in Figure 6-25.

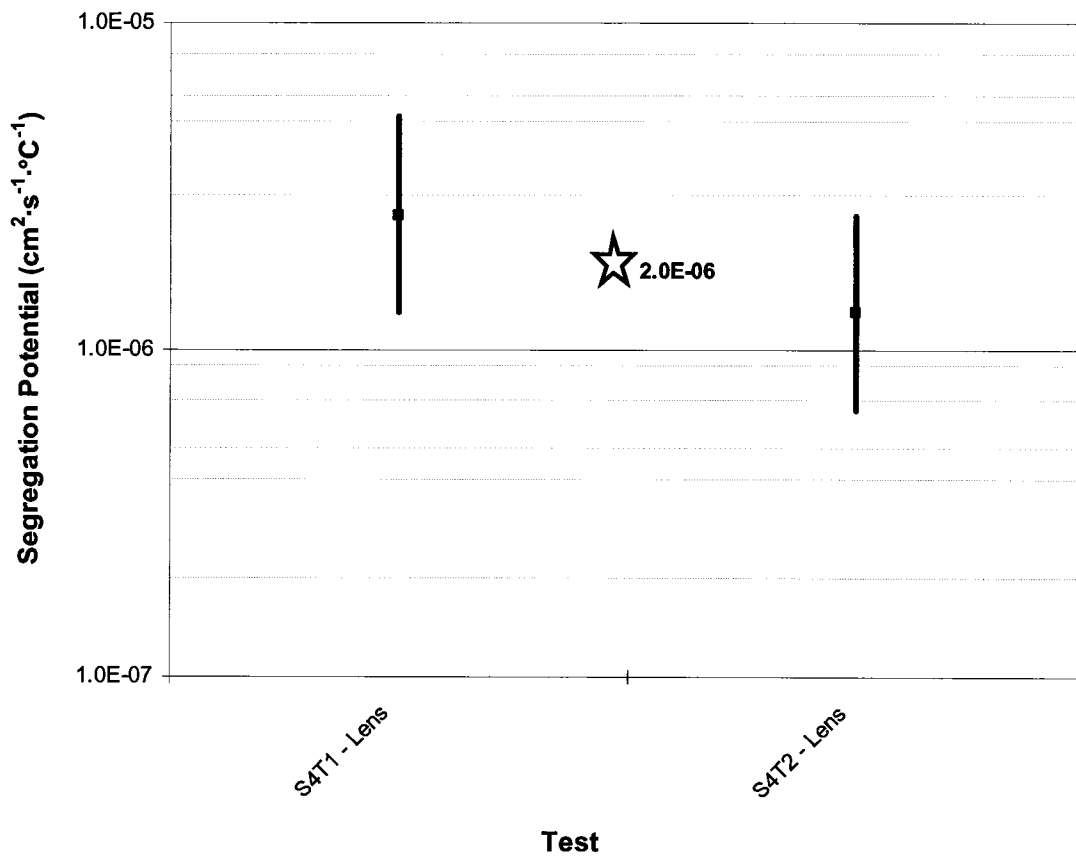


Figure 6-24 - Segregation Potential of MFT Sump Frozen Core

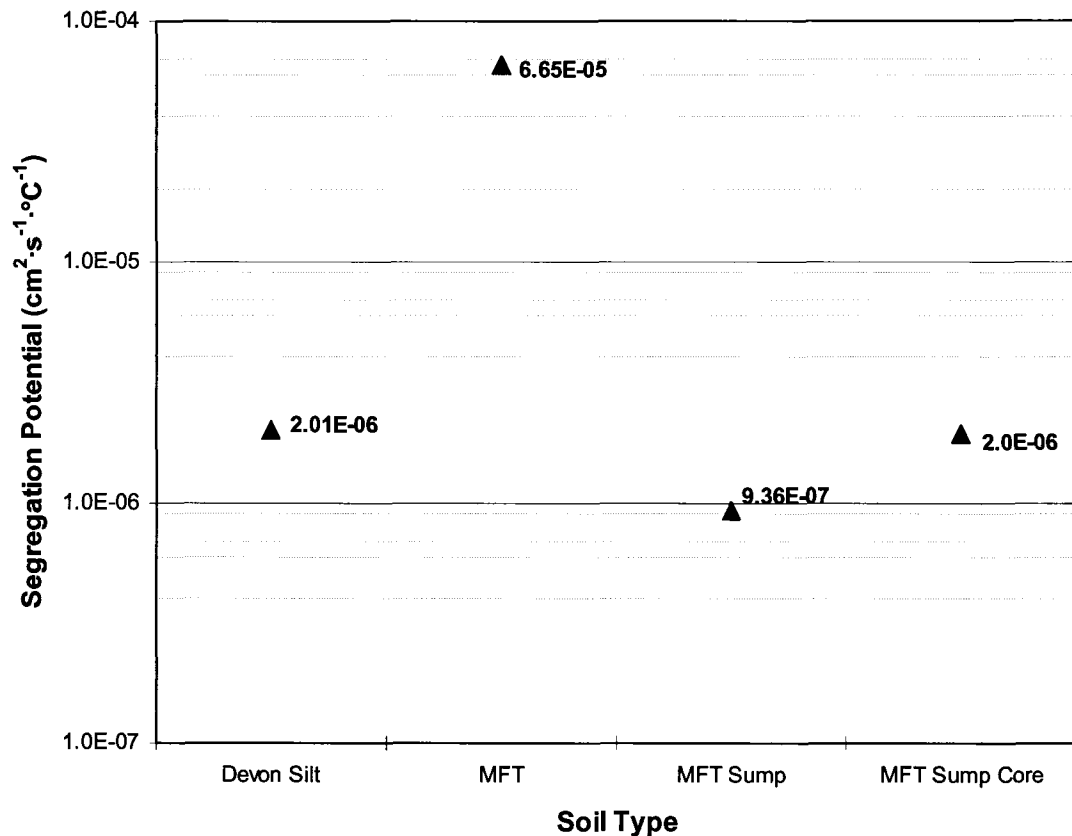


Figure 6-25 - Average Segregation Potential of All Soils Tested

It is of interest to note that the segregation potential of the Devon Silt, the MFT sump, and the frozen MFT sump cores are approximately equal. However, the segregation potential of the MFT is much greater.

6.6 Solids Content Distribution After Freezing

The solids content was determined for several of the freezing tests. Figure 6-26 presents the solids content for the MFT tests. Both S1T3 and S1T4 were obtained after the sample had been through two freeze-thaw cycles. Following the final thaw, the samples were then rapidly frozen from the bottom with liquid nitrogen and were then sectioned with a diamond saw. Sample S2T2 was frozen for one 12-day cycle, and was then placed in a freezer without allowing thaw. The sample was sectioned with a diamond saw in the same manner as the S1 tests.

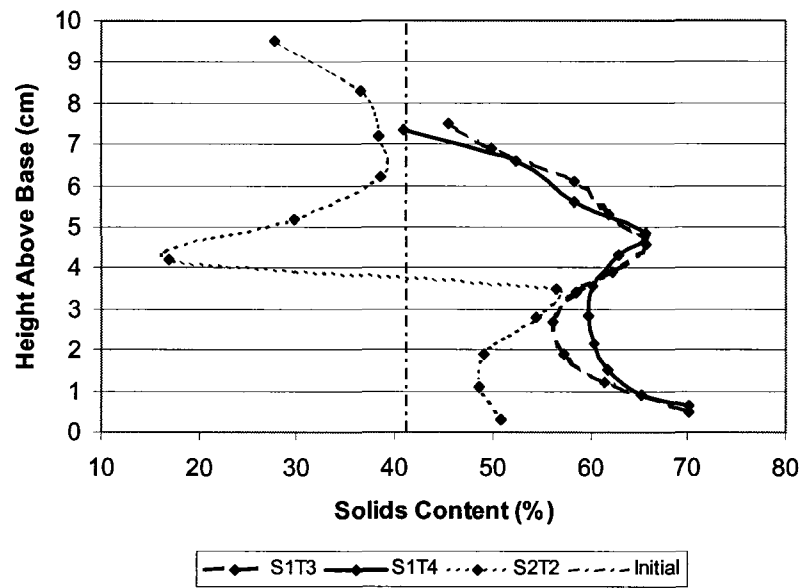


Figure 6-26 - Solids Content After Freezing for MFT

Figure 6-26 shows that all test data exhibit a similar shape. Above the final ice lens (4-5 cm), the solids content decreases towards the surface. For the S1 tests, this is due to the consolidation of the soil peds during freezing. Since the sample was thawed, and then frozen again before determining the solids content, the peds were allowed to collapse and the ice lenses melted and drained towards the surface. The collapsed peds caused an increase in the solids content with depth due to the greater self-weight, and to the more extensive ped formation near the final ice lens.

For the S2 test where there was no thaw cycle, the water from the ice lenses was not allowed to drain, giving a decrease in solids content due to the ice lens near the 4 cm depth. This test still exhibits a decrease in solids content near the surface but the cause is unknown.

Below the final ice lens, all tests show both an increase in solids content above the initial condition, and a “C” shape. The shape of this portion of the curve is of interest. It was expected that the greatest solids content would be immediately below the final ice lens due to the consolidation from suction near the lens. What was not expected was the increase in solids content at the base of the sample at the drainage boundary. Note that the shape of this curve is analogous to the shape of a pore pressure distribution in a soil

layer that has experienced an increase in pore pressure, with top and bottom drainage, and has been allowed to partially dissipate the excess pore pressure. Two processes are likely responsible here:

- The samples did not heave. The volume change due to the expansion of water to ice was constrained resulting in an increase in pore pressure in the thawed soil. This increase in pore pressure was allowed to dissipate near the drainage boundary at the base, increasing the solids content near the boundary. All the excess pore pressure had not yet dissipated when the test was terminated.
- Consolidation beneath the ice lens occurred, attracting water to the ice lens from the thawed soil, and increasing the solids content.

Finally, the S1 tests that experienced thaw cycles have increased in solids content beneath the final ice lens to a higher degree than the S2 test that was not thawed. This may be due to the extra time for pore pressure dissipation that the S1 tests were allowed while they were left in a thawed state.

Figure 6-27 presents the solids content for the MFT sump bulk sample tests. These results were obtained by scooping the thawed material from the test cell after the sample had been through one freeze-thaw cycle. As in Figure 6-26, there is an increase in solids content with depth down to the final ice lens (4 cm). The greatest increase in solids content is below the final ice lens. Sampling by hand is a much cruder method of determining the solids content //compared with using a diamond saw to section a frozen sample, hence the conclusions made in interpreting Figure 6-27 must be more general than were made for Figure 6-26.

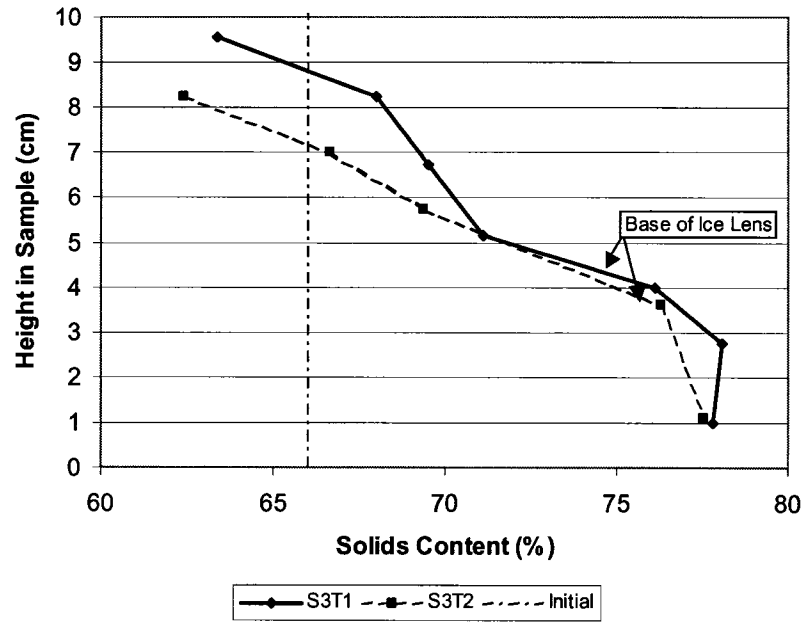


Figure 6-27 - Solids Content After Freezing for MFT Sump - Bulk Sample

The solids content for the frozen core from the MFT sump tests are given in Figure 6-28. These cores were taken from different depths, but all had an initial solids content of approximately 62% ($\pm 2\%$). The shapes of the curves are similar to those shown in Figure 6-27.

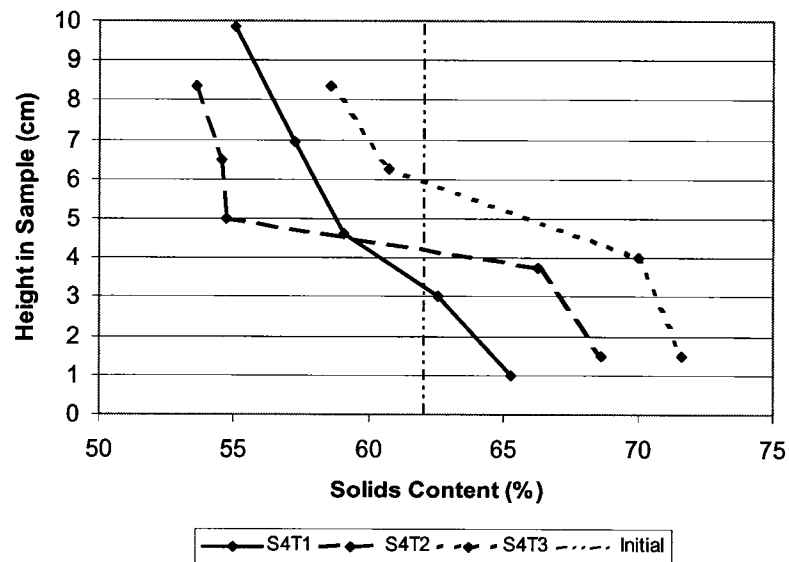


Figure 6-28 - Solids Content After Freezing for Frozen Core from MFT Sump

The solids content from S5 (Figure 6-28) was unique in that it shows a uniform distribution after freezing. In this test, two freezing cycles were performed so that there

was more ice lensing throughout the sample, down to about 3 cm height. After freezing, the consolidation pressure was reapplied to close the lenses that remained open due to friction with the wall of the cell. This allowed water to drain away from the peds, and 6% thaw strain resulted. The initial solids content prior to freezing was not measured.

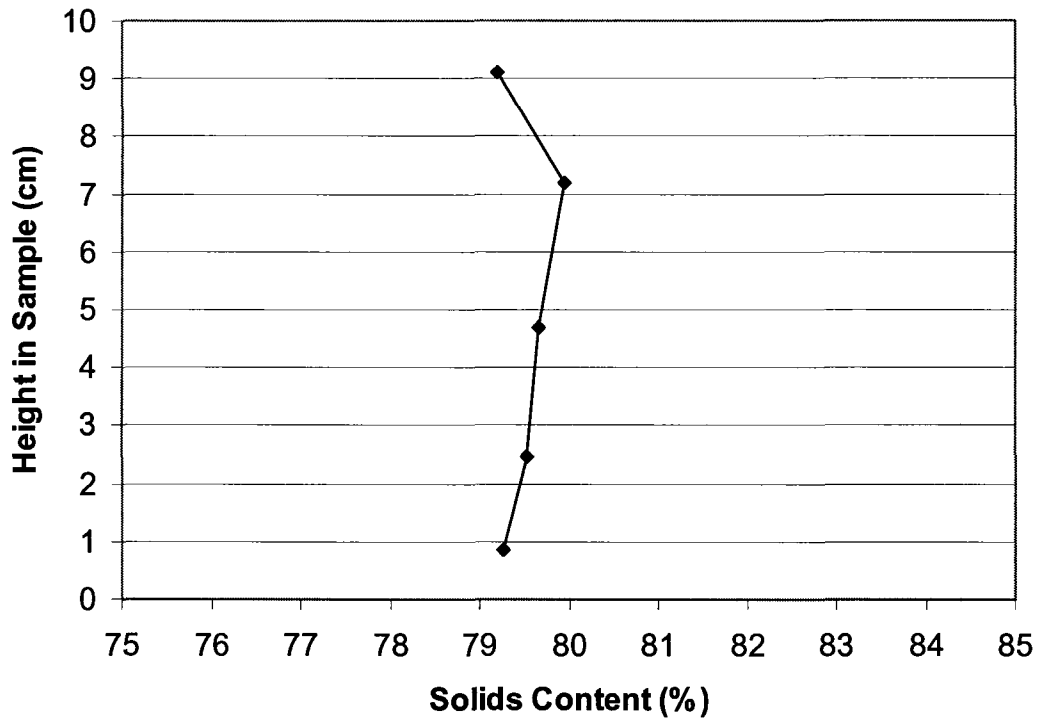


Figure 6-29 – Solids Content After Freezing and Re-application of Consolidation Pressure for Series 5 Tests

6.7 Photographs from Freezing Tests

Several phenomena were observed during the freezing tests through the use of time-lapse photography that are worthy of note.

The ice structure varies considerably between the Devon Silt and the MFT, likely due to the vastly different moisture contents. It may be possible to correlate the shape of the ice structure during transient freezing with the Liquidity Index, which is an indication of the amount of water contained in the soil, relative to the amount of water the soil can normally contain. A Liquidity Index of 1 represents a soil at its liquid limit, and a value

of 0 indicates a soil at the plastic limit. The Devon Silt used in these tests had a LI of approximately 0.7, while the MFT was roughly 3.4.

Figure 6-30 and Figure 6-31 show the final ice lens structure, at approximately the same scale, for Devon Silt and MFT respectively. The Devon Silt was prepared and frozen with water of the same salinity as the MFT (10 g/L NaCl). Note that the ice structure of the Devon Silt appears to surround peds, with a mainly horizontal ice structure. Also, the lenses are skewed at slight angles, and there are small vertical lenses extending beneath the final ice lenses.

Figure 6-31, showing the final ice structure for MFT, demonstrates a primarily vertically oriented ice structure, appearing as needles of ice. Near the final ice lens, the lenses become horizontally aligned, but are not as continuous as the Devon Silt. Two processes may help to explain these differences:

- The MFT, with a LI 4.9 times greater than the Devon Silt, has much more water in the voids that is available to form ice lenses. More extensive ice lensing during transient freezing (the upper portion of the photographs), may occur for this reason.
- Soils with high plasticity are known to develop shrinkage cracks during freezing (Chamberlain, E.J., Gow, A.J. 1979). The Plasticity Index (PI) for Devon Silt and MFT is approximately 24 and 43 respectively. It is expected that the MFT will develop more shrinkage cracks during freezing. Once shrinkage cracks develop, they could then be more easily penetrated by the advancing ice front, develop into vertical ice lenses, and continue to draw water towards the lens laterally from the adjacent MFT.

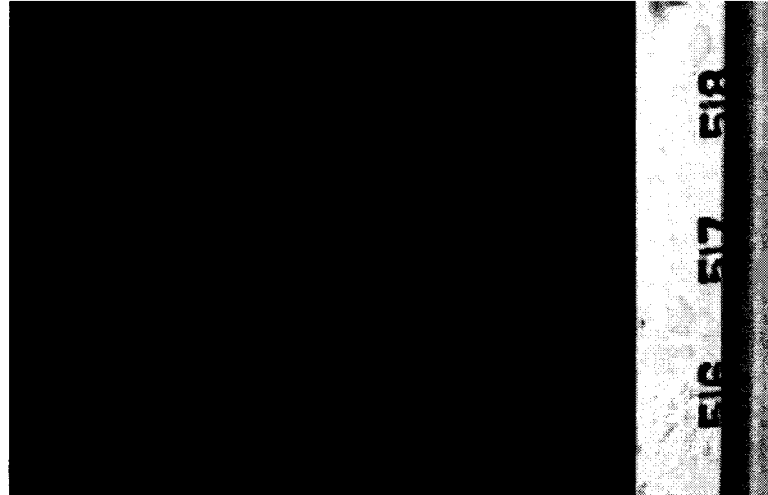


Figure 6-30 - Ice Structure in Devon Silt (10g/L NaCl)



Figure 6-31 - Ice Structure in MFT

Figure 6-32 provides an example of how the ice lenses develop during the transient freezing of MFT. The ice lenses nearest the frozen fringe are vertically aligned. As steady thermal conditions are approached, the ice structure becomes horizontal.

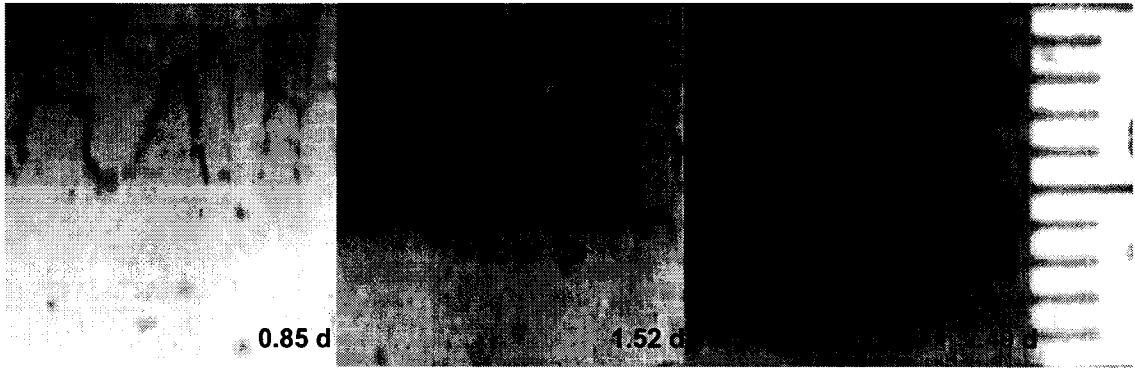


Figure 6-32 - Advancing Freezing Front in MFT Bulk Sump - S5T1

Examining Figure 6-32, it is noted that the vertically aligned ice lenses near the frozen fringe are forming well in advance of any horizontal lenses. It has been suggested that vertical ice lenses form during periods of restricted flow from below, forcing water to be drawn laterally from within the frozen fringe, and forming peds (Andersland and Ladanyi 2004). Shrinkage cracks formed in the frozen fringe also allow the ice to form vertically. Further growth of these ice lenses occurs until a horizontal ice lens develops and stops the flow of water from below. By this mechanism, peds could begin to form before a horizontal ice lens is developed.

Figure 6-32 also indicates that after the final ice lens has developed; vertical ice needles continue to form in the frozen fringe beneath the lens. This may be due to shrinkage cracks in the fringe. Xia also noted an ice structure forming beneath the final ice lens that matches the observations made here (Xia 2006).

6.8 Thaw Strain

Thaw strain was calculated for most of the tests performed. Some difficulty exists in determining the soil-water interface due to the presence of a hindered settling zone, with low solids content materials. Some judgment is required to estimate the soil-water interface. Also, the presence of bitumen that bonds to the cell wall after thaw makes it difficult to view the soil-water interface. Placing a light behind the sample is helpful in determining this interface, but this technique was not discovered until after several tests had been performed. Tests that are known to be inaccurate are either not included in the following plots, or are marked as being erroneous (Err).

The following graph in Figure 6-33 presents the thaw strain for different samples. Thaw strain is an indication of the change in the soil structure during freezing, and is simply the change in height divided by the height of the soil that was frozen. For an incompressible soil this is a simple measurement. However for compressible soils, the thaw strain is complicated due to the simultaneous occurrence of consolidation in the thawed portion of the soil.

Separating the consolidation portion of the thaw settlement from the thaw strain was found to be quite difficult. Several techniques were attempted to estimate the amount of consolidation settlement that had occurred, and to remove this amount from the total thaw settlement. Techniques include:

- Using the final moisture content distribution, the reduction in moisture content in the thawed soil was used to estimate the amount of consolidation that had occurred. This technique did not yield good results.
- Suction measurements were not sufficient to determine the shape and magnitude of the suction profile, and hence the consolidation due to suction was not applicable using this method.
- The horizontal ice lens thickness represents the amount of water withdrawn from the thawed soil for the cases where the external water supply rate was negligible. Unfortunately, photographs were not taken of the full sample profile and the determination of the total horizontal ice lens thickness was not possible.

The results from the technique that was found to produce reasonable results are shown in Figure 6-33, presenting a summary of all the thaw strain measurements. By plotting the thaw strain versus the number of days that the sample was frozen, the effect of consolidation is dealt with indirectly. When temperatures reach steady state (two days), the soil has been frozen to its maximum depth. Beyond this time, thaw strain should not increase further. Applying linear regression to the data, and reading the thaw strain at 2 days indicates how much of the thaw strain was due to the freezing of the soil, and not

the consolidation. Only the MFT was frozen over long durations, allowing this type of analysis. This technique assumes that the consolidation occurs at a constant rate after the onset of steady thermal conditions. This seems reasonable based on the water inflow plots for the MFT tests, which remain constant under steady thermal conditions.

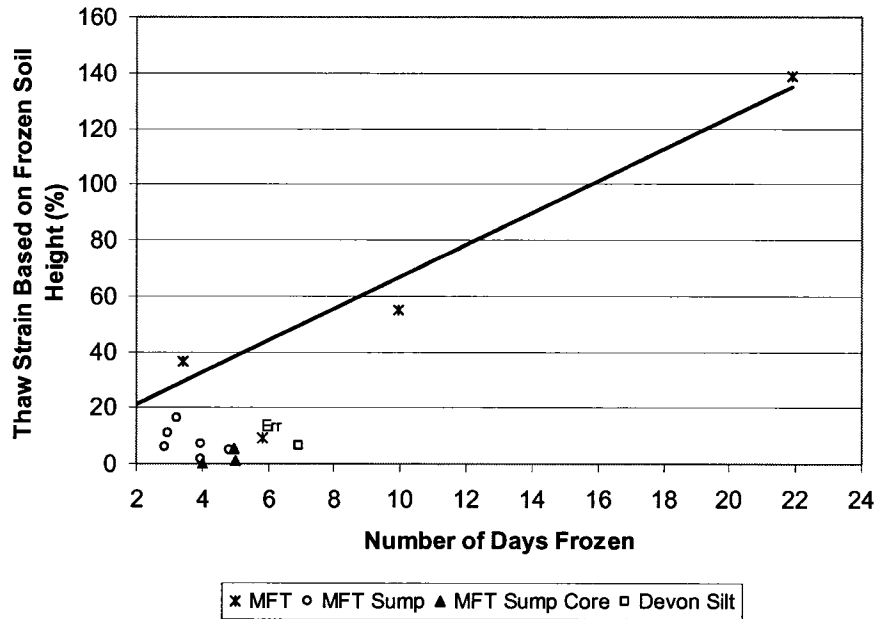


Figure 6-33 - Thaw Strain for All Tests

Since only the MFT can be analyzed with this technique, the thaw strain was simply averaged for the other soils. It is expected that these thaw strains are slightly higher than they should be due to some consolidation that has occurred. Since the sump fines and the Devon Silt had a higher solids content than the MFT, and hence a lower Liquidity Index, the amount of consolidation will be less. Also, these tests were frozen for a shorter duration, allowing less overall consolidation of the unfrozen soil to occur.

The average thaw strains presented in Figure 6-37 are compared with published thaw strain values for McKenzie Valley soils in Figure 6-34 and Figure 6-35 (Andersland and Ladanyi 2004). Both figures show that the mine tailings exhibit thaw strain values that lie outside of the range of the McKenzie Valley soils.

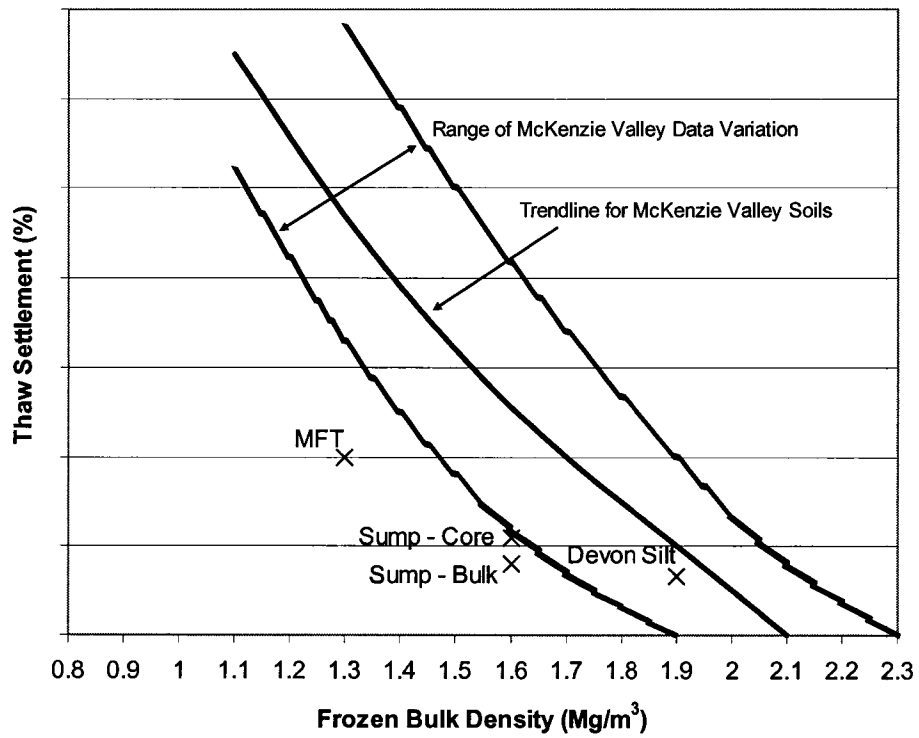


Figure 6-34 – Thaw Strain vs. Density for Soils Tested and McKenzie Valley Soils (Modified after Andersland and Ladanyi 2004)

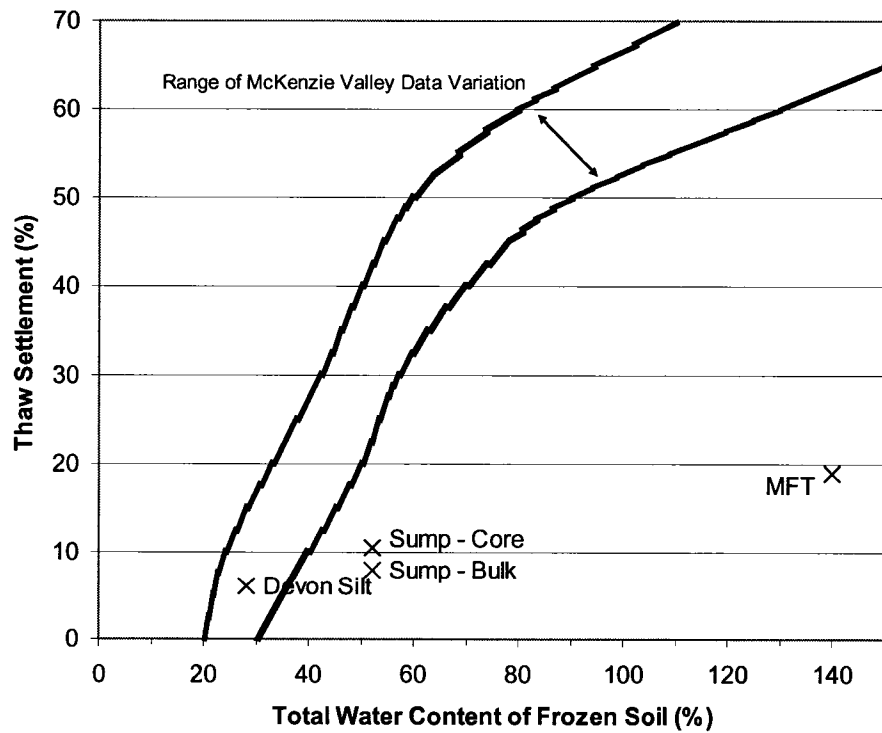


Figure 6-35 - Thaw Strain vs. Water Content for Soils Tested and McKenzie Valley Soils (Modified after Andersland and Ladanyi 2004)

To compare thaw strains determined in these tests to values found in the literature, which are usually reported in terms of initial and thawed solids content, it was necessary to convert these thaw strains to a thawed solids content. This description of this technique is presented in Section 4.1. This is easily accomplished by using the initial solids content and the thaw settlement as inputs, assuming the specific gravity of the soil, and solving for the final solids content. The results of this technique are given later in this section in Table 6-4.

Figure 6-36 shows the thaw strain for the MFT bulk sump tests, which were designed to study the effects of multiple freeze and thaw cycles. Due to difficulty in interpreting the soil-water interface, there are errors in this figure. During cycle 1 and 2, the thaw strain was likely underestimated. After cycle 3, when the test cell was dismantled, the true location of the top of the MFT sample was determined. Thus, the cumulative thaw strain at cycle 3 is accurate. It was expected that cycle 1 would have the greatest thaw strain, with diminutive thaw strains for subsequent cycles. The duration of the freezing test for each cycle was approximately the same.

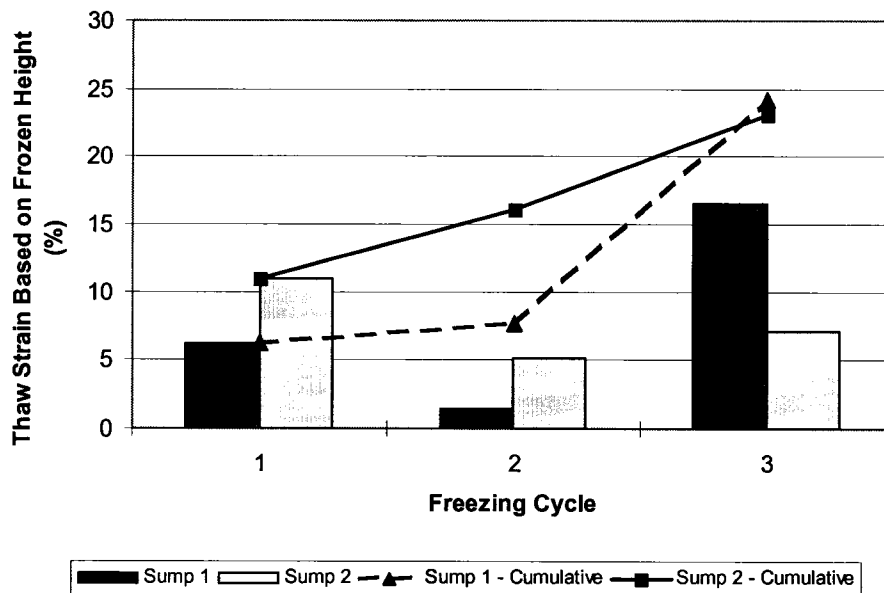


Figure 6-36 - Thaw Strain for Test Series 3

Figure 6-37 demonstrates the thaw strain that was measured using the MFT sump frozen core samples. These samples were tested in two ways. The Series 4 tests were performed in the freezing cell, where the sample was allowed to thaw initially before the load plate was lowered to the soil surface, and another freeze-thaw cycle followed in the laboratory. The Series 6 tests consisted of only a thaw cycle, placing the samples into a container without any load plate on top. Examining Figure 6-37, it is noted that the Series 4 tests indicate an increase in thaw strain with depth within the sump. This was expected, due to the greater extent of the ice lensing with depth (See Appendix C). It is difficult to see a trend with depth in the Series 6 tests due to a lot of scatter in the data. The scatter may be due to the shape of the container that was used for thaw. Some samples were taller than their width, leading to more support being provided by the wall of the container. Wider containers would provide less interference. It is thought that the use of the freezing cell for Series 4 allowed a better measure of the thaw strain by applying a slight pressure to the soil when it was lowered before the second freezing cycle. This slight pressure likely caused a collapse of the ped structure. The lack of any pressure in the Series 6 tests likely resulted in the scatter in the test data. As a result, only the Series 4 tests were used to determine an average thaw strain for the frozen core. The average depth of these tests was 30 cm, and the initial solids content was approximately 64%.

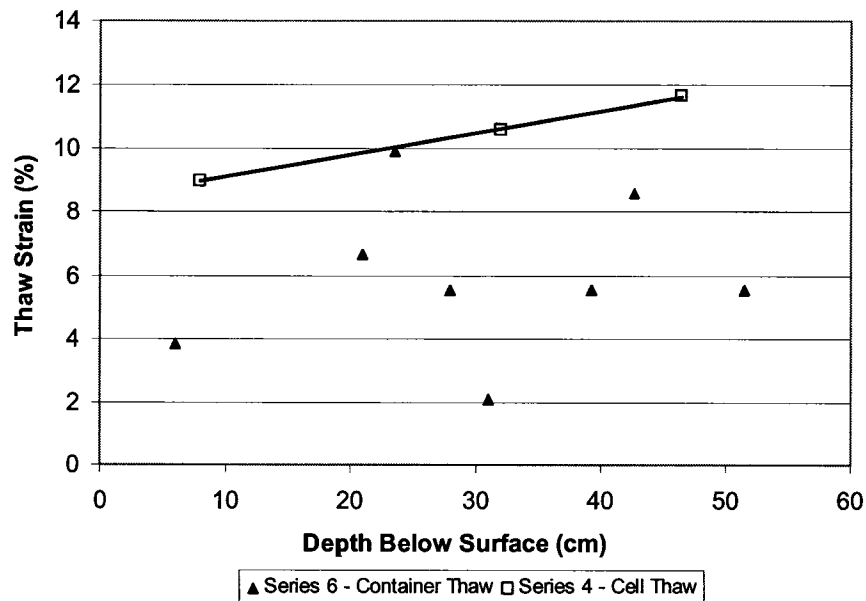


Figure 6-37 - Thaw Strain For MFT Sump Frozen Core

Figure 6-38 contains the initial thaw strain from the first thaw of the frozen core, as well as the cumulative strain after the laboratory freeze-thaw test for the Series 4 tests. Two of the tests showed an increase in thaw strain following the second freeze-cycle, while one did not. Possible reasons for the lack of increased thaw strain may be swell after thaw, or error in determining the soil-water interface. The latter is not likely, due to the ease of viewing the interface for the sump material.

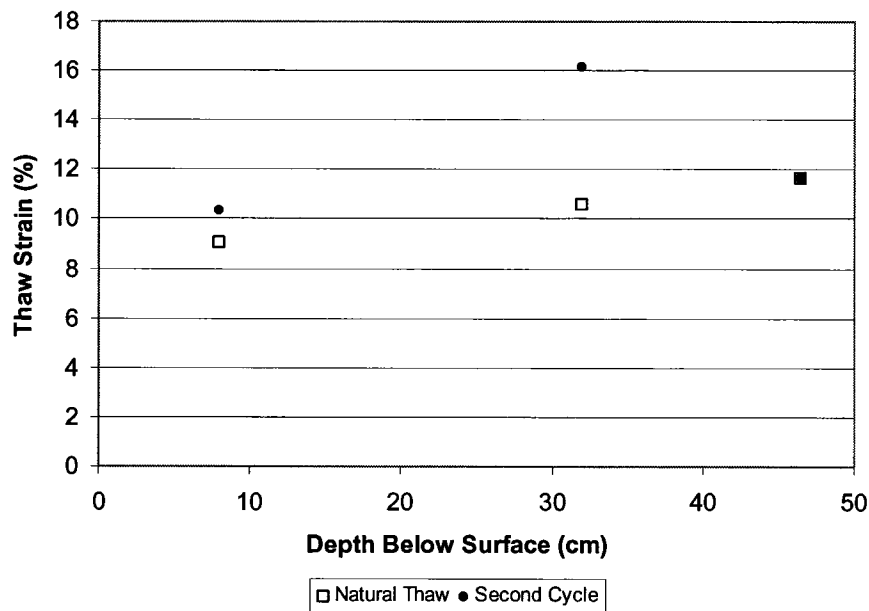


Figure 6-38 - Thaw Strain for MFT Sump Frozen Core - Series 4

Table 6-4 - Summary of Average Thaw Strain and Corresponding Solids Content

Material	Initial Solids Content (%)	Final Solids Content (%)	Measured Thaw Strain (%)
MFT	41	48	20
MFT Bulk Sump	66	69	8
MFT Sump Core	64	69	10
Devon Silt	77.2	79.5	6*

*- No consolidation. Initial solids content back-calculated.

Using Table 6-4, the final solids content that corresponds with the measured thaw strain is presented in Figure 6-39 and Figure 6-40. Figure 6-39 contains the thaw strain data from Proskin's work in 1992. Of interest is the trend line for the Suncor untreated tails. The thaw strain found in this work closely matches this data. This indicates that the test method used to measure the thaw strain has yielded results in line with other work. Also shown for comparison are the thaw strain values for the SWSS sump at the Syncrude site, which lie out of the range of Proskin's work.

Figure 6-40 presents a comparison for the Suncor MFT tested as part of this research with the bench-scale tests performed by Dawson (Dawson et al. 1999). The freezing rate impacts thaw strain, and may account for the slight variation between the thaw strain calculated in this work and that presented by Dawson.

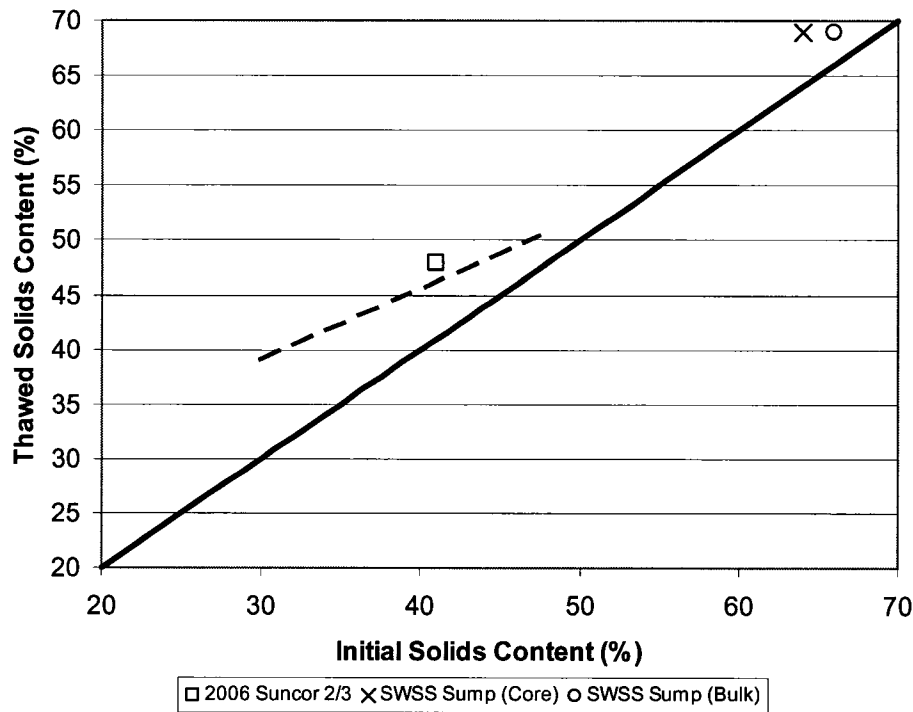


Figure 6-39 - Freeze-Thaw Dewatering of 1992/93 Suncor Field Core (Modified after Proskin et al. 1996)

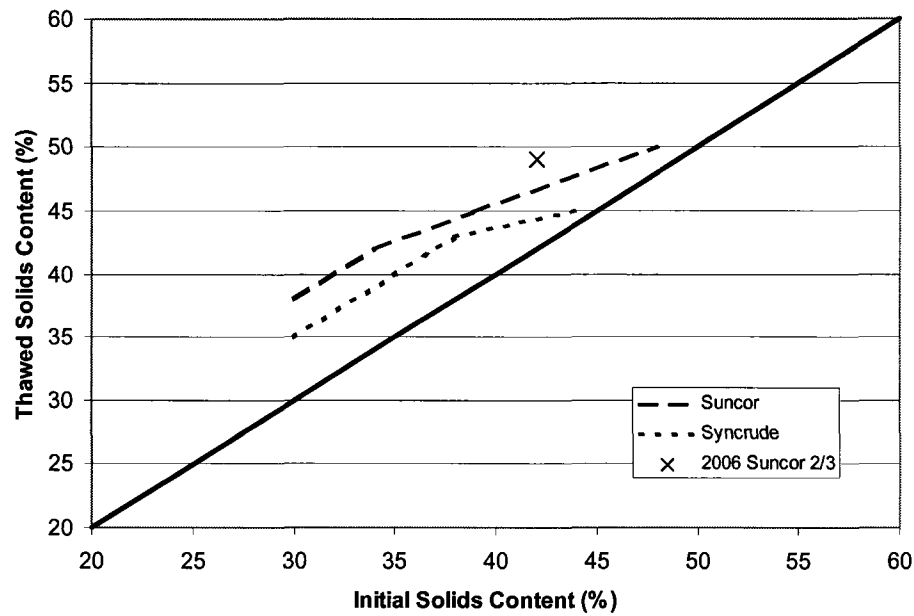


Figure 6-40 - Bench Scale Freeze-Thaw Dewatering – (Modified after Dawson et al. 1999)

6.9 Conclusions

Pore pressure sensors indicated that the maximum suctions generated in any tests were in the range of 20-70 kPa. These suctions represent the average pressure over the diameter of the sensor, which was 5 mm. The measurable suction profile extended to a maximum depth of only approximately 4 mm below the active lens.

The amount of heave measured at the surface relative to the actual thickness of the ice lenses that developed is related to the Liquidity Index of the soil. Repeated freeze-thaw cycles cause a compressible sample to transition towards a non-compressible behaviour that exhibits surface heave and a net inflow of water from the external supply.

The temperature measurements and photographs of the ice lenses allowed the segregational freezing temperature to be interpreted, as -0.6°C for MFT. At steady state, the frozen fringe was approximately 1 cm thick. Steady state was obtained after approximately 48 hours of freezing.

Segregation potential can be calculated in several ways. Using the surface heave or water inflow rates is suitable only for incompressible soils. Only the Devon Silt that was

consolidated could be analyzed in this manner. Time-lapse photographs of the final ice lens indicated if the soil is behaving in an incompressible, purely compressible, or partly compressible manner. It also showed if the final ice lens is the only active lens. The Segregation potential of partially compressible soils can be determined by correcting the final ice lens thickness from time-lapse photographs.

There are several factors that contribute to errors when calculating the SP using time-lapse photography. These include the limited field of view in the photograph, influence of the room temperature at the cell wall boundary, and heat conduction by the scale embedded with the soil.

The values of the SP determined by the time-lapse photography method, and by conventional heave and flow technique are similar. Other techniques that were used to determine the SP were the penetration rate of the base of the ice lenses and the final moisture content distribution.

Segregation potential was expected to increase with repeated freeze-thaw cycles, as the freezing front advanced into fresh, never before frozen soil with each cycle. This was not the case, likely due to the effects of consolidation of the underlying unfrozen soil, which resulted in a soil with a lower void ratio immediately below the ice being frozen with subsequent cycles.

The moisture content distributions after freeze and thaw indicate that the unfrozen soil may have experienced an increase in pore pressure due to constrained heave, as well as suctions beneath the ice lens, when no surface heave was observed.

Photographs of the ice lenses during freezing indicate that the ice structure may be related to the Liquidity Index. A soil with a high Liquidity Index develops a more vertically aligned, needled structure. These vertical needles develop in advance of any horizontal lenses. This may be due to the development of shrinkage cracks in soils with higher plasticity and Liquidity Index.

The determination of thaw strain is complicated for compressible soils, due to the occurrence of consolidation of the unfrozen soil. By plotting the thaw strain over the freezing period for several tests, the thaw strain can be inferred at the end of the transient freezing period. It appears that calculation thaw strain in a freezing cell with a load plate allows a reasonably accurate measurement due to the slight pressure that can be applied to collapse the ped structure. Thaw strains for MFT determined in this chapter correlate well with previous work reported in the literature.

6.10 References

Andersland, O. B., and Ladanyi, B. (2004). *Frozen Ground Engineering*. John Wiley & Sons, Inc., Hoboken, New Jersey.

Chamberlain, E.J., and Gow, A.J. (1979). "Effect of freezing and thawing on the permeability and structure of soils." *Engineering Geology*, 13 73-92.

Dawson, R. F., Segó, D. C., and Pollock, G. W. (1999). "Freeze-thaw dewatering of oil sands fine tails." *Canadian Geotechnical Journal*, 36(4), 587-598.

Hereygers, C. (2006). "Various laboratory tests of soil properties." Performed at the University of Alberta.

Konrad, J. M. (1989). "Effect of freeze-thaw cycles on the freezing characteristics of a clayey silt at various overconsolidation ratios." *Canadian Geotechnical Journal*, 26(2), 217-226.

Konrad, J. M. (1987). "Procedure for determining the segregation potential of freezing soils." *Geotechnical Testing Journal*, 10(2), 51-58.

Konrad, J. M., and Morgenstern, N. R. (1980). "Mechanistic theory of ice lens formation in fine-grained soils." *Canadian Geotechnical Journal*, 17(4), 473-486.

Proskin, S. A., Segó, D. C., and Burns, R. (1996). "Field tests evaluating freeze-thaw dewatering of fine tailings." *Proceedings of the 1996 3rd International Conference on Tailings and Mine Waste, Jan 16-19 1996*, Fort Collins, CO, USA, 189-198.

Segó, D. C. (2006). "Thesis progress meeting, May 2006."

Xia, D. (2006). "Frost heave studies using digital photographic technique." M.Sc. thesis, Department of Civil and Environmental Engineering, University of Alberta, Edmonton, Alberta.

Xia, D., Arenson, L. U., Biggar, K. W., and Segó, D. C. (2005). "Freezing process in Devon Silt – Using time-lapse photography." *Submitted to Canadian Geotechnical Journal*.

Chapter 7 - Modeling for Field Predictions

To better appreciate the freezing characteristics of the MFT and the bulk samples from the SWSS at Syncrude, a prediction of frost heave due to climatic conditions at Fort McMurray has been performed. The frost heave model is based on the segregation potential theory, and is outlined in Figure 7-1.

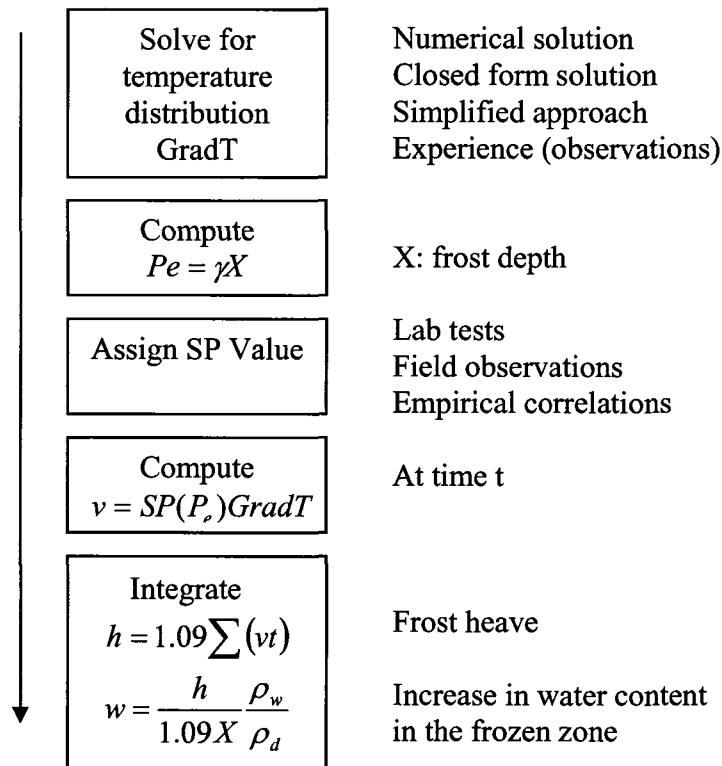


Figure 7-1 - Flow Chart for Frost-Heave Prediction (Modified after Konrad 1999)

The analysis for frost heave presented in Figure 7-1 allows the determination of the frost heave due to the formation of ice lenses. It does not represent the actual surface heave, which would need to include the expansion of the pore water in the frozen zone. The frost heave due to ice lens formation is due to the volume of water that was either supplied from consolidation of the underlying unfrozen soil, or from an external water supply. Freezing tests performed on the MFT and the sump material demonstrated that for the insitu void ratio of these soils, the external water supply rate is negligible. Therefore, the formation of the ice lenses is due almost entirely to water supplied from consolidation of the underlying unfrozen soil. The calculation of heave then represents the consolidation of the unfrozen soil below the active ice lens. Once the consolidation of the unfrozen soil

is known for the freezing period, thaw strain calculations can be applied to the soil that was frozen to provide a total thaw settlement prediction.

This model requires input of the temperature distribution, frost penetration, segregation potential, and other basic geotechnical soil properties. These parameters are outlined in the following sections.

7.1 *Temperature Distribution*

Any solution of the temperature distribution in a freezing soil will require assumptions of the boundary conditions and soil properties. These are outlined in the following sections. TempW, by GEO-SLOPE International Ltd., was used for the analysis. TempW is a finite element software that can be used to model the temperature changes in a soil.

7.1.1 Bottom Boundary Condition

For this analysis, the bottom boundary condition was assumed to be a constant 5°C at 8 m depth.

7.1.2 Upper Boundary Condition

The upper boundary condition was based on the average daily temperature at Fort McMurray, obtained from Environment Canada's records for the period of 1983-2003 (Meteorological Service of Canada 2002). The mean daily temperature and the snow depth on the ground were averaged over the 20-year period to obtain the results presented in Figure 7-2.

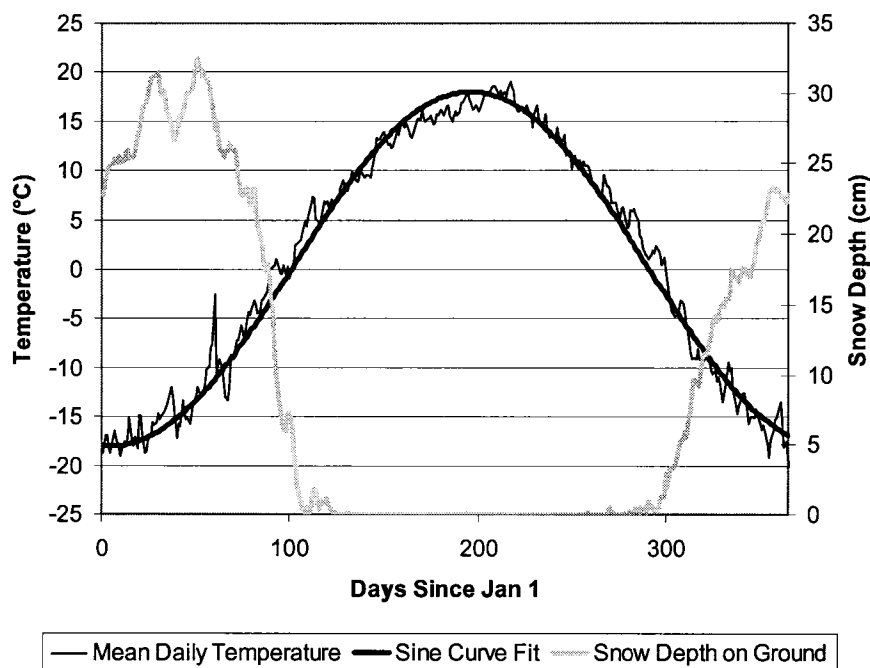


Figure 7-2 - Average Daily Temperature and Snow Depth at Ft. McMurray from 1983-2003

A sine curve was fit to the mean daily temperature plotted in Figure 7-2. The equation for this curve is given below:

Equation 7-1

$$T = 18\sin[0.0165(d + 280)]$$

where T is the temperature in degrees Celsius, d is the number of days since January 1st, and radians are used in the sine function. The freezing and thawing periods are 175 and 190 days respectively, with freezing beginning on October 26th. The amplitude of the sine curve is $\pm 18^\circ\text{C}$. Snow is present throughout the entire freezing period. It is assumed that the snow cover will be highly reflective and will not allow the ground to be warmed above the air temperature by the sun. During the summer, it was assumed that the grey, dry soil would be hotter than the air by a factor of 1.3. This value is based on the low range for gravel (Krahn 2004). The transition from a snow covered surface to a bare soil surface was assumed to occur from a ground temperature of -0.5°C to 0°C .

7.1.3 Basic Geotechnical Parameters

The following parameters, listed in Table 7-1 and Table 7-2, were either determined using basic geotechnical equations, or were obtained from published sources.

Table 7-1 - Parameters for Thermal Analysis for Sump Material

Parameter		Value	Source
Moisture Content	w	51.5 %	Measured
Specific Gravity	G _s	2.45	Measured
Saturation	S	1.0	Assumed
Bulk Density	γ _b	16.2 (kN/m ³)	Measured
Dry Density	γ _d	10.7 (kN/m ³)	Measured
Specific Heat Capacity of Soil Grains	c _s	0.71 (kJ/kg·°C)	(Krahn 2004)
Specific Heat Capacity of Water	c _w	4.187 (kJ/kg·°C)	(Krahn 2004)
Specific Heat Capacity of Bitumen	c _b	1.63 at 0°C (kJ/kg·°C)	(Mochinaga et al. 2006)
Specific Heat Capacity of Ice	c _i	2.094 (kJ/kg·°C)	(Krahn 2004)
Density of Bitumen	ρ _b	1030 (kg/m ³)	(Mochinaga et al. 2006)
Bitumen Content		2%	(McKenna and Dawson 1999)
Thermal Conductivity of Ice	k _i	2.23 (W/m·°C)	(Krahn 2004)
Thermal Conductivity of Water	k _w	0.605 (W/m·°C)	(Krahn 2004)

Table 7-2 - Parameters for Thermal Analysis for MFT

Parameter		Value	Source
Moisture Content	w	141%	Measured
Specific Gravity	G _s	2.42	(Proskin 1998)
Saturation	S	1.0	Assumed
Bulk Density	γ _b	13.0 (kN/m ³)	Measured
Dry Density	γ _d	5.4 (kN/m ³)	Measured
Specific Heat Capacity of Soil Grains	c _s	0.71 (kJ/kg·°C)	(Krahn 2004)
Specific Heat Capacity of Water	c _w	4.187 (kJ/kg·°C)	(Krahn 2004)
Specific Heat Capacity of Bitumen	c _b	1.63 at 0°C (kJ/kg·°C)	(Mochinaga et al. 2006)
Specific Heat Capacity of Ice	c _i	2.094 (kJ/kg·°C)	(Krahn 2004)
Density of Bitumen	ρ _b	1030 (kg/m ³)	(Mochinaga et al. 2006)
Bitumen Content		2%	(McKenna and Dawson 1999)
Thermal Conductivity of Ice	k _i	2.23 (W/m·°C)	(Krahn 2004)
Thermal Conductivity of Water	k _w	0.605 (W/m·°C)	(Krahn 2004)

7.1.4 Thermal Analysis Parameters

Using the parameters listed in Table 7-1 and Table 7-2, as well as empirical relationships, the inputs for the thermal analysis were determined and are outlined in the following sections.

7.1.4.1 Unfrozen Water Content

The unfrozen water content variation with temperature was determined in the laboratory using time domain reflectometry technique (TDR). TempW requires an unfrozen water content function as an input parameter. The function shown in Figure 7-3 was entered into the analysis for both the MFT and the sump material.

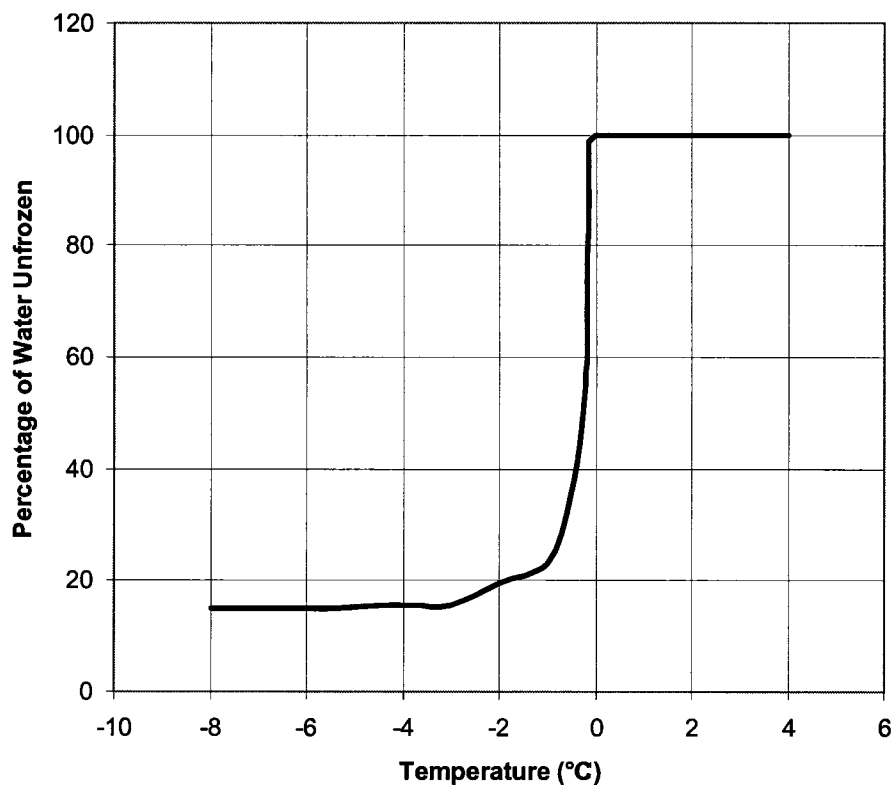


Figure 7-3 - Unfrozen Water Content for Sump Material

7.1.4.2 Heat Capacity

TempW uses the volumetric heat capacity of the soil, which is a function of the unfrozen water content. The volumetric heat capacity can be approximated by the dry density of

the soil and the specific heat capacities of its components. This is shown in Equation 7-2 (Krahn 2004).

Equation 7-2 (Krahn 2004)

$$c = \gamma_d (c_s + c_w w_u + c_i w_f)$$

where:

- γ_d is the dry density in kN/m^3
- c_s, c_w, c_i are the specific heat capacities of the soil grains, water, and ice respectively ($\text{kJ/kg}\cdot^\circ\text{C}$)
- w_u and w_f are the unfrozen and frozen volumetric water contents, respectively

The specific heat capacity of the solids was taken to be a weighted average, based on the volume of bitumen and soil particles. The volumetric heat capacities of the MFT and sump material are presented in Figure 7-4.

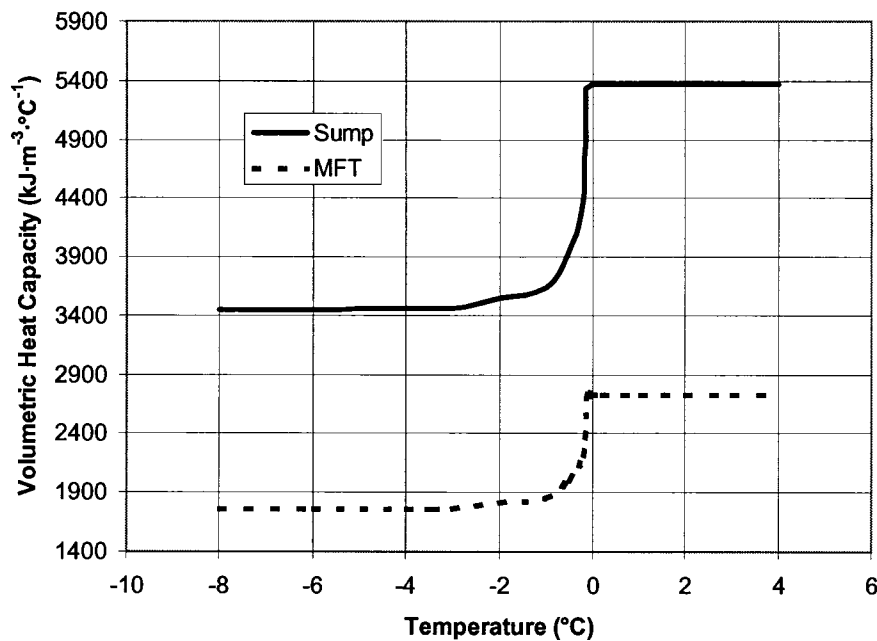


Figure 7-4 - Volumetric Heat Capacity Function for MFT and Sump

7.1.4.3 Thermal Conductivity

Thermal conductivity can be calculated from empirical relationships or measured directly. For the MFT, the thermal conductivity reported by Proskin was used (Proskin

1998). The thermal conductivity was found by interpreting freeze and thaw tests performed in the laboratory. The values for Suncor MFT at 33% solids content were found to be 1.05 W/m·°C for the thawed state, and 2.18 W/m·°C for the frozen state. This corresponds to a soil mineral thermal conductivity of 3.02 W/m·°C (by using a weighted average). Since the solids content of the MFT used in this testing was 41%, Proskin's value was adjusted based on the new solids content. Equation 7-3 gives the frozen thermal conductivity based on thermal conductivity of the soil components.

Equation 7-3 (Farouki 1986)

$$k_{sat} = k_s^{(1-n)} k_i^{(n-\theta)} k_w^\theta$$

where:

- k_s , k_i , and k_w are the thermal conductivity of the soil grains, ice, and water respectively
- n is the porosity
- θ is the volume fraction of the unfrozen water per unit soil volume

Using Equation 7-3 and using the soil thermal conductivities found by increasing the solids content to 41%, the thermal conductivity of MFT was estimated. The values are slightly different than those reported by Proskin, possibly due to inaccuracies with using Equation 7-3.

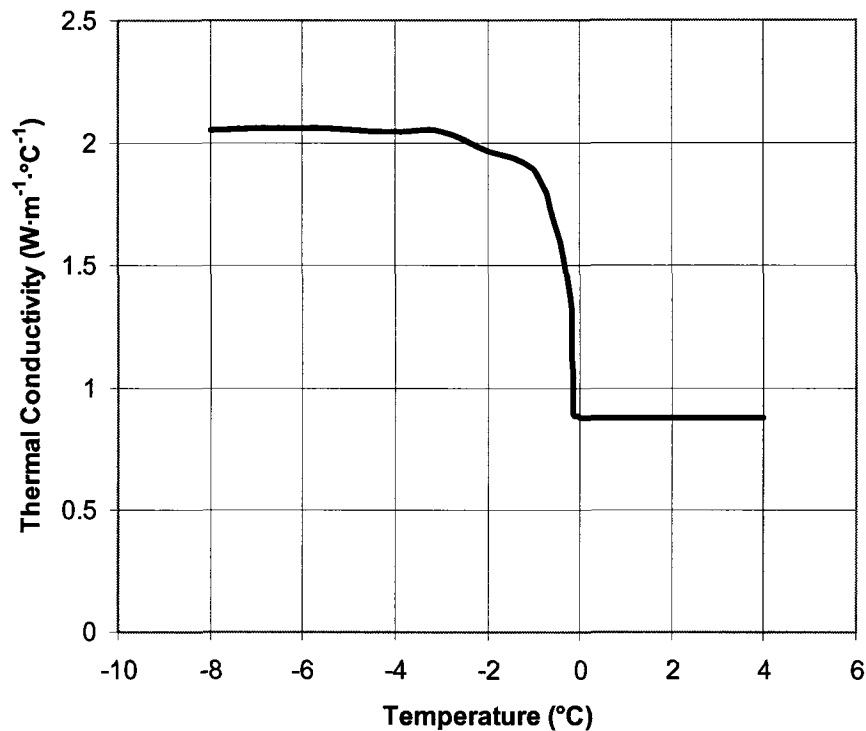


Figure 7-5 – Thermal Conductivity of MFT

Since the grain size distribution of the sump material is different than the MFT, and the mineral constituents are unknown, an estimate was made based on the method suggested by Johansen, shown in Equation 7-4 (Andersland and Ladanyi 2004).

Equation 7-4

$$k_s = k_q^q k_o^{1-q}$$

where:

- k_q , and k_o are the thermal conductivities of quartz and other minerals, respectively
- q is the quartz fraction of the solids in the soil

The thermal conductivity of the other minerals is 2.0 W/m·°C, and 7.7 W/m·°C for quartz (Andersland and Ladanyi 2004). For the sump, which contains 14% quartz sand, this method yields a thermal conductivity of 2.4 W/m·°C for the soil particles. Including the bitumen for the thermal conductivity of the solids lowers this value to 2.27 W/m·°C.

Using Equation 7-3, Figure 7-6 was created.

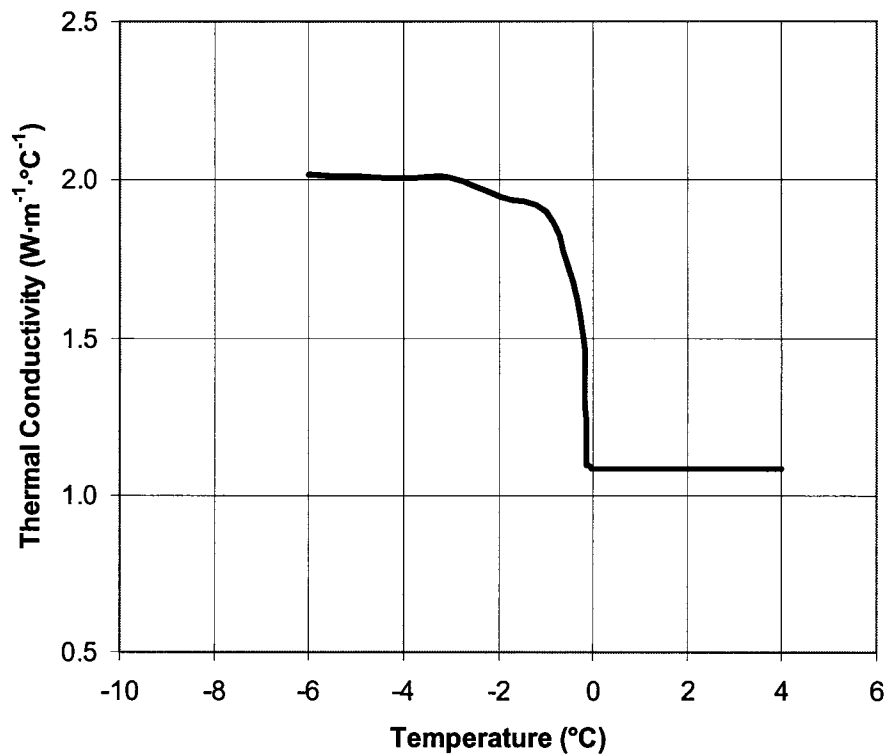


Figure 7-6 - Thermal Conductivity for Sump Material

The thermal conductivity is highly dependant on the unfrozen water content and can be assumed to be constant when the soil is completely frozen or thawed (Krahn 2004).

7.1.5 Numerical Analysis Method

There are several methods that are suitable for determining the temperature distribution in the soil, and hence the temperature gradient at the freezing front. The Stefan solution is commonly used, but involves several simplifying assumptions. A more rigorous method is the solution of the differential equation for heat flow, which is used by TEMP/W, and is given in Equation 7-5.

Equation 7-5 (Krahn 2004)

$$\frac{\partial}{\partial x} \left(k_x \frac{\partial T}{\partial x} \right) + \frac{\partial}{\partial y} \left(k_y \frac{\partial T}{\partial y} \right) + Q = \lambda \frac{\partial T}{\partial t}$$

where:

- T is the temperature,
- k_x is the thermal conductivity in the x-direction,

- k_y is the thermal conductivity in the y-direction,
- Q is the applied boundary flux,
- λ is the capacity for heat storage,
- T is the time.

TEMP/W uses a finite element solution to the differential equation. The mesh for the analysis is presented in Figure 7-7.

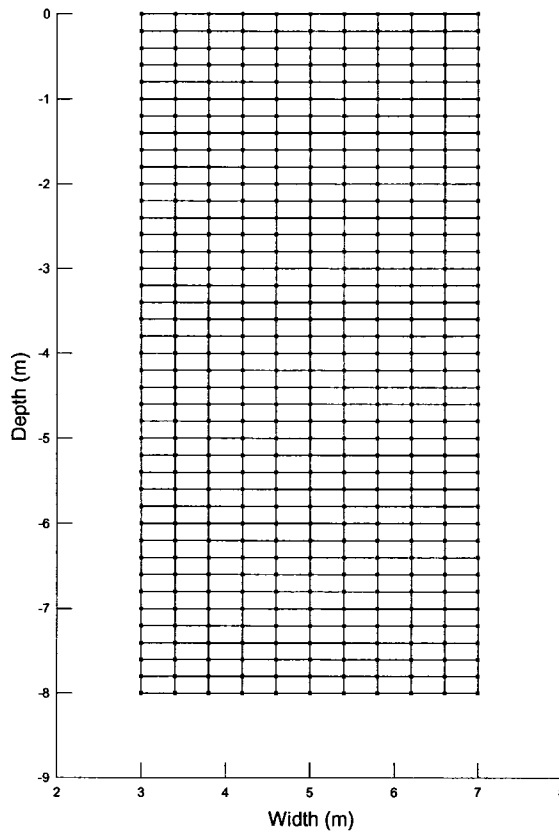


Figure 7-7 - Mesh for Finite Element Analysis

7.1.6 Numerical Analysis Results

The results of thermal modeling with TempW, as well as the determination of frost heave are presented in the following sections.

7.1.6.1 Initial Temperature Distribution

Using the climatic data shown in Figure 7-2, and allowing TempW to run through ten years, until the conditions at October 26th became stable, the initial temperature

distribution was determined. Adaptive time stepping was used to prevent large temperature gradients from upsetting the results. Figure 7-8 presents the initial temperature distribution for the sump and the MFT on October 26th, representing the beginning of the freezing period.

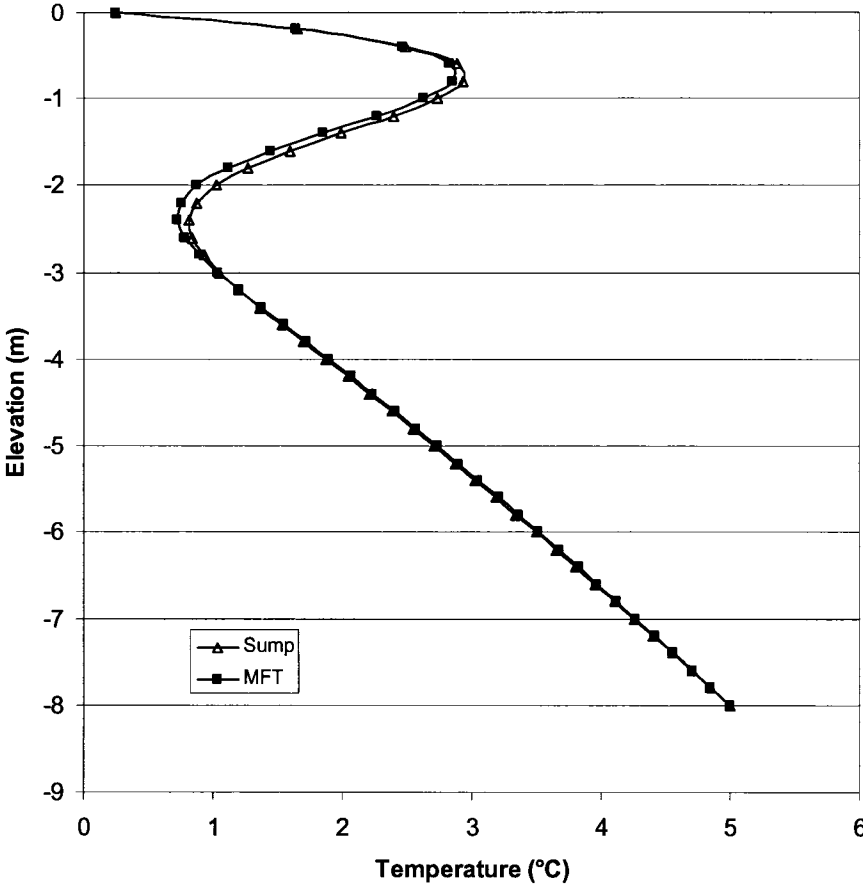


Figure 7-8 - Initial Temperature Distribution of Sump and MFT Deposits at Start of Freezing Period

The temperature variation within the deposits throughout the year is shown in Figure 7-9.

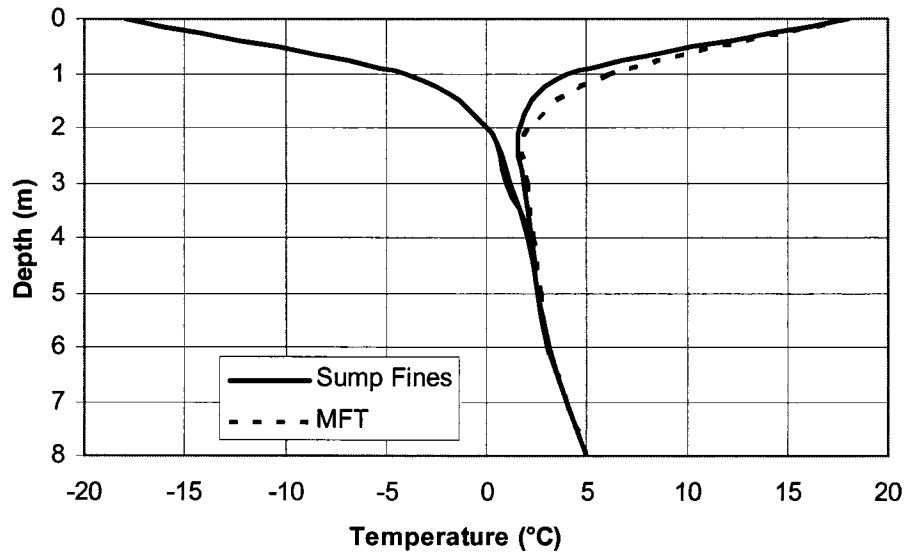


Figure 7-9 - Annual Soil Temperature Variation in Sump and MFT

7.1.6.2 Frost Penetration

The frost penetration for the sump and the MFT are given in Figure 7-10. The freezing front was assumed to retreat after 175 days. The depth of frozen ground shown in Figure 7-9 is slightly greater than the depth illustrated in Figure 7-10, due to modeling error.

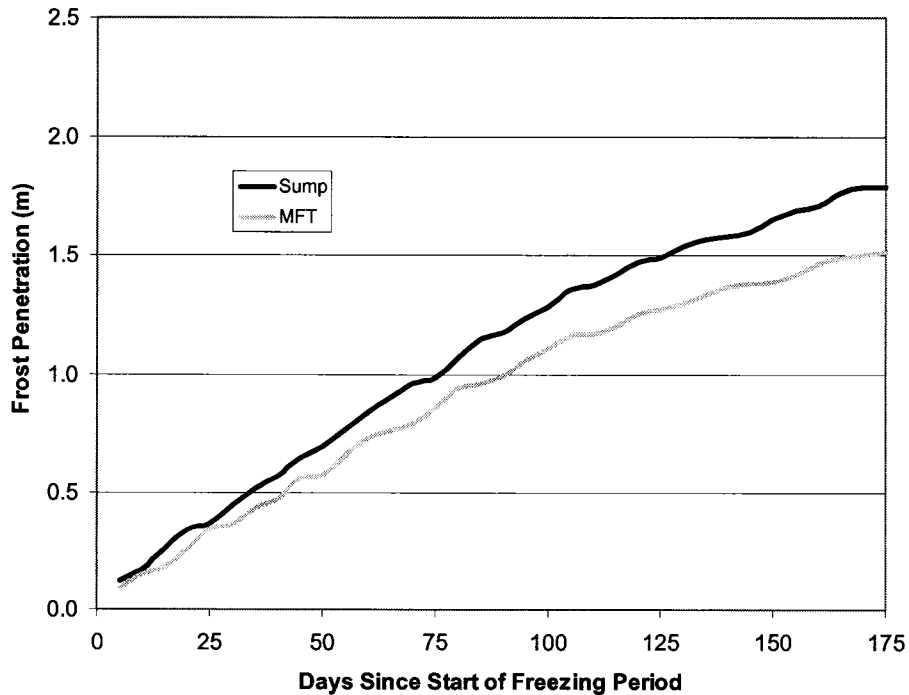


Figure 7-10 - Frost Penetration for Sump and MFT

7.1.6.3 Temperature Gradient

The temperature gradients at the freezing front for the Sump and the MFT are plotted in Figure 7-11. The oscillations are due to numerical errors within the model.

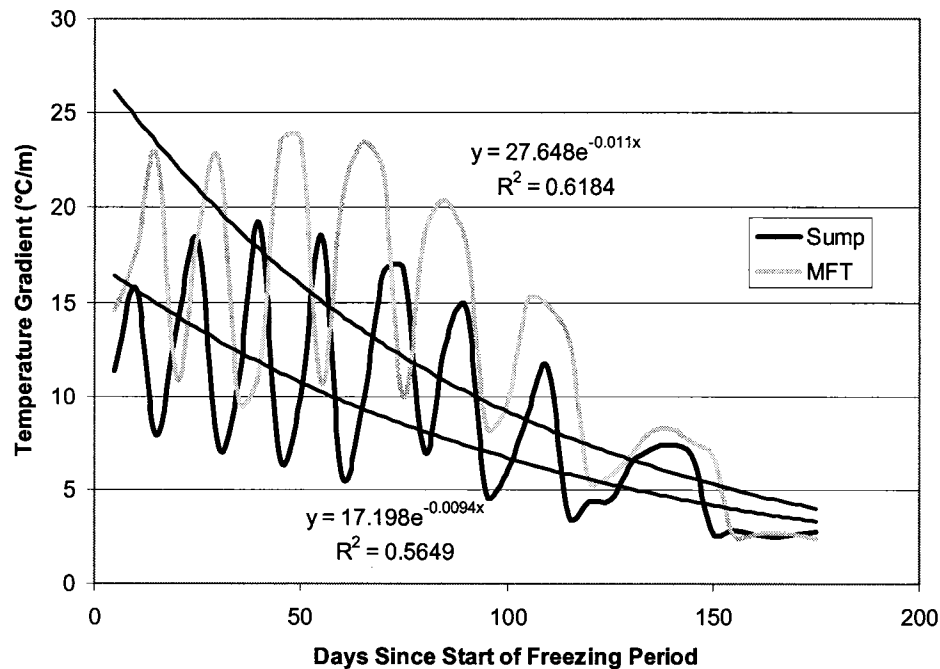


Figure 7-11 - Temperature Gradient at Freezing Front for Sump and MFT

7.2 Segregation Potential

The segregation potential for each material was calculated and presented in Chapter 6. The calculated segregation potential was found without overburden pressure (SP_0). Since the depth of frost penetration is approximately 2 meters, the maximum overburden pressure is no more than 40 kPa. It is assumed that the segregation potential will be approximately equal to the SP_0 value since the overburden pressure is small. The segregation potential used for the analysis is given in Table 7-3.

Table 7-3 - Segregation Potential Used for Frost Heave Analysis

Soil	Segregation Potential ($\text{cm}^2 \cdot \text{s}^{-1} \cdot \text{°C}^{-1}$)
MFT	6.7E-05
Sump	9.4E-07

7.3 Frost Heave Determination

After the temperature distribution in the soil was modeled for the freezing period, 5 day time steps were selected and the temperature gradient at the freezing front was determined for each. The temperature gradient and the segregation potential were then substituted into the equations listed in Figure 7-1 to find the heave for each period. The sum of each period represents the total water thickness accumulated at the ice lens for the freezing period. This is plotted in Figure 7-12.

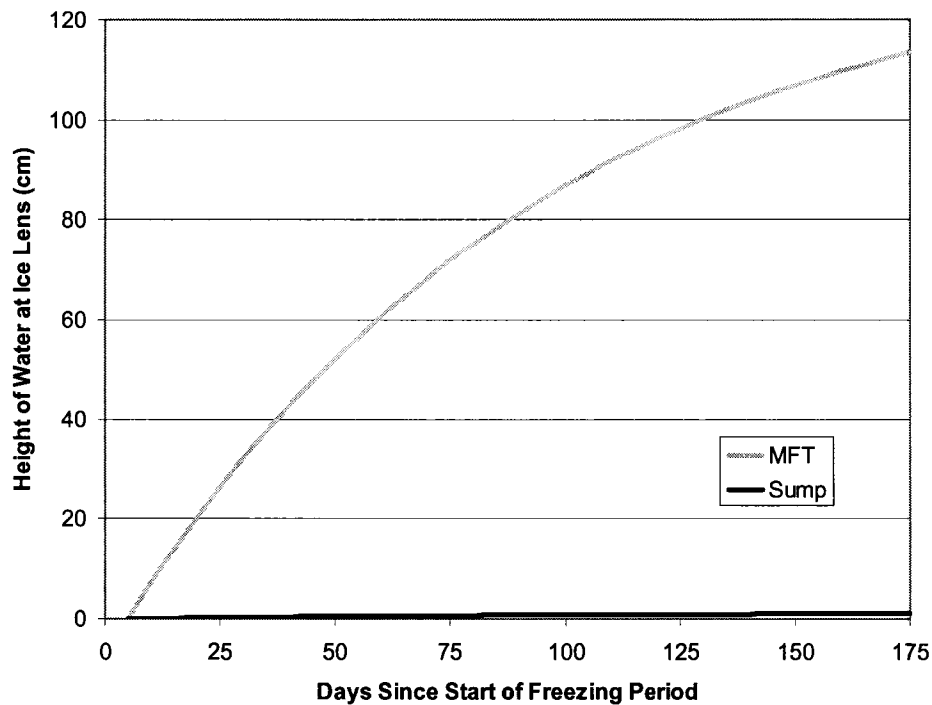


Figure 7-12 - Frost Heave During Freezing Period

It is important to realize the approximate nature of using this type of frost heave prediction. The temperature gradient does not vary greatly by changing the analysis. The segregation potential, however, can vary by over an order of magnitude between subsequent freezing tests. By using the high and low values for SP for the MFT (from Figure 6-20), the frost heave ranges from 1.7 cm to 13.5 m. Similarly, by using the extreme values for the sump (from Figure 6-21), the heave ranges from 0.3 to 3.5 cm. In order to obtain better predictions, more freezing tests could be performed. Alternatively, the temperature gradient and heave could be measured, and the SP determined by back calculation. This would allow greater certainty of the SP and thermal conditions and

would enable more accurate modeling. The MFT shows a much higher potential for frost heave than the sump.

7.3.1 Thaw Strain and Consolidation

The thaw strain was determined in Chapter 6. The average values to be used in this analysis are 20% for the MFT and 8% for the sump. These values are accurate for only the first cycle of freeze-thaw. Based on the frost penetrations shown in Figure 7-10, the thaw settlement would be 30 cm for the MFT, and 14 cm for the sump. The solids content for the MFT would have increased from 41% to 48% in the upper, frozen zone. The solids content of the sump would increase from 66% to 69%. Combined with the volume reduction due to the consolidation of the underlying soil due to ice lens growth, this gives a total height reduction of 146 cm for the MFT, and 15 cm for the sump

7.4 Conclusions

Using TempW software, the thermal conditions in a deposit of Syncrude sump fines and Suncor Pond 2/3 MFT were modeled. The frost penetration was found to be 1.75 m for the sump, and 1.5 m for the MFT. Based on the thaw strains observed in the laboratory testing, this would result in 30 cm and 14 cm of thaw settlement for the sump and MFT, respectively.

In addition to the thaw settlement due to the structural changes in the frozen soil, the underlying soil would be dewatered by an amount proportional to the frost heave. This calculation was found to be highly dependant on the segregation potential, which can vary greatly. The height of water drawn to the ice lens from the underlying soil was approximately 1 cm for the sump, and 1.2 m for the MFT. These predictions may be in error by one order of magnitude. More freezing tests would allow a better determination of the segregation potential. Comparison with field conditions is also possible for calibrating the model.

By performing more freezing and thaw strain tests, the segregation potential and thaw strain could be determined over a range of solids contents. The frost heave model could

then be used to analyze the effect of freeze-thaw over several years, with increasing solids content after each cycle.

7.5 References

Andersland, O. B., and Ladanyi, B. (2004). *Frozen Ground Engineering*. John Wiley & Sons, Inc., Hoboken, New Jersey.

Farouki, O. T. (1986). *Thermal properties of soils. Series on rock and soil mechanics*. Trans Tech Publications, Clausthal-Zellerfeld, Germany.

Konrad, J. M. (1999). "Frost susceptibility related to soil index properties." *Canadian Geotechnical Journal*, 36(3), 403-417.

Krahn, J. (2004). *Thermal modeling with TEMP/W. An engineering methodology*. GEO-SLOPE International Ltd., Calgary, Alberta.

McKenna, G., and Dawson, R. (1999). "1995/1996 MFT freeze-thaw prototype at Syncrude's Base Mine Lake." Syncrude Ltd, Edmonton, Alberta.

Meteorological Service of Canada. (2002). "2002 CDCD West CD." National Archives and Data Management Branch, Downsview, Ontario.

Mochinaga, H., Onozuka, S., Kono, F., Ogawa, T., Takahashi, A., and Torigoe, T. (2006). "Properties of Oils sands and Bitumen in Athabasca." CSPG / CSEG / CWLS Joint Convention, Calgary, Alberta.

Proskin, S. A. (1998). "A geotechnical investigation of freeze-thaw dewatering of oil sands fine tailings." PhD thesis, University of Alberta, Edmonton, Alberta.

Chapter 8 - Summary, Conclusions, and Recommendations

8.1 Summary of Thesis

The reclamation of high moisture content mine tailings is a problem that has plagued the oil sand industry in Alberta since early in its development. One potential technique for reclamation is to use the natural processes of freeze-thaw, desiccation, and evapotranspiration to dewater and strengthen these weak deposits. The focus of this thesis was on the suitability of using freeze-thaw cycles to dewater the tailings. Two types of mine tailings were studied: Mature Fine Tailings (MFT) from Suncor Limited's Pond 2/3, and MFT rich sump fines from the South West Sand Storage (SWSS) external sump at Syncrude Limited. The sump fines were sampled during their first winter in which they were allowed to freeze. Both frozen core samples, and unfrozen bulk samples were obtained. The MFT was sampled in an unfrozen state, from material that had never been frozen. Comparisons of the ice structure developed insitu and during laboratory tests were made. Thaw strain was measured. The segregation potential (SP) was calculated for use in a model for frost heave to predict the effectiveness of freeze-thaw dewatering for these materials.

The sump samples, Suncor MFT, and Devon Silt were tested in the laboratory to determine material characteristics for comparison. The sump material and Devon Silt had nearly the same grain size distribution, while the MFT was finer. The solids content of the MFT and sump fines was 41.0 and 66.1 respectively. The Liquidity Index was greatest for the MFT (3.4). The sump fines and Devon Silt had Liquidity Index values that were much lower (2.6 and 0.7 respectively).

When freezing tests were performed on the samples, it was found that typical testing procedures were useful only for the preconsolidated Devon Silt. The sump and MFT samples were compressible, and consolidation occurred in the underlying unfrozen soil during the test. This resulted in an underestimation of the soils potential for frost heave.

A test method to include the effect of consolidation by measuring suction in the unfrozen soil was found to be ineffective. The suction profile in the unfrozen soil was too localized to measure so the consolidation theory could not be applied. The test did measure large increases in pressure in the frozen soil, likely aligned perpendicular to the test cell walls. This stress may have caused the soil to lock against the test cell, and not allow heave to occur. A third test method was developed that allowed the determination of the SP at steady thermal conditions through the use of digital time-lapse photography. The method was found to yield results comparable to the conventional method, but is expected to produce less precise results. This method was also found to be useful in assessing the validity of using the conventional test methods.

The maximum suction that was measured during a freezing test was 70 kPa, occurring immediately beneath the frozen soil. This is likely the maximum suction generated by the ice lens, however it is the average over the diameter of the pressure sensor (5 mm). The measurable suction profile extended only approximately 4 mm below the active ice lens for MFT.

Segregation potential was expected to increase with repeated freeze-thaw cycles, as the freezing front advanced into fresh, never before frozen soil with each cycle. This was not the case, likely due to the effect of consolidation on the underlying unfrozen soil, which resulted in a soil with a lower void ratio being frozen with subsequent cycles.

The moisture content distribution measured in the sample after freezing suggests that the thawed soil experiences consolidation due to suction generated at the ice lens above, and a pressure increase due to constrained heave.

Thaw strain is a difficult parameter to determine from freezing tests for soils that are compressible since consolidation occurs simultaneously with freezing. A method to remove the settlement due to consolidation from the total thaw settlement was found and requires the knowledge of the time required for the test to reach steady thermal conditions, and thaw strains for several tests of varying freezing duration.

TempW thermal modeling software was used to predict the temperature gradients within a deposit of MFT and sump fines during an average winter in Fort McMurray. By determining the frost penetration with the model, and applying the thaw strain measured in the lab, it was predicted that the deposits of MFT and sump fines would have thaw settlements of 30 cm and 14 cm, respectively. In addition to the thaw settlement, the amount of ice lens development, and hence dewatering of the underlying deposit was also predicted by combining the thermal model with the measured SP. It was predicted that the sump would develop 1 cm of ice lenses, while the MFT would have 1.2 m of ice lenses. These values are highly dependant on the SP, which is known to have a variation of up to 1 order of magnitude between subsequent freezing tests. Better frost heave testing or calibration with field conditions would allow better predictions to be made in the future.

8.2 Conclusions

- The ice observed in the cores of naturally frozen sump material differed slightly from the ice lensing observed in the laboratory tests. Temperature fluctuations caused the naturally frozen samples to exhibit variable ice lens structure. The natural samples generally exhibited the same ice structure as was created in the laboratory, although the peds and ice lenses were larger in the natural soil.
- Vertically aligned ice structures appear to have caused stresses to be locked against the test cell wall and restricted heave.
- The segregation potential of high moisture content mine tailings cannot be determined with tradition freezing test methods. Suction within the unfrozen soil is localized very near the ice lens and is too difficult to measure with typical sensors.
- Time-lapse photography is a suitable method for determining the segregation potential of high moisture content mine tailings; the method has less precision than conventional test methods.
- The amount of heave that is measured at the top of the sample appears to be related to the Liquidity Index (LI) of the soil. Soils with a high LI are

compressible and do not exhibit surface heave even though extensive ice lens formation does occur. Repeated freeze-thaw cycles cause the LI to decrease, and the amount of measured heave to increase.

- Photographs of the ice lenses during freezing indicate that the ice structure may be related to the LI. A soil with a high LI develops a more vertically aligned, needled structure. These vertical needles develop in advance of any horizontal lenses. This may be due to the development of shrinkage cracks in soils with higher plasticity.
- The segregation potential of the MFT was found to be much greater than that of Devon Silt or the sump material, which were approximately equal. This indicates potential for using freeze-thaw to assist with dewatering of MFT.
- Consolidation can be removed from the total thaw strain for high moisture content mine tailings by using freezing tests of varying duration.
- Field-scale frost heave predictions can be performed with the knowledge of the thermal conditions, soil thermal characteristics, and soil frost susceptibility. These predictions are highly dependant on the segregation potential, which is a difficult parameter to determine precisely.

8.3 Recommendations

Freezing tests performed on typical soils require only the measurement of surface heave or water supply. This is adequate for soils that are stiff. It is recommended that when tests are performed on softer soils, digital photographs of the final ice lens should be taken to ensure that the soil is incompressible. If the photographs show a final ice lens with a stationary base, the assumption of incompressibility is valid. Using digital photographs from freezing tests for a range of soils, it should be possible to correlate parameters such as LI or shear strength with the amount of consolidation that occurs during freezing. The segregation potential may also be affected by the LI. Using time-lapse photography would allow this relationship to be studied for a soil over a wide range of moisture contents.

The SP was determined for only two types of mine tailings. More testing on samples of varying solids content would allow for future modeling of the tailings that are currently awaiting reclamation.

Segregation potential is a sensitive parameter that can have a large impact on field scale predictions. It is recommended that SP be measured carefully, or be estimated from field measurements. With better SP measurements, and by performing more freezing and thaw strain tests at different solids contents, the segregation potential and thaw strain could be determined over a range of insitu physical states of MFT. The frost heave model could then be used to analyze the influence of freeze-thaw over several years, with increasing solids content after each cycle. This would be a useful tool for deciding how to reclaim high moisture content mine tailings by means of a natural process.

Appendix A - Summary of Test Results

Table A-1 - Overview of Tests

Test	Material	Number of Cycles	Core Pressure Measured	Preconsolidation Pressure (kPa)	Temperature Gradient at Final Lens (°C/cm)
S1T1b	Devon Silt	1	No	Unknown (<100)	0.66
S1T2	MFT	1	No	0	0.55
S1T3	MFT	2	No	0	0.31
S1T4	MFT	2	No	0	0.37
S2T2	MFT	1	Yes	0	0.41
S2T3	MFT	1	Yes	0	0.31
S2T4	MFT	1	Yes	0	0.50
S3T1	Bulk Sump	3	Yes	Unknown	0.51
S3T2	Bulk Sump	3	Yes	Unknown	0.55
S4T1	Sump Core	1	Yes	Unknown	0.72
S4T2	Sump Core	1	Yes	Unknown	0.63
S4T3	Sump Core	1	No	Unknown	N/A
S5T1	Devon Silt	1	No	100	0.39
S5T2	Devon Silt	1	No	100	0.38
S6T1	Sump Core	0	N/A	Unknown	N/A
S6T2	Sump Core	0	N/A	Unknown	N/A
S6T3	Sump Core	0	N/A	Unknown	N/A
S6T4	Sump Core	0	N/A	Unknown	N/A
S6T5	Sump Core	0	N/A	Unknown	N/A
S6T6	Sump Core	0	N/A	Unknown	N/A
S6T7	Sump Core	0	N/A	Unknown	N/A
S6T8	Sump Core	0	N/A	Unknown	N/A

A.1 Test Series 1

A.1.1 S1T1 – Devon Silt

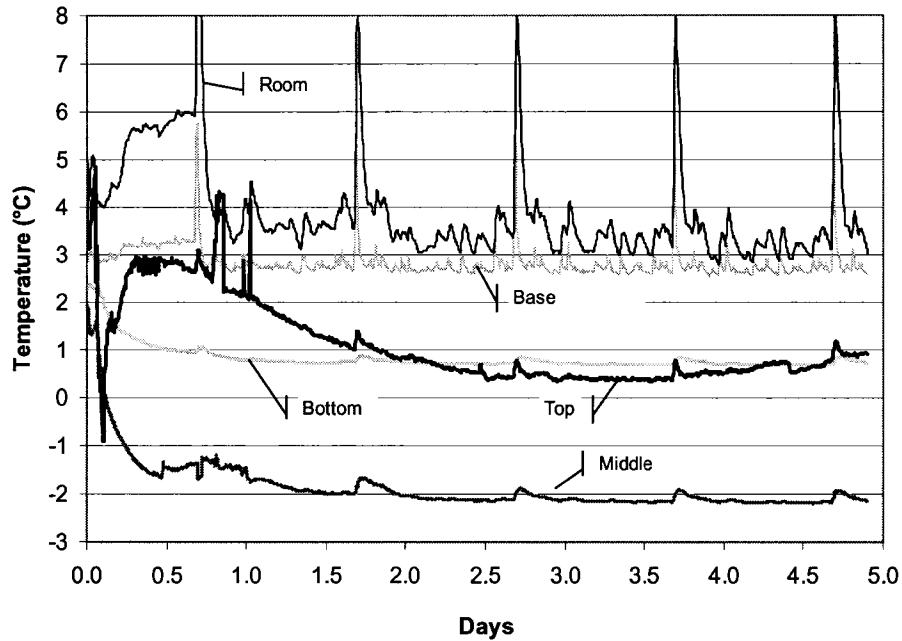


Figure A-1 – Temperature in Sample During Test – S1T1

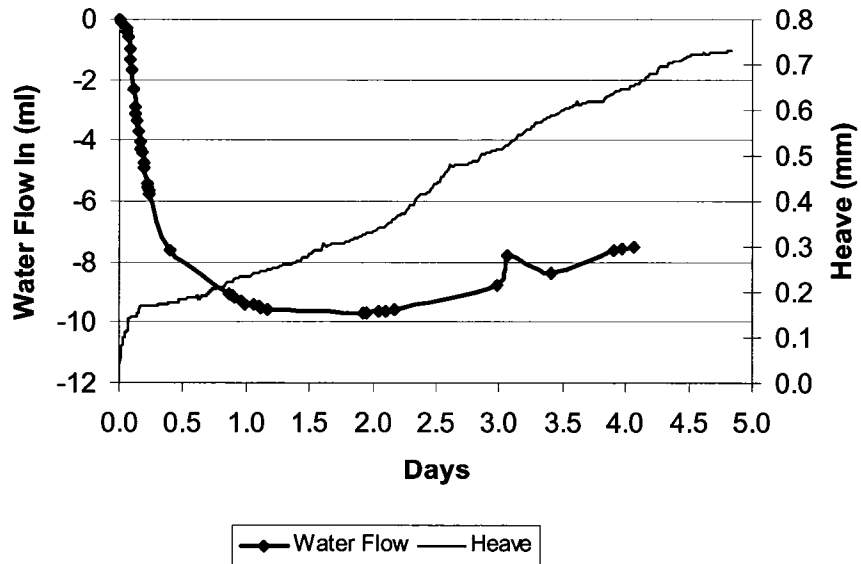


Figure A-2 - Water Supply and Heave - S1T1

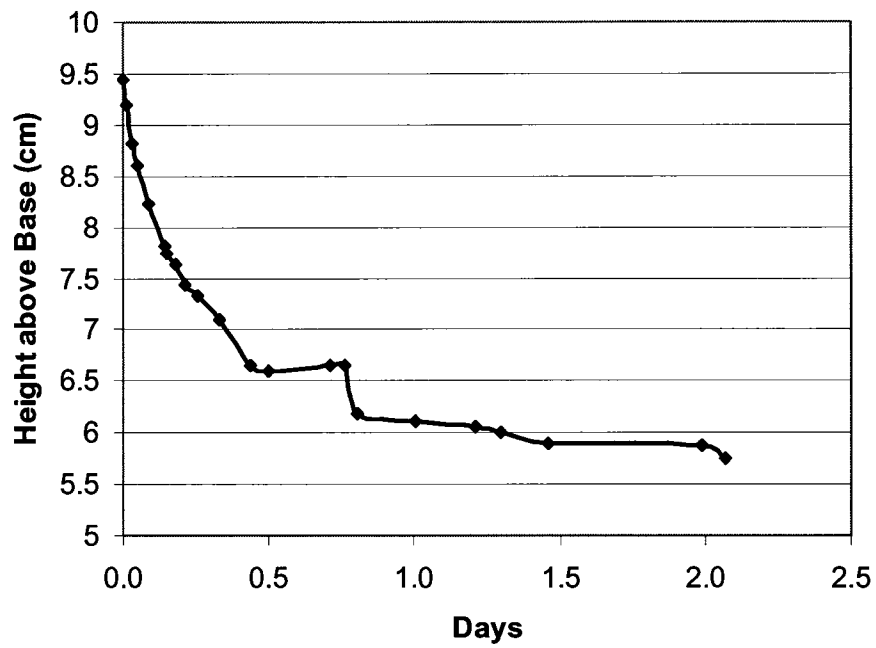


Figure A-3 - Base of Ice Lens Penetration - S1T1

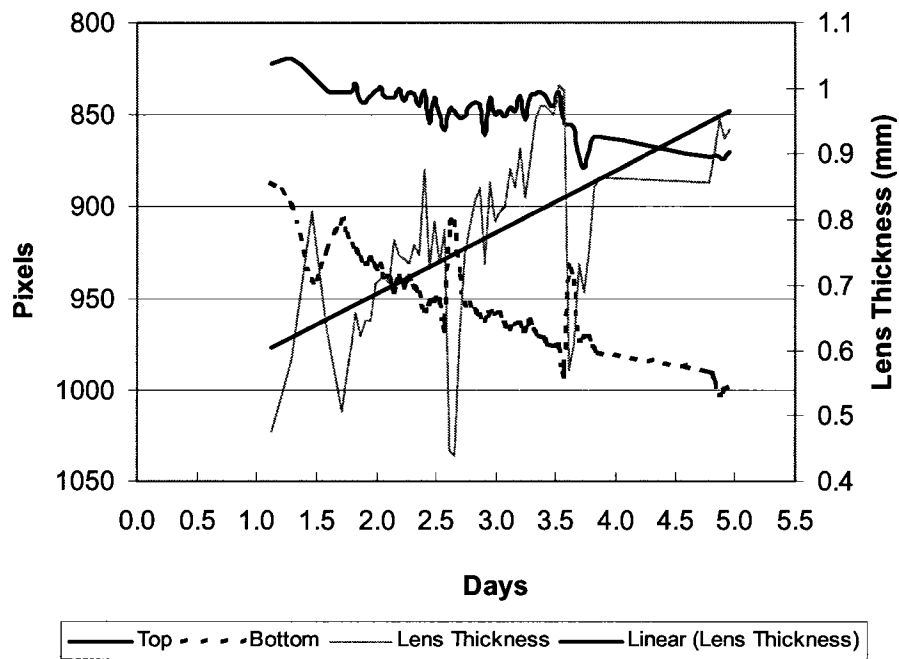


Figure A-4 - Final Ice Lens Growth - S1T1

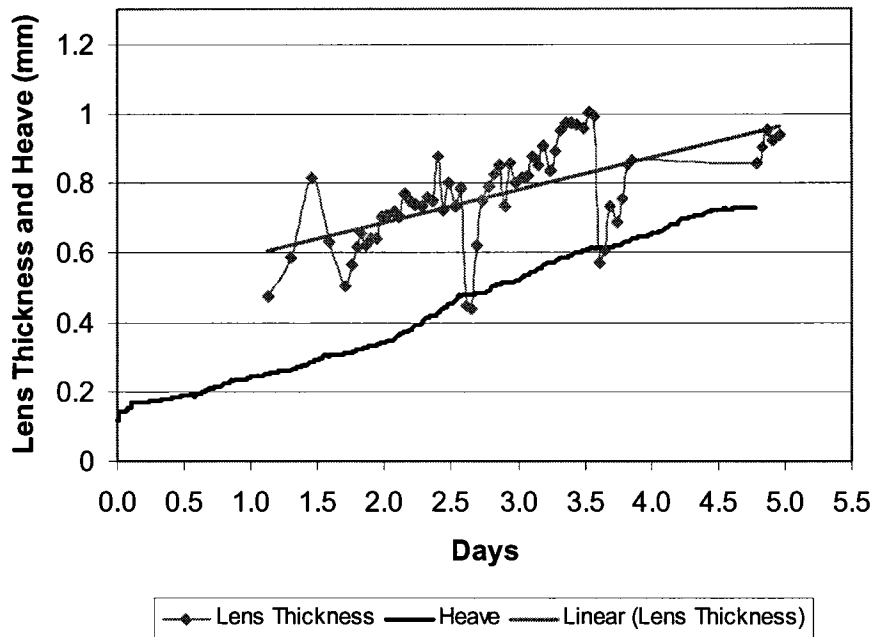


Figure A-5 - Surface Heave and Final Ice Lens Growth - S1T1

A.1.2 S1T2 – Suncor Pond 2/3 MFT

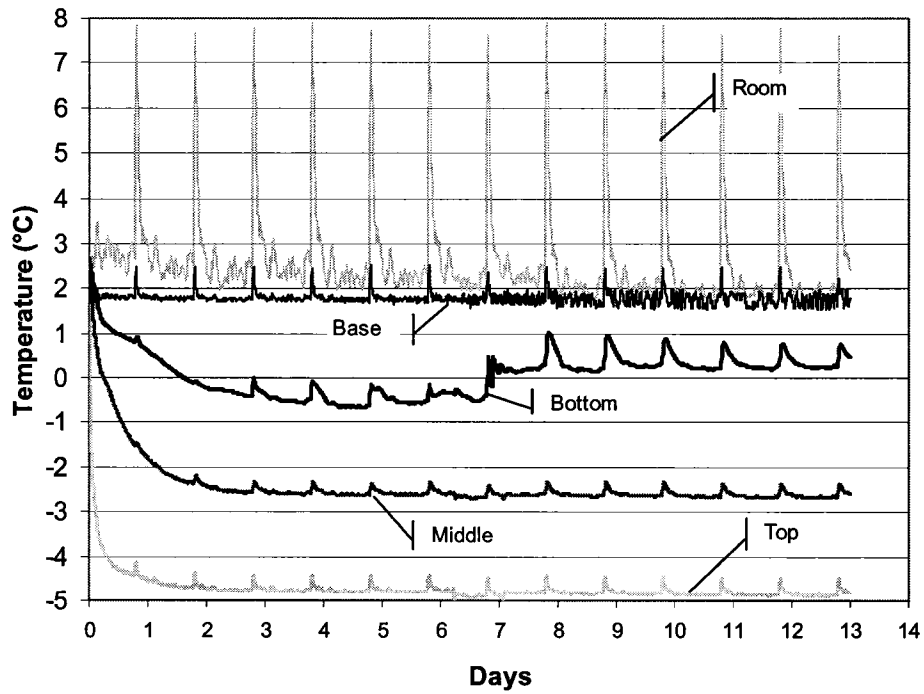


Figure A-6 - Temperature in Sample During Test - S1T2

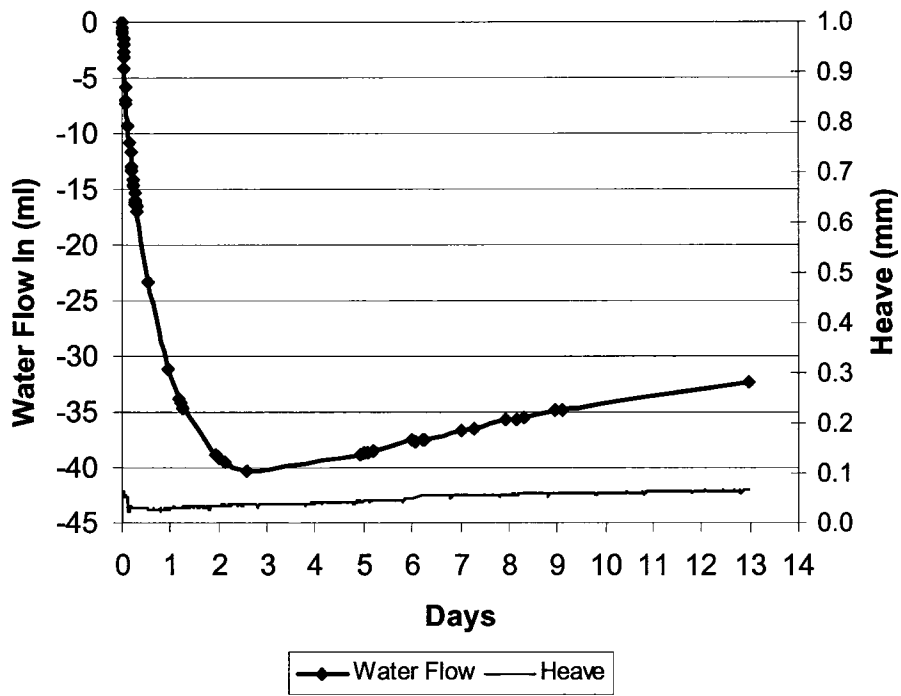


Figure A-7 - Water Supply and Heave - S1T2

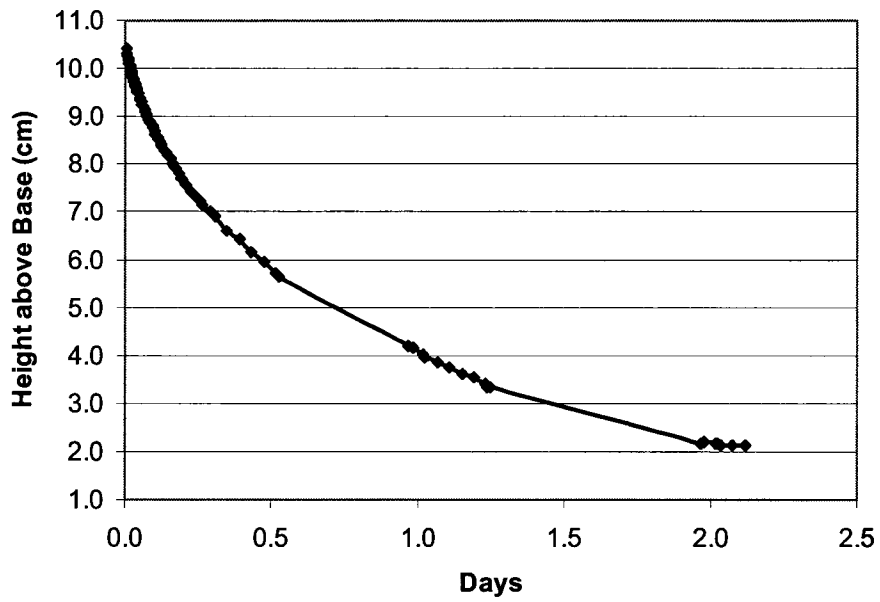


Figure A-8 - Base of Fringe Penetration - S1T2

A.1.3 S1T3 – Suncor Pond 2/3 MFT

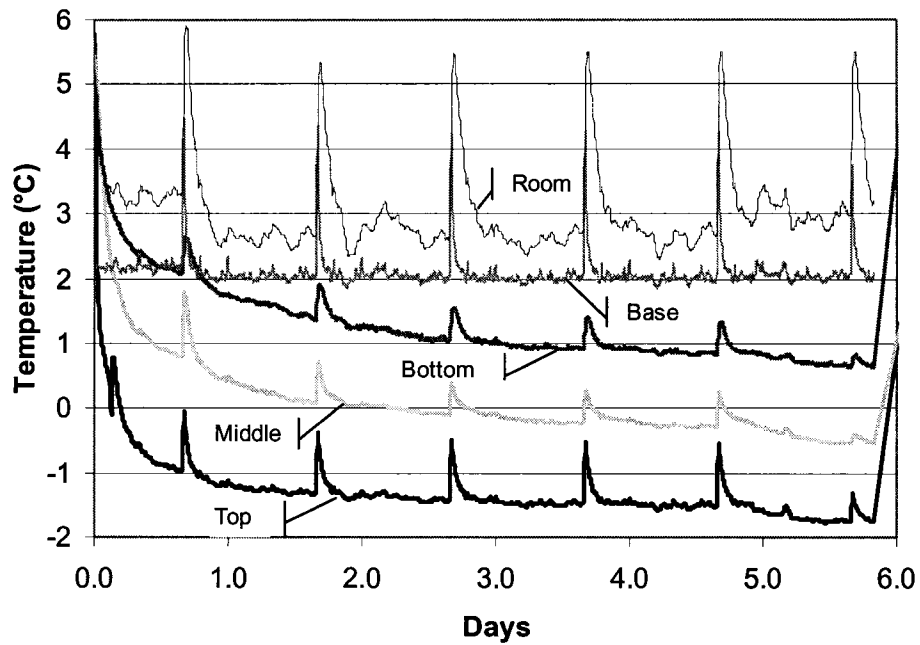


Figure A-9 - Temperature in Sample During Test - Cycle 1 - S1T3

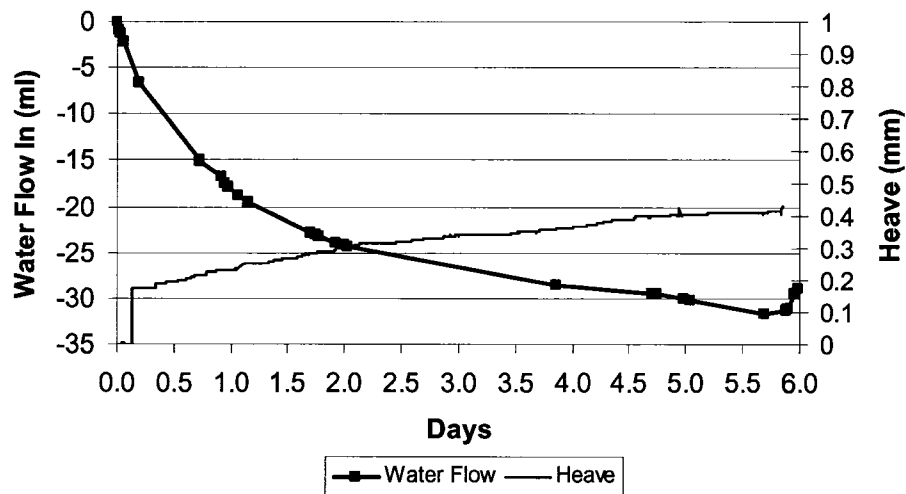


Figure A-10 - Water Supply and Heave - Cycle 1 - S1T3

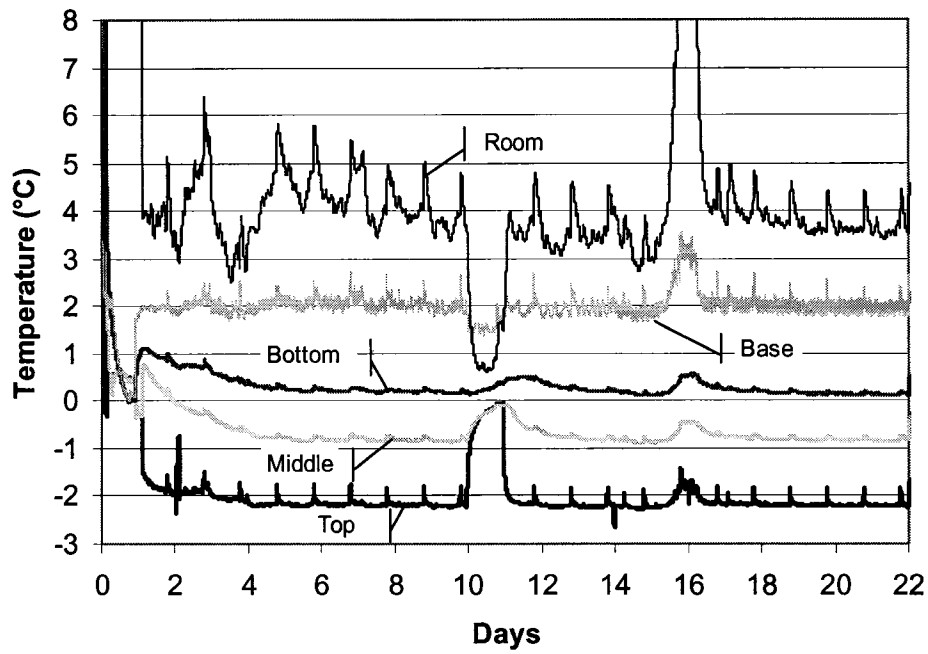


Figure A-11 - Temperature in Sample During Test - Cycle 2 - S1T3

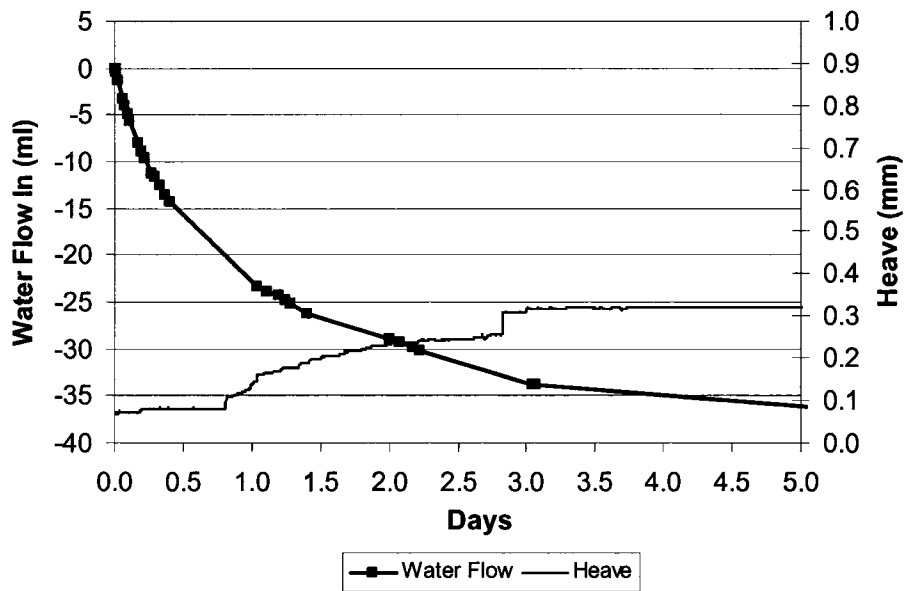


Figure A-12 - Water Supply and Heave - Cycle 2 - S1T3

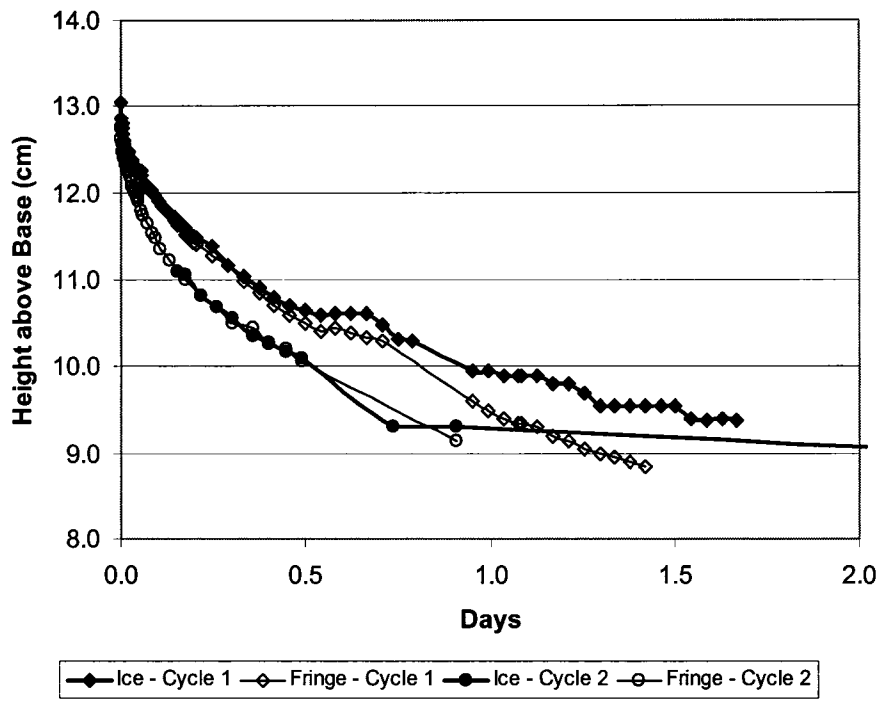


Figure A-13 - Ice and Fringe Penetration - S1T3



Figure A-14 - Solids Content Profile – After 2 Cycles - S1T3

A.1.4 S1T4 – Suncor Pond 2/3 MFT

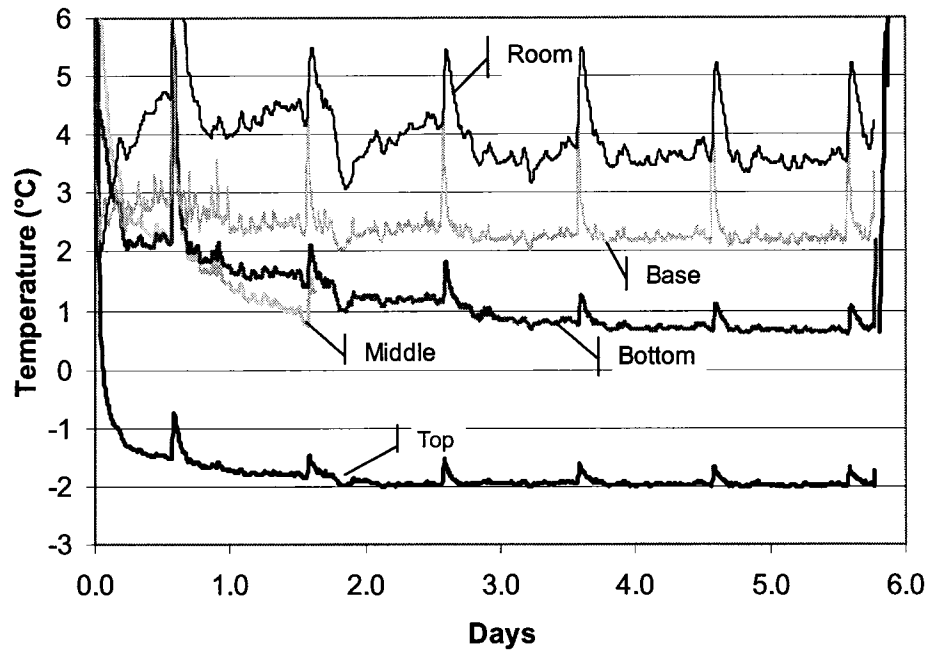


Figure A-15 - Temperature in Sample During Test - Cycle 1 - S1T4

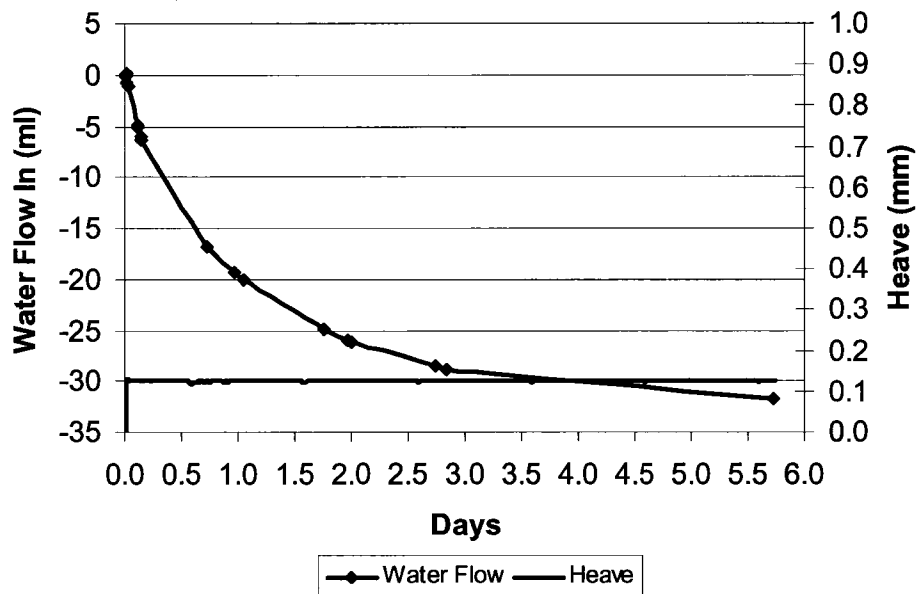


Figure A-16 - Water Supply and Heave - Cycle 1 - S1T4

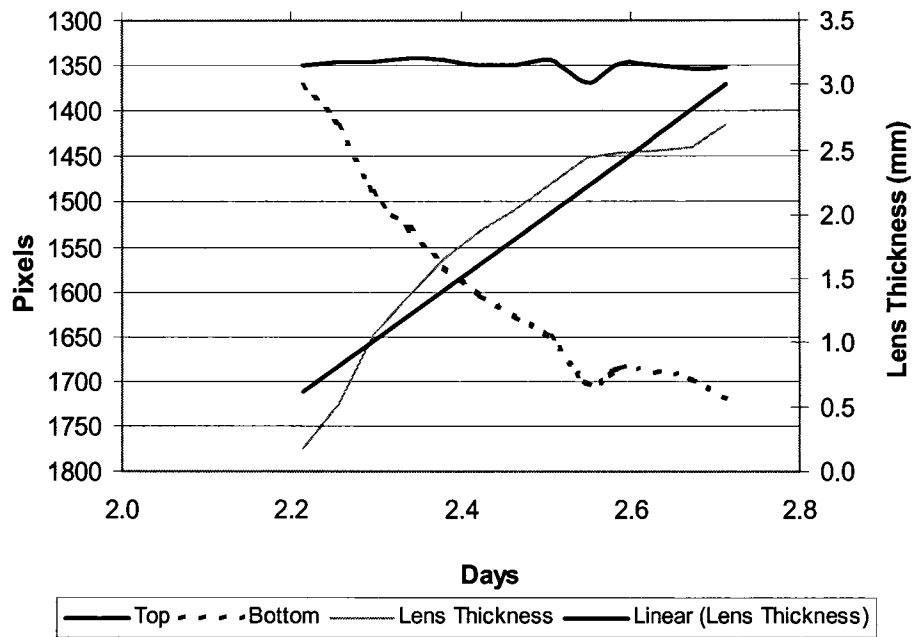


Figure A-17 - Final Ice Lens Growth - Cycle 1 - S1T4

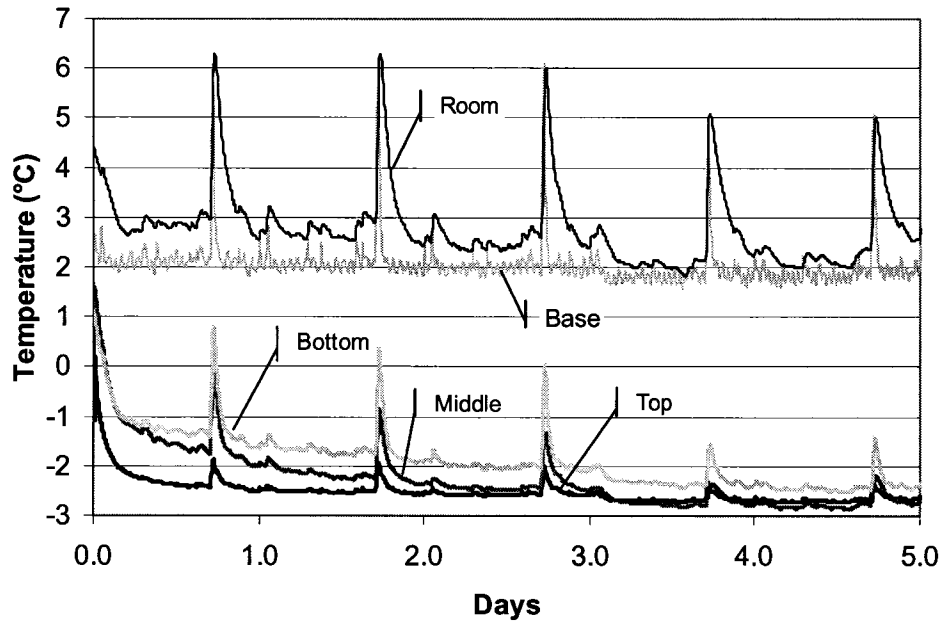


Figure A-18 - Temperature in Sample During Test - Cycle 2 - S1T4

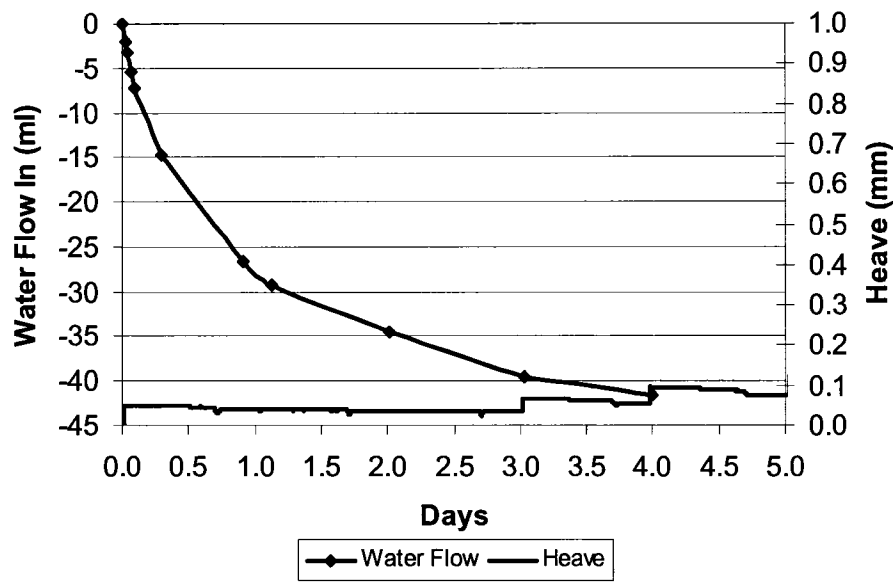


Figure A-19 - Water Supply and Heave - Cycle 2 - S1T4

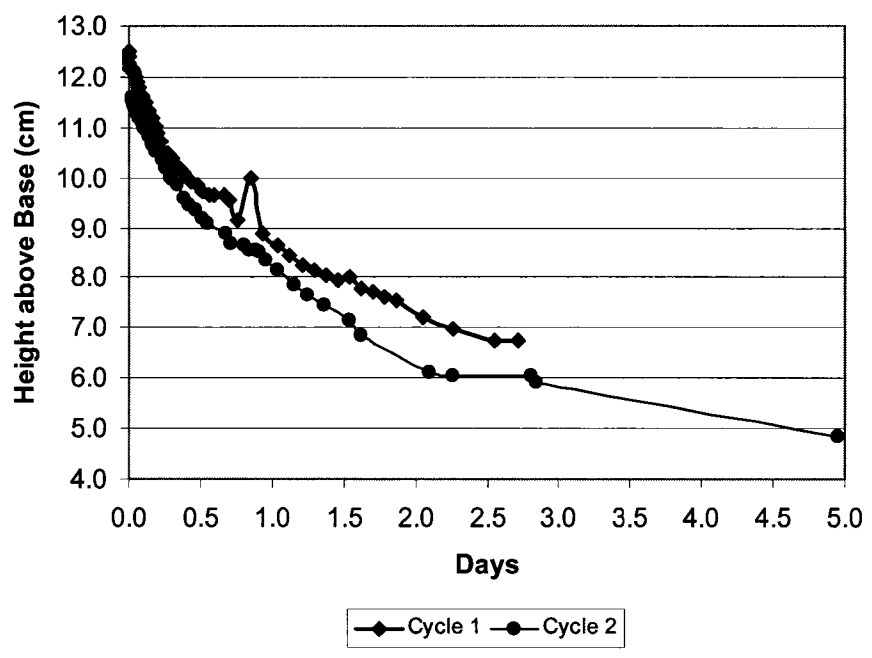


Figure A-20 - Base of Ice Lens Penetration - S1T4

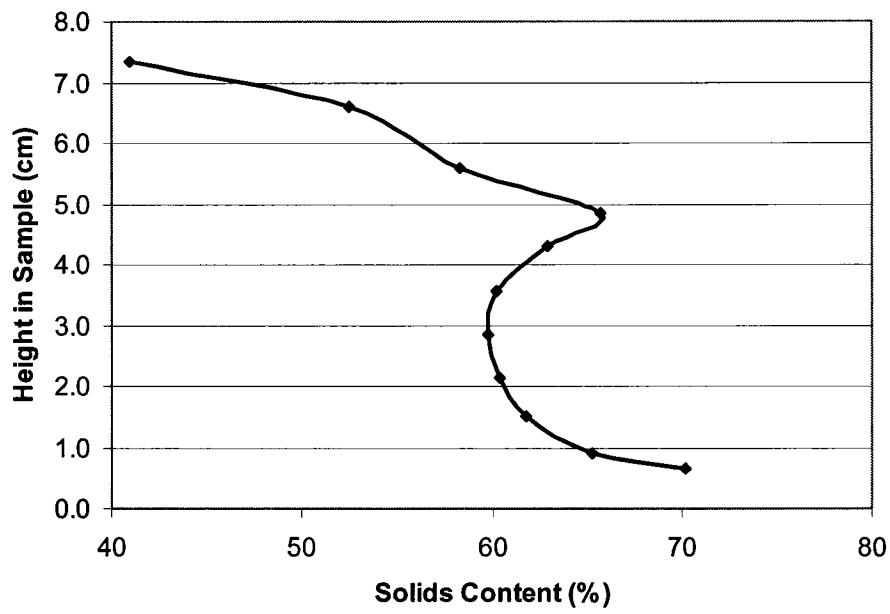
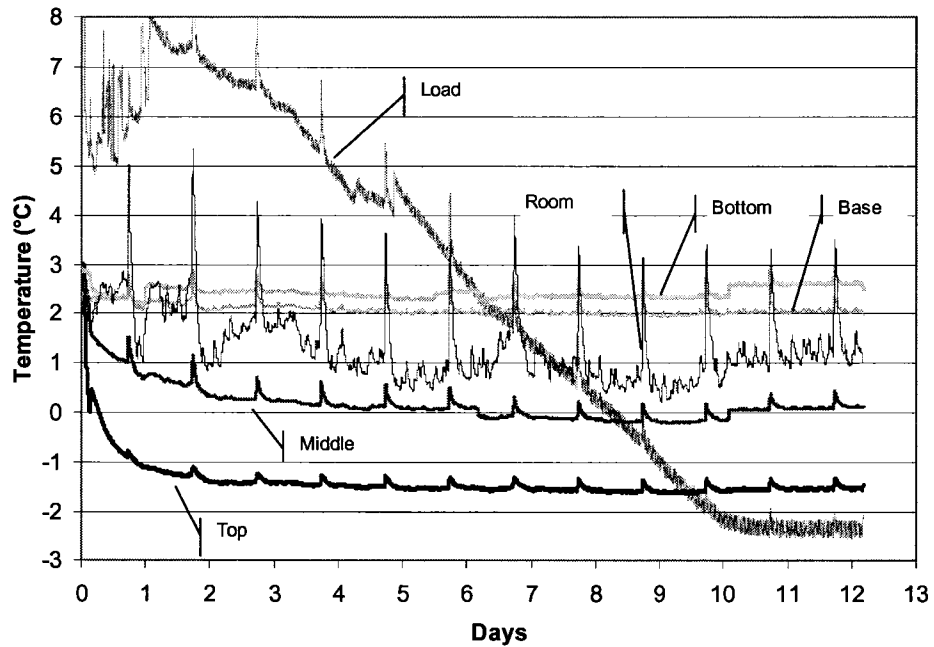


Figure A-21 - Solids Content Profile - After 2 Cycles - S1T4

A.2 Test Series 2

A.2.1 S2T2 – Suncor Pond 2/3 MFT



A-22 - Temperature in Sample During Test - S2T2

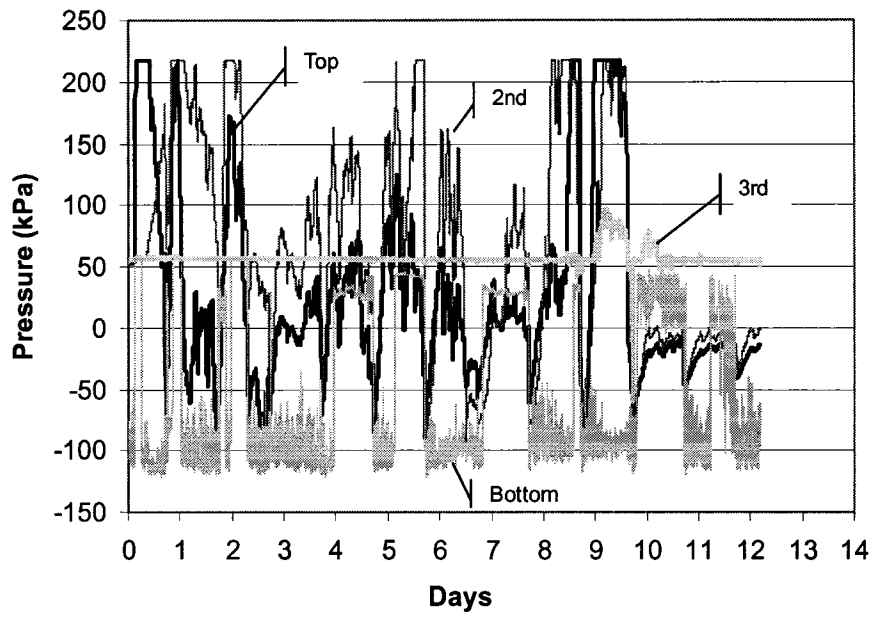


Figure A-23 - Pore Pressure During Freezing - 54.6 kPa Back-Pressure - S2T2

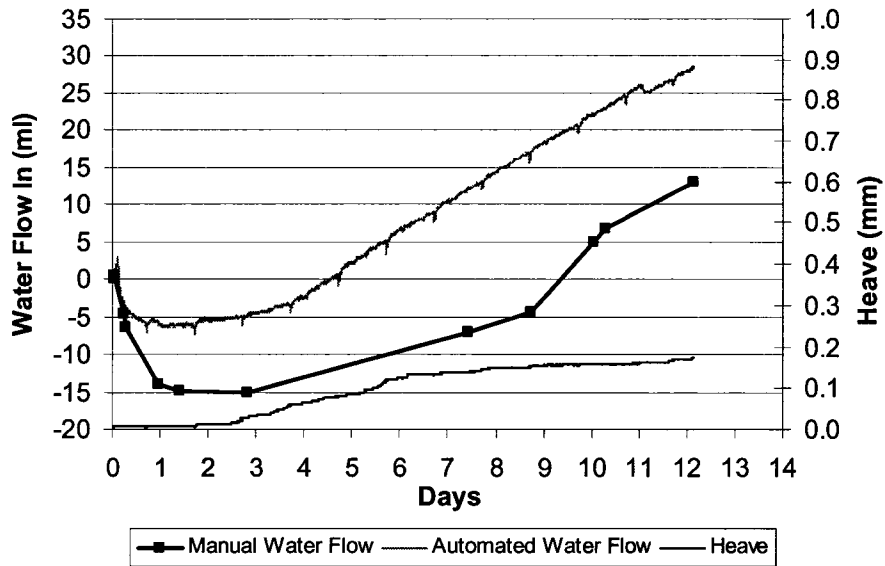


Figure A-24 - Water Supply and Heave - S2T2

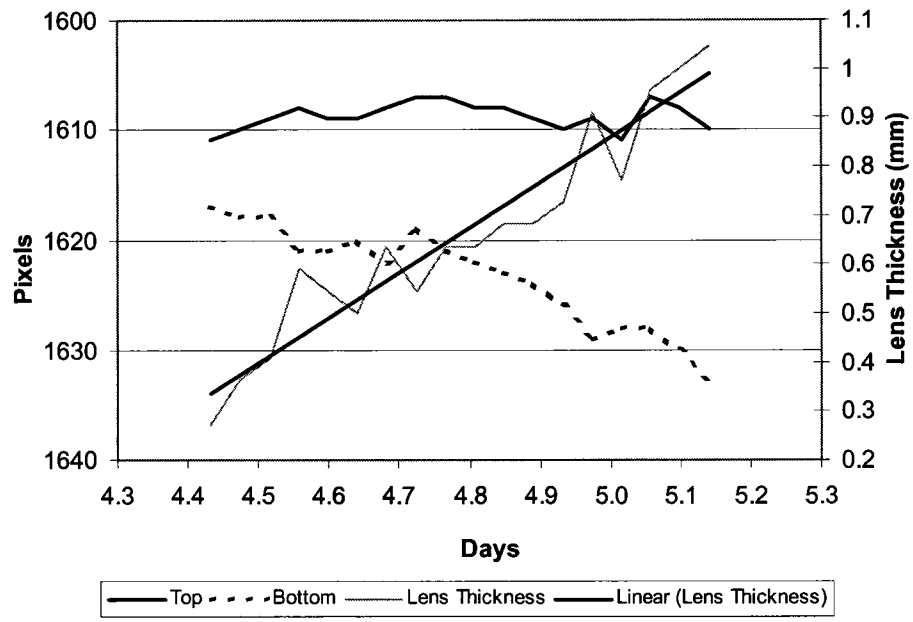


Figure A-25 - Final Ice Lens Growth - S2T2

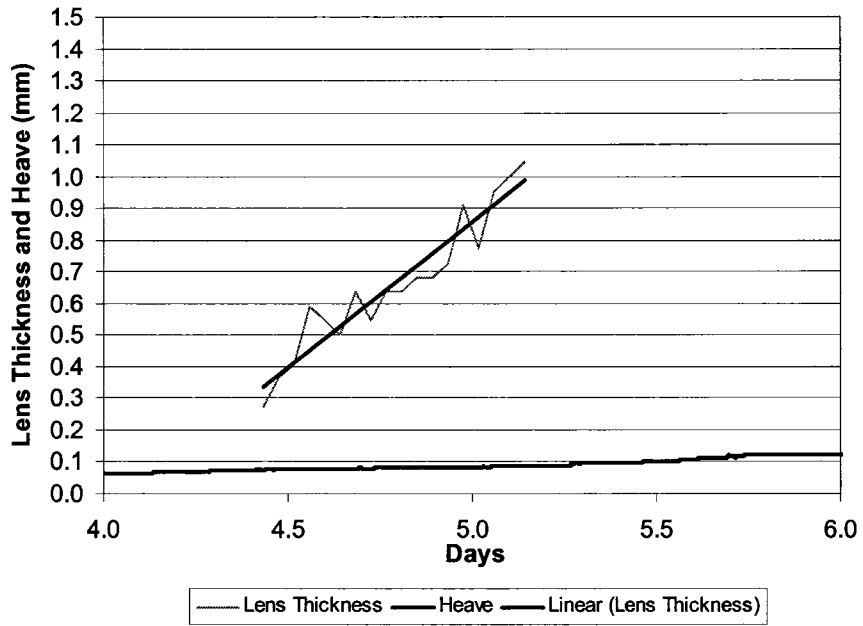


Figure A-26 - Surface Heave and Final Ice Lens Growth - S2T2

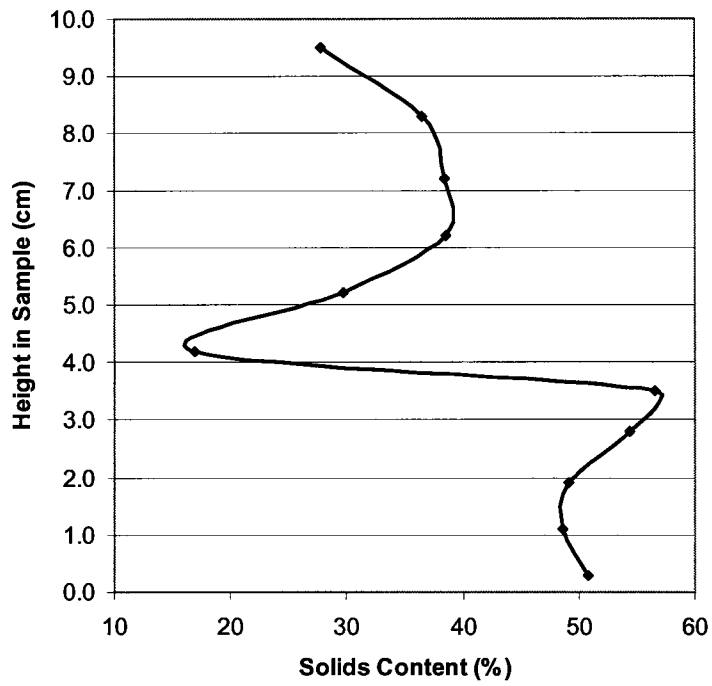


Figure A-27 - Solids Content Profile - S2T2

A.2.2 S2T3 - Suncor Pond 2/3 MFT

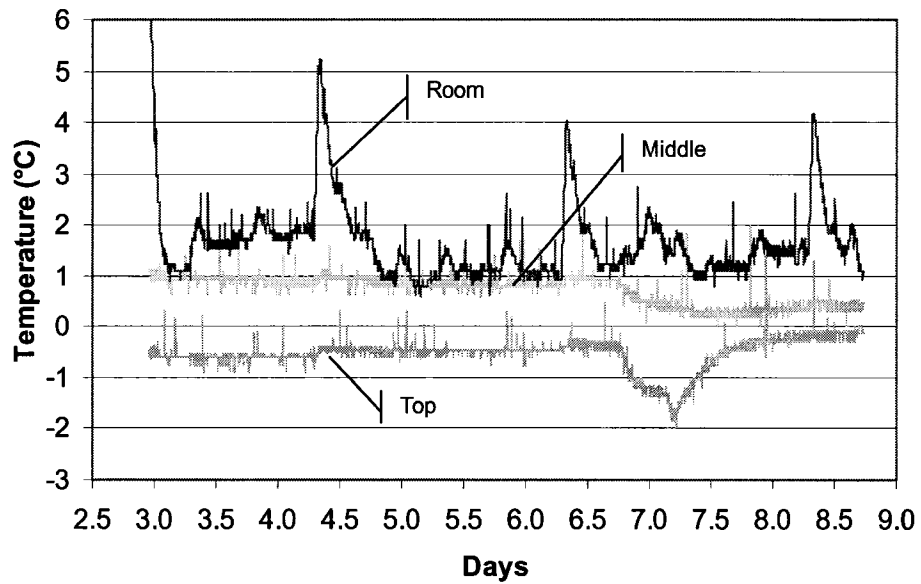


Figure A-28 - Temperature in Sample During Test - S2T3

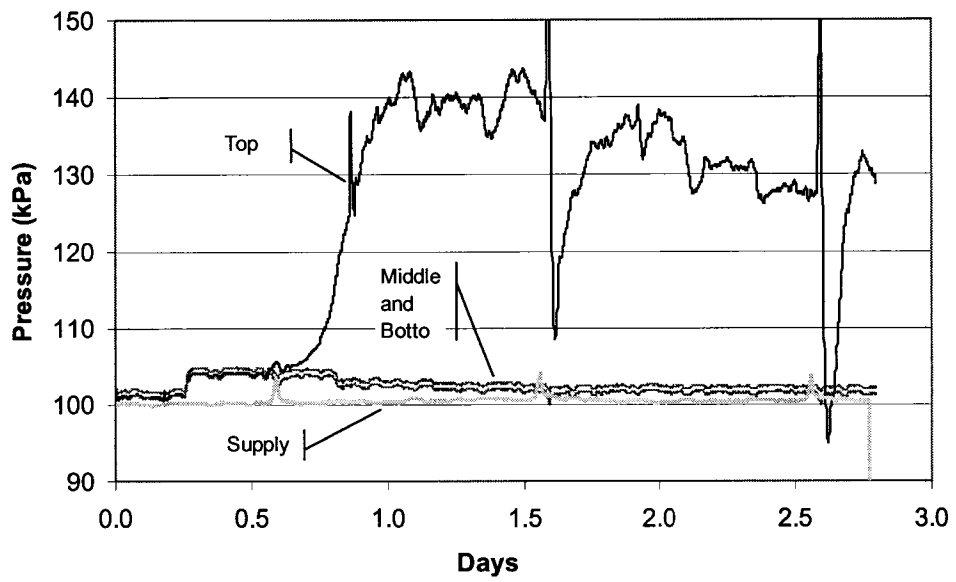


Figure A-29 - Pore Pressure During Freezing – S2T3

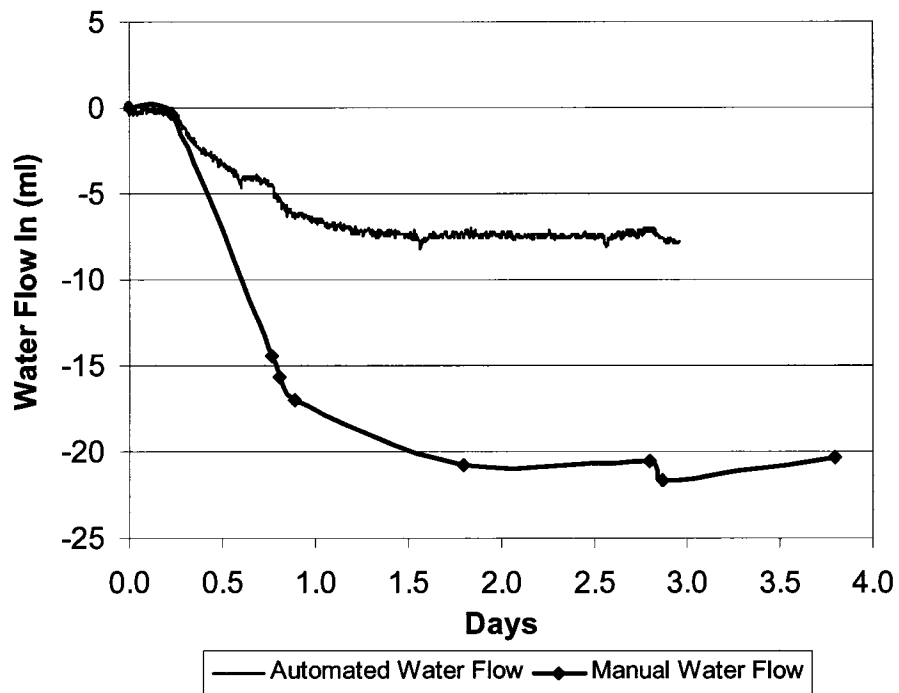


Figure A-30 - Water Supply – S2T3

A.2.3 S2T4 – Suncor Pond 2/3 MFT

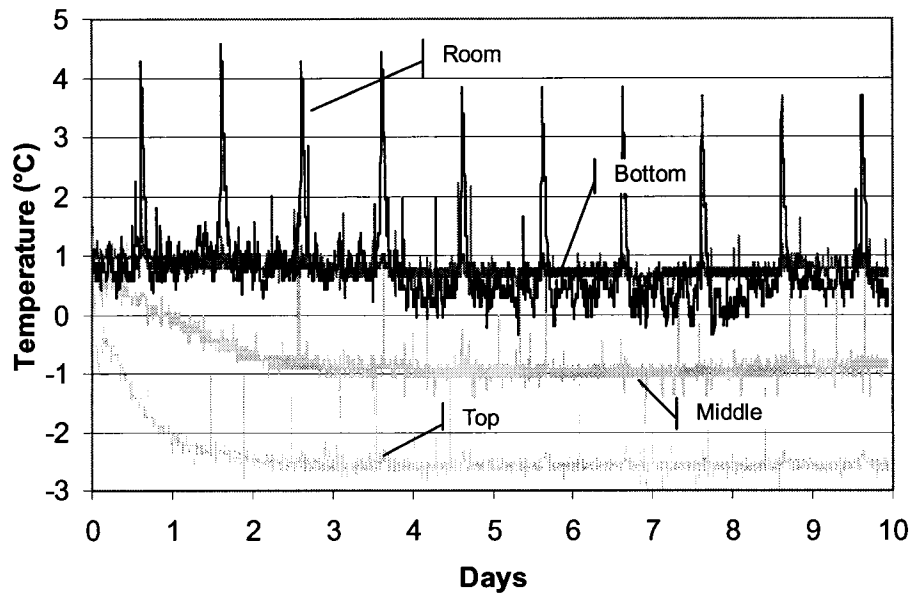


Figure A-31 - Temperature in Sample During Test – S2T4

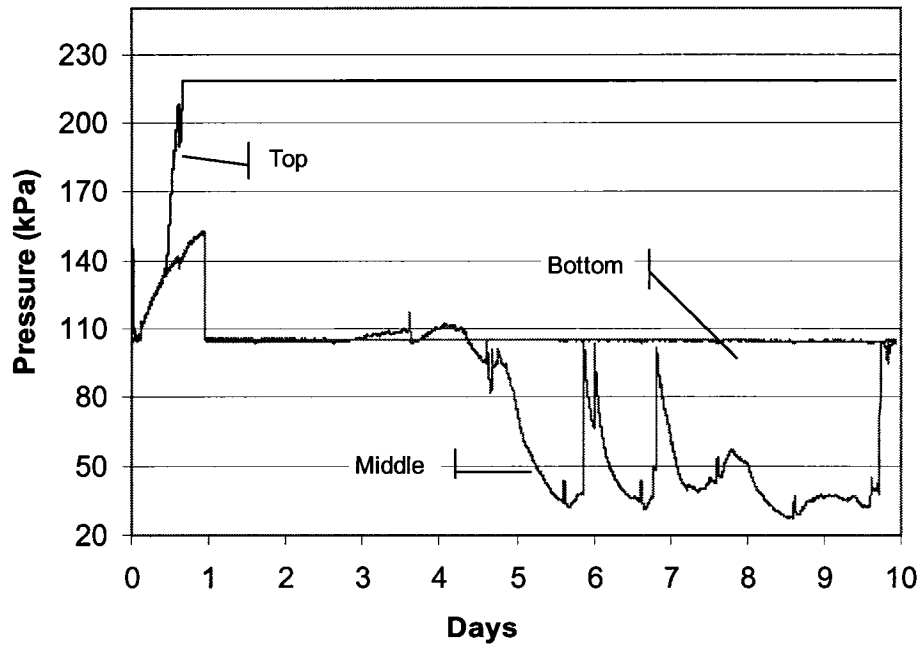


Figure A-32 - Pore Pressure During Freezing – 106 kPa Back Pressure – S2T4

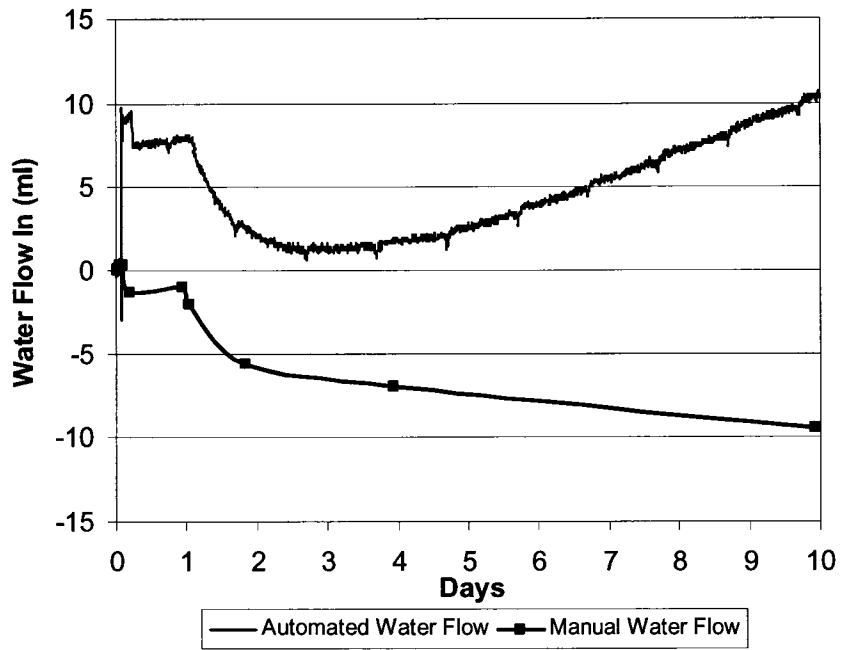


Figure A-33 - Water Supply – S2T4

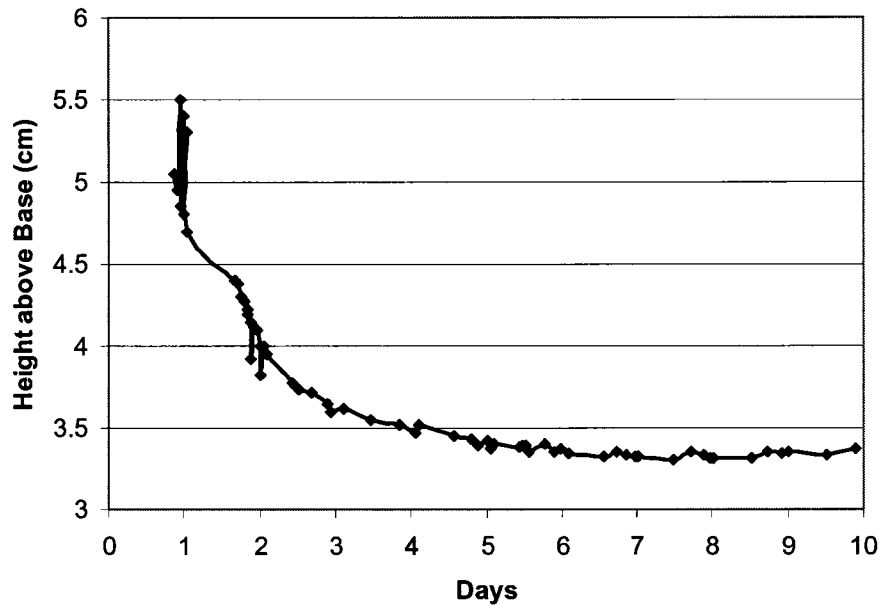


Figure A-34 - Base of Ice Lens Penetration – S2T4

A.3 Test Series 3

A.3.1 S3T1 – Syncrude SWSS Sump Fines - Bulk

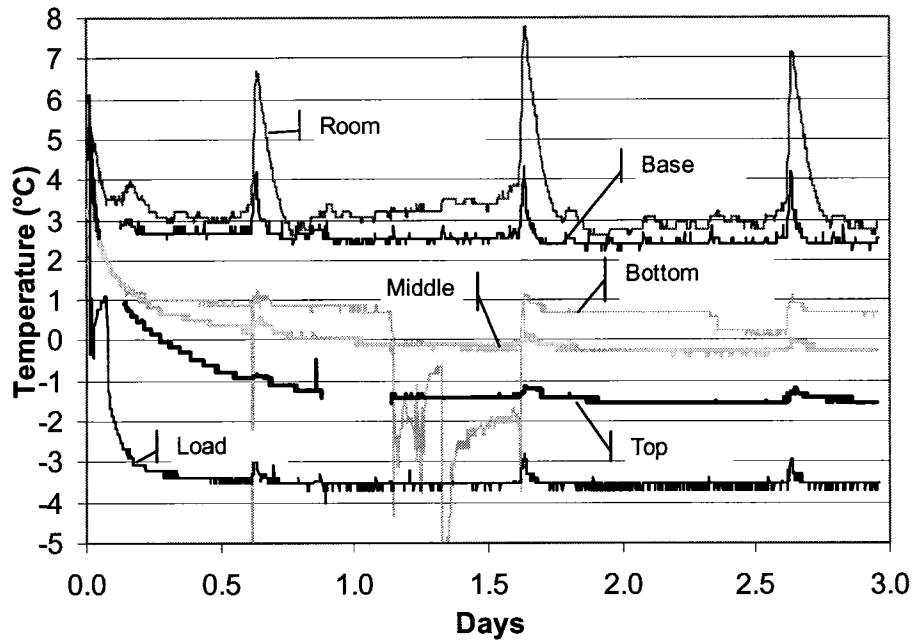


Figure A-35 - Temperature in Sample During Test - Cycle 1 – S3T1

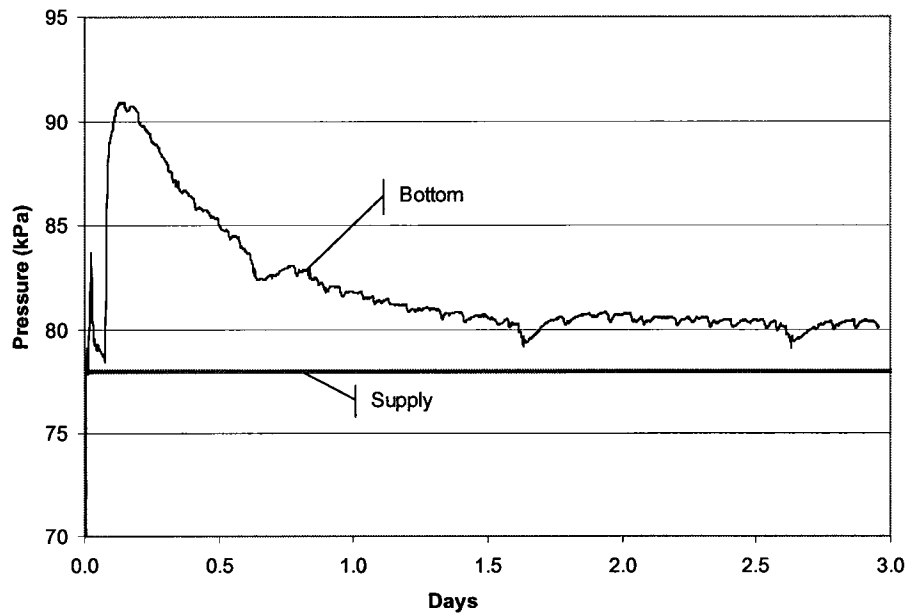


Figure A-36 - Pore Pressure During Freezing - 78 kPa Back-Pressure – Cycle 1 – S3T1

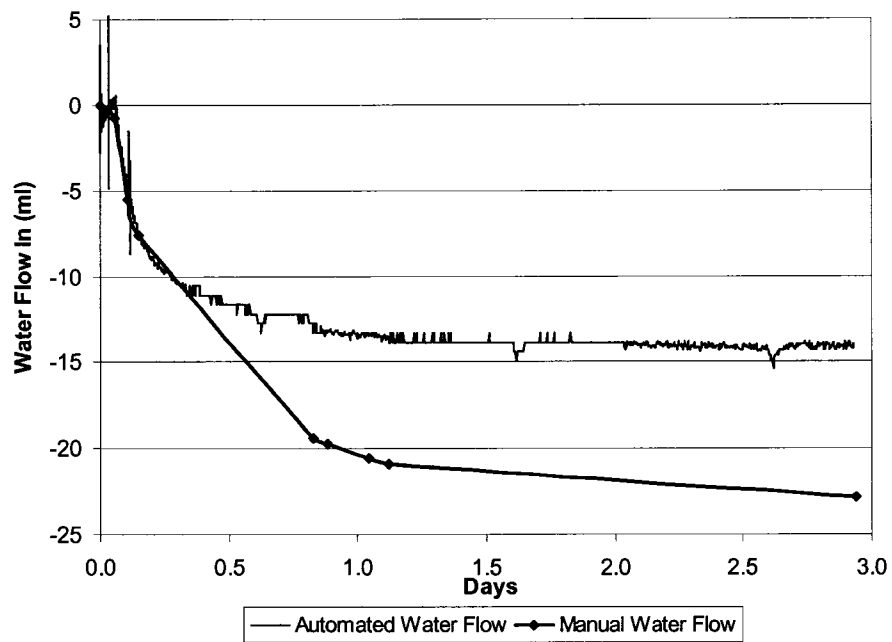


Figure A-37 - Water Supply - Cycle 1 – S3T1

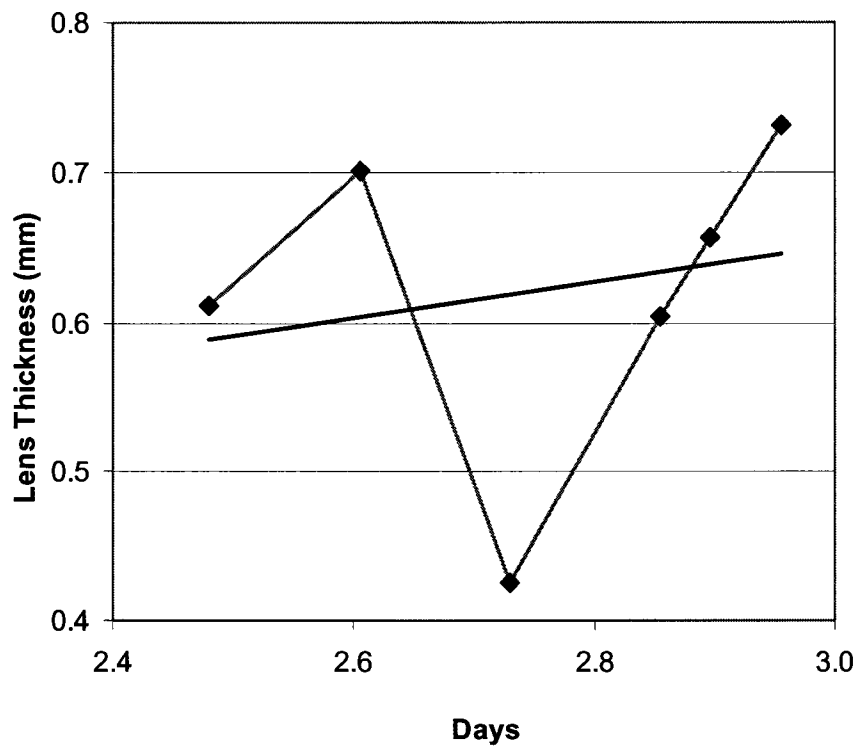


Figure A-38 - Final Ice Lens Growth – S3T1

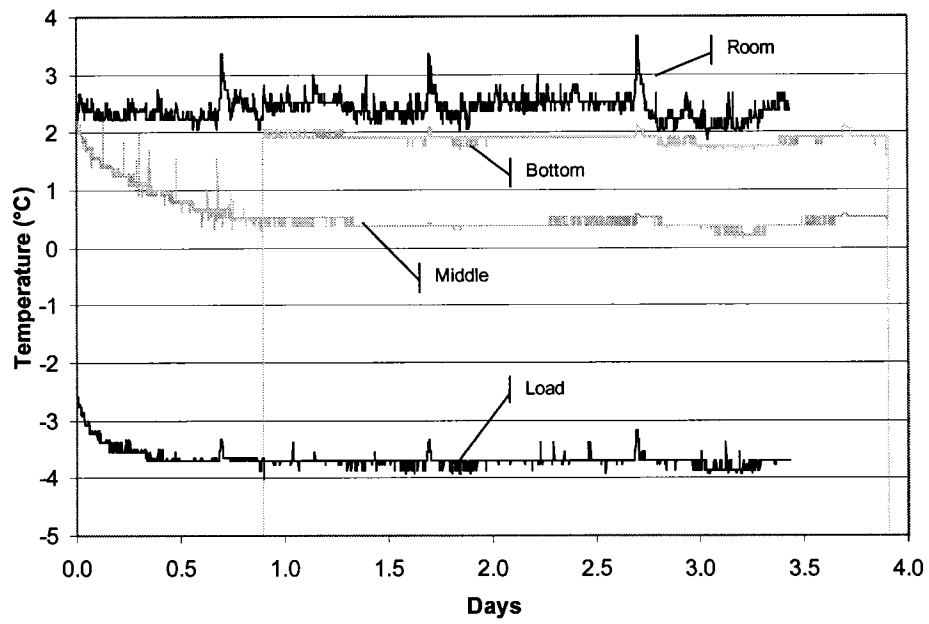


Figure A-39 - Temperature in Sample During Test - Cycle 2 - S3T1

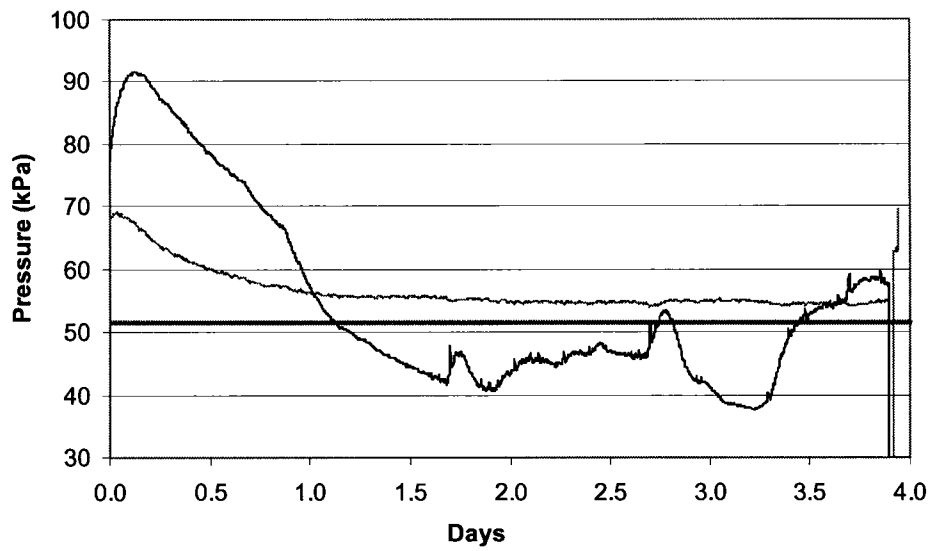


Figure A-40 - Pore Pressure During Freezing - Cycle 2 - S3T1

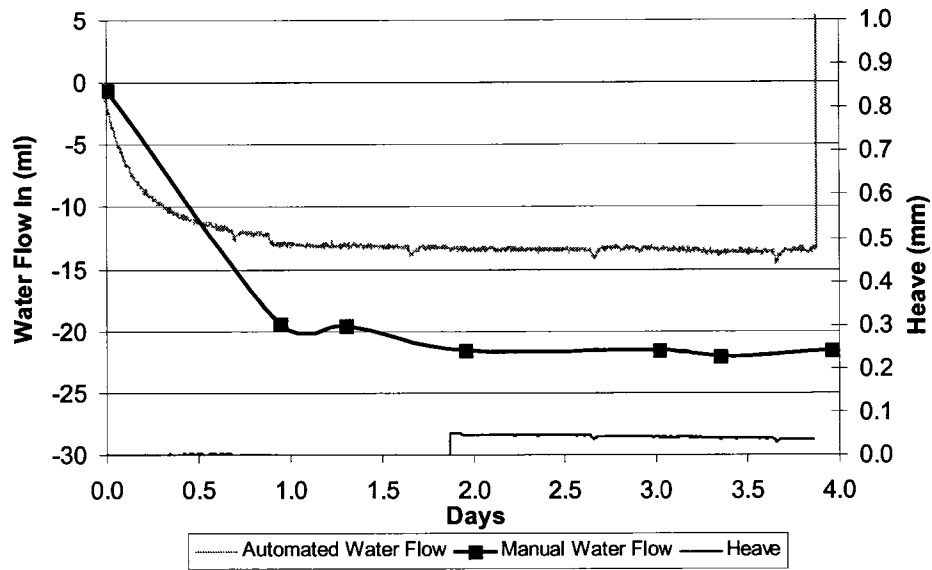


Figure A-41 - Water Supply and Heave - Cycle 2 - S3T1

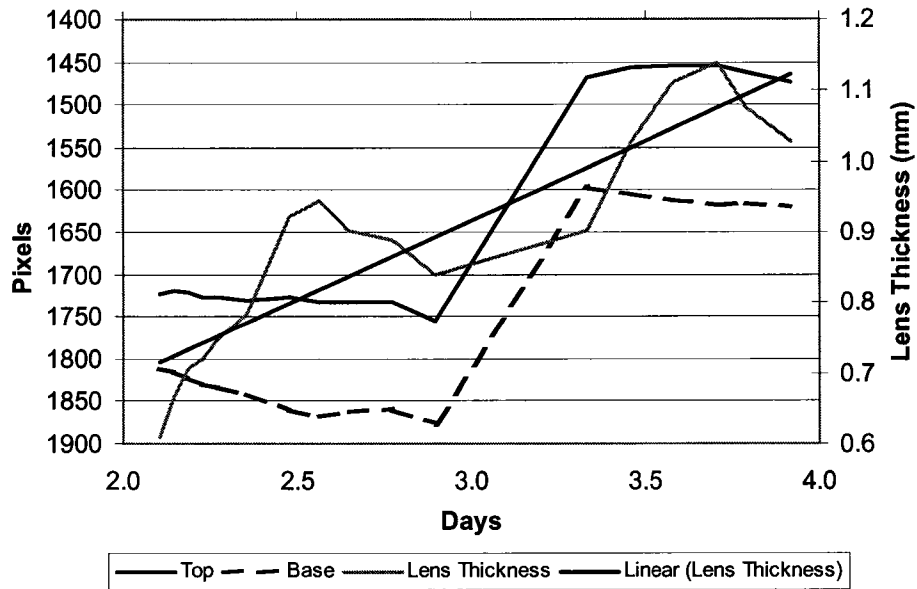


Figure A-42 - Final Ice Lens Growth - Cycle 2 - S3T1

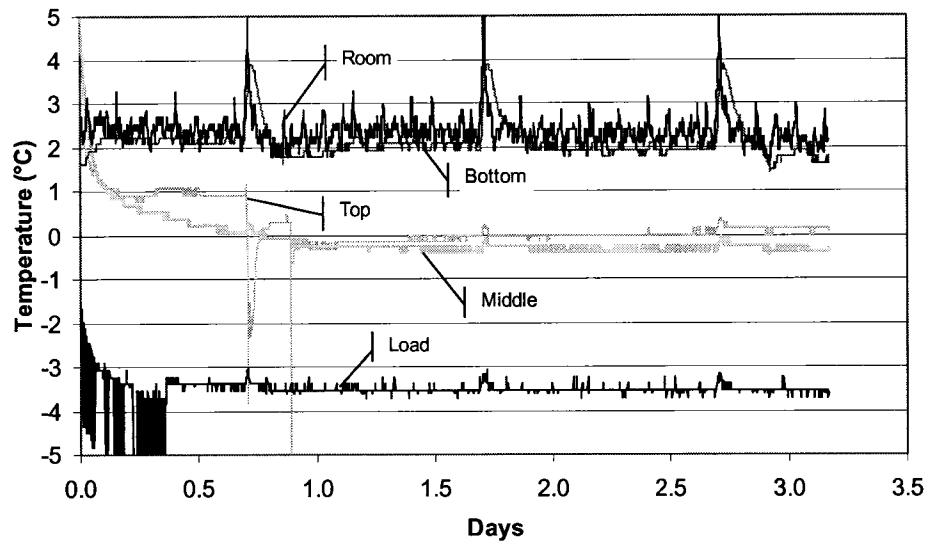


Figure A-43 - Temperature in Sample During Test - Cycle 3 - S3T1

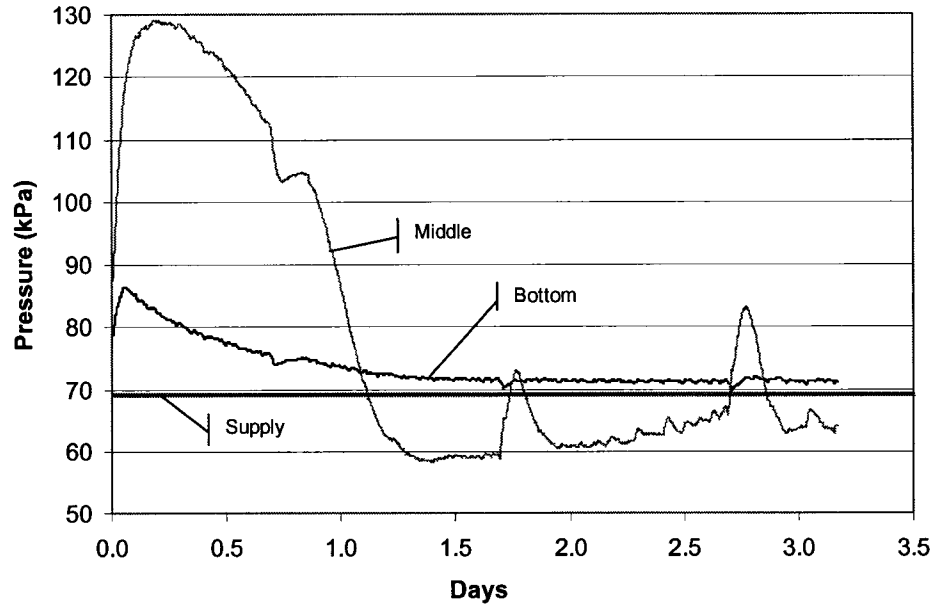


Figure A-44 - Pore Pressure During Freezing - Cycle 3 - S3T1

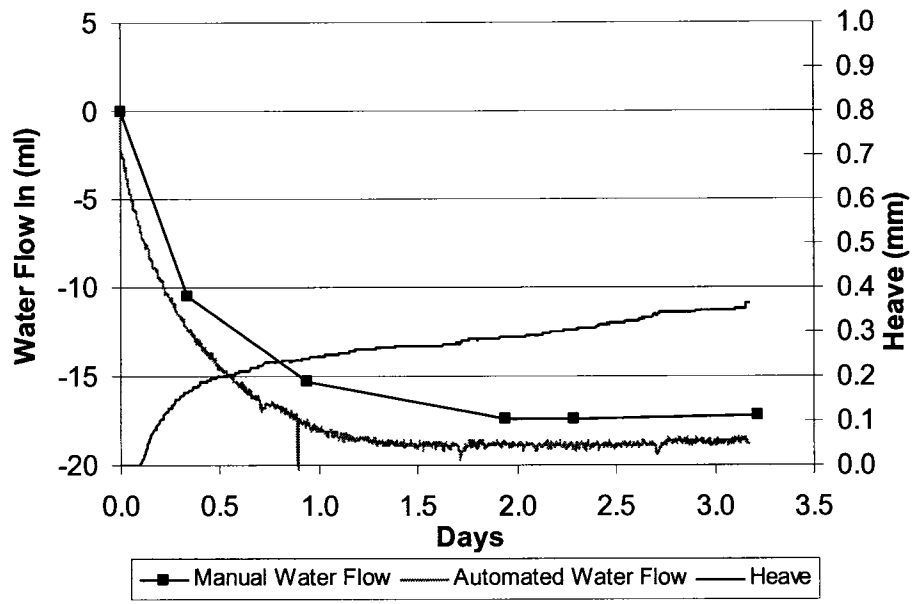


Figure A-45 - Water Supply and Heave - Cycle 3 - S3T1

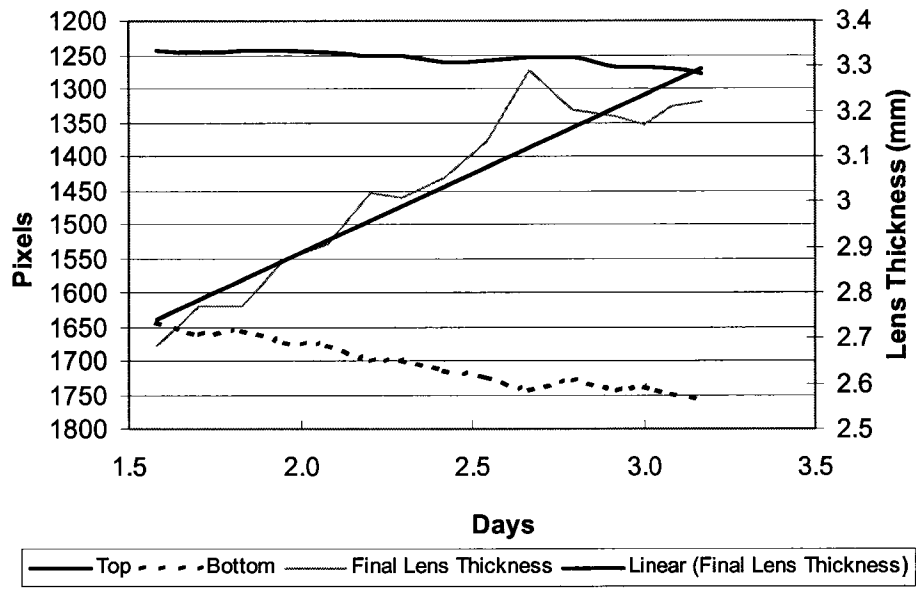


Figure A-46 - Final Ice Lens Growth - Cycle 3 - S3T1

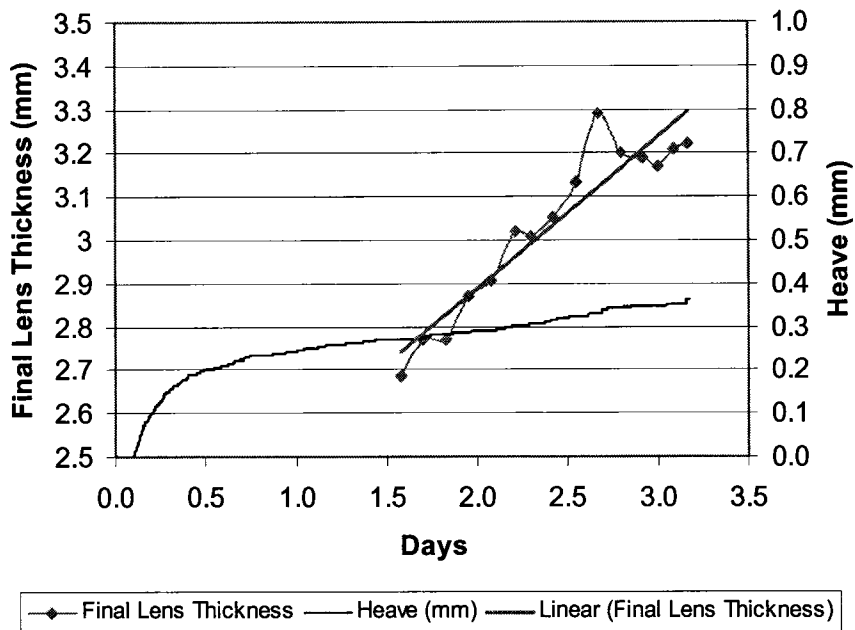


Figure A-47 - Surface Heave and Final Ice Lens Growth - Cycle 3 - S3T1

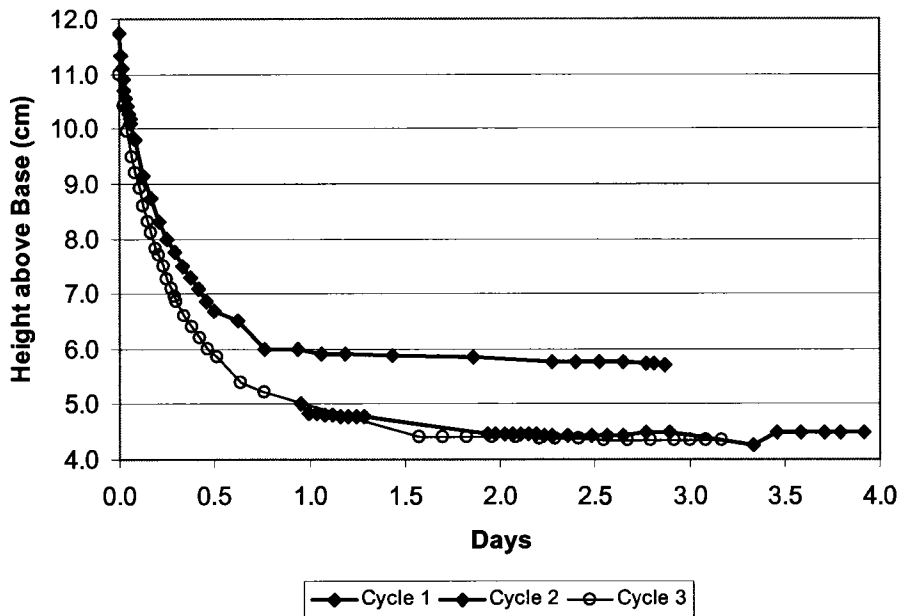


Figure A-48 - Base of Ice Lens Penetration - S3T1

A.3.2 S3T2 – Syncrude SWSS Sump Fines - Bulk

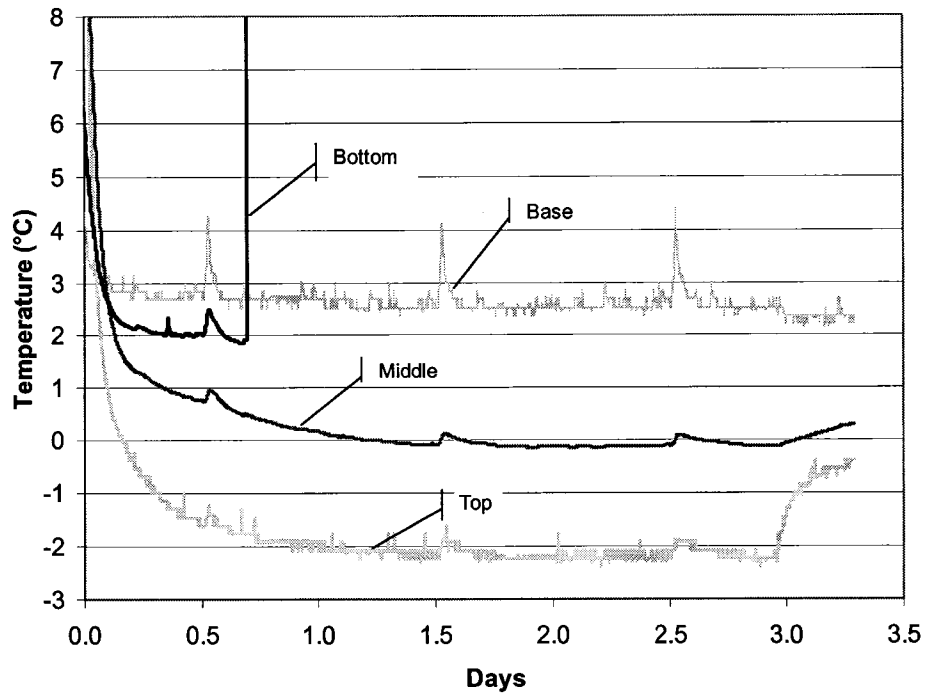


Figure A-49 - Temperature in Sample During Test - Cycle 1 – S3T2

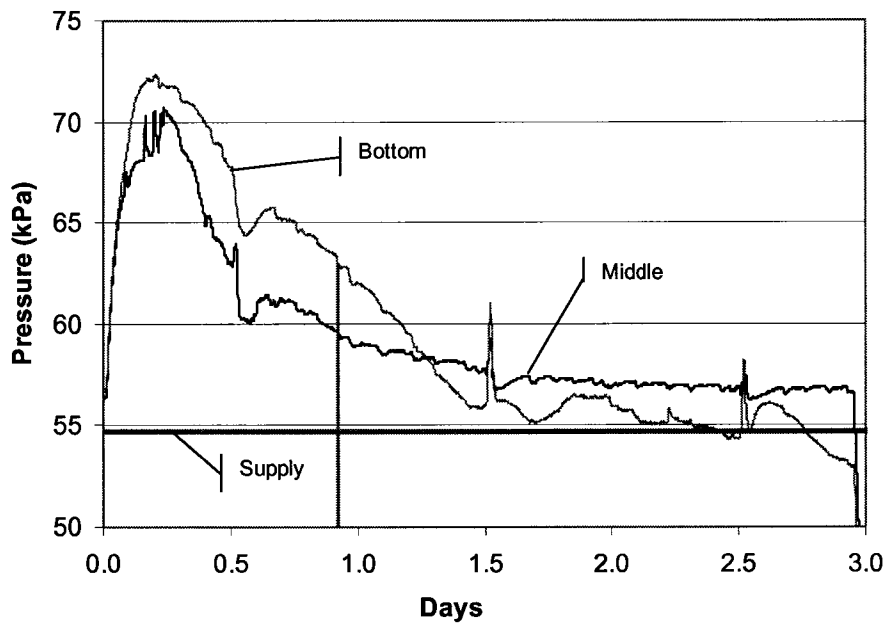


Figure A-50 - Pore Pressure During Freezing - Cycle 1 – S3T2

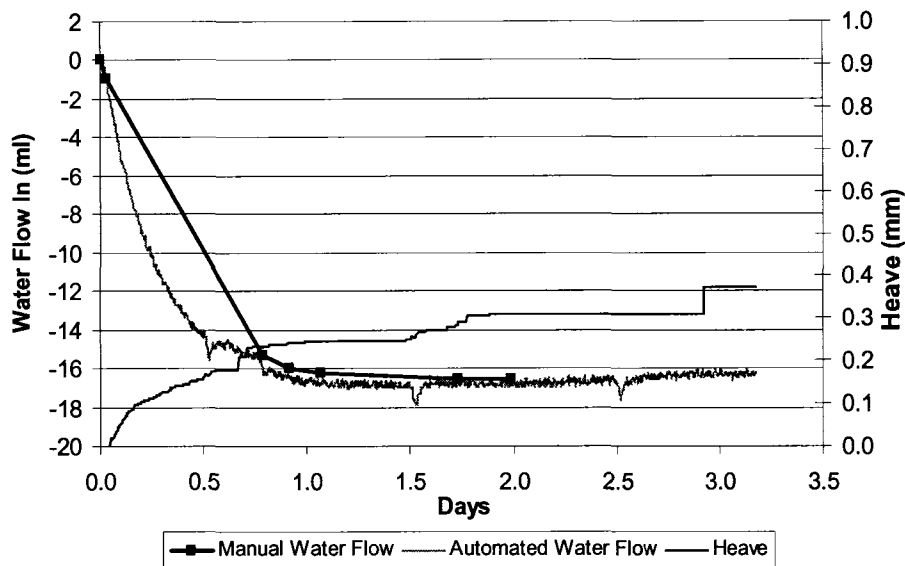


Figure A-51 - Water Supply and Heave - Cycle 1 - S3T2

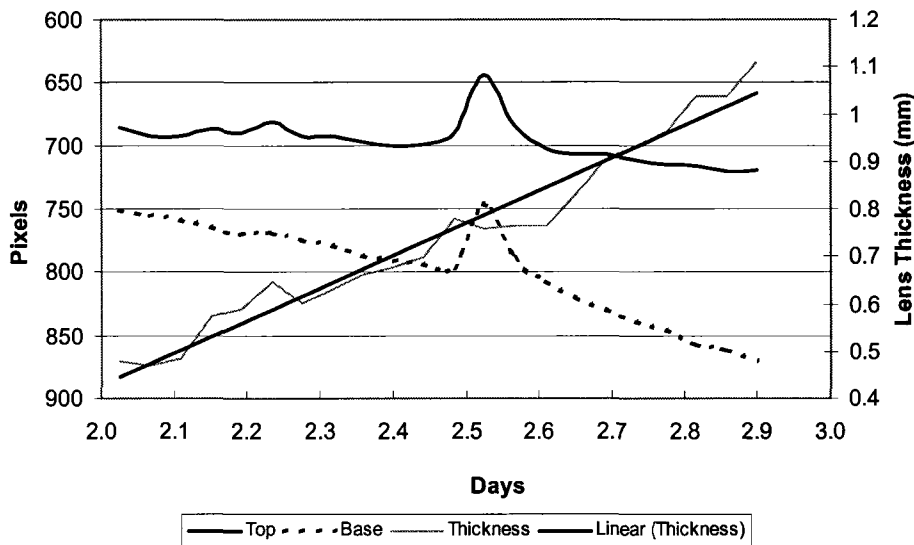


Figure A-52 - Final Ice Lens Growth - Cycle 1 - S3T2

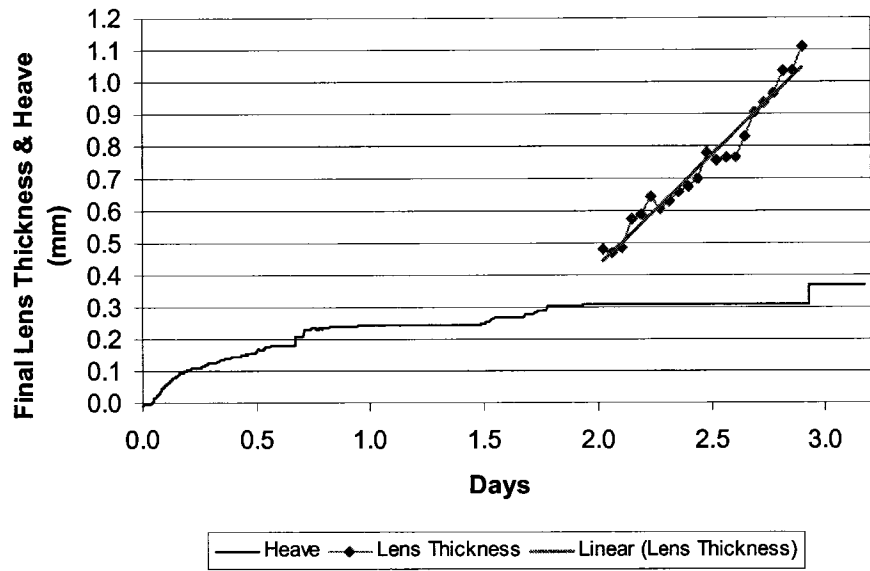


Figure A-53 - Surface Heave and Final Ice Lens Growth – Cycle 1 – S3T2

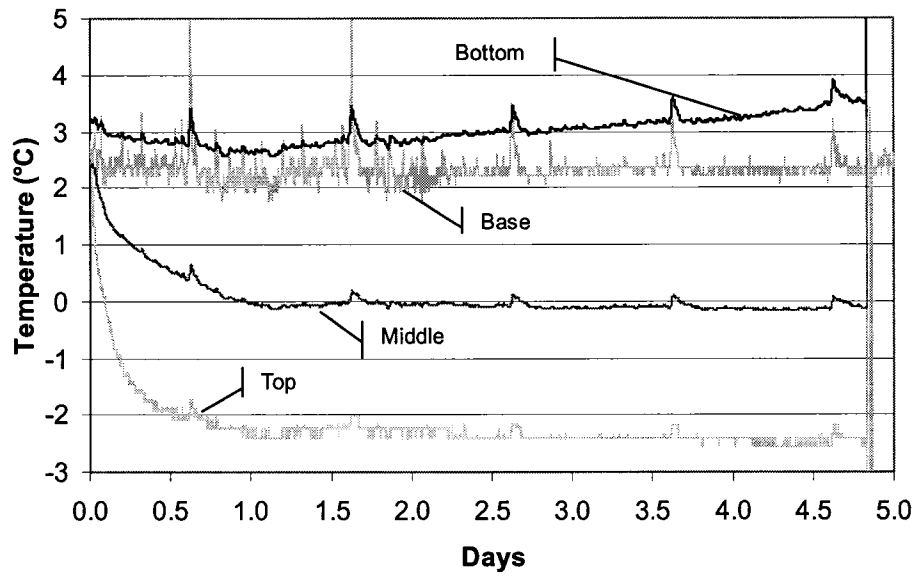


Figure A-54 - Temperature in Sample During Test – Cycle 2 – S3T2

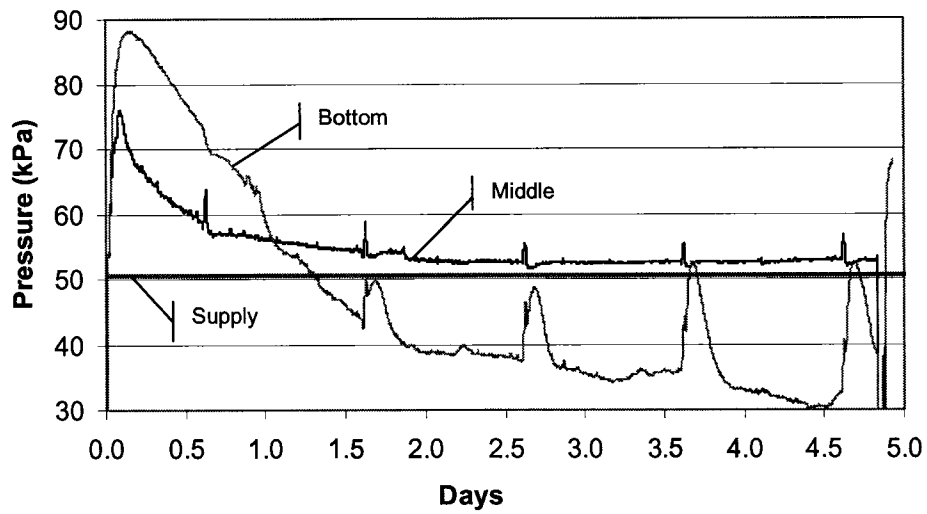


Figure A-55 - Pore Pressure During Freezing – Cycle 2 – S3T2

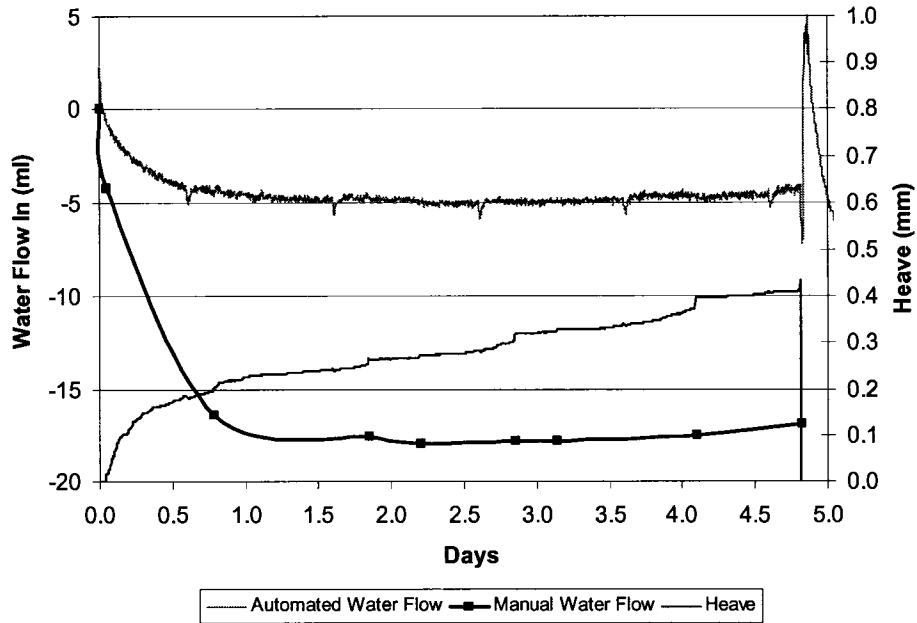


Figure A-56 - Water Supply and Heave – Cycle 2 – S3T2

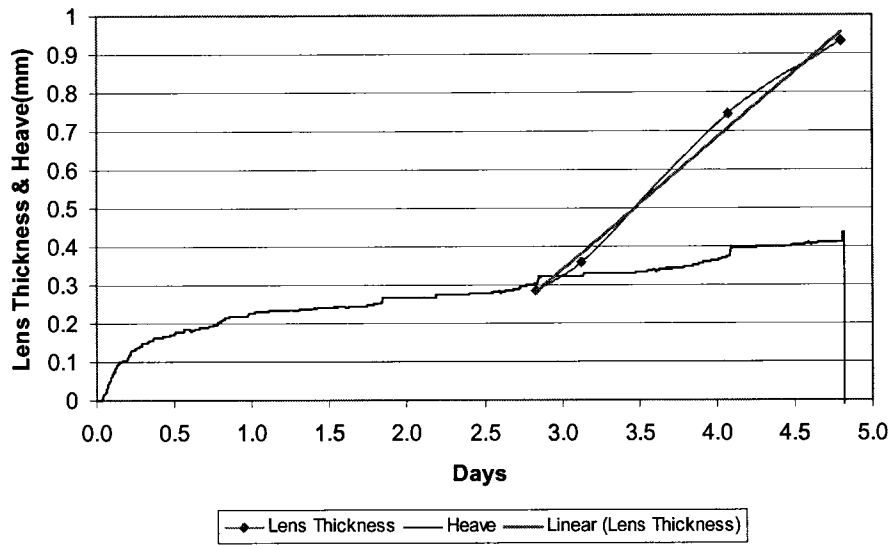


Figure A-57 - Surface Heave and Final Ice Lens Growth - Cycle 2 - S3T2

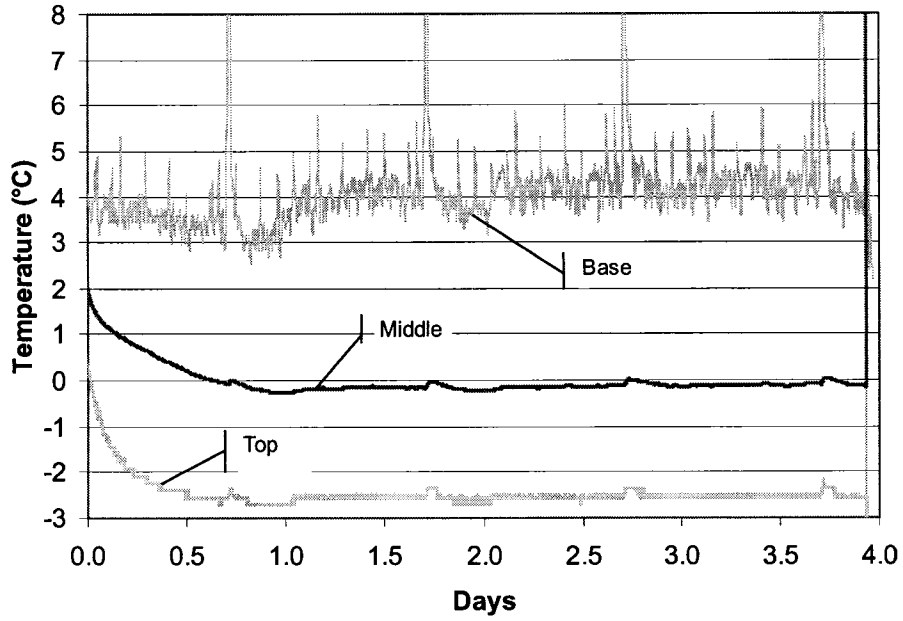


Figure A-58 - Temperature in Sample During Test - Cycle 3 - S3T2

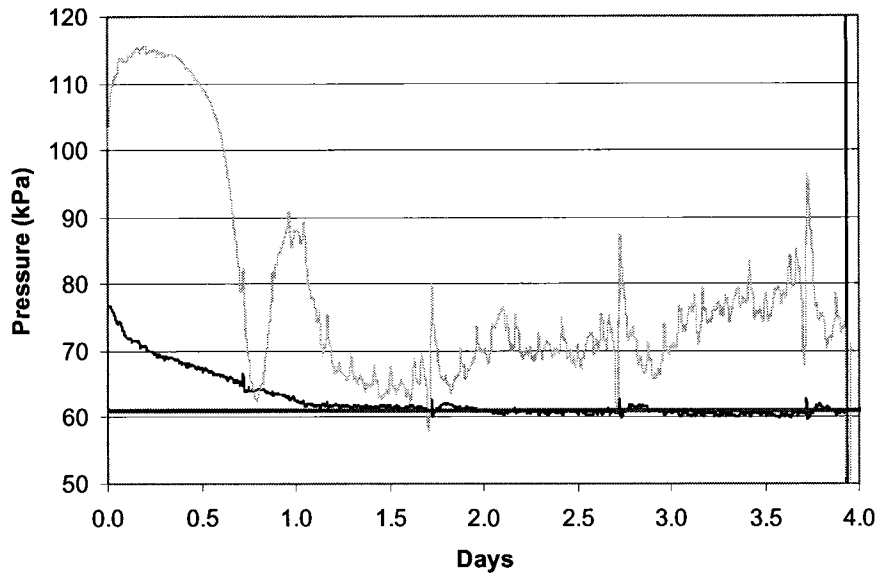


Figure A-59 - Pore Pressure During Freezing - Cycle 3 - S3T2

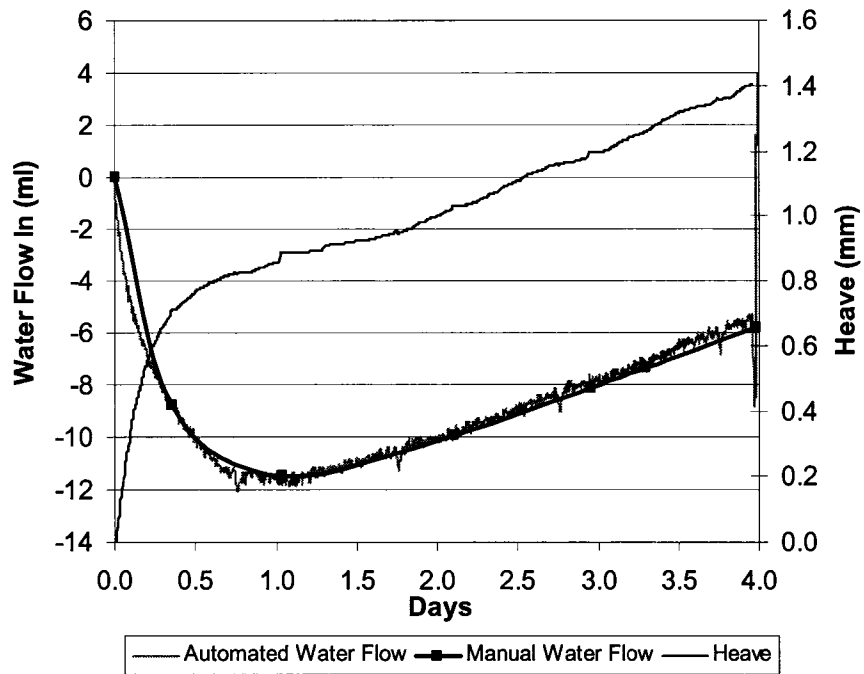


Figure A-60 - Water Supply and Heave - Cycle 3 - S3T2

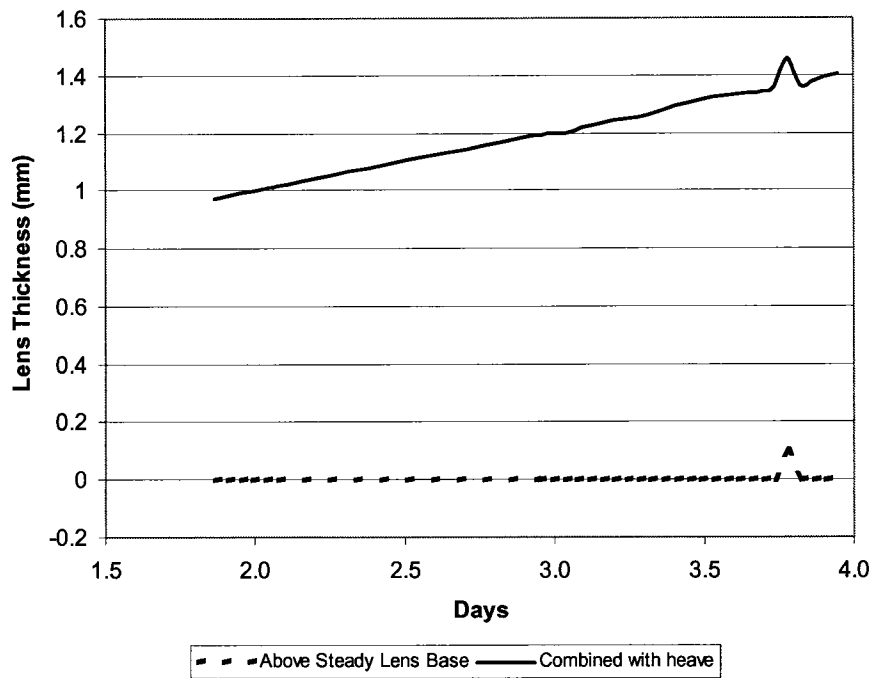


Figure A-61 - Base of Final Lens and Heave - Cycle 3 - S3T2

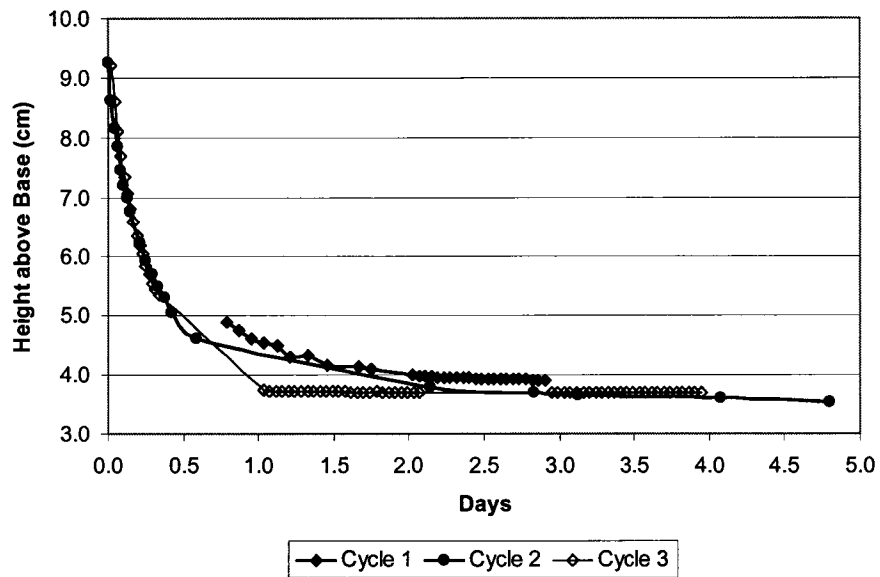


Figure A-62 - Base of Ice Lens Penetration - S3T2

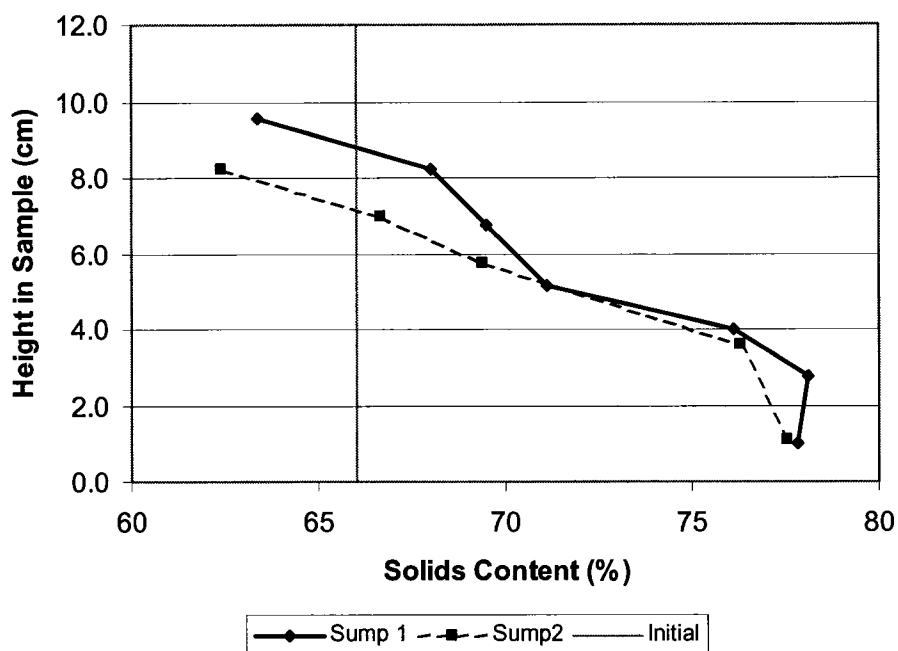


Figure A-63 - Solids Content Profile After 3 Cycles – S3T2

A.4 Test Series 4

A.4.1 S4T1 - Syncrude SWSS Sump Fines – Frozen Core

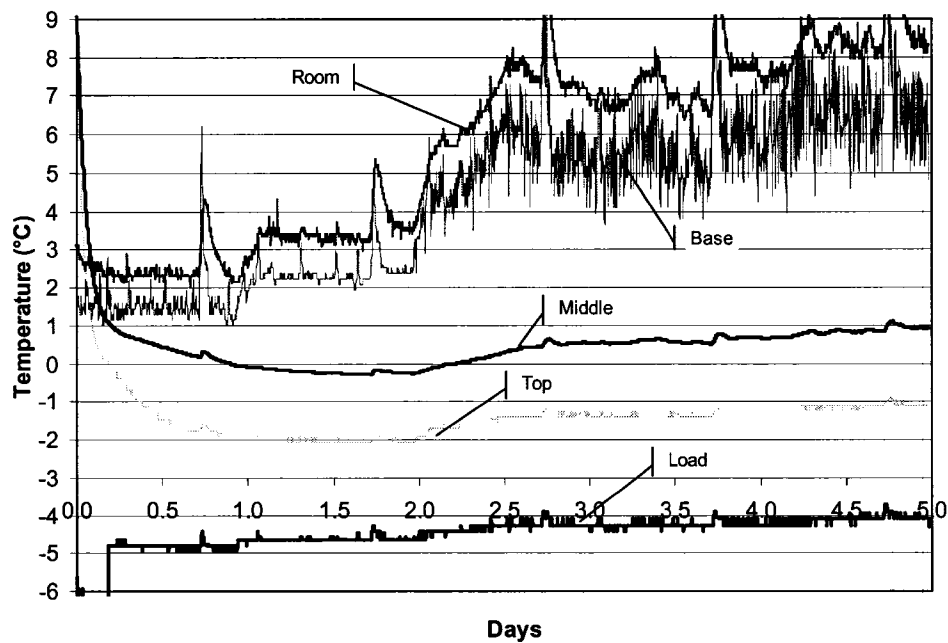


Figure A-64 - Temperature in Sample During Test – S4T1

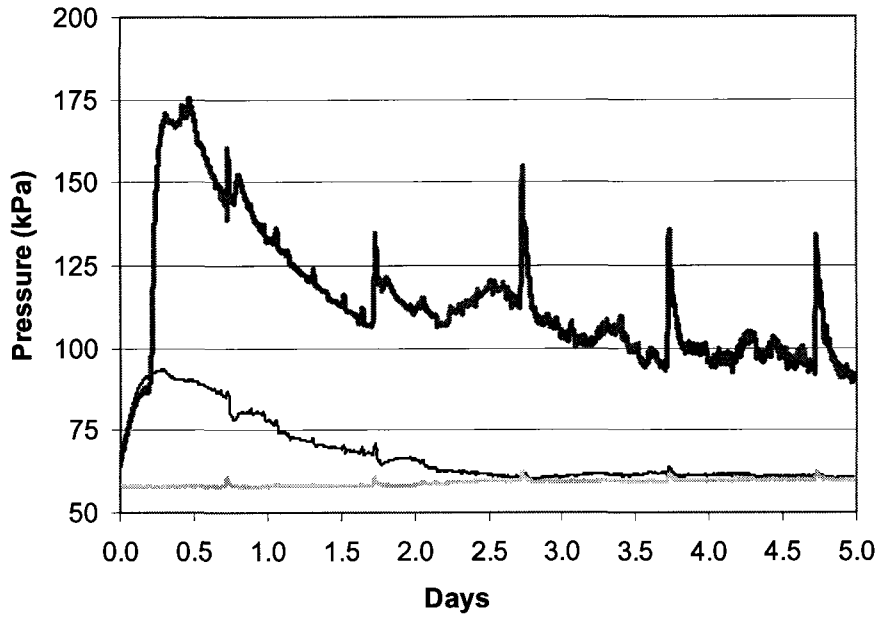


Figure A-65 - Pore Pressure During Freezing – S4T1

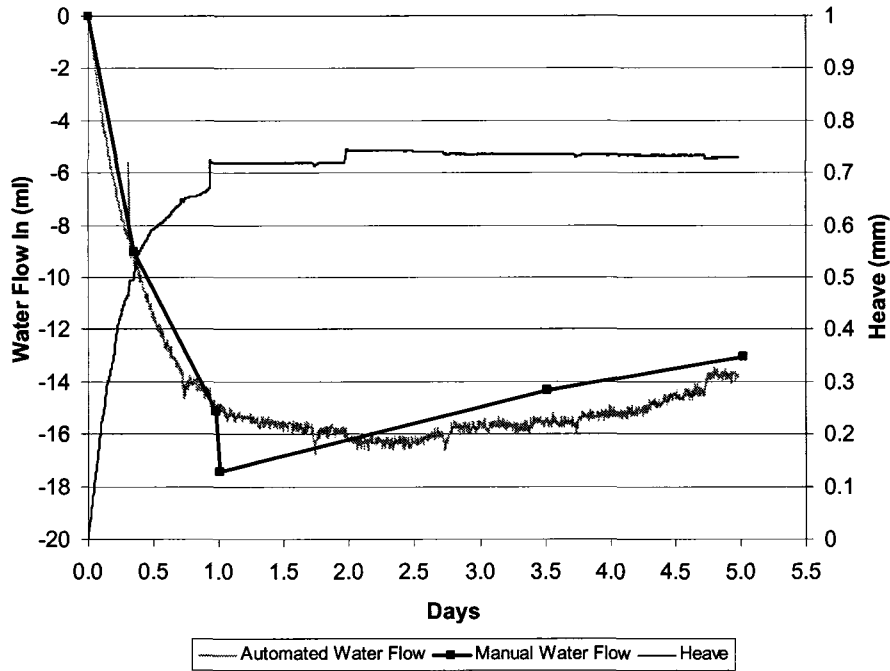


Figure A-66 - Water Supply and Heave – S4T1

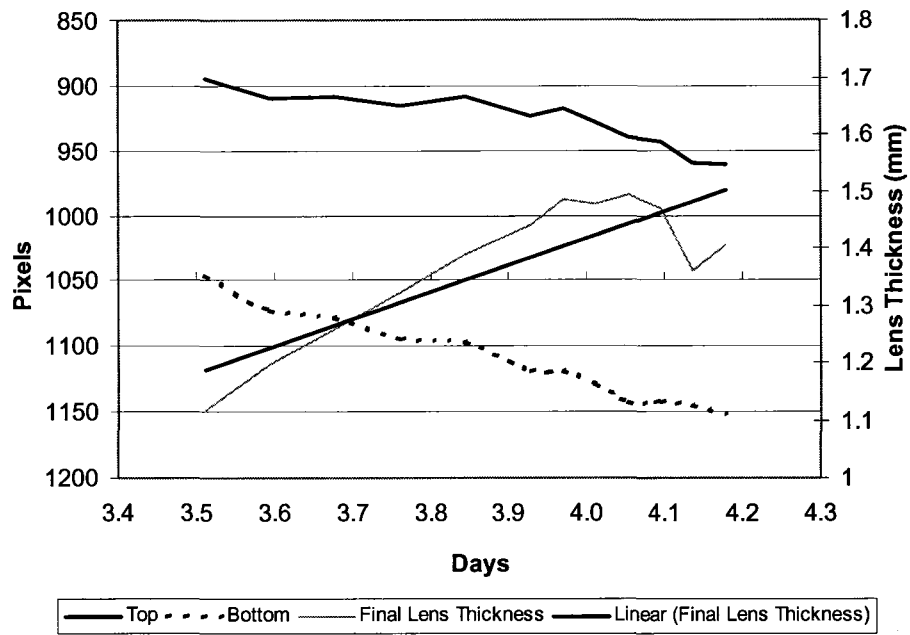


Figure A-67 - Final Ice Lens Growth - First Ice Lens - S4T1

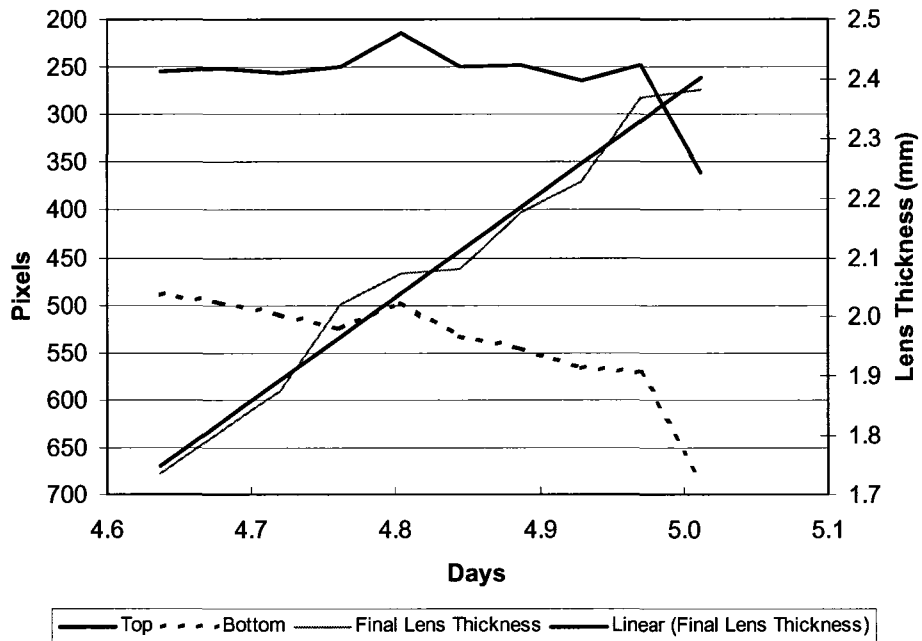


Figure A-68 - Final Ice Lens Growth - Retreated Ice Lens - S4T1

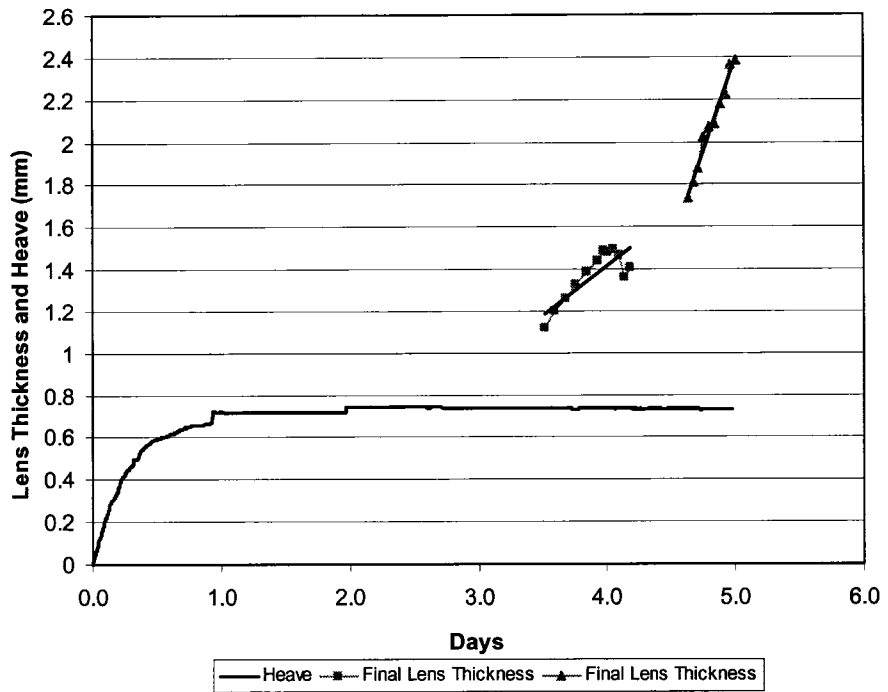


Figure A-69 - Surface Heave and Final Ice Lens Growth - S4T1

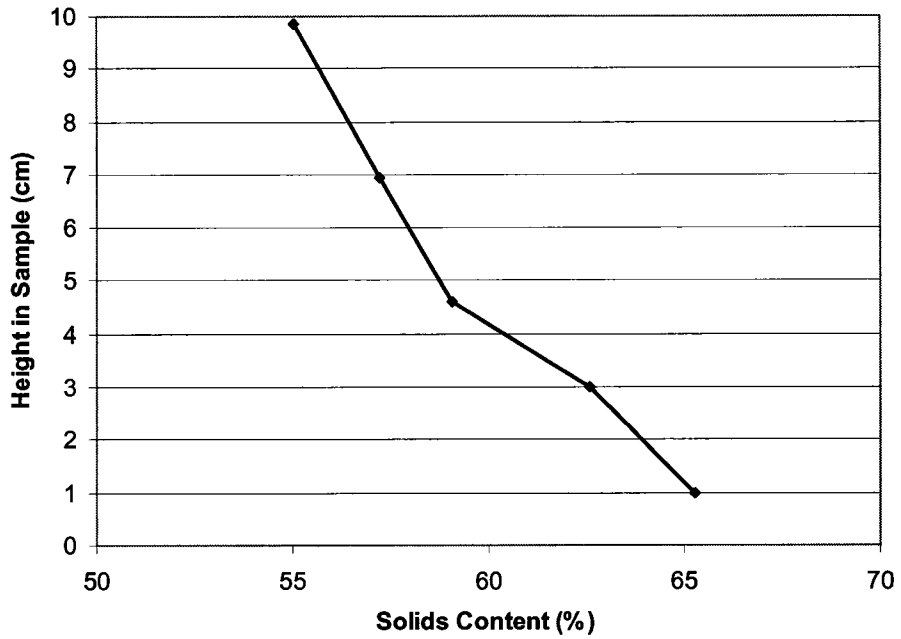


Figure A-70 - Solids Content Profile After Thaw - S4T1

A.4.2 S4T2 - Syncrude SWSS Sump Fines – Frozen Core

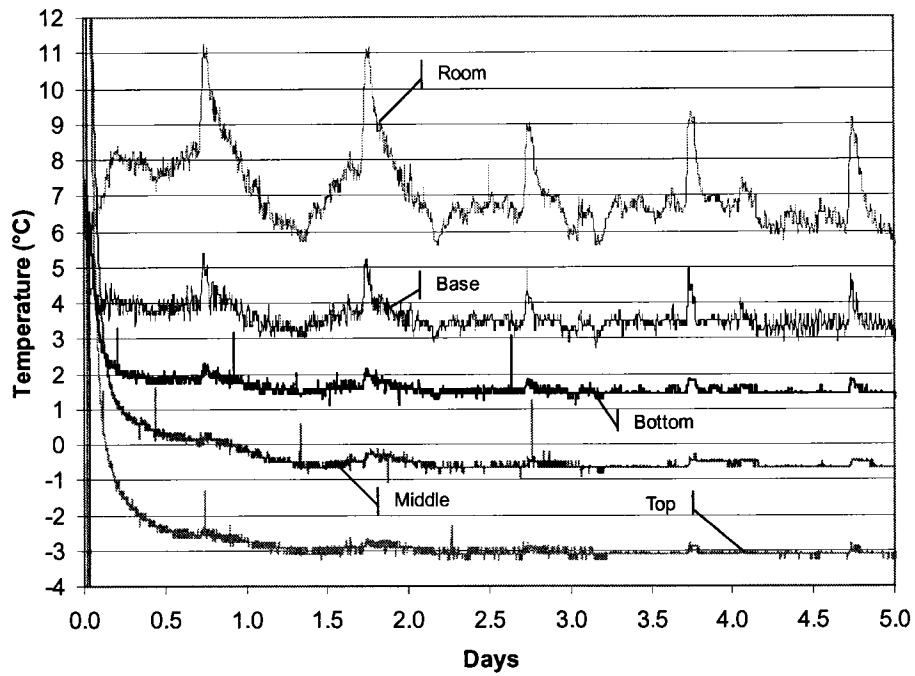


Figure A-71 - Temperature in Sample During Test – S4T2

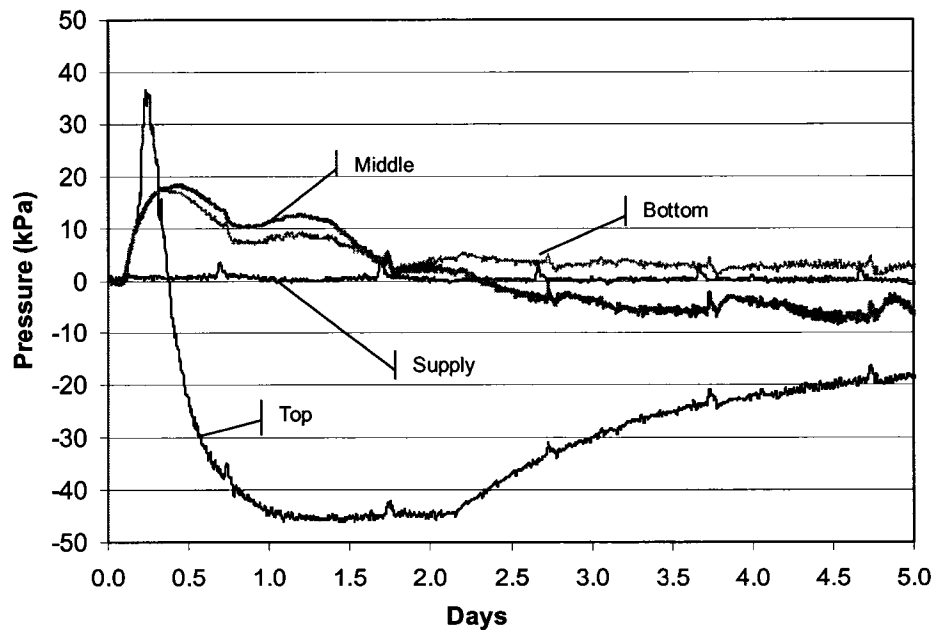


Figure A-72 - Pore Pressure During Freezing – S4T2

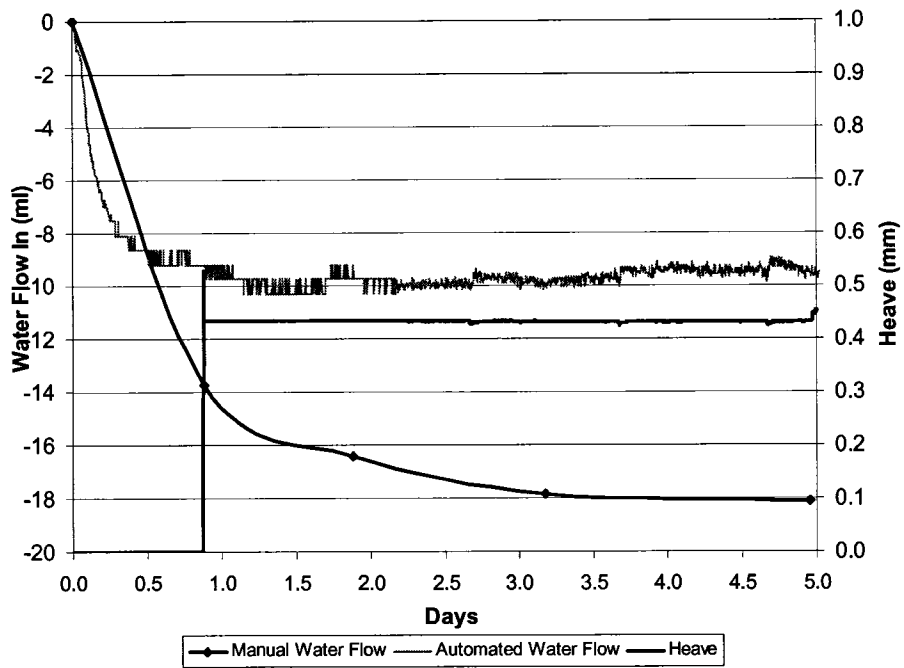


Figure A-73 - Water Supply and Heave - S4T2

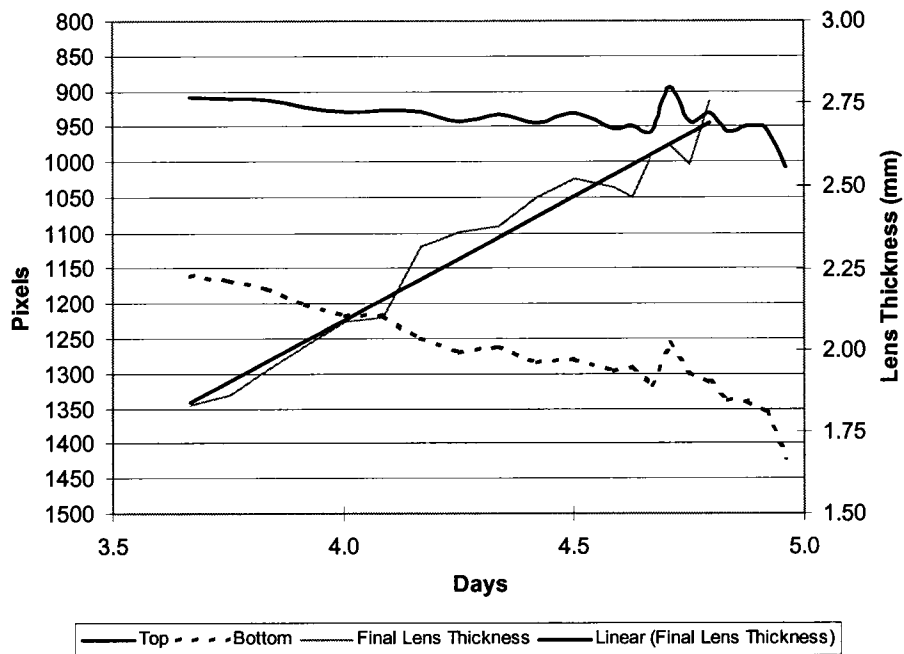


Figure A-74 - Final Ice Lens Growth - S4T2

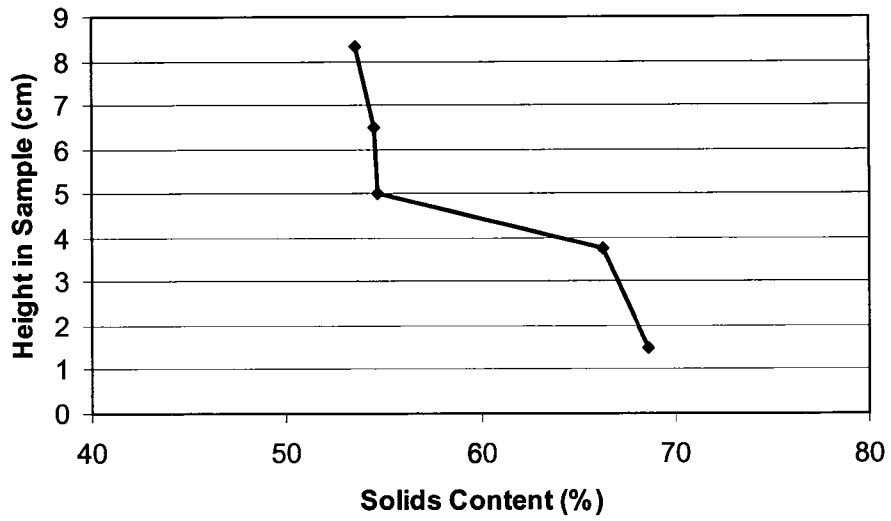


Figure A-75 - Solids Content Profile After Thaw – S4T2

A.4.3 S4T3 - Syncrude SWSS Sump Fines – Frozen Core

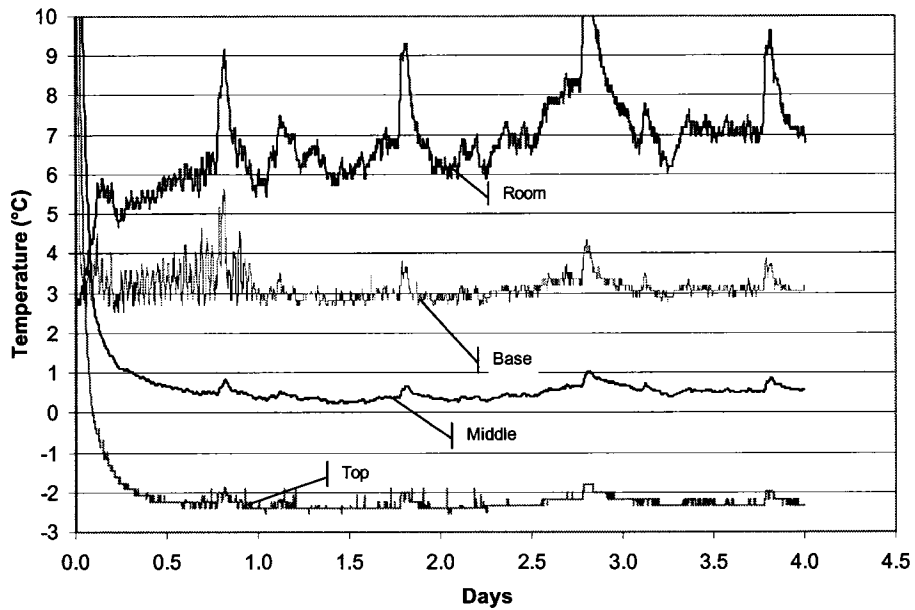


Figure A-76 - Temperature in Sample During Test – S4T3

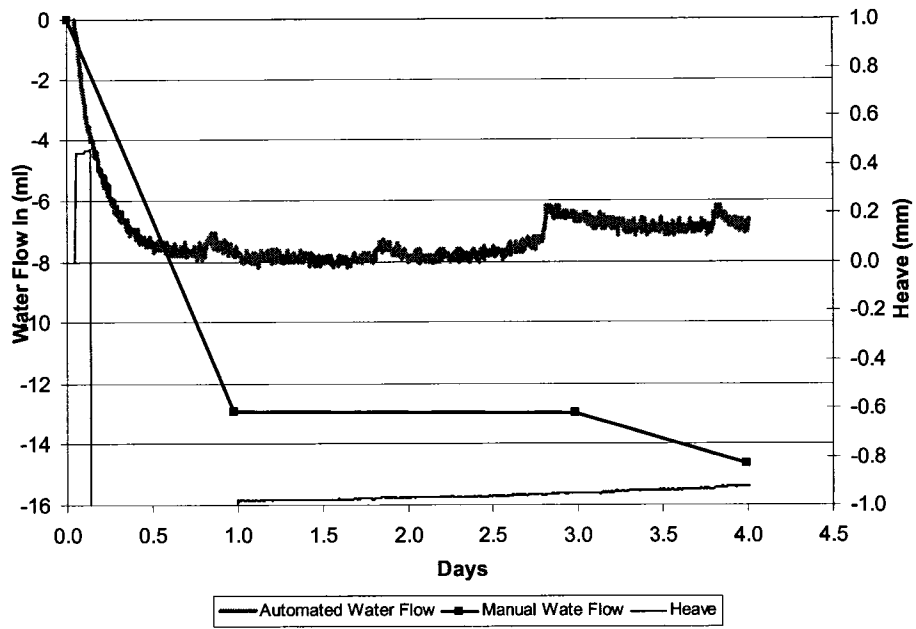


Figure A-77 - Water Supply and Heave – S4T3

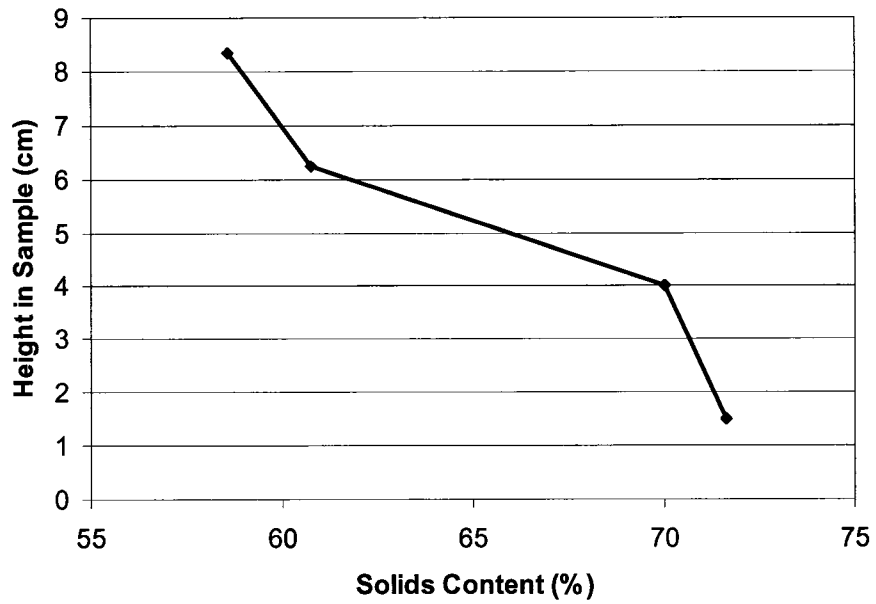


Figure A-78 - Solids Content Profile After Thaw – S4T3

A.5 Test Series 5

A.5.1 S5T1 and S5T2 – Devon Silt

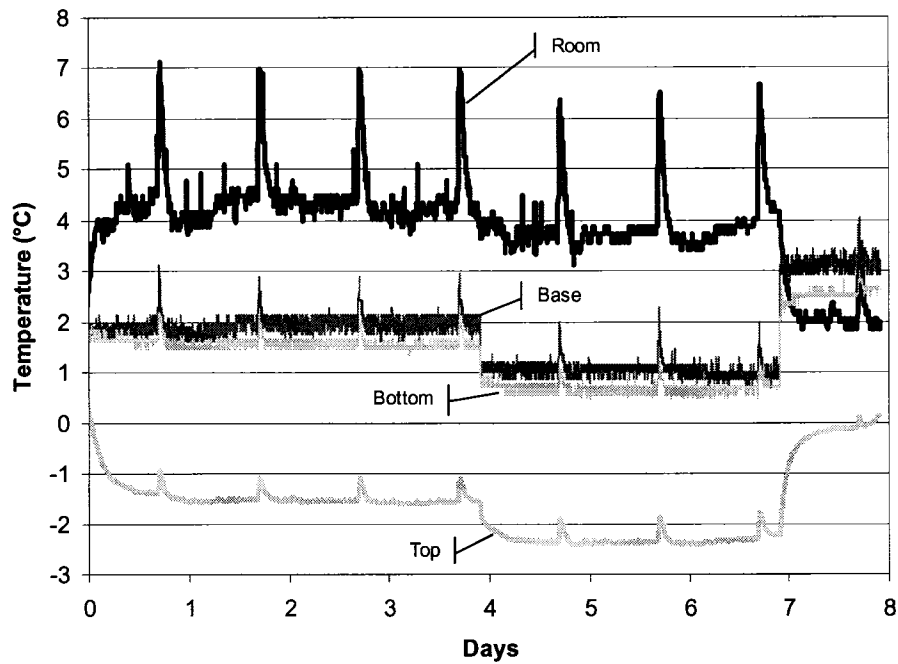


Figure A-79 - Temperature in Sample During Test - S5T1 and S5T2

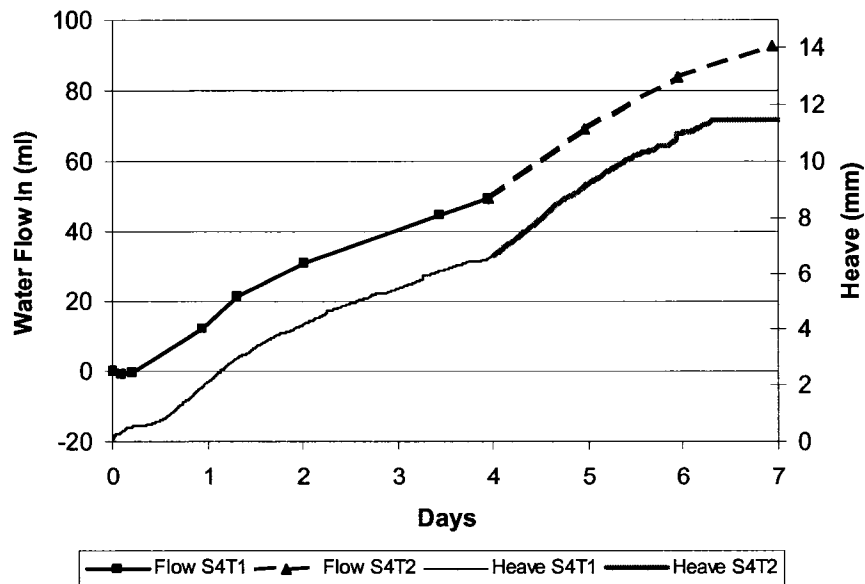


Figure A-80 - Water Supply and Heave - S5T1 and S5T2

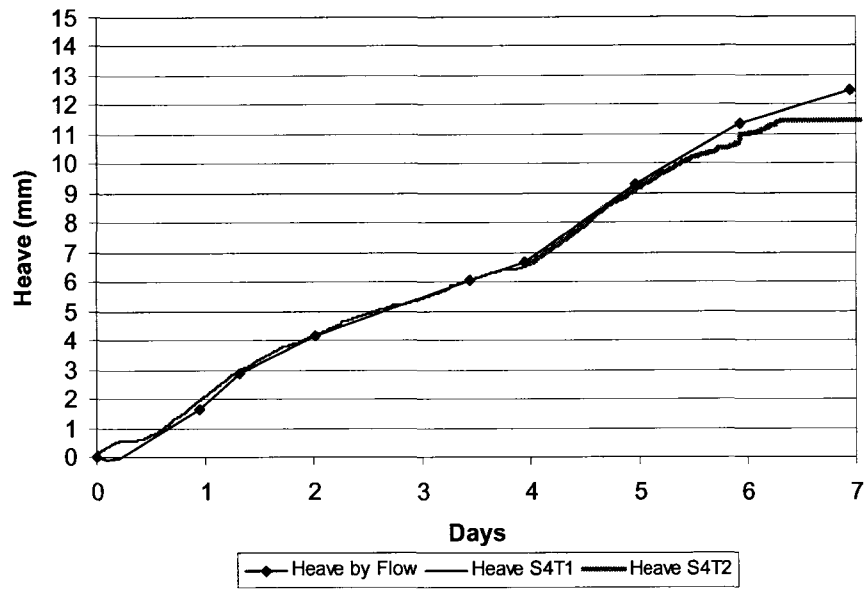


Figure A-81 - Measured Heave and Heave Due to Inflow - S5T1 and S5T2

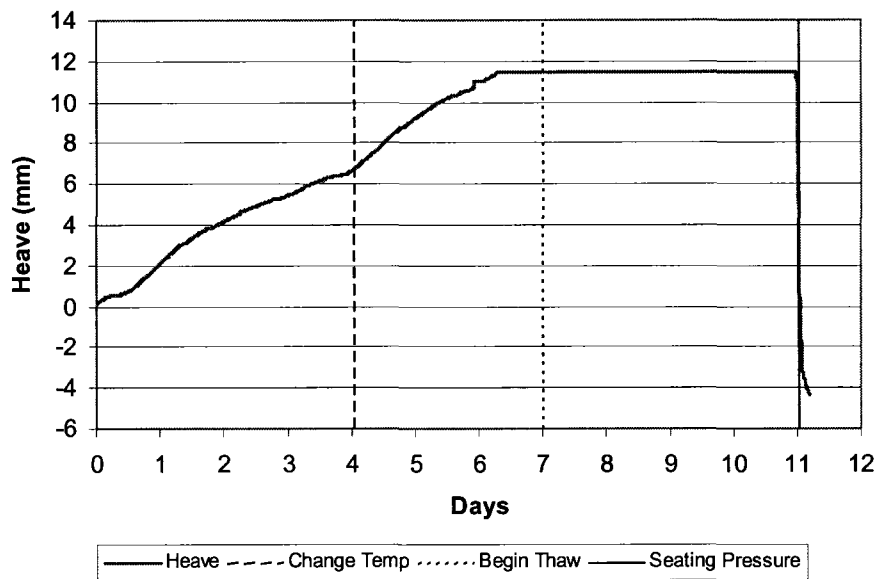


Figure A-82 - Heave Throughout S5T1 and S5T2 Freeze and Final Thaw

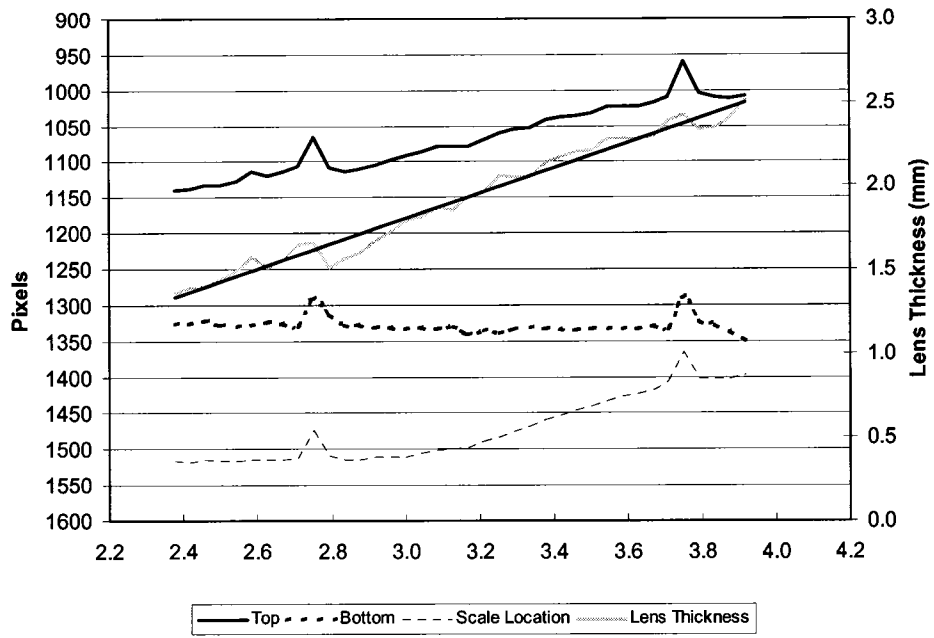


Figure A-83 - Final Ice Lens Growth - S5T1

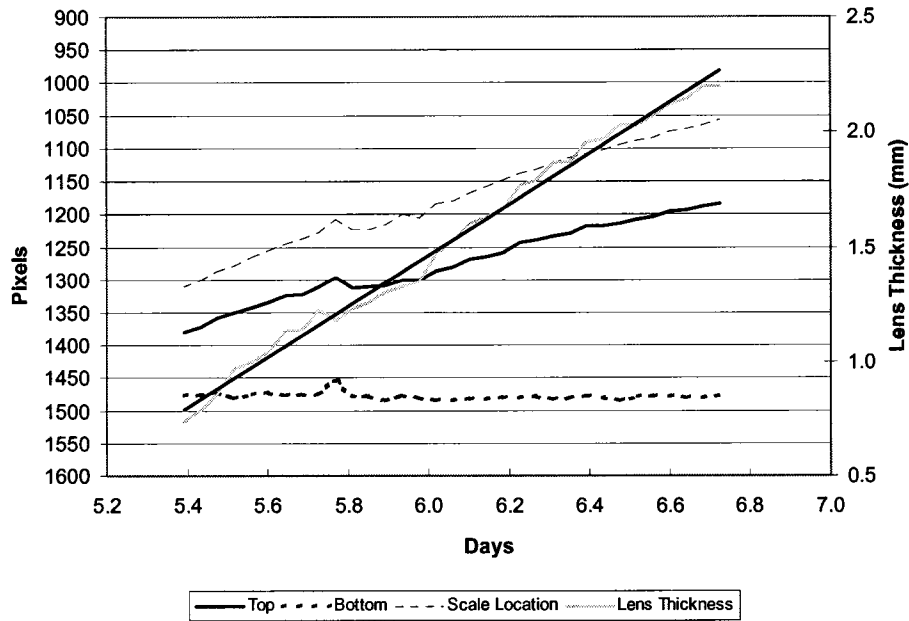


Figure A-84 - Final Ice Lens Growth - S5T2

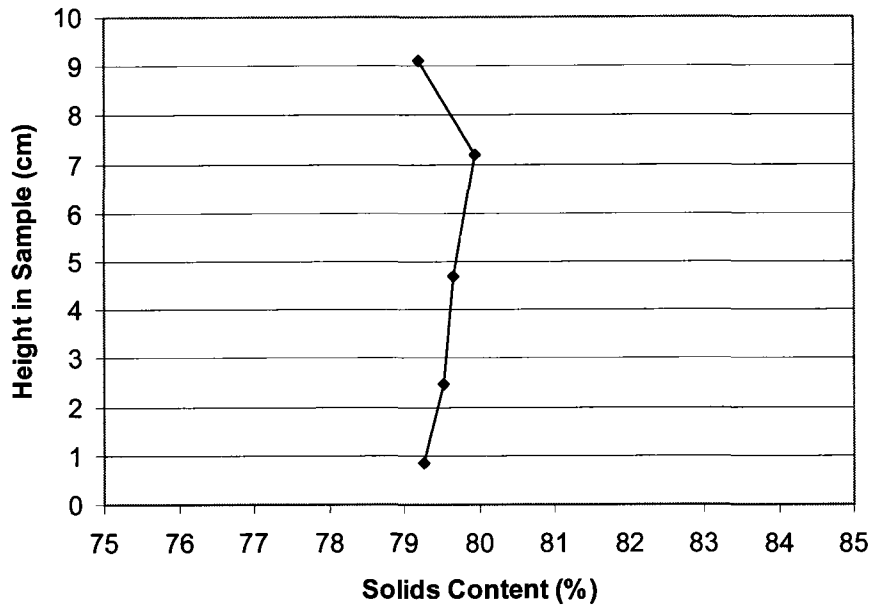


Figure A-85 - Final Solids Content After Thaw and Re-application of Consolidation Pressure – S5T1 and S5T2

A.6 Test Series 6

A.6.1 Syncrude SWSS Sump Fines – Frozen Core

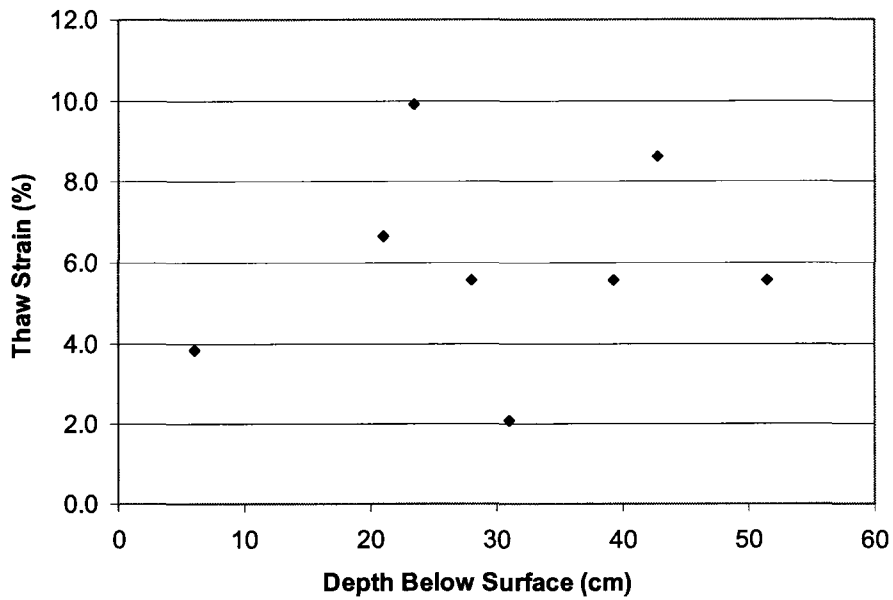


Figure A-86 - Thaw Strain for Test Series 6

Appendix B - Testing Procedure and Details

B.1 Sample Preparation

B.1.1 Bulk MFT Samples

1. Weigh the container that will be used for mixing the sample.
2. Using an impeller, stir the entire bulk sample thoroughly.
3. Withdraw a sample for testing from the bulk sample with a container immediately after mixing.
4. Weigh the container and the tailings.
5. Based on the known moisture content determined from the bulk sample, determine the volume of water in the sample, and add 5g/L fluorescein ($C_{20}H_{12}O_5$).
6. Use a stand mixer to stir the tailings and fluorescein for 10 minutes.
7. Remove a small sample from the batch for initial moisture content determination.
8. Place the testing cell on a shaker table, and vibrate the cell while pouring the tailings into the cell with a funnel. Pour the desired sample height into the cell in one lift to avoid a bitumen skin forming mid sample.
9. Place a vacuum pressure on top of the cell of 60 kPa. Allow the vacuum and shaker table approximately 1 hour to remove any air from the sample.
10. Assemble the top portion of the cell.

B.1.2 Frozen Sump Core

1. In a cold room maintained at a freezing temperature, cut the frozen core sample perpendicular to its long axis using a diamond blade saw.
2. Place the core in a lathe and trim the sample down to the testing cell diameter.
3. Place the trimmed core in the testing cell.

B.1.3 Devon Silt

1. Obtain a sample of Devon Silt and use a mechanical grinder to remove any clumps.

2. Weigh the dry soil and add water to increase the moisture content to 50%.
3. Allow the sample to soak overnight.
4. Follow the procedure from Step 5 in Section B.1.1.

B.2 Material Characterization

Tests to determine the material characteristics are listed in Table B-1, along with the relevant ASTM standard.

Table B-1 - Material Characteristics and Associated ASTM Standards

Parameter	ASTM Standard
Freezing Point Depression	D5918-96(2001) Standard Test Methods for Frost Heave and Thaw Weakening Susceptibility of Soils
Grain Size Distribution	D422-63(2002) Standard Test Method for Particle-Size Analysis of Soils
Atterberg Limits	D4318-05 Standard Test Methods for Liquid Limit, Plastic Limit, and Plasticity Index of Soils
Specific Gravity	D854-06 Standard Test Methods for SPECIFIC GRAVITY of SOIL Solids by Water Pycnometer
Moisture Content	D2216-05 Standard Test Methods for Laboratory Determination of Water (Moisture) Content of Soil and Rock by Mass

B.3 Equipment Accuracy

The accuracy of the instruments used for each testing setup is presented in this section. See Section 5.2, 5.3, and 5.4 for a description of each test method.

Table B-2 - Equipment Accuracy for Test Setup 1

Instrument	Type	Accuracy
Thermistor	YSI 44007, 5000 Ohm	±0.2°C
Displacement Gauge for Heave	Novotechnik TR50	0.002 mm
Burette for Water Supply	50 mL Capacity	±0.01 mL
Differential Pressure Sensor for Air Supply	Omega PX26-030DV	±2.0 kPa
Photograph Scale	Steel Ruler	±0.2 mm

Table B-3 - Equipment Accuracy for Test Setup 2 and 3

Instrument	Type	Accuracy
Thermistor	YSI 44007, 5000 Ohm	±0.2°C
Displacement Gauge for Heave	Novotechnik TR50	0.002 mm
Burette for Water Supply	Plastic Glass Manometer with Embedded Ruler	±0.065 mL
Differential Pressure Sensor for Air Supply	Omega PX26-030DV	±2.0 kPa
Differential Pressure Sensor for Water Supply	Validyne DP103	±0.55 mL
Gauge Pressure Sensor for Pore Pressure	Omega PX26-015GV	±0.69 kPa
Photograph Scale	Steel Ruler	±0.2 mm

B.4 Testing Procedures

B.4.1 Setup 1

1. Use clear silicone to bond a steel measuring tape to the inner wall of the testing cell.
2. Saturate any water supply ports in the freezing cell.
3. Place a boiled pore stone and filter paper on the bottom of the freezing cell.
4. Grease the cell walls with clear silicone vacuum grease.
5. After the sample has been placed in the cell (See B.1.1 - B.1.3), remove the end caps from the temperature ports and quickly insert the thermistors. Allow the sample a few hours to dissipate excess pore pressure if the hydraulic conductivity is known to be low.

6. Assemble the top of the testing cell.
7. Place the cell in the cold room and allow it to cool to the ambient air temperature near 0°C.
8. Connect the air pressure lines, water supply lines, and coolant supply lines.
9. Assemble the vertical displacement-measuring device.
10. Take initial readings of sample height and water supply level.
11. Insulate the sample by wrapping the cell with fiberglass insulation. Use a window with a closed air gap to photograph through if photos are desired.
12. Turn on the cold end supply to begin freezing.
13. Open the valves for the water supply.
14. Setup ultraviolet lighting far enough from the sample to not heat it excessively. Turn off any white light sources.
15. Using a digital camera with a macro lens, take photos remotely at regular intervals. Set the camera to a low focal length ($f4.0$), and a slow shutter speed (20-30"). The photo interval must reflect the rate of freezing if the advancement of freezing front is to be measured accurately. Use a 15-minute interval for the first several hours, increasing to 1-hour intervals when steady state is approached.
16. Sample temperature at intervals of 5 minutes using an automatic data collection system (Data Dolphin).
17. Record water supply levels at 15-minute intervals initially, increasing to 6 hours when steady freezing conditions have been established.

B.4.2 Setup 2

1. Follow the same procedure used in Section B.4.1. At step 5, also install the pressure sensors.
2. At step 10, determine the initial pressure sensor reading for the manometer.
3. At step 16, also record the manometer pressure readings at 5-minute intervals.

B.4.3 Setup 3

1. Follow the same procedure used in Section B.4.2.

B.5 Final Solids Content Determination

The final solids content after completion of the freezing test can be performed several ways.

B.5.1 Frozen Sample

Samples that are to be extruded from the cell in a frozen state will destroy the instruments embedded within. Re-freezing after thaw allows the instruments to be saved. After freezing, a hydraulic extruder was used to push the sample from the test cell. The sample was then cut into sections using a diamond blade saw, and the solids content determined.

B.5.2 Refreezing from Thawed Sample

To sample a sample after it has thawed, the testing cell was placed atop a liquid nitrogen cooled base plate, and allowed to freeze rapidly. The top of the cell was dismantled to allow heave. Freezing was completed in less than one hour.

B.5.3 Freezing Remainder of Frozen Sample

Samples that were already frozen were placed in a -25°C cold room to freeze the remaining thawed soil beneath the ice lens. Freezing was completed in less than one hour.

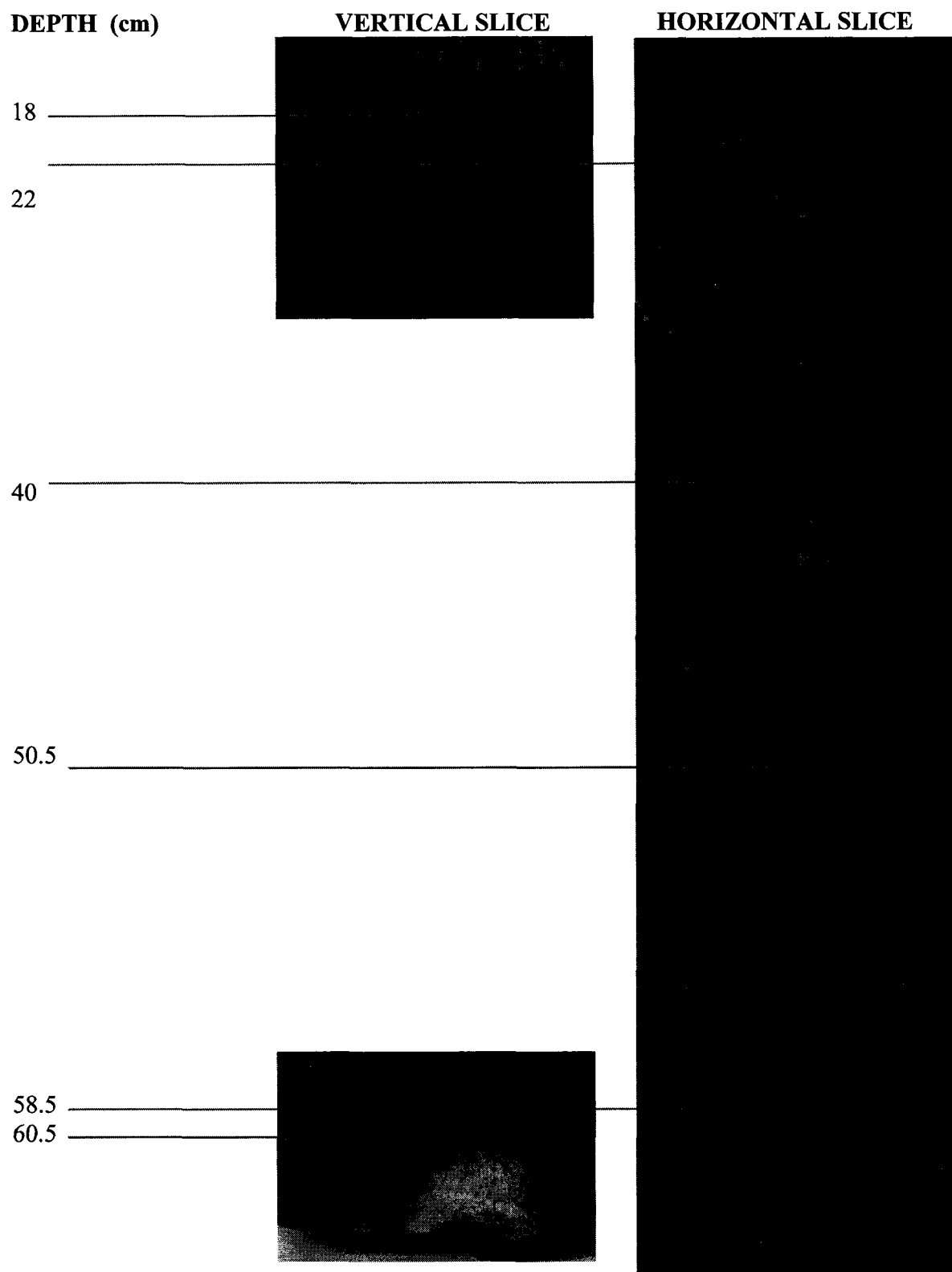
B.5.4 Thawed Sample

The solids content of several samples was determined by hand sampling. This was done by scooping the soil from the cell in uniform layers, and measuring the remaining height.

Appendix C - Frozen Core Photographs

The following photographs are from the field-sampling program. Frozen core from sites S2 and S3 were sectioned in the laboratory and are presented here to demonstrate ice lens formation in naturally frozen soil. All photographs are of the same scale and are of a soil sample 7.0 cm wide.

C.1 Sampling Location S2



C.2 Sampling Location S3

SCALE (cm)

VERTICAL SLICE

HORIZONTAL SLICE

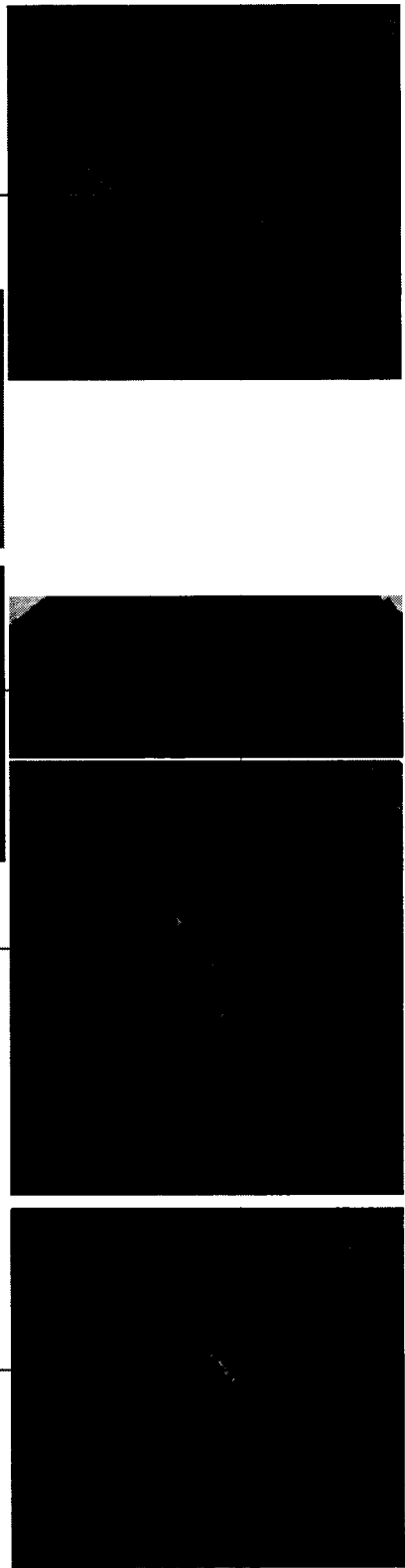
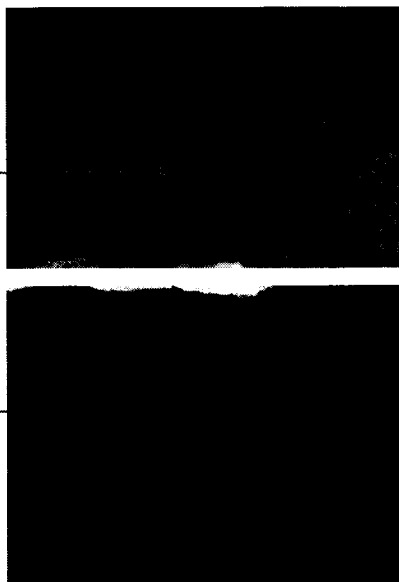
10

15

21

25

31

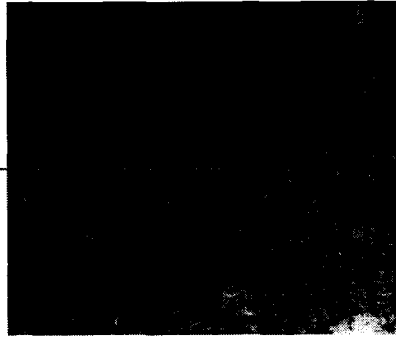


SCALE (cm)

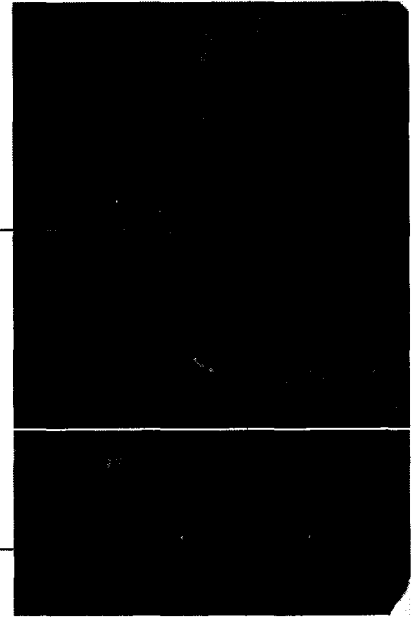
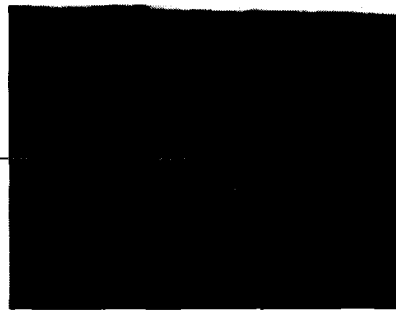
VERTICAL SLICE

HORIZONTAL SLICE

36



39



50



59

197